Impact Studies

Victor L. Masaitis *Editor*

Popigai Impact Structure and its Diamond-Bearing Rocks

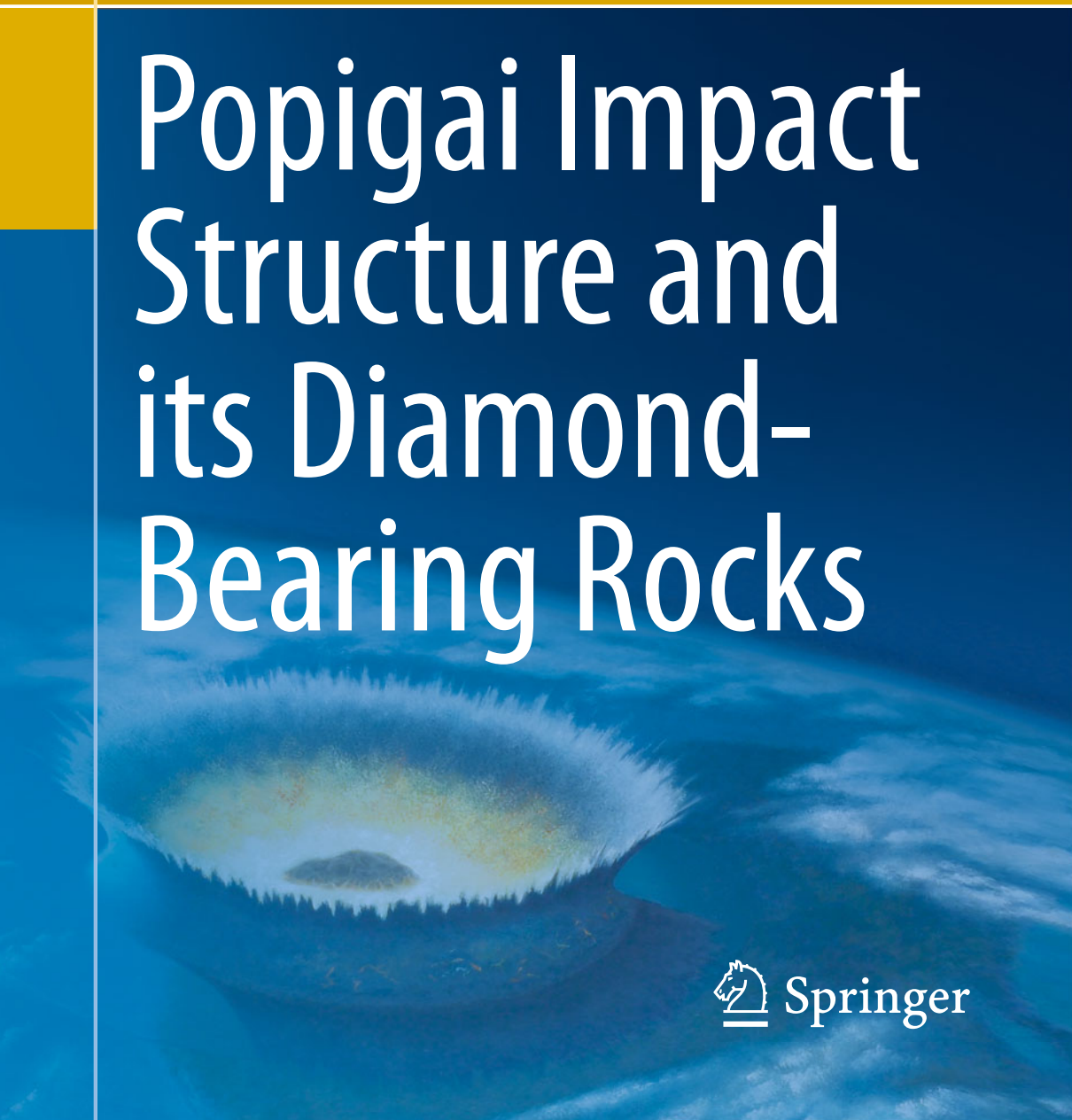

Springer

Impact Studies

Within the past two decades, research on impact cratering mainly gained attention throughout the world after the theory that a large impact event caused the extinction of ca. 50% of all living species, including the dinosaurs, approximately 65 million years ago was proposed. Impact craters are formed when a large meteorid crashes into a larger planetary body with a solid surface.

The interdisciplinary series, **Impact Studies**, aims to include all aspects of research related to impact cratering—geology, geophysics, paleontology, geochemistry, mineralogy, petrology, planetology, etc. Experimental studies on shock metamorphism, investigations of individual impact craters, comparative planetology, and paleontological research on the effects of impact events are just a few topics that are treated in this series. All contributions are peer-reviewed to ensure high scientific quality.

More information about this series at http://www.springer.com/series/4698

Victor L. Masaitis
Editor

Popigai Impact Structure and its Diamond-Bearing Rocks

Springer

Editor
Victor L. Masaitis
A. P. Karpinsky Russian Geological
Research Institute (VSEGEI)
St. Petersburg
Russia

ISSN 1612-8338
Impact Studies
ISBN 978-3-319-77987-4 ISBN 978-3-319-77988-1 (eBook)
https://doi.org/10.1007/978-3-319-77988-1

Library of Congress Control Number: 2018935219

Cover illustration: Dona Jalufka, Vienna, Austria

Printed on acid-free paper

This Springer imprint is published by the registered company Springer International Publishing AG
part of Springer Nature
The registered company address is: Gewerbestrasse 11, 6330 Cham, Switzerland

Preface to the English Edition

The basis of this publication is the book "Diamond-bearing Impactites of the Popigai Astrobleme," printed in Russian by VSEGEI Publishing House (St. Petersburg) in 1998, and contained a description of the Popigai impact structure in the north of Siberia. Although a number of concerning articles appeared in certain English-language journals and collections of papers over the past twenty years, some important features of this impact structure, of its impact breccias and diamond-bearing impactites are missing in the scientific literature in English.

The translation of the mentioned book into English under the title "Popigai Impact Structure and Its Diamond-bearing Rocks" in general follows the content presented in Russian. However, it is somewhat modified. Additions were input to the chapters dealing with the mineralogy of impact diamonds, the characteristics of their deposits, the genesis of diamond-bearing impactites, and others. The sections concerning various post-impact formations have been included as well, but on other hand, the description of other diamond-bearing impact structures has been deleted. For some refinements were used papers published in the last two decades and written mainly by authors, who have performed additional field observations and partial revision of previous ones. A number of illustrations have been replaced, and they are supplemented with new photographs. The list of references is also expanded.

Authors acknowledge to Alexander Deutsch, Falco Langenhorst, Boris Ivanov, Richard Grieve, Phillipe Claeys, Mark Pilkington,@ and Doreen Ames for fruitful discussions held during the joint geological excursion to Popigai crater undertaken in August 1997 (IPEX-97). Oleg Simonov and Mikhail Goncharov are also appreciated for essential help in our studies of the Popigai. Especially, we thank A. Deutsch and F. Langenhorst for assistance in various research, and collaboration in analytical study on Popigai impactites and its diamonds.

The original English translation was made in VSEGEI by T. I. Vasilieva with some additions by V. L. Masaitis and M. V. Naumov, and the translation was subjected to the necessary linguistic processing in the Springer Publishing House.

The preparation of the manuscript “Popigai Impact Structure and Its Diamond-bearing Rocks” was carried out by V. L. Masaitis, M. V. Naumov, T. V. Selivanovskaya, and V. T. Kirichenko with participation of I. G. Fedorova and M. S. Mashchak.

St. Petersburg, Russia Victor L. Masaitis

Preface to the Previous Book "Diamond-bearing Impactites of the Popigai Astrobleme" (1998)

The role and significance of diamonds in the life of the modern industrial society are well known, due to which the search and revealing of the new deposits of diamond raw materials are one of the priority trends of subsurface studies. During more than 120 years, kimberlites were the only diamond-bearing bedrock in the world; they are described in tens of thousands of scientific publications. First discovered in South Africa in the nineteenth century, and then on other continents, they are up to now of great interest not only as the source of valuable minerals, but also as the source of information on Earth's upper mantle horizons, their composition and the processes occurring within them.

The last decades were not only marked by discoveries of new diamond-bearing provinces of kimberlites and related rocks in different regions of the world (Eastern Siberia, Eastern and Northern Europe, South-Eastern Asia, Australia, northwest and west of North America, some regions of Africa, etc), but also by revealing of new genetic types of diamond-bearing rocks earlier unknown. Among them are impactites, first discovered at the beginning of the 70s in the northern Siberian Platform, and formed by melting of crystalline rock under the impact of a cosmic body. Impactites occur within the Popigai impact structure (or astrobleme) of about 100 km across that appeared at the end of Eocene. Polycrystalline diamonds enclosed in impactites resulted from transformation of graphite of initial target gneisses under shock compression.

An assumption of a possible discovery of diamonds of shock origin in the flanks of large lunar craters was first made at the middle of 1960s. However, the studies of lunar rocks demonstrated the lack of perceptible amounts of graphite and other carbon minerals in them that minimized or totally excluded such a possibility. As is known, diamonds of shock origin were initially discovered in meteorites, i.e., ureilites and octahedrites, where they formed at the expense of carbonaceous substance of these cosmic bodies under high-velocity impacts in space or on the Earth's surface. Sources of unusual polycrystalline diamonds, discovered in 1960s in placers in the Ukraine and northeastern Yakutia, are long remained unknown. And it is only after discovery of diamonds in impactites of the Popigai impact

structure, it became obvious that they appeared in placers during destruction of similar primary rocks.

Diamond-bearing impactites are up to now not well known to geologists. This prevents the discovery and studies of similar formations in other impact structures, and also leads to errors in description of these rocks, sometimes even resulting in different conjectures concerning their composition, mode of occurrence, relationships with other rocks and, particularly, their origin. This is, to a major extent, due to fact that detailed characteristics of impactites, which were studied in particular detail in the Popigai structure, up to recent time were not accessible for publication, similar to the data on the therein diamonds enclosed.

The Popigai structure belongs to the first dozen of the largest impact sites on the Earth's surface. Its size, good preservation from erosion, diversity of structural elements, as well as an extensive range of different rock types subjected to shock metamorphism and crater excavation, make this object rather favorable for elaboration of many issues connected with impact cratering. It is necessary to emphasize that the total volume of impact melt solidification products in the Popigai crater is inferior on the Earth's land surface only to the Proterozoic Sudbury impact structure in Canada. Study of distribution, composition, and mode of origin of impactites and breccias developed in the Popigai structure is of great significance for the reconstruction of processes of impact cratering including those on the surfaces of other planets where rocks crushed and re-melted by large falling space bodies, cover extensive areas, particularly in large impact basins.

The Popigai depression described for the first time in the middle 1940s by D. V. Kozhevin was considered for a long time as a volcanic–tectonic structure. However, in 1970, geologists of All-Union Geological Research Institute (VSEGEI) headed by V. L. Masaitis recognize and substantiate the impact origin of the Popigai structure; in addition, they reveal specific diamonds in impact-derived rocks filling the depression. This initiates an extensive exploration of the Popigai resulting in discovering of unique diamond deposits and thorough investigation of the impact crater and enclosed impact-generated formations.

Diamond-bearing impactites of the Popigai structure were the object of comprehensive geological (including geological surveying of medium and large scales) and specialized research, conducted in 1970–1985 and partly in later years. Geological exploration conducted during the period of 1972–1984 and accompanied by extensive diamond drilling (more than 800 boreholes) and geophysical observations enables to determine more precisely the subsurface structure of the impact structure, mode of occurrence and relationships of different rock types, as well as to reveal the specific features of diamond distribution in impactites. Geological, petrographic, mineralogical, geochemical, and other studies allowed giving a rather complete characteristics of impactites, as well as of enclosed within them impact diamonds, etc.

Geological surveying of the Popigai impact structure and specialized research were conducted by authors of the present work, as well as by V. V. Geern, M. M. Goncharov, A. N. Danilin, V. T. Kirichenko, G. G. Lopatin, L. A. Lopatina, L. A. Markovich, V. A. Maslov, A. V. Medvedev, M. V. Mikhailov, A. Yu.

Romanovsky, V. V. Khailov, and some other geologists. Geological prospecting and borehole drilling were conducted under the leadership of L. M. Zaretsky, N. A. Donov, V. T. Kirichenko, V. G. Mezhubovsky, and other specialists, who were also evaluating diamond resources in impactites. V. I. Vaganov, V. I. Batrak, and some others also participated in these evaluation works. A major contribution to the study of impact diamonds was made by M. A. Gnevushev, G. K. Erjomenko, G. S. Rumyantsev, Yu. A. Polkanov, and E. D. Nadezhdina-Bondarenko; certain rock and mineral groups were investigated by S. A. Vishnevsky, V. A. Ezersky, N. A. Pal'chik, and J. V. Orlova. Geophysical observations conducted under the leadership of Yu. M. Shulgin, E. K. Germanov, R. T. Guibadullin, and V. S. Yakupov were of great significance for deciphering subsurface structure of the impact structure. Important results were obtained by M. I. Plotnikova, V. V. Chernoknizhnikov, and other geologists during the studies of loose Pliocene–Quaternary deposits and diamond-bearing placers resulting from in the course of erosion of impact rocks.

The authors of the present work conducted geological and other type of research in the Popigai structure from 1970 to 1985; route observations covered its entire area. The cores from more than 400 boreholes were described and petrographically characterized; the total number of thin sections of rocks studied during the indicated period amounts to several thousands. In the process of observation, numerous analyses of the chemical composition of rocks and minerals were conducted, and specific features of their transformation were studied using different analytical techniques, with major emphasis on the analysis of diamond content in impactites. Most of analytical works were carried out in VSEGEI Labs. Some information on geology of the Popigai structure, on characteristics of rocks and their minerals, etc., including that concerning the reconstruction of specific features of the impact event, was published by the authors and other researchers as a monograph (1975) and separate articles; these data were also included as sections into the other publications.

To analyze and generalize the material presented under its separate sections, some data obtained by above-mentioned researchers were used in addition. Account was also taken of the information concerning geological structure of territories adjacent to the Popigai crater and obtained in the course of the state medium-scale geological surveying.

The monograph was prepared at A. P. Karpinsky Russian Geological Research Institute (VSEGEI) with support of the Russian Foundation for Basic Research, grant 95-05-30509, during 1995–1997. The following specialists participated in its compilation: V. L. Masaitis, M. S. Mashchak, A. I. Raikhlin, T. V. Selivanovskaya, and G. I. Shafranovsky. Some materials were prepared with participation of E. L. Balmasov and I. G. Fedorova; some geological sections and schemes for certain areas were compiled by M. V. Naumov. E. L. Balmasov and S. M. Gadasina performed the important work on presentation of the materials and their computer processing. The general guidance and editing was undertaken by V. L. Masaitis.

1998

Contents

Abbreviations

Bh	Borehole
CVD	Chemical vapor deposition
DSDP	Deep-sea drilling project
DTA	Differential thermal analysis
EMP	Electron microprobe
EPR	Electron paramagnetic resonance
FWHM	"Full width at half maximum" (Raman spectroscopy)
HRTEM	High-resolution transmission electron microscopy
HT	High temperature
INA	Impulse neutron activation analysis
LOI	Loss of ignition
LT	Low temperature
MT TNT	Megatons of trinitrotoluole
ODP	Ocean-drilling project
RAS	Russian Academy of Science
RFBR	Russian Foundation for Basic Research
SEM	Scanning electron microscopy
SFS	Super-fine structure
TEM	Transmission electron microscopy
UF	Ultraviolet
VSEGEI	A. P. Karpinsky Russian Geological Research Institute

Abbreviation of mineral species (according to recommendations of the International Mineralogical Association (IMA))

Ab	Albite
An	Anorthite
Bt	Biotite
Cord	Cordierite
CPx	Clinopyroxene

Di	Diamond
Fsp	Feldspar
Gr	Graphite
Grt	Garnet
OPx	Orthopyroxene
Ort	Orthoclase
Pl	Plagioclase
Qu	Quartz
Scap	Scapolite
Sill	Sillimanite

Chapter 1
Main Geological Features of the Impact Structure

Victor L. Masaitis, Mikhail S. Mashchak and Mikhail V. Naumov

The Popigai crater centered at 71° 28′N, 110° 11′E formed in the Siberian Platform, at the northeastern margin of the Anabar Shield due to a large-scale impact event. This region is characterized by a two-layered geological structure: Archean and Paleoproterozoic crystalline basement is overlain by a gently dipping northeastwards platform cover consisting predominantly of carbonate and terrigenous Mesoproterozoic, Neoproterozoic, Paleozoic, and Mesozoic rocks (Fig. 1.1); the Early Mesozoic hypabyssal basic intrusions also occur. All these rocks are disturbed along flanks of the impact structure. Various impact breccias and impactites filling the crater represent the allochthonous formations. Allogenic breccias and impactites also occur outside the crater as eroded remnants of the ejecta blanket. Loose Pliocene-Quaternary and Quaternary deposits overlie breccias and impactites within the Popigai hollow, which is clearly expressed in the modern relief.

1.1 Topography of the Popigai Depression

The Popigai hollow is located in the northern part of the Middle Siberian plateau, at the border of the forest-tundra and tundra spreading to the north. The topography of the hollow inherits generally the morphostructure of the impact crater strongly modified by erosion and accumulation of Pliocene and Quaternary deposits. Usually, the Popigai hollow of about 75 km in diameter is regarded not only as a flat rounded depression with attitude of its floor of 20–80 m (Fig. 1.2), but it including at western and southern sectors several arched elevations. The latter rise for 100–250 m over the plain and appear as discontinuous chains of hills, in places with flat summits (Suon-Tumul, Ubaybyt-Kerikete, Mayachika-Kerikete and others). At west and southwest,

V. L. Masaitis (✉) · M. S. Mashchak · M. V. Naumov
A.P. Karpinsky Russian Geological Research Institute, Sredny prospekt, 74, 199106 Saint Petersburg, Russia
e-mail: vcmsts@mail.ru; victor_masaitis@vsegei.ru

M. V. Naumov
e-mail: m_naumov@mail.ru

V. L. Masaitis (ed.), *Popigai Impact Structure and its Diamond-Bearing Rocks*,
Impact Studies, https://doi.org/10.1007/978-3-319-77988-1_1

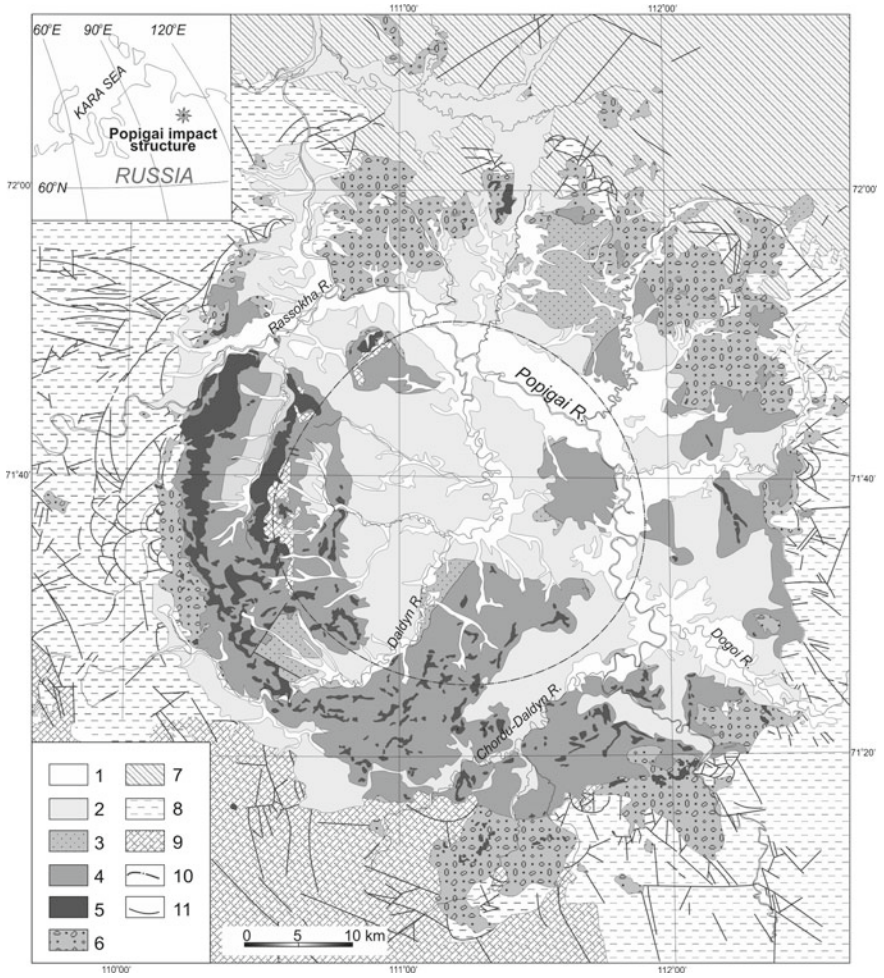

Fig. 1.1 Geological map of the Popigai impact structure. 1—Recent alluvium, 2—Neogene to Quaternary deposits, 3—polymict allogenic microbreccia, 4—suevite, 5—tagamite, 6—polymict allogenic megabreccia, blocky and rubble breccia, 7—Upper Paleozoic and Mesozoic sedimentary and igneous rocks, 8—Mesoproterozoic, Neoproterozoic and Cambrian sedimentary rocks, 9—Archean and Early Proterozoic crystalline rocks, 10—central line of peak ring, 11—faults

the hollow is restricted by a weakly undulating plateau with absolute attitude of 300–500 m, while at north and east, it is merging imperceptibly to a ridged plain elevating 100–150 m above the floor of the central part of the hollow. The swampy floor of the hollow abounds in lakes. The rivers draining the hollow and its framework show arched concentric orientation, some valleys have radial directions, though. Geomorphologic features of the Popigai impact structure and evolution of its relief have been described in detail by Plotnikova (1990).

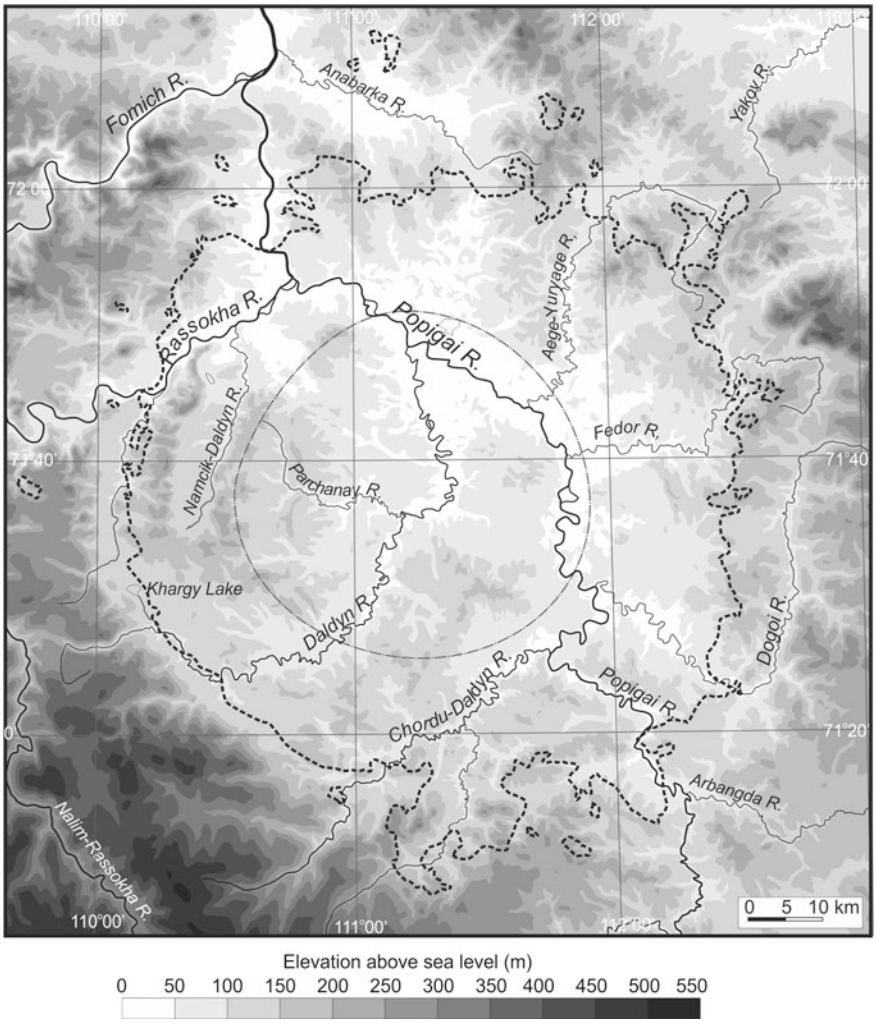

Fig. 1.2 Topography of the Popigai impact crater. Dotted line: extent of the impactites and allogenic breccias; dashed line: central line of peak ring

1.2 Crystalline Basement

The crystalline basement in the northeastern Anabar Shield is represented by various gneisses and plagiogneisses, which are granitized and migmatitized in places. These are alternating hypersthene-biotite-garnet, biotite-garnet-hypersthene, biotite-garnet-sillimanite, and garnet-sillimanite-cordierite gneisses with subsidiary lenses of salite-scapolite lithology, calcyphyre, and marble. Garnet, biotite-garnet and other gneisses and plagiogneisses often contain graphite. All these lithologies

belong to the Upper Anabar and Khapchan Series. The former is characterized by the strong predominance of leuco- and mesocratic hypersthene and bipyroxene gneisses and plagiogneisses, while the latter is composed of mostly garnet-bearing gneisses. The total thickness of these two series is estimated to be as much as 8–9 km (Markov 1983; Mashchak 2015). U-Pb dating of zircons from unaltered crystalline rocks of the Upper Anabar Series showed age values ranging from 2750 to 2180 Ma, of the Khapchan Series, from 2020 to 1865 Ma (Gusev et al. 2013). This points to two principal tectono-magmatic events occurring mainly at the Archean/Proterozoic (2600–2500 Ma) and Paleoproterozoic/Mesoproterozoic (2200–1800 Ma) boundaries correspondingly; some datings show the presence of relics of Neoarchean formations.

Metamorphic basement rocks form steep north-west striking folds; different faults are common, accompanied by cataclastic and mylonitization zones. They include numerous intrusions ranging from Archean to Neoproterozoic age.

Rare, small metamorphosed bodies of dunite, peridotite, and pyroxenite (commonly amphibolized) occasionally occur. Porphyroblastic hypersthene granite (charnokite) form lenticular bodies in hypersthene gneisses. Granulite metamorphism and radiological dating of all these plutonic rocks (results of U-Pb dating range from 3125 to 2700 Ma) allow assigning them to the Archean.

The Paleoproterozoic intrusions are represented by both granitoids and mafics. The former appear as minor masses, lenticular bodies, and fields of migmatites. They are composed of monzodiorite, quartz monzonite, porphyroblastic biotite-amphibole granite, leucocratic biotite granite, and alaskite-type granite. U-Pb dating of zircons from these lithologies (2120–1960 Ma) points to their formation during the Paleoproterozoic. Metagabbro and metagabbro-norite are of similar age (2100 Ma).

Quartz dolerites and gabbrodolerites cutting metamorphic rocks are considered to be Mesoproterozoic, proceeding from the fact that they are overlain by Mesoproterozoic carbonate rocks with weathering crust at the base, and their radiological dating (1190–1580 Ma).

1.3 Platform Cover

The platform cover comprises the Mesoproterosoic, Neoproterozoic, Lower and Middle Cambrian, Carboniferous, Lower Permian, Lower Triassic, Middle Jurassic, and Cretaceous deposits, as well as different genetic types of Pliocene and Quaternary deposits (Markov 1983; Vasilyeva 1985, 1989; Kulikov et al. 1987; Proskurnin 2013; Mashchak 2015).

Mesoproterozoic deposits are represented by the Ilya, Burdur, Labaztach, and Kotuikan formations, while the Neoproterozoic, by the Starorechensk Formation. The deposits of two former formations are widespread west of the Popigai structure where they lie with a sharp angular unconformity on the eroded surface of the crystalline basement (Fig. 1.3). They have a similar lithological composition and are represented by red-brown and pink-grey quartz sandstones, minor arkoses,

Fig. 1.3 Relief of the northeastern part of Anabar shield. Crystalline rocks are covered by horizontally bedded Mesoproterozoic quartzite, occurred on flat hill summits

quarzites, quartzitic sandstones, gritstones, and rare conglomerate lenses. Their total thickness is of about 500–700 m. Southeast of the impact structure, the Mesoproterozoic deposits are developed locally and are represented by Labaztach and Kotuikan formations. The former (of 60 m thick) is mainly composed of the quartz sandstones and quartzite sandstones. The Kotuikan Formation (up to 150 m thick) overlie conformably the Labaztach sandstones; it consists of alternating variegated stromatolith-bearing and clayey dolomites, quartz sandstones with glauconite, containing gritstones and conglomerate interbeds up to 65 m thick. The Starorechensk Formation occurs only southeast of the structure where it overlies unconformably both Mesoproterozoic sediments and Early Precambrian crystalline rocks. It is represented by a homogeneous 120–140 m thick sequence of grey and brownish-grey stromatolith-bearing, sandy, and clayey, often bituminous dolomites with sandstone and conglomerate interbeds.

Cambrian deposits, which overlie unconformably on the Mesoproterozoic and Neoproterozoic formations, are widespread both northwest and east of the Popigai structure. In the northwestern area, a continuous sequence of total thickness up to 600–700 m embraces an interval from the Ediacarian to the Middle Cambrian. The sequence is subdivided into seven formations. At its base, the Nemakit-Daldyn Formation (Ediacarian—Lower Cambrian) of little thickness (no more than 30 m) is distinguished. It is composed of grey and brownish-grey limestone, dolomite and

gritstone with basal sandstone and conglomerate. The Lower Cambrian of total thickness of 150–200 m is dominated by limestone and clayey limestone; dolomite and minor marls occur in addition. It is subdivided into Medvezhinskaya (red and violet-red limestones with marl interbeds), Parphen-Yuryakh (variegated clayey limestones, dolomite, marls), Kijeng-Yuryakh (light-coloured dolomite), and Popigai (greenish-grey and brownish-grey limestone and dolomite) Formations. The Middle Cambrian of 240–300 m thick is composed of light-coloured, predominantly greenish-grey dolomites including algal, clayey and bituminous varieties. It is subdivided into Chumnakh and Dalbykh Formation; the former contains some sandstone and marl interbeds in its base while the latter is characterized by appearance of chert nodules throughout the sequence.

East of the Popigai structure, the Nemakit-Daldyn Formation is thicker (up to 70 m); it comprises quartz sandstones in the base, variegated limestones, subordinate dolomites and marls. The Lower Cambrian is composed of brownish-grey bituminous limestone and marls with interbeds of algal limestone and siliceous lithologies of the Emyaksin Formation of 80–100 m thick. The Middle Cambrian is represented by the Anabar Formation up to 400 m thick, which is composed of uniform light-coloured dolomite with interbeds of algal and clayey dolomite and chert lenses. The actual contact between Emyaksin and Anabar Formations southeast of the Popigai structure is more probably tectonic.

Carboniferous and Permian deposits are widespread northeast and north of the Popigai structure. They overlie the eroded Cambrian surface and include three formations (Bobrov et al. 1990, unpublished data; Proskurnin 2013): (1) Khanar Formation of the Middle to Upper Carboniferous (up to 80 m thick) composed of greenish-grey polymict sandstones and siltstones with coal interbeds and lenses of shale, limestone, marlstone, conglomerate, and gravelite; (2) Kotuy Formation of the Lower Permian (40–140 m thick): light-grey sandstones with mudstone, silstone, shale, and coal interbeds, and (3) Potokoy Formation of the Middle Permian (60–80 m thick): predominant arkose sandstones with siltstone, mudstone, coaly shale interbeds and coal lenses.

Lower Triassic comprises sedimentary-volcanic rocks of Pravaya Boyarka Formation (basaltic tuffs, tuffites, tuffaceous sandstones, with local and thin, up to 10 m, basalt flows). It forms discrete fields among the Permian deposits extending up to 800 km^2 at the northern framing of the Popigai structure (sources of Anabarka and Mayan Rivers). Their visible thickness peaks 70–85 m.

Jurassic deposits are recorded in an only site—at Anabarka River north of the Popigai structure where they are made up of leptochlorite arkose sandstones, characteristic of the Middle Jurassic Series in contiguous areas. Possibly, this Jurassic patch represents a large ejected block—erosional remnant of allogenic breccia. Sandstones with fauna of Aalenian and Plinsbachian occur as fragments in lithic impact breccias and impactites, which points to the former occurrence of Jurassic sequences in this region.

Rock fragments with fossils of the Berriasian stage and the Lower Valanginian substage of the Lower Cretaceous occurring in a similar environment, indicate that the formations of this age has been spread in the region. Proper Valanginian deposits

of 20–30 m thick overlyimg on the eroded surface of the Permian at 50–60 km north of the impact structure, is composed of sands with clay interbeds formations (Bobrov et al. 1990, unpublished data). The Upper Cretaceous deposits have been retained on small areas around the periphery of the Popigai structure where they overlie on the Cambrian carbonate rocks. These are quartz-feldspare sands and sandstones with interbeds of clay, lignite coals, gritstone, and conglomerate lenses with the total thickness up to 10–15 m. Fragments and blocks of similar rocks occur within various lithic breccias in the inner part of the impact structure.

Igneous rocks within the sedimentary cover are represented by the Early Triassic dolerite, gabbrodolerite and trachydolerite. They form dykes, sills, and irregular cutting bodies within Carboniferous, Permian and, rarely, Cambrian sequences. Their thickness ranges from the first meters to several dozens meters. In the contiguous areas, they are overlain by the Jurassic deposits.

Sedimentary rocks in the considered area have a general gentle monoclinal dip northeasterly; near the shield boundaries, the dip is 2°–3°; far to the northeast, dip angles are flattened to 0° 30′. Locally, the general gentle bedding is complicated by gentle folds, flexures, and extensive faults. Northwest and northeast-striking faults prevail; their length peaking 10–15 km, displacement amplitude, several dozens meters. Early Triassic dolerite dike swarm of WNW strike is aligned northwest and northeast of the impact structure.

All above-described geological formations including igneous ones, may be regarded as target rocks, which were subjected to a variable extent to the influence of the impact.

Pliocene and Quaternary deposits occur ubiquitously; however, they are most widespread within the Popigai hollow where overlie various impact breccias and impactites. Their largest occurrence areas are in its eastern part (see Chap. 3).

1.4 Gravitational and Magnetic Fields

The data on gravity and magnetic fields, vertical electric surveying, and petrophysical measurements of rock samples (Masaitis et al. 1975, Yakupov 1972; Pilkington et al. 2002; unpublished data of Shul'gin 1977; Germanov et al. 1975; Antonovich et al. 1977; and others) enable to reveal the main features of the inner structure of the Popigai. These data are in good agreement with both geological observations on the surface and drilling.

The observed gravity field (Fig. 1.4) reached a minimum of −52 mGal with respect to the general level of the regional field of −17 mGal. The anomaly is essentially a gravity low with a lateral extent of 80–110 km, its minimum occurs in the southeastern portion of the structure. The ring gravity high of ~45 km in diameter is coincident with the peak ring of shocked and brecciated basement rocks. Strong NNW-SSE anomalies (up to 30–35 mGal) reflecting the structure of the crystalline basement influence the periphery of the crater-derived gravity anomaly.

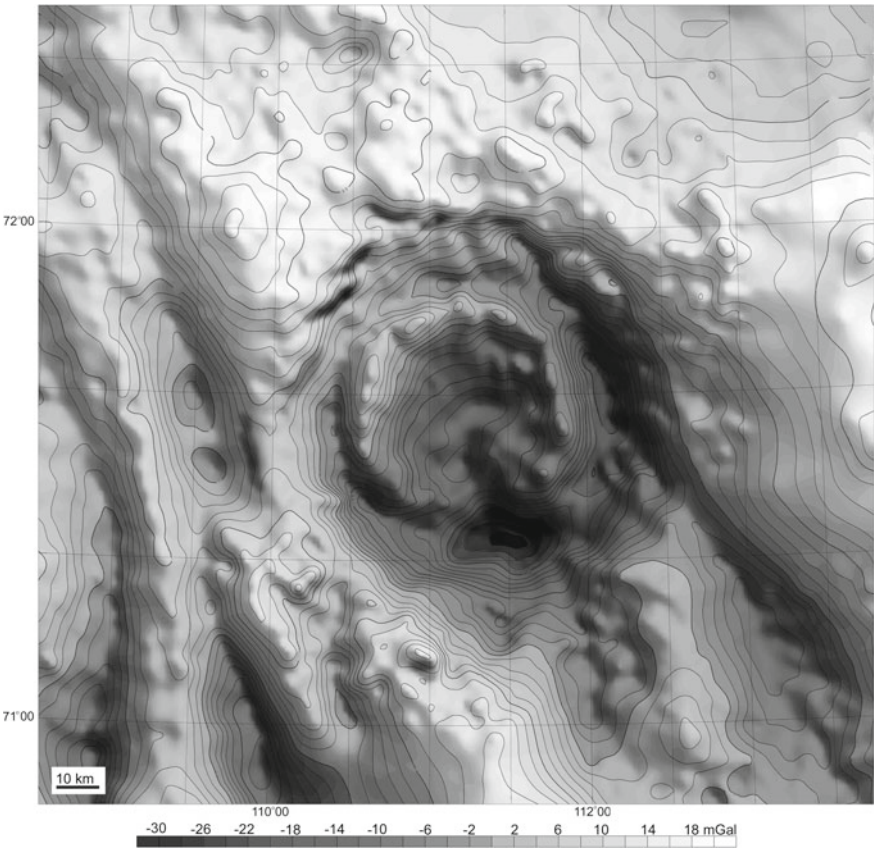

Fig. 1.4 Gravity map (Bouguer anomaly) of the Popigai impact crater and adjacent area. Extracted from the gravity map of the Taymyr region (courtesy of V.V. Koshevoi). Compiled by Institute VNIIGeophysika, based on the data of the Geophysical Expedition #3 FGUP "Krasnoyarskgeologia"

The main elements of the crater structure that are revealed from gravity evidence are well correlated with variations of the density of different rocks occurring here (Table 1.1) as well as with their mode of occurrence. Density of impact breccias and impactites is generally 0.35–0.45 g/cm^3 lower than that of the initial crystalline basement rocks and Mesoproterozoic and Cambrian sedimentary rocks; density of all these lithologies subjected to shock metamorphism and crushing, is also reduced.

The Popigai structure as a whole is also expressed as a negative magnetic field anomaly, with the average amplitude of about −300 to 500 nT (Fig. 1.5). This anomaly seems to break the alternate field of band-like, northwesterly striking high-contrasting magnetic anomalies reflecting specific features of basement composition and structure, which is characteristic of the region and mostly aroused by them. This trend related to the basement structure is similar to observed gravity field. However, the configuration of magnetic field does not coincide with the crater's structural

Table 1.1 Average density of target rocks, impactites, and impact breccias

Lithological group	n	σ, g/cm^3	
		$\overline{X}$	S
Gneisses of the crystalline basement	32	2.83	0.25
Shocked target gneisses	70	2.57	0.19
Quartzitic sandstone of Mesoproterozoic[a]		2.70	
Dolomite, limestone, and marlstone of Cambrian	26	2.67	0.17
Sandstone and aleurolite of Upper Paleozoic	7	2.23	0.18
Fine-clastic lithic allogenic breccia (microbreccia)	8	2.07	0.11
Suevite	97	2.24	0.33
Tagamite	82	2.48	0.28

[a]Data are provided by D. I. Savrasov and Yu. M. Shul'gin
$\overline{X}$—mean value. S—standard deviation

elements revealed by gravity survey. The maximal negative anomalies (up to −600 to 700 nT) locate in southwest and southeast parts of the crater and outside of its southeast periphery.

Modeling of gravity profile, magnetic and electric surveying data across the Popigai impact structure suggest the presence beneath the crater floor of large volume of brecciated target material characterized by reduced density, magnetization and electric resistance. The maximum thickness of the lens of such rocks may reach as much as 5–6 km. It is possible that the lower boundary of this lens is strongly disturbed by displacements of true crater bottom at the modification stage of the cratering. For the gravity field case, the observed anomaly is a combination of the simple circular gravity low due to the fractured basement and shorter wavelength gravity effects resulting from the crater floor (true crater bottom) topography. The topographic variations lead to the ring-shaped gravity high that is well coincided with the mapped position of the annual basement uplift (peak ring). For the magnetic field case, the anomaly over the crater is the sum of the magnetic effects of the crater fill and the underlying fractured basement. Both of these are essentially non-magnetic compared to the highly magnetized crystalline basement in the framework. Petrophysical measurements suggest that the remanent magnetization effects are negligible and that magnetic anomalies related to internal crater morphology are not expected.

The absence of any magnetic signature related to the extensive impact melt rocks highlights the differences in the types of anomalies observed in different craters. At the Popigai, a mineralogical alteration of ferromagnetic minerals is very weak or lacking. When compared with unaffected target gneisses, the Fe_2O_3/FeO ratio of both varieties of impactites is reduced. It may partly explain the lack of magnetite and, hence, the absence of significant magnetic anomalies associated with impactites (Pilkington et al. 2002).

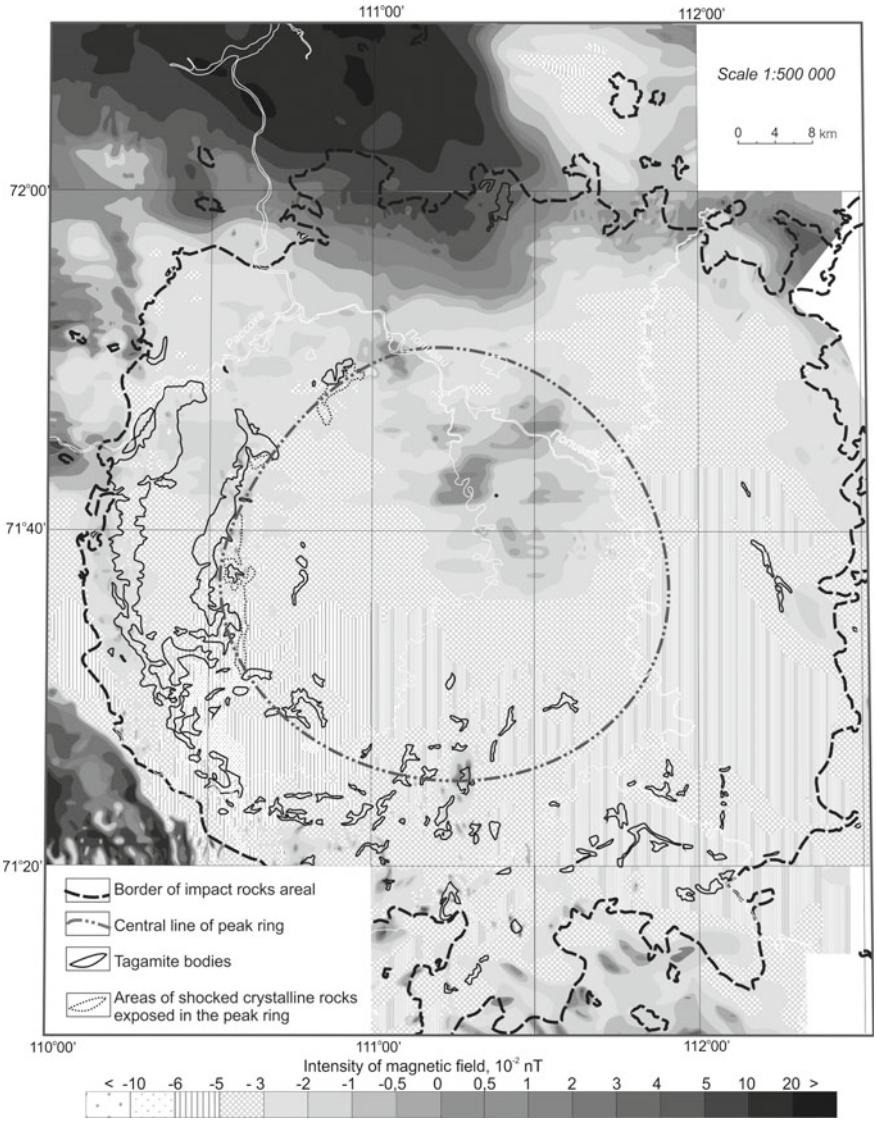

Fig. 1.5 Magnetic anomaly map of the Popigai impact structure. Compiled from unpublished data of Germanov et al. (1977) and Antonovich et al. (1977)

1.5 Morphology and Inner Structure

Geological mapping, drilling, geophysical observations as well as aerial photography and space image deciphering enable to regard the Popigai crater as a complex multi-ring structure (Figs. 1.1 and 1.4). Its diameter is of about 100 km, the depth about

2 km or little more (Masaitis 2002; Masaitis et al. 2005). Its main morphostructural elements, which are visible against the relief of the surface of deformed target crystalline and sedimentary rocks, are: (1) central depression with insignificant central uplift, (2) peak ring, (3) annual (ring) trough or depression, and (4) outer terrace-like surface of deformed sediments, inclined towards the centre of the structure. At this terrace in the northwestern, northern, and northeastern sectors, some discontinuous chains of low hills (up to 150 m) of uplifted bedrock may be regarded as the remnants of an outer structural rim.

The central depression is reconstructed mostly from geophysical evidences, and partly from drilling data. The thick sequence of various impact lithic breccias and impactites develops there; it overlies the true crater bottom made of brecciated crystalline rocks. The hypsometric position of the crater floor in the depression is assumed to reach 2 km; thus, the impact allogenic breccia and impactite sequence in the central part of the structure can also have a such total thickness.

The most characteristic element is the peak ring of about 45 km in diameter. Crystalline rocks are exposed on its surface in the northwestern sector of the crater where they are highly brecciated. In other sectors they are covered by impactite and allogenic breccia. The transverse profile of peak ring is asymmetric: steepness of the inner slope is 3°–20° while that of the outer one, 5°–30°, in places, up to 45°. The peak ring has a block structure; in places, the crystalline rocks are injected by veins of crushed and melted material.

The annular trough, with diameter of its axis of about 55–60 km, has the relative depth from 1.2 to 1.5 km in the northwest and up to 1.7–2.0 km in the southeast (Masaitis et al. 2005). The floor relief is characterized by significant variations of elevations, which are established from drilling evidences. The thickness of the retained breccias and impactites within the trough peakes 2.0 km in the southeastern sector. The outer slope of the trough varies in steepness from 10°–20° to 3°–5°; the latter occurs in radial trenches, which complicate the annular trough. These second-order structural elements, traceable radially approximately from the outer edge of the annual trough, are up to 10–15 km wide. The thickness of allogenic impact breccias and impactites developed in radial troughs ("ploughing tongues") reaches several hundred meters and increases from their rear to frontal parts. These structures impart a festoon image of the outer limit of fields of fall-out impact rocks. The sedimentary and, partly crystalline target rocks surrounding the crater are deformed within the ring outer terrace-like zone of about 10 km wide. There are complicated combinations of centrifugal arched thrusts, upthrows, klippe, minor folds, and faults in rock continuity, generally attenuating radially. It is frequently observed there that older rocks are overthrusted upon the younger ones. Lateral displacement amplitudes can reach several kilometers. Radial faults occur in addition. Slight rocks deformations are traced within the radius of 70 km from the center of the impact structure. Within the same radial distance, remnants of impact ejecta preserved from erosion occur in places on watershed areas and valley slopes. These are composed of both allogenic breccias and suevites, and, less frequently, tagamite. The maximum area of certain remnants is up to 3–5 km^2; the thickness of locally preserved ejecta can reach the first dozens of meters.

Precambrian crystalline rocks exposed in peak ring, crater edge and penetrated by boreholes in different sectors of the crater are of slightly different composition. In the northwestern sector of peak ring, at the Majachika Upland, graphite-bearing biotite-garnet gneisses and plagiogneisses, in places with sillimanite and cordierite, plus similar subsidiary biotite-garnet rocks with pyroxene occur. In the southwestern sector of the peak ring, biotite-bipyroxene gneisses and plagiogneisses with bands and lenses of biotite-garnet, biotite-hypersthene, biotite-salite gneisses and plagiogneisses prevail. At the base of the annular through in this part of the structure, alternating biotite-salite, biotite-bipyroxene, biotite-hypersthene, in places garnet-bearing gneisses and plagiogneisses with marble and calciphyre lenses develop. At the southern edge of the structure, salite and scapolite-salite lithologies plus calciphyre occur along with biotite-garnet gneisses. Crystalline rocks are often granitizied there; charnokites are also developed in places.

1.6 Crater Fill and Composing Impact Rocks

The crater fill of the Popigai includes various impact breccias and impactites that are exclusive variable by structure and composition and appearing in numerous continuous exposures in different sectors of the impact structure (Masaitis et al. 1975, 1998, 2004 etc.). Displaced lithic impact breccias and impactites form in general a composite system of extensive lenticular sub-horizontal bodies, locally intercalated to one another, splitted and wedging-out. At the same time, a general succession of various impact lithologies in the vertical section of the crater fill can be outlined quite confidently (Fig. 1.6) (Raikhlin 1996; Masaitis 2003). In general, the crater fill is subdivided into three main members overlying the crushed and partly displaced crystalline basement and sedimentary cover formations (parautochthon, authigenic breccia). The lower member represents mostly by klippe and blocky allogenic lithic breccias (partly cemented by impactites). They are overlain by the middle member including proper impactites—tagamite and suevite enriched in impact glass. The upper member consists of suevites, which contain significant admixture of lithic fragments, and lithic microbreccias. Local crater fill sequences vary considerably throughout the crater area; in some areas, some lithological units may be missing.

Local geological bodies composed of different impact lithologies and distinguished within the crater fill have either gradational or sharp contacts. Most of these contacts and planar inner features dip toward the crater center at angles of up to 30°. The principal feature of the internal structure of most such bodies is the peculiar distribution of clastic material, melt particles, and glass bombs. This distribution can be regarded as irregularly banded at mega-, macro- and microscales in vertical section. The bedding planes also show in places some linear features manifested by chains of large clasts, impact glass fragments and bombs, or deformed and stretched rock fragments. Most of these linear features are radially oriented relative to the crater center. Thus, the internal structure of the crater fill can be considered as linear-planar, reminiscent of similar features in some volcanic units (Fisher and Schmincke 1984).

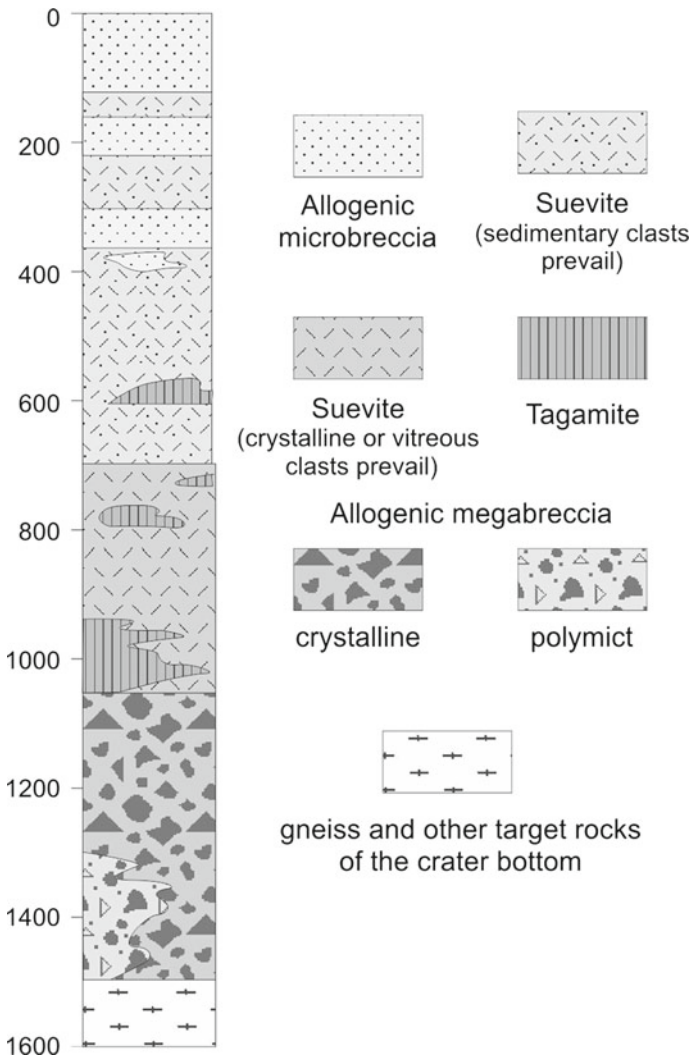

Fig. 1.6 A generalized column of the crater fill of the Popigai impact structure

Impact breccias and impactites rocks overlain by the Pliocene-Quaternary deposits to a major extent are exposed on the surface at area of about 1000 km^2 (see Chap. 2). In the central part of the impact structure, the total thickness of allogenic breccias and impactites can exceed 2 km, tagamites and suevites contributing up to 2/3 to this amount. Allogenic lithic breccias display the greatest thickness in the axial part of the annular trough; this is recorded in northwestern, southeastern, and southwestern sectors. On the southwestern edge of the crater, as well as in some other areas, impactites lie directly on deformed crystalline or sedimentary rocks. The gravity

center of the numerous composite impactite bodies is slightly displaced southwest of the geometric center of the impact structure. Most of large sheet-like and irregular tagamite bodies are concentrated in western and southwestern sectors.

Some comments should be made concerning subdivision and names of impact rocks, composing the Popigai crater fill and remnants of ejecta blanket as well as the highly disturbed target rocks. Two main groups of impact-influenced and impact-generated rocks may be recognized: (1) autochtonous monomict lithic breccias and (2) allochtonous polymict lithic breccias and impactites. The former are partly transformed and brecciated target rocks, which retain its initial composition and, especially, its texture. The latter represent highly transformed rocks, which lost previous texture, structure and, in some cases, composition.

Approaches of their systematic, classification and nomenclature follow the principles adopted in igneous and metamorphic petrology. Impact rocks subjected to various types of transformations (compression, brecciation, melting, ejection, etc.), are subdivided in accordance with their composition and structure and on the base of quantitative evaluations of constituent parts. Proper root names are used for certain kinds of rocks. Rock names are not descriptive and do not characterized the former state of material, mode of origin, mode of occurrence etc. Initial rocks subjected to any alteration, but retaining main features of their previous composition and texture, which may be easily recognized, attributed by qualifiers as "brecciated", "cataclased", "shocked" etc. Totally transformed rocks, which acquire new textures, structures and, in some cases, composition, are assigned as "impact lithic breccias" or "impactites". the last contain more then 10% of chilled or crystallized impact melt in the form of coherent groundmass or fragments of impact glass. The use of the term "impactite" for all types of rocks subjected to shock metamorphism was considered as erroneous (Gary et al. 1972; Murawski 1977), and it is preferable to return it original meaning. Thus, both tagamite and suevite regarded as impactite.

The general scheme of subdivision of allochtonous impact lithologies (Fig. 1.7) is based on studies of rocks occurring in impact craters on the territory of Russia and some other countries (Masaitis et al. 1975, 1978, 1980, 1992; Masaitis 1983, 2005). It corresponds to modern requirements for petrolographic nomenclature (Petrographic Code 2009). The used terms in general coincide with those proposed in some works concerning impact lithologies (French 1998; Stöffler and Grieve 2007), but differ in the certain approaches. A more detailed description of all these rocks, their names, constituents, textures and other features, are given under Chaps. 2 and 3. In general, suevites are subdivided according to amount of various clasts (vitroclasts, sedimentary or crystalline lithoclasts), and size of fragments (ash, lapilli, agglomerate); tagamites, in turn, are subdivided according to their crystallinity and other petrographic features, which allow consider these rocks as low- or high-temperature varieties.

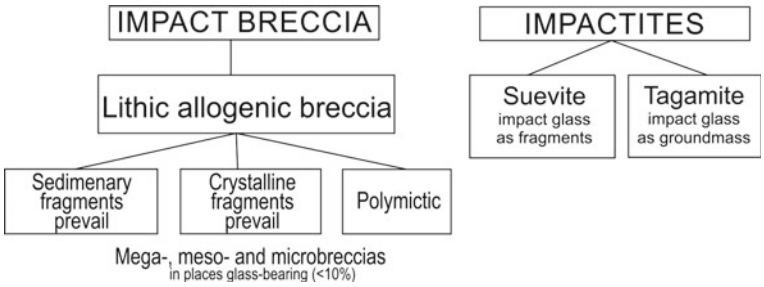

Fig. 1.7 Classification scheme of main groups of allochthonous impact rocks. Impact breccia can contain up to 10% melted substance while impactites contain from 10 to 90% chilled or crystallized impact melt

1.7 Crater Age

Inferred from geological evidences, the age of the Popigai impact event falls within the interval between the Late Cretaceous and Pliocene. K-Ar radiological dating on bulk samples of tagamites and impact glass, as well as dating using uranium fission track technique gave age values from 29 to 45 Ma, averaging at 38.9 Ma (Masaitis et al. 1975; Komarov and Raikhlin 1976), which corresponds to the Middle Eocene pursuant to the modern geochronological scale (Gradstein et al. 2012). ^{40}Ar-^{39}Ar dating of tagamite and impact glass specimens selected by us enabled to specify this dating; in accordance with information obtained, the time of the impact event is evaluated at 35.7 ± 0.2 Ma (Bottomley et al. 1993, 1997). Therefore, it can be presumed that the crater appeared in the end of Eocene. The last value is, apparently, most close to the real time of cratering, it needs a confirmation by different techniques using more extensive and carefully selected material, though.

In connection with a more precise dating of the Popigai event, emphasis should be placed on the data concerning the presence of minor shocked quartz clasts in a thin clay interbed enriched in iridium and occurring at the Eocene/Oligocene boundary wthin a thick strata of carbonates and other rocks in Central Appenine Peninsula, in Massignano area (Montanari et al. 1993; Langenhorst and Clymer 1996). This interbed dated by argon-argon technique using volcanic ash fragments at 35.7 ± 0.4 Ma, is proposed to form with a simultaneous precipitation of powder particles ejected to high horizons of the atmosphere during an impact event.

The fine spheroids of impact melt (microkrystites) and particles of shock-transformed minerals (shocked quartz etc.) are found also in the Late Eocene deposits in Spain and in deep drillholes DSDP and ODP in subequatorial area of oceans and in the southern part of Atlantic ocean (Glass and Koeberl 1999; Vonhof and Smit 1999; Montanari and Koeberl 2000, etc). The bulk compositions of impactites from Popigai and tiny spheroids (microkrystites) recovered from core of the drillholes are similar. Moreover, isotope researches of particles and spheroids and their dating compared to corresponding data on impactites specify that they have arisen due to

the material, which has been thrown out from Popigai crater (Vonhof and Smit 1999; Kettrup et al. 2001).

References

Bottomley RJ, York D, Grieve RAF (1993) Age of the Popigai impact event using the ^{40}Ar-^{39}Ar method [abs]. Lunar and Planetary Sciences XXIV. Houston, pp 161–162

Bottomley R, Grieve R, York D, Masaitis V (1997) The age of the Popigai impact event and its relation to events at the Eocene/Oligocene boundary. Nature 388:365–368

Fisher RV, Schmincke HU (1984) Pyroclastic rocks. Springer, Berlin, 472 pp

French BM (1998) Traces of catastrophe. A handbook of shock-metamorphic effects in terrestrial meteorite impact structures. LPI Contribution No. 954. Houston, 120 pp

Gary M, McAfee R, Wolf CL (eds) (1972) Glossary of geology. Amer Inst of Geol, Washigton DC, 586 pp

Glass BP, Koeberl C (1999) Ocean Drilling Project Hole 689B spherules and upper Eocene microtektite and clinopyroxene-bearing spherule strewn fields. Meteorit Planet Sci 34:197–208

Gradstein F, Ogg JG, Schmitz MD, Ogg GM (eds) (2012) The geologic time scale. Elsevier, 1144 pp

Gusev NI, Rudenko VE, Berezhnaya NG, Skublov SG, Larionov AN (2013) Isotope features and dating (SHRIMP-II) of metamorphic and magmatic lithologies from the Kotuikan-Monholo Zone of the Anabar Shield (in Russian). Regionalnaya Geologija and Metallogenija 54:48–59

Kettrup B, Deutsch A, Masaitis VL (2001) The late Eocene spherules represent distal Popigai ejecta [abs]. Meteorit Planet Sci 36(suppl):A96–A97

Komarov AN, Raikhlin AI (1976) Comparison of fission track and potassium-argon dating of impactites (in Russian). Trans (Dokl) Acad Sci USSR 228:673–676

Kulikov YP, Vladimirov AI, Vtyurin VG, Golubev VM, Kudrin AN (1987) State geological map of the USSR of 1:200 000 scale. Sheet R-48-XI, XII; R-49-I, II; R-49-VII, VIII; R-49-XIII, XIV; R-49-XI, XII. Explanatory notes (in Russian). Ministry of Geology of USSR, Moscow, 194 pp

Langenhorst F, Clymer AK (1996) Characteristics of shocked quartz in late Eocene impact ejecta from Massignano (Ancona, Italy): clues to shock conditions and source craters. Geology 24:487–490

Markov FV (ed) (1983) Explanatory notes to geological map of the USSR of 1:1 000 000 scale (new series), sheet R-48-(50) (in Russian). Nedra Press, Moscow, 192 pp

Masaitis VL (ed) (1983) Textures and structures of impact breccias and impactites (in Russian) Nauka Press, Leningrad, 159 pp

Masaitis VL (2002) Popigai impact crater: general geology. In: Plado J, Pesonen LJ (eds) Impacts in Precambrian shields. Springer, Berlin, pp 81–86

Masaitis VL (2003) Obscure-bedded ejecta facies from the Popigai impact structure: lithological features and mode of origin. In: Koeberl C, Martinez-Ruiz FC (eds) Impact markers in the stratigraphic record. Springer, Berlin, pp 137–162

Masaitis VL (2005) Morphological, structural and lithological records of terrestrial impacts: an overview. Aust J Earth Sci 52:509–528

Masaitis VL, Mikhailov MS, Selivanovskaya TV (1975) The Popigai meteorite crater (in Russian). Nauka Press, Moscow, 124 pp

Masaitis VL, Raikhlin AI, Selivanovskaya TV (1978) Principal criteria for classification and nomenclature of explosion breccia and impactites (in Russian). Lithologija i poleznye iskopaemye 1:125–133

Masaitis VL, Danilin AN, Mashchak MS, Raikhlin AI, Selivanovskaya TV, Shadenkov EM (1980) The geology of astroblemes (in Russian). Nedra Press, Leningrad, 231 pp

Masaitis VL, Raikhlin AI, Selivanovskaya TV (1992) Impactites and impact breccia. In: Classification and nomenclature of metamorphic rocks (in Russian). Nauka Press, Novosibirsk, pp 168–187

Masaitis VL, Mashchak MS, Raikhlin AI, Selivanovskaya TV, Shafranovsky GI (1998) Diamond-bearing impactites of the Popigai astrobleme (in Russian). VSEGEI Press, St. Petersburg, 182 pp

Masaitis VL, Mashchak MS, Naumov MV (2004) Popigai impact crater: guide of geological excursions. VSEGEI Press, St. Petersburg, 55 pp

Masaitis VL, Naumov MV, Mashchak MS (2005) Original diameter and depth of erosion of the Popigai impact crater Russia. In: Kenkmann T, Hörz F, Deutsch A (eds) Large meteorite impacts and planetary evolution III. Geol Soc of America Spec Pap 384, pp 131–140

Mashchak MS (ed) (2015) State geological map of Russian Federation of 1:1 000 000 scale (3rd generation), sheet R-48. Explanatory notes (in Russian). VSEGEI Press, St. Petersburg, 398 pp

Montanari A, Koeberl C (eds) (2000) Impact stratigraphy: the Italian record. Lecture notes in earth sciences 93. Springer, Heidelberg, 364 pp

Montanari A, Asaro F, Michel HV, Kennett JP (1993) Iridium anomalies of late Eocene age at Massignano (Italy) and ODP site 689B (Maud Rise, Antarctic). Palaios 8:420–437

Murawski H (1977) Geologische Wörterbuch. Enke Verlag, Stuttgart, 373 pp

Petrographic Code (2009) Magmatic, metamorphic, metasomatic, and impact rocks, 3rd edn (in Russian). VSEGEI Press, St. Petersburg, 128 pp

Pilkington M, Pesonen LJ, Grieve RAF, Masaitis VL (2002) Geophysics and petrophysics of the Popigai impact structure, Siberia. In: Plado J, Pesonen LJ (eds) Impacts in Precambrian shields. Springer, Berlin, pp 87–108

Plotnikova MI (1990) Essay on post-Oligocene history of the Popigai impact morphostructure (in Russian). Meteoritika 49:154–164

Proskurnin VF (ed) (2013) State geological map of Russian Federation of 1:1 000 000 scale (3rd generation), sheet S-49. Explanatory notes (in Russian): VSEGEI Press, St. Petersburg, 275 pp

Raikhlin AI (1996) Suevite from the Popigai crater: inner structure and mode of origin. Sol Syst Res 30(1):11–15

Stöffler D, Grieve RAF (2007) Impactites, Chapter 2.11. In: Fettes D, Desmons J (eds) Metamorphic rocks: a classification and glossary of terms, recommendation of the International Union of Geological Sciences. Cambridge University Press, Cambridge, pp 82–92

Vasilyeva MN (1985) State geological map of the USSR of 1:200 000 scale. Sheet R-49-XI, XII. Explanatory notes (in Russian). Ministry of Geology of USSR, Moscow, 86 pp

Vasilyeva MN (1989) State geological map of the USSR of 1:200 000 scale. Sheet R-49-V, VI. Explanatory notes (in Russian). Ministry of Geology of USSR, Moscow, 92 pp

Vonhof HB, Smit J (1999) Late Eocene microkrystites and microtektites at Maud Rise (Ocean Drilling Project Hole 689B; Southern Ocean) suggest a global extension of the approximately 35.5 Ma Pacific impact ejecta strewn field. Meteorit Planet Sci 34:747–756

Yakupov VS (1972) On genesis of the Popigai depression (in Russian). Trans (Dokl) Acad Sci USSR 206(5):1185–1186

Chapter 2
Concentric Structural Zones and Lithology of Distributed Impact Rocks

Mikhail S. Mashchak, Victor L. Masaitis, Anatoly I. Raikhlin, Tatjana V. Selivanovskaya and Mikhail V. Naumov

Principal features of occurrence and inner structure of allogenic breccia and impactite sequences in the Popigai impact structure were revealed in the course of medium- and large-scale geological mapping as well as during drilling works (Masaitis et al. 1975, 1980, 1998, 1999, 2004; Danilin 1982; Mashchak and Selivanovskaya 1988, etc.). Certain areas described below are located in different sectors of the crater and characterize the structure of its three concentric zones: (1) inner zone of the central depression, (2) intermediate zone of peak ring and annular trough, and (3) outer ring terrace-like zone (Fig. 2.1). These areas also differ by the depth of erosion, as well as by the mode of exposure and state of drilling.

2.1 Terrace-like Zone and Outer Slope of the Annular Trough

2.1.1 Sogdoku Upland Area

The study area (Fig. 2.1) is located on the flank of the impact structure, in its northwestern sector where a continuous field of impactite and breccia borders with deformed Mesoproterozoic and Lower Cambrian sedmentary sequences. All these rocks are cropping out in extensive exposures along the valleys of Buordakh, Sakha-Yuryage Creeks and their tributaries, and along the right flank of the Rassokha River valley. These exposures extend mainly along western slopes of flat Sogdoku-Kerikete Upland (in the north) and Suon-Tumul Upland (in the south), a relative elevation of which reaching 200 m. Good exposure makes this area rather favorable

M. S. Mashchak · V. L. Masaitis (✉) · A. I. Raikhlin · T. V. Selivanovskaya · M. V. Naumov
A.P. Karpinsky Russian Geological Research Institute, Sredny prospekt, 74, 199106 Saint Petersburg, Russia
e-mail: vcmsts@mail.ru; victor_masaitis@vsegei.ru

M. V. Naumov
e-mail: m_naumov@mail.ru

V. L. Masaitis (ed.), *Popigai Impact Structure and its Diamond-Bearing Rocks*,
Impact Studies, https://doi.org/10.1007/978-3-319-77988-1_2

for detailed observations; the results were partly described earlier (Masaitis et al. 1975; Danilin 1982).

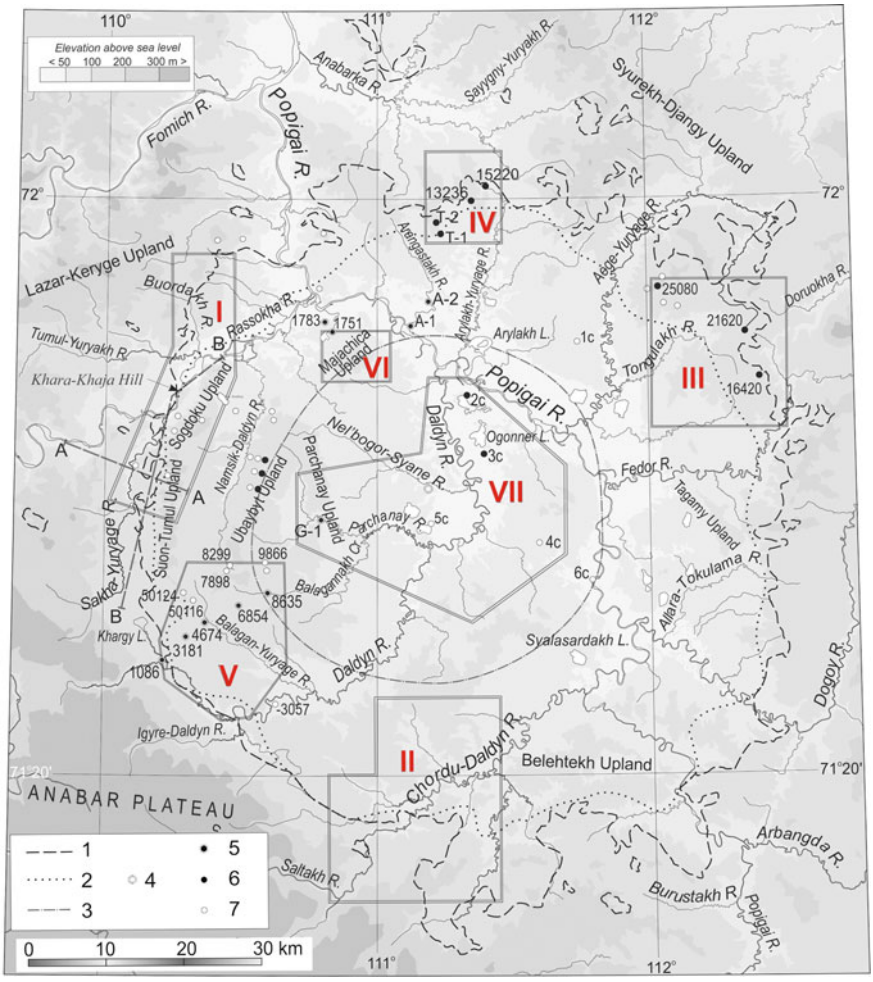

Fig. 2.1 Scheme of location of certain areas described in detail within the Popigai impact structure. The areas are shown by double lines and numbered: I—Sogdoku Upland, II—Chordu-Daldyn area, III—Tongulakh area, IV—Arylakh-Yuryage area, V—Balagan-Yuryage area, VI—Mayachika Upland, VII—Lower Daldyn area. Lines of geologic cross-sections at the Sogdoku Upland area are shown by dashed lines (AA—Fig. 2.2, BB—Fig. 2.4). The scale of grey hues shows the topography. 1—The outer limit of the continuous distribution of allogenic lithic breccias and impactites, 2—outer edge of annular trough, 3—axis of the peak ring, 4—geometric center of impact structure, 5—Structural boreholes (450–1520 m deep), 6—Key boreholes within drilling areas, 7—other boreholes outside of detailed drilling areas

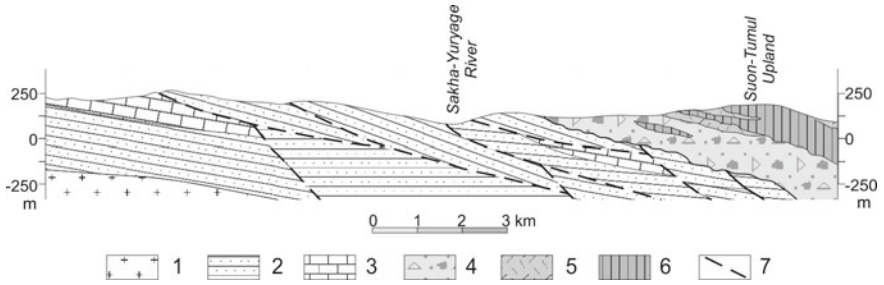

Fig. 2.2 Geological cross-section of the western edge of annular trough in the upper course of the Sakha-Yuryage River. 1—Archean to Paleoproterozoic gneisses, 2—Mesoproterozoic quartzite, 3—Lower Cambrian carbonate rocks, 4—polymict megabreccia, blocky, and rubble breccia, 5—suevite, 6—tagamite, 7—overthrusts

Mesoproterozoic quartzitic sandstones, as well as dolomites, limestones, marls of the Lower Cambrian, are generally gently dipping northwards; however, their occurrence is dusturbed by multiple arcuate listric low-angled and high-angled thrusts, the planes of which dipping eastwards and southeastwards (Figs. 2.2 and 2.3). Quartzitic sandstones are overthrusted on carbonate rocks in many sites; some thrust sheets are from 1–2 to 5–8 km across, the thickness of the displaced plates ranging from several dozens to a hundred of meters. The separations are evaluated to be some km. In some cases, the thrust sheets appear as isolated asymmetric arched hills with older rocks on the summits. In places, remnants of coal-bearing Cretaceous sands are recorded along thrust surfaces. Minor folds of different orientation occur there, as well as small zones of intense crushing; in places, coal-bearing sands fill fractures in denser rocks. At the southward extension of the ring deformation zone, at the Sakha-Yuryage River source, thrust sheets also comprise blocks of crystalline basement rocks.

Polymict allogenic breccia, suevites, and tagamites overlie the deformed sedimentary cover and are subsiding southeastwards in the considered area. At the same time, the base of breccias and impactites (Fig. 2.4) has a lower hypsometric position in the north. The surface of the base is uneven; in general, several troughs or grooves, incised into the sedimentary rocks, are recorded. These troughs are filled with polymict breccias and impactites and oriented radially relative to the crater centre (Masaitis et al. 1975). Radial troughs, which are peculiar morphostructural elements of the second order, are from 1 to 4–6 km wide; the incision depth is evaluated at 100–300 m. The largest radial trough (“Buordakh tongue”) is located in the northern part of the area, it has a trough-shaped profile and is traceable for 9 km at strike (Fig. 2.3).

Allogenic polymict breccias are mainly represented by block and klippe varieties with fine clastic psammitic-silty microbreccia. Continuous exposures of these lithologies occur on the Rassokha River bank downstream from the Sakha-Yuryage River mouth (so called “Variegated Cliffs”, Fig. 2.5) and on the Sakha-Yuryage River bank at about 10 km far from its mouth. In places, the groundmass of the lithic breccia is represented by crushed and grounded material of dense sedimentary and crystalline

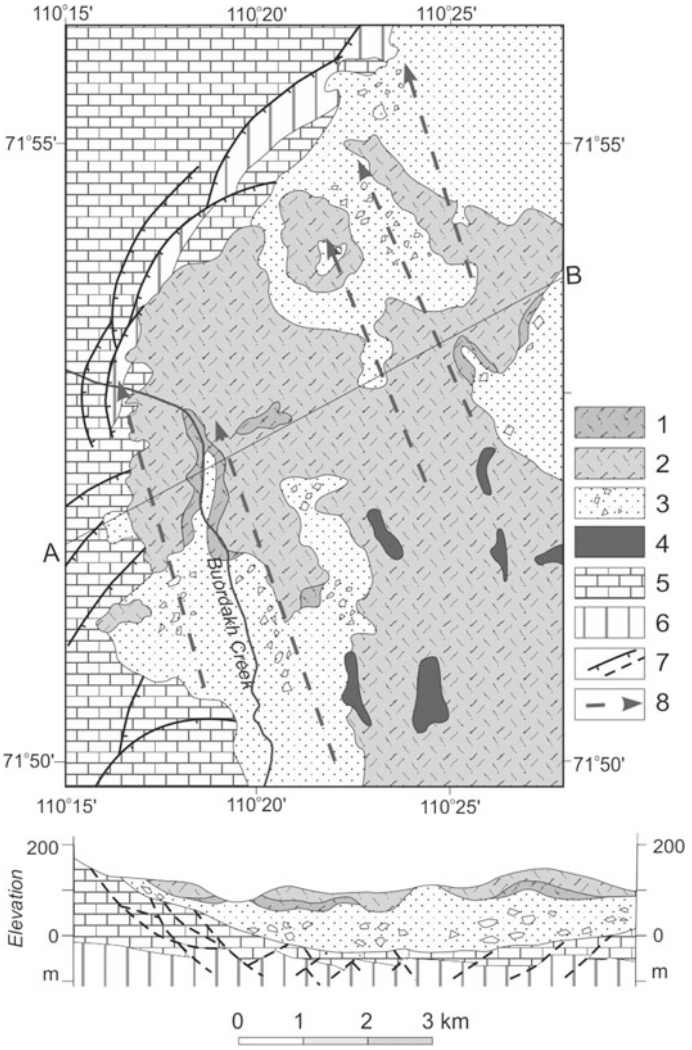

Fig. 2.3 Sketch geological map of the Buordakh area. 1 and 2—Suevites composed mainly of clasts of crystalline rocks: 1—agglomerate-sized, 2—lapilli-sized; 3—polymict allogenic megabreccia, 4—tagamites, 5—Lower Cambrian carbonate rocks, 6—Mesoproterozoic quartzite, 7—thrusts [a—on the map, b—on the section (assumed)], 8—axes of ridge-like projections of the roof of lithic megabreccia

rocks making up fragments, blocks, and klippe of differing sizes. Their sizes reach many dozens and even the first hundreds of meters across. On the average, the size of blocks ranges from dozens of centimeters to first meters of first dozens of meters. In some cases, large klippe and their accumulations seem to be "floating" in the breccia cement or microbreccia. At the same time, in certain exposures (particularly in the

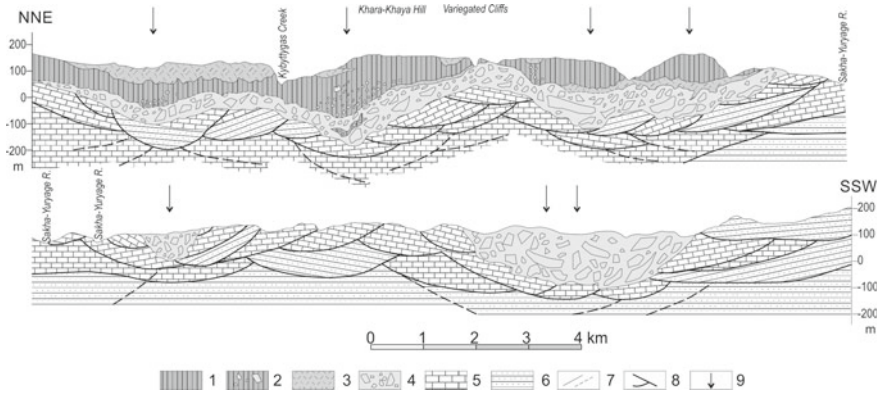

Fig. 2.4 A longitudinal geological section along the western edge of the Popigai crater (western slopes and foothill of Sogdoku and Suon-Tumul Uplands). 1—Tagamite, 2—tagamite containing blocks of shocked gneisses, 3—suevite, 4—polymict allogenic megabreccia and mesobreccia, 5—Lower Cambrian carbonate rocks, 6—Mesoproterozoic quartzite, 7—geological boundaries (fixed and assumed), 8—tectonic borders, fixed or assumed, 9—axes of radial trenches

downstream part of the Sakha-Yuryage River valley), microbreccia is almost devoid of large blocks and mainly comprises psammitic rock debris with minor inclusions of impact glass (Fig. 2.6). In some places, large blocks of sedimentary or crystalline rock are crossed by thin fissures (from 1–2 to 10–15 cm) filled with microbreccia or coaly microbreccia, containing small fragments of various rocks, petrified wood and impact glass fragments. In same cases, the specific roll-like inclusions occur indicating the turbulent displacement of the breccia mass. These are fragments of solid sedimentary rocks of 20–50 cm across wrapped round by plastic clayey material.

The most clear shock features are recorded in rocks, which make up the clastic material in breccias. These rocks are various gneisses and plagiogneisses containing predominantly pyroxenes, biotite, and garnet as main dark minerals; they often enclose impregnation of sulfides and graphite. These rocks are to a variable extent and irregularly brecciated, cataclased, cut by breccia and tagamite veins, and, in places, by thin dike-like tagamite bodies. In some cases, rocks subjected to shock alterations to a variable degree up to transformation to an aggregate of diaplectic glass and monomineral fusion glass (e.g. lechatelierite) domains inheriting original mineral grains. Fusion glass particles during mixing of the material are often passing into partially or fully homogenized impact glass containing small particles of shocked minerals, predominantly quartz and feldspars. Small particles of such glass (commonly altered) are often found in microbreccia, which is locally characterized by fluidal structure; accumulations of such particles form suevite-like lenses.

In addition to crystalline rocks, fragments and blocks are represented by quartzitic sandstone, different carbonate rocks, coal-bearing sandstones and siltstones, dolerites, and coal-bearing sands containing sideritized wood. These are destruction products of various sedimentary cover formations, from Mesoproterozoic

Fig. 2.5 An exposure of polymict allogenic megabreccia covered by an erosional remnant of the tagamite sheet. "Variegated Cliffs", Rassokha River. The sheet base subsides to the left where tagamites are exposed as Khara-Khaya bluff (background left)

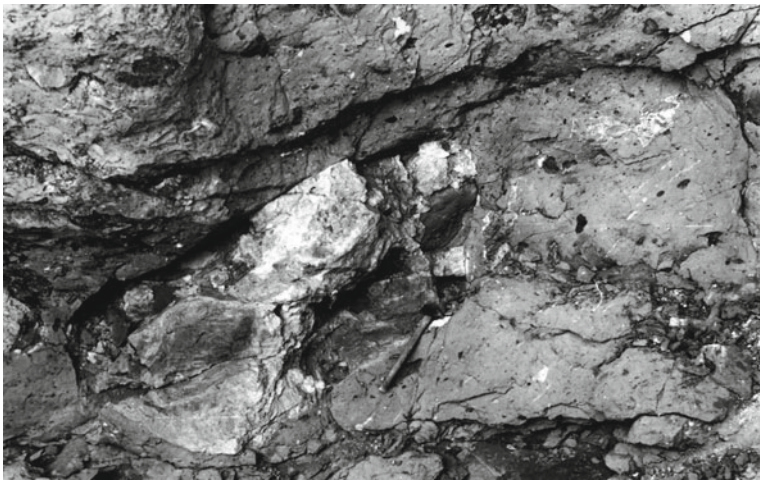

Fig. 2.6 Microbreccia containing small clasts of different sedimentary and crystalline rocks as well as impact glass particles. In the center of the picture—a large block of quartzite. Hammer for scale. "Variegated Cliffs", Rassokha River

to Cretaceous ones. The visible thickness of the polymict allogenic breccia in the considered area is up to 80–100 m; this is also confirmed by drilling. The maximum thickness can be as much as two times more.

Polymict lithic breccia is ubiquitously overlain by suevites and tagamites; the surface of their lower contact is quite irregular, variations in elevation reach 200 m within the distance of 2–3 km. In the Buordakh Creek basin, this surface is complicated by ridges and grooves parallel to the radial trough direction (NW 325°–340°). These ridges of 0.5–1.0 km wide are traceable for 4–6 km; they rise for 30–80 m, the steepness of their slopes ranges from 5°–10° to 25°. Contacts between polymict breccia and overlying suevite are more abrupt on crests and less expressed within grooves where agglomerate suevite prevail; the latter is crowded by fragments of intensely shocked crystalline rocks, the entire suevite sequence being composed of lapilli-sized fragments, though (Danilin 1982). In the frontal part of the Buordakh tongue, the allogenic breccia is wedging out, so that suevites lie directly on upthrusted quartzitic sandstones and carbonate rocks (Fig. 2.3).

Tagamites and suevites in the study area form an extensive complex sheet-like body; its thickness reaches 200–250 m in the north, but it is gradually decreasing southwards where it does not exceed 50–80 m. Suevite bodies overlie tagamites, thin irregular bodies of the latter occur among suevites in places, though. The thickness of the suevite varies from the first dozens to 130 m. These are predominantly lapilli-sized vitroclastic suevites, which are sintered near contacts with larger tagamite bodies and often composed of flattened impact glass bombs (Fladen) with surfaces reminding those of ropy lavas. Contacts between suevites and tagamites are commonly abrupt; in places, however, tagamite forms minor apophyses into overlying suevite.

On the surface of the plateau formed by Sogdoku-Kerikete and Suon-Tumul Uplands, there is exposed a partly eroded upper part of a tagamite sheet extending for more than 30 km from north to south and having a width from 6 km in the north to 1 km in the south. The maximum visible thickness of the sheet reaches locally 200 m; however, it varies highly. In the middle part of the plateau, allogenic breccia underlying the tagamite is exposed; it is also penetrated by boreholes there. The lower horizontal contact of the sheet body with the allogenic breccia is clearly visible in the Variegated Rocks cliff (Fig. 2.5). Tagamite close to this contact is glassy and of the fluidal texture caused by a linear distribution of cavities and minor gneiss inclusions.

The most complete vertical section of the tagamite sheet is observed in a exposure of these rocks of 140 m high at the Khara-Khaya Hill (Fig. 2.5) where a characteristic columnar jointing is well-expressed in tagamite. There, the lower part of the sheet comprises abundant large blocks of shocked gneisses up to 10–20 m across; they comprise to 30–40 vol%. In fact, this horizon represents the megabreccia of crystalline rocks cemented by tagamite. The upper two-thirds of the observed section are composed of tagamite enriched by smaller inclusions of thermally altered shocked rocks and minerals; the size of fragments ranges there from several dozens of cm to shares of a mm. They are rather regularly distributed and contribute 10–15% of the rock volume (Fig. 2.7). Among biotite-garnet gneiss inclusions, there are varieties enriched in shocked graphite and containing diamonds. In the upper part of the exposure, there is a sag of the roof of the tagamite sheet, filled in by suevite; however, this might be only a remnant of a partly eroded suevite lens. The roof of the sheet is exposed on the right bank of Rassokha River, downstream of the mouth

Fig. 2.7 Tagamite with numerous inclusions of shocked gneisses. Hammer for scale. Right bank of the Rassokha river

of Buordakh Creek. It has an undulating surface and overlain by suevites with thin tagamite apophyses.

Some post-impact faults, which are collateral to the crater edge, are revealed in this area. They divide slightly uplifted and subsided blocks of impactites.

The following main structural features of the Sogdoku Upland area should be emphasized:

1. Very irregular relief of the base of the crater fill formations;
2. Occurrence of polymict lithic breccias in the lower part of the section, and suevites and tagamites in the upper one;

3. Reduction of the thickness of the composite impactite body from north to south;
4. Upward in the vertical section, there occurs flattening of relief of the base of the lenticular and sheeted impactite bodies, which in the upper part have a sub-horizontal occurrence;
5. Upward in the section, from parauthochton to suevites and tagamites there occurs a significant increase in the horizontal displacement amplitudes of the ejected allochtonous material.

2.1.2 Chordy-Daldyn Area

The area embraces the basin of the middle course of the Chordy-Daldyn River that includes a portion of the southern sector of the impact structure (Fig. 2.1). A gently undulating relief with elevations up to 200 m alternates there with extensive lowland areas. In the northern part of the area, the annular trough axis trends sub-latitudinally. The central and southern parts are confined, respectively, to the outer slope of this trough and to the ring deformation zone within the outer terrace of the crater. The surface of the latter is complicated by a submeridional radial trough, the axis of which passing in the eastern part of the area (Mashchak and Selivanovskaya 1988).

Suevites developed in the northern part of the area, are represented mainly by lapilli and agglomerate varieties. Their matrix consists of disintegrated terrigenous sedimentary rocks, or fragments of crystalline rock minerals. Lapilli suevites form sheeted bodies up to 80–100 m thick; agglomerate suevites occur within them as lenses up to 15–20 m thick. At different levels in vitro-lithoclastic suevites, accumulations of shocked rock blocks and debris and glass bombs occur frequently. In these cases, the suevites are dominated by fragments of Paleozoic and Mesozoic terrigenous sedimentary rocks. Agglomerate litho-vitroclastic suevites are characterized by the abundance of automorphic, fresh, massive black glass (in the form of drops, ribbons, bombs etc.), along with subsidiary volumes of devitrified porous and slaggy glass. Irregular lenses of lithic microbreccia occur mainly in lowland areas; their spatial interrelations with suevites are complicated. Withun suevites, there are minor irregular tagamite bodies and shocked gneiss blocks up to 3–5 m across, forming aureoles around larger tagamite bodies. Such peculiar aureoles in suevites are commonly extending submeridionally and are traceable for the several dozens of meters along the their long axes.

At the downstream of the Chordy-Daldyn River (some kilometers to the east from the northeast corner of the represented map, Fig. 2.8), approximately at 10 km upstream of its mouth, in the terrace escarpment of about 20 m high (Fig. 2.9), a suevite sequence consists of three parts. The lower part is composed of a litho-vitroclastic variety containing large (30–40 cm) inclusions of dolomites and other rocks (Masaitis 2003). The intermediate composite layer dipping to the crater center at angles 30°–40°, consists of obscure-bedded litho-vitroclastic suevite about 2 m thick. Some vague layers and lenses of sorted fragments in the considered suevites, predominantly fine clastic ones, are of 10–30 cm thick. There are also accumulations

of accretionary lapilli of 10–20 mm in diameter, some of them are broken (Fig. 2.10). This layer is overlain by vitroclastic suevites displaying no sorting of clastic material and containing many lithic fragments, glass bombs and gneiss bombs to 20 cm across coated by glass. In places, their outer surface appears a bread-crust structure. It is interesting to note that in nearby suevite outcrops on the left bank of Chordu-Daldyn River, charred wood branches were found. Some of them are up to 5 cm thick and carbonized from the outside (Fig. 2.11). They looks as charred fragments of arboreal vegetation existed on the surface at the time of impact. All these observations enable to reconstruct some conditions of transportation and accumulation of ejected material forming these suevites.

Within the main occurrence field of suevites, there are abundant tagamite bodies; the largest one covers an area of 1.5 × 5.0 km. Presumably, these exposures are in certain cases apical parts of thick sheeted bodies, occurring at depth in the annular trough and similar to those penetrated by boreholes in the Balagan-Yuryage River Basin (see Sect. 2.2.1). Smaller bodies of 0.5–1.0 km across occur in suevites within a band of about 6–8 km wide, adjoining to the crystalline rock range, tracing the southern flank of the annular trough. Commonly, such bodies are surrounded by accumulations of relatively large blocks of shocked gneisses and impact glass bombs. Tagamites from large bodies (their visible thickness is first dozens of meters) are in places holocrystalline, but more frequently, hemicrystalline; the content of inclusions varies considerably, attaining 20–30% of the volume in places. In this area, both low-temperature and high-temperature tagamites are identified; some bodies display peculiar eutaxites where one tagamite variety is enclosed into another one. In particular, on the Chordu-Daldyn River bank near the Saltakh-Yuryage Creek mouth, a low-temperature tagamite body encloses abundant flattened lump-shaped high-temperature tagamite inclusions of a glassy habit (Fig. 2.12). They are of 1–5 cm thick and up to 20–30 cm long, being oriented in the same direction. Abrupt contacts between two varieties are observed.

A ridge of partly deformed crystalline rocks extending latitudinally and adjoining in the southwest to their continuous occurrence field (its relative elevation above the surface of crystalline rocks in the outer terrace is about 150–200 m) separates the area of suevites and tagamites in the north from the zone of predominant occurrence of polymict megabreccias in the south (Fig. 2.8). The extent of this range is about 9 km; it also extends eastwards for a dozen and a half of two dozens kilometers. However, it passes into accumulations of large displaced klippe of crystalline rocks there. The ridge is composed of pyroxene, amphibole-pyroxene and garnet gneisses and plagiogneisses. In the western part of the range where its width is of about 1 km, gneisses display a sub-latitudional attitude. Here, the gneisses bear no visible features of shock metamorphism, unlike similar rocks exposed from under the polymict allogenic megabreccia cover in the east. At the south and southwest where crystalline basement rocks are overlain by allogenic megabreccia of 100–150 m thick, its strike changes to trend northwesterly.

Suevites adjoining from the north to the crystalline basement rock range, which as if marks the outer edge of annular trough, are locally underlain by the polymict allogenic megabreccia, projecting on the left side of the Kychypkynaakh River—the

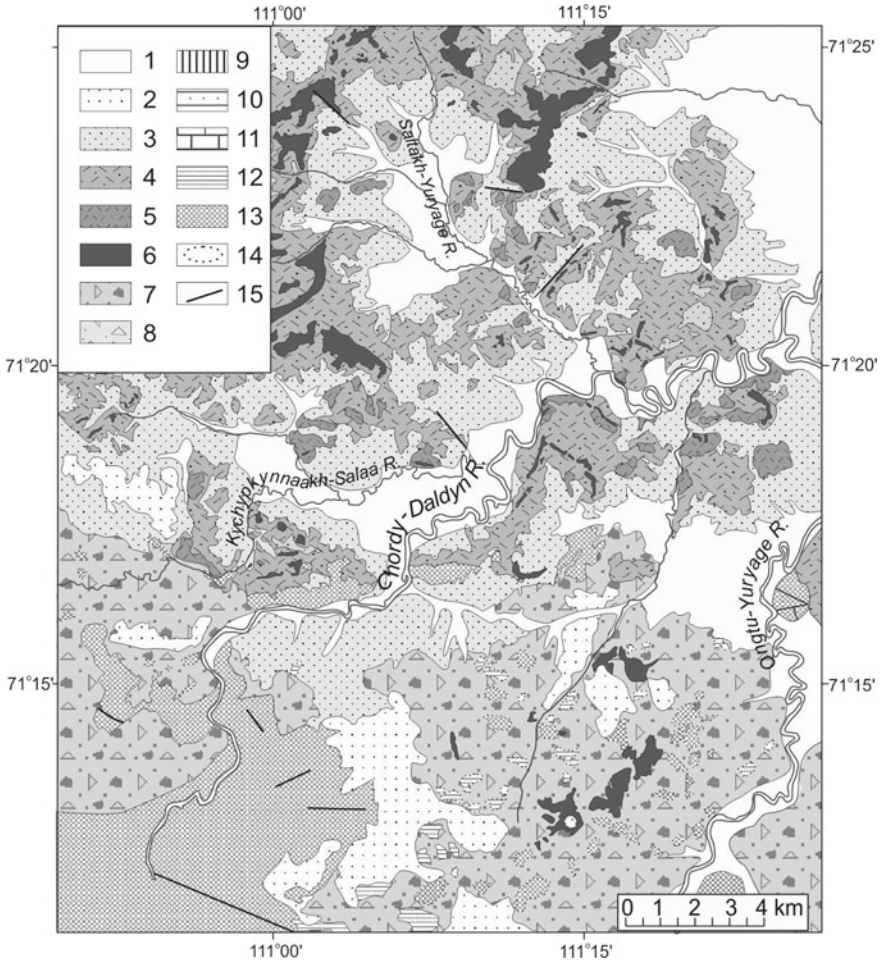

Fig. 2.8 Geological map of the Chordu-Daldyn area. 1—Quaternary sediments, 2—Neogene-Quaternary deposits. 3—Polymict allogenic microbreccia, 4—Vitro-lithoclastic and litho-vitroclastic suevite, 5—Vitroclastic suevite, 6—Tagamite, 7—Polymict allogenic megabreccia, 8—Allogenic megabreccia composed of sedimentary blocks. 9—Upper Triassic dolerite, 10—Upper Paleozoic sandstone, argillite, aleurolite, 11—Cambrian carbonate rocks, 12—Mesoproterozoic quartzite, 13—Archean to Paleoproterozoic crystalline rocks. 14—Contours of large klippen within allogenic breccias. 15—Faults

left tributary of the Chordy-Daldyn River. Another part of the suevite section is exposed along the submeridional two-kilometer part of the Kychypkynaakh River, on its right bank. The suevite sequence there of 60–100 m of estimated thickness is noted for obscure bedding and complex inner structure (Masaitis 2003). The lower part of this unit is made up of vitroclastic suevites, which have no any directive structure and contain small tagamite bodies. Upward in the section, suevites are

Fig. 2.9 A thin layer of obscure-bedded suevite (it dips left at angle of 30°–40°, central part of the outcrop) underlies by massive suevite supported of large dolomite fragments (lower part of the outcrop), and overlies by suevite, supported by glass and gneiss bombs (upper part of the outcrop). The suevites are mainly lapilli-sized, some coated gneiss bombs peaking 30–50 cm across. Chordu-Daldyn River, lower course. The exposure is of 30 m high

characterized by some features pointing to their ordered sedimentation. These are exceptionally vitro-lithoclastic varieties, which are fine-clastic (more rarely, medium-clastic), with clearly expressed and vaguely outlined beds from 5–10 to 30–50 cm or more in thickness, composed of clastic material of the various size and admixture of lithic fragments (Fig. 2.13). The general northward dip of these rocks is at an angle of 30° or steeper, but the bedding undulates considerably. Fine-clastic material of these suevites locally encloses separate large (to 20–30 cm) glass bombs and coated

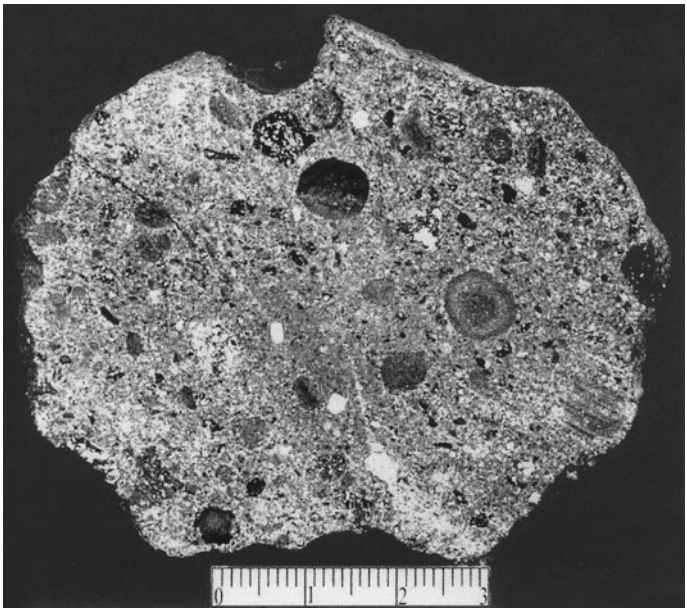

Fig. 2.10 A sample from the layer of obscure-bedded suevite shown on the Fig. 2.9. The suevite contains accretionary lapilli of rim- and multi-rim types, some of them are broken

gneiss bombs. Locally, lenticular accumulations of carbonate rocks, gneiss blocks, glass fragments, and bombs are visible. In places, gneiss bombs are embedded into fine-grained suevites and form bomb sags (Fig. 2.14). Within this part of the section, fine-clastic suevites contain the accumulations of rounded accretionary lapilli of 0.5–1 cm across.

The upper part of the considered unit is predominantly composed of vitro-lithoclastic suevites, which are made up of fragments of psammitic-silty and psephytic size. Suevites display vaguely outlined beds and lenses from 20–30 cm to 1 m thick or more characterized by homogenous distribution of fine-clastic material. At the same time, the upper part of the section displays beds with a gradational distribution of pebble-sized fragments. Numerous irregularly-dispersed accretionary lapilli (their diameter is approximately 0.5 cm) and small particles of fresh glass were observed as well. In some places, obscure cross-bedding exists. Although the suevite sequence described above locates close to a crystalline basement occurrence, their lithofacial features are typical to the upper member of the crater fill. It is possible that the block of these rocks was subsided in the form of small graben during a later stage of cratering.

Within the extensive fields of the above-mentioned allogenic megabreccias in the southern part of the area, there are accumulations of large blocks and klippe of gneisses, quarzitic sandstone and carbonate rocks in places. In most cases, they do not display clear features of shock metamorphism. Only in relatively small quartzite

Fig. 2.11 The fragment of charred wood in litho-vitroclastic suevite. The piece of partly petrified wood was charred from the outside in the explosion cloud during the impact. A camera lid for scale. Chordu-Daldyn River

blocks, a mortar structure is observed. At the same time, minor blocks often contain shocked gneisses subjected to shock compression with the amplitude up to 25–35 GPa. They are accompanied by impact glass bombs and small tagamite bodies. The klippe and block allogenic breccias are cemented by the grounded material of rocks making up their coarse-clastic fraction. However, in places the clastic matter is represented by a mixture of debris and smaller fragments, up to the appearance of areas where a silty-psammitic fragment size and lithic microbreccia.

In the field of polymict allogenic megabreccia, some irregular in plan erosional remnants of tagamite occur. They occupy the uplands and are from the first meters to several hundred meters and the first kilometers across. The thickness of the preserved bodies is up to 30–50 m; the composing rocks are commonly porous and contain up to 10% of crystalline rock inclusions. Tagamites are of a glassy habit; in places, they are weakly crystallized. Inferred from petrographic features, they can be assigned mainly to the high-temperature variety (see Chap. 4).

The main structural features of the described area are as follows:

1. Crystalline rocks uplifted along the outer flank of the annular trough form a sub-latitudionally trending range of a block structure;

Fig. 2.12 LT tagamite with thin orientated lenses of HT tagamite (light). In the center there is a large gneiss inclusion. Hammer for scale. Chordu-Daldyn River, close to the mouth of the Saltakh-Yuryage Creek

2. Polymict allogenic megabreccias occurring over the crystalline basement on the outer terrace include the accumulations of thrust slices of different rocks up to several km across;
3. Within a partly eroded ejecta cover occurring south of the above-mentioned range, sheet-like tagamite bodies are preserved accompanied by aureoles of minor bodies and bombs of solidified melt;
4. Small bodies of low-temperature tagamites enclose fine lenses of high-temperature tagamites; this results in generation of oriented structures and point to their simultaneous displacement in a plastic state;
5. Suevite sequence contains certain units, which are characterized by some features of material sorting and characterized by sinuous bedding, which is, possibly, due to their deposition from the water saturated hot gaseous media moved in centrifugal direction.

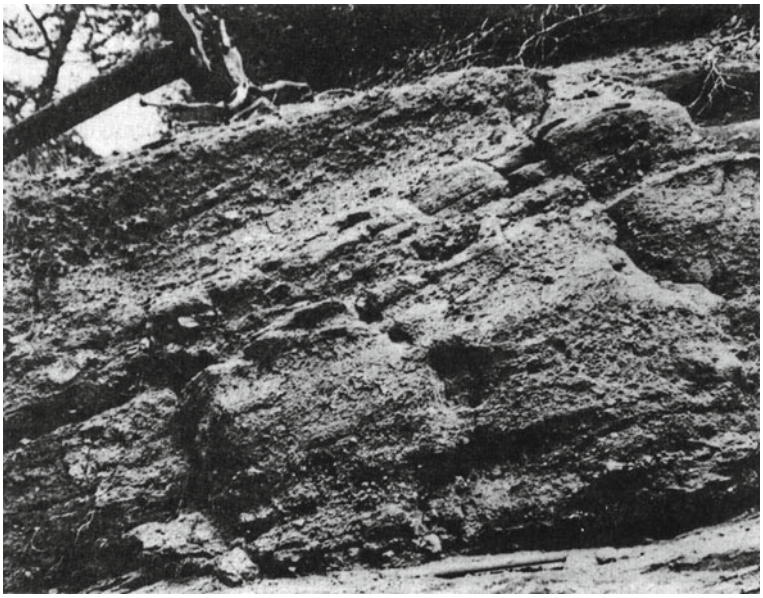

Fig. 2.13 A pack of obscure-bedded vitro-litoclastic, predominantly lapilli, suevite. Weakly expressed cross-bedding is seen at the right side of the outcrop. Hammer for scale (center bottom). Lower course of the Kychypkynaakh-Salaa River

2.1.3 Tongulakh Area

The Tongulakh area is located at upper reaches of the Tongulakh, Fedor, and Aege-Yuryage rivers. It belongs to the ring deformation zone on the northeastern flank of the outer crater zone (Fig. 2.1). This is a gently undulating plain with the maximum elevations of 150–180 m passing southwestwards into a swampy lowland of the Popigai hollow. Deformed Cambrian carbonate rocks are developed there; in places, thin Permian terrigenous rock sequences injected by gabbrodolerites overlie above them. All these formations are exposed only in the eastern part of the study area; over the rest of the area, a continuous cover of allogenic megabreccia is developed with small remnants of suevites, overlying it (Fig. 2.15). The structure of impact rock sequences in the area was specified by the study of core of about two dozen boreholes, which were drilled to the depth of 100 m.

The surface of deformed target rocks is gently subsiding southwestwards at an angle no more than 10°–15°. The character of these deformations can be established from observations of minor exposures, but mainly from results of aerial photography deciphering, including those of contiguous areas. Carbonate rocks within a belt of about 15–18 km wide (including its part hidden by the ejecta blanket) are intensely fractured; their bedding is disturbed in most cases. Dip angles are up to 50°, but commonly they do not exceed 10°–20°. The carbonate rocks are cut by faults into

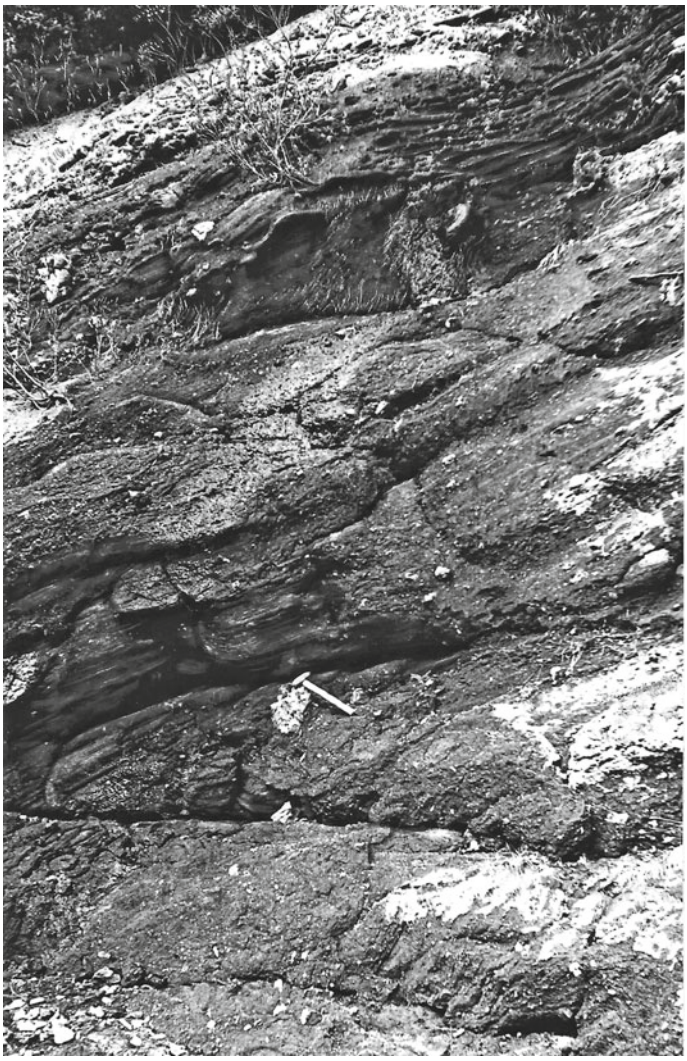

Fig. 2.14 Obscure-bedded suevite (bedding dips at an angle of 30°–40°). A large rounded bomb of shocked gneiss coated with impact glass occupies a bomb sag (lower left). Hammer for scale. Kychypkynaakh-Salaa River

blocks from several hundred meters to the first kilometers across. In places, minor folds of different orientation are recorded. In rare cases, blocks seem to be adjoined along gentle thrust planes; however, the most of faults are steeply dipping; they trend predominantly northeasterly.

The surface of the deformed base of impact rocks is irregular. Elevation variations reach many dozens and, possibly, the first hundreds of meters. A festoon character of

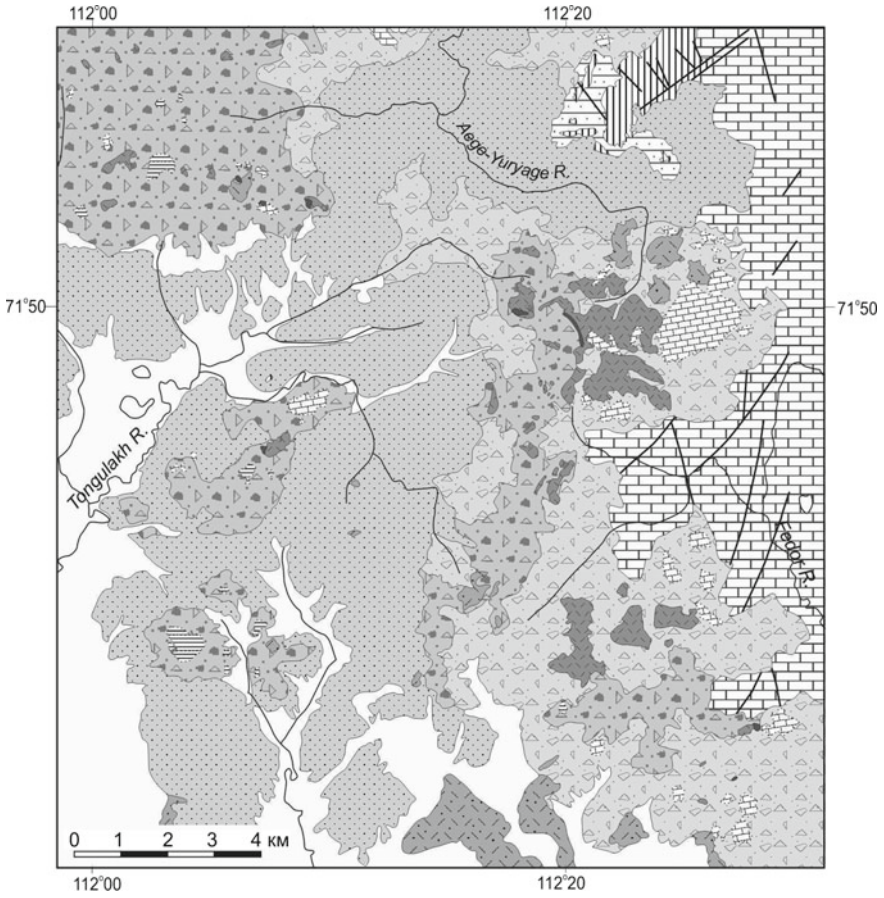

Fig. 2.15 Geological map of the upper course of the Tongulakh Creek. For legend, see Fig. 2.8

allogenic megabreccia field borders points to a possible existence of grooves or shallow troughs, which are transverse to the crater flank. The thickness of megabreccia is variable and ranges from the first meters to many dozens and, possibly, to 100–200 m in the southwestern part of the area.

The lower part of the breccia sequence is dominated by megabreccias and debris-block monomict scattered breccias after sedimentary rocks, commonly grading up in the section into polymict megabreccias and debris-block breccias, containing both sedimentary and crystalline rock material. Fragments in the lower part are ubiquitously dominated by the Middle Cambrian carbonate rocks; in the northeast of the region they contain abundant Permian sandstones and dolerites. There are accumulations of flattened blocks and klippe of carbonate rocks, some of them peaking 2–3 km across in plan. Polymict breccia is manifested on the surface by fields of scree and debris of shocked crystalline rocks, quartzitic sandstones, carbonate rocks, in places

Fig. 2.16 Shatter cones in a limestone fragment from allogenic breccia. Aege-Yuryage River

with shatter cones (Fig. 2.16). Some blocks are up to several dozens meters or even much greater. In places where crystalline blocks are recorded, scattering of impact glass bombs and tagamite debris are common as well. The thickness of polymict breccias, obviously, does not exceed 150–200 m; the maximum penetrated thickness in boreholes is 82 m. A significant part of polymict breccias (frequently, more than 50%) is contributed by microbreccia. The latter is lacking in large rock blocks; it is up to 30 m thick un places from drilling data. Microbreccias are also cropping out at a number of small exposures, but commonly they being destroyed and appear as debris or talus deposits.

The suevite form separated fields from several dozen square meters to 4–5 km^2 occupying the most elevated parts of the area. This allows presuming that they overlie the polymict breccia. This is also confirmed by drilling evidences. At the same time, along the eastern boundary of the allogenic breccia field where the latter consists mostly of sedimentary material, suevites rest directly on these breccias or on the deformed carbonate and other target rocks.

In boreholes drilled at the Tongulakh Creek source area, the thickness of suevites ranges from 56.6 to 85.5 m. The suevites are characterized by a large size of clastics (up to 2 m or more) making up a significant part of the rock and composed mostly of intensely (up to 30–50 GPa) shocked garnet-bearing gneisses with graphite. There are also fragments of sedimentary rocks of different formations. The cement matter of these suevites is made by mixture of rock fragments and vitroclasts; it constitutes 50–60 vol%.

Suevites dominated by clasts of sedimentary rocks are developed mainly in the northeastern part of the area. They are commonly associated with allogenic breccias also composed mainly of disintegrated material of carbonate and terrigenous lithologies. As is shown by drilling evidence, these suevites enclose in places microbreccia lenses and irregular patches. Contacts between suevite and microbreccia observed

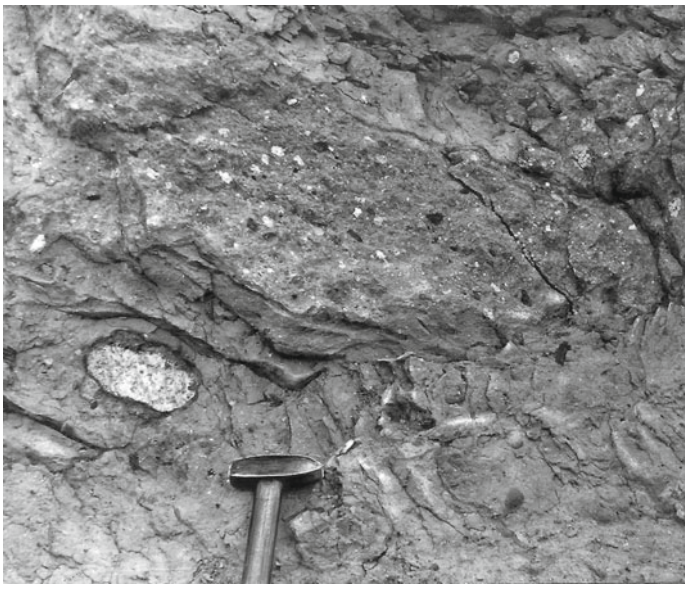

Fig. 2.17 The interrelation between suevite and microbreccia, which include gravel-sized fragments of target rocks and a rounded gneiss bomb coated with impact glass. The contact surface is undulated and show evidences of the thermal influence on microbbreccia. Hammer for scale. Aege-Yuryage River

in some outcrops show that at the moment of deposition, the suevite substance was hot and partly sintered the psammitic material of microbreccia (Fig. 2.17).

Tagamite forms several minor (no more than the first dozens of meters across) bodies, noted for the high content (30–35%) of shocked gneiss inclusions.

So, the study area is characterized by the following main structural features:

1. Irregular surface of the target composed of deformed sedimentary rocks is gently plunging southeastwards;
2. A relatively thin ejecta of polymict (more rarely, monomict) allogenic megabreccia, is noted for a significant role of fine clastic facies—microbreccia;
3. Although shocked crystalline rocks contribute essentially to the impact ejecta, the role of completely remolten material in them is insignificant;
4. Suevites form small, thin remnants, so that a significant portion of these rocks seems to have been eroded.

2.1.4 Arylakh-Yuryage Area

The area between Arangastakh and Arylakh-Yuryage Creeks belongs to the northern flank of the outer deformation zone (Fig. 2.1). The topography of the area follows

the original crater morphostructre; from south northward, a low lacustrine-alluvial plain is replaced by an undulating plain where meridionally elongated low hills (with elevations up to 160 m) are separated by wide swampy valleys of Nastuja Yuryakh and Arylakh-Yuryage Creeks. The area is noteworthy for the appearance of the bedrock of the outer crater rim, which is exposed in the northern part of the area. South of the rim, allogenic breccia comprising relatively small bodies of impactites is widespread throughout the area (Fig. 2.18). Due to some drilling (25 boreholes up to 136.5 m dip are drilled there), the inner structure of impact-generated ejections can be revealed in detail.

The reconstruction of the relief of the base of the allogenic megabreccia and impactites (Masaitis et al. 2005) shows that the contour line +150 m of the surface of the target rocks may be considered as the outer border of the outer gently-dipping terrace outlined by discontinuous remnants of the bedrock of the crater rim. The distance of this contour line from the crater's center in the northern sector is about 48 km. It is important to note that north of the considered area, numerous remnants (up to 7 km^2 of area and up to 25 thick) of polymict allogenic megabreccia composed mostly of sedimentary rock fragments occur at the altitudes of +25 to +100 m. These are observed at the distances up to 18–20 km from the crater rim.

Inferred from the altitudes of the base of impact breccias both inward and outward of the crater rim, its elevation peaks no less than 150–190 m. The rim is generated by both Upper Paleozoic terrigenous rocks intruded by numerous dolerite bodies (which contribute up to 40% of the Upper Paleozoic) and intensely disturbed Middle Cambrian dolomite. The former is only slightly deformed: close to contacts with impact-generated formations, Carboniferous sandstone and aleurolite as well as conformable dolerite sills at the western part of the area dip steeply (20°–50°) northerly. However, as far as at 200–300 m outward from the contact, they dip very gently (1°–2° dip). Alternatively, west of Kurdyagolakh Lake, the crater rim is composed of blocks of intensely deformed Cambrian rocks that upthrust over the Upper Paleozoic. This remnant of the bedrock rim is of about 2 km wide; its southern (inward) border is vague because it is replaced by allogenic megabreccia composed of large fractured dolomite klippen with minor admixture of other lithologies (dolerite, sandstone) and patches of the microbreccia. Cambrian blocks are suggested to be moved for 2–3 km at least.

From aerial photography deciphering, the remnant consists of angled dolomite blocks up to 2 km across with very variable attitudes. Inward to the crater, the uneven surface of deformed target rocks is modelled to subside gently southwards at an angle not more than 10°.

The surface of the deformed rim as well as of adjoining klippen breccia is uneven. It abounds in small pits where eight suevite remnants from 30 × 100 to 80 × 110 m across are preserved. This fact indicates in addition that the structural rim occurred before the deposition of the ejected allogenic material.

The above-mentioned remnant of the structural rim occurs in the front of a radial trough, which causes a lobate shape of the allogenic breccia field. The radial trough is remarkable for the occurrence of a large impactite body (of about 2 km^3) while

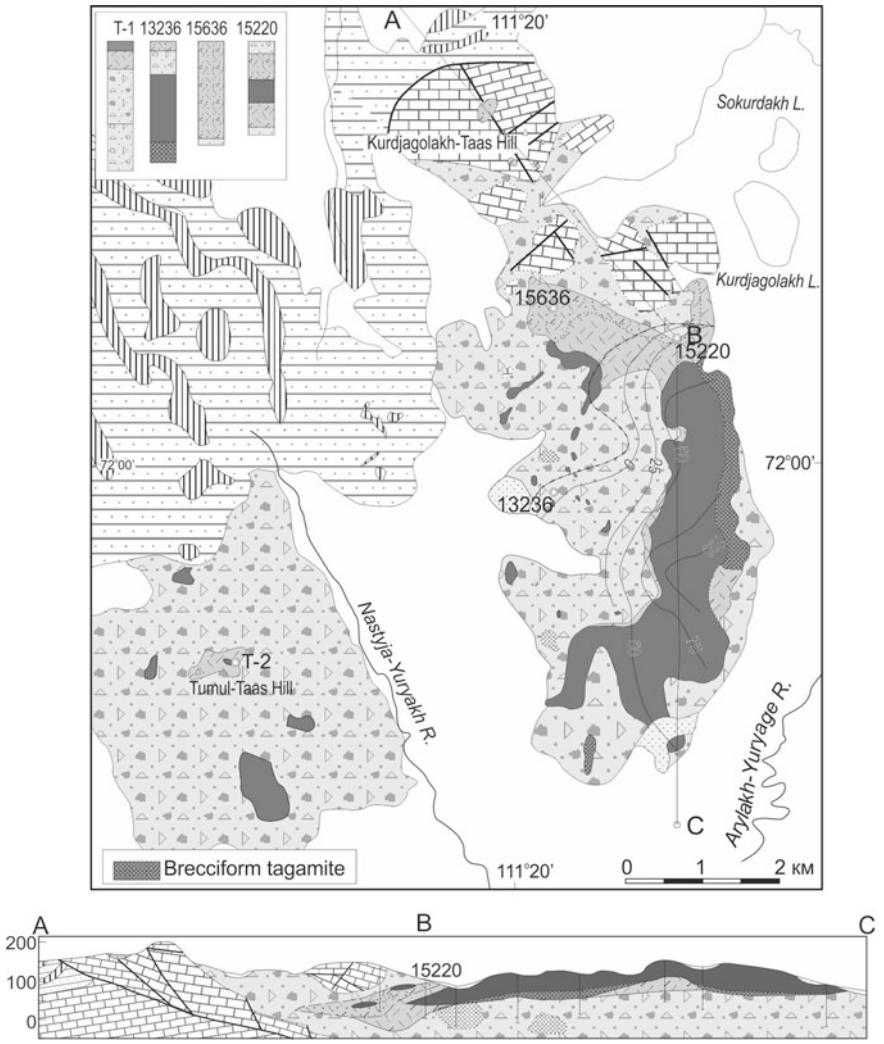

Fig. 2.18 Geological map of the Arylakh-Yuryage River area. For main legend, see Fig. 2.8; a symbol for brecciform tagamite is added. The location of the cross-section is shown by the A-B-C line. At top left, general sections of key boreholes are shown; these boreholes are put into the map as well

outside of the trough impactite (mostly suevite) form patches no more than 0.1 km^2; however, some small tagamite ejections as thick as 10 m.

Polymict allogenic megabreccia is a dominated impact lithology in the area. The maximum thickness is estimated to be no more than 225 m; an incomplete thickness opened by borehole peaks 99 m. The megbreccia is composed of blocks and klippe of different target lithologies—Precambrian gneisses, Mesoproterozoic sandstone,

Cambrian dolomite, Upper Paleozoic terrigenous rocks, Triassic dolerite and volcanoclastics, and Jurassic and Cretaceous sandstone, coaly aleurolite, and clay. These fragments range from some cm to many hundreds meters across and are cemented by microbreccia or suevitic matter. Two lithological varieties develop changing gradually to one another: (1) Polymict megabreccia containing both sedimentary and crystalline rock material, and (2) Megabreccia and rubble-block breccias after sedimentary rocks. Contacts between them are indistinct. Commonly, these varieties are laterally separated: the former as a rule, envelops impactite bodies—both larger ones and small patches, while the latter is commonly forming continuous field lacking in impact melt ejections; in addition, it composes fallout patches of breccia. Only at Tumul-Taas hill, a gradual replacing of polymict megabreccia by "sedimentary" megabreccia downward in the section is observed; more probably, this is due to limited thickness of the polymict breccia there (13–53 m).

The polymict megabreccia consists of rubble, blocks and klippen of all target lithologies except for Upper Mezozoic sedimentary rocks, which occur very rarely. Crystalline rocks—biotite-garnet and biotite-pyroxene gneisses—are greatly dominated; in borehole sections, they constitute from 35 to 75%, while carbonate lithologies, up to 25%; other rocks compose no more than 5%.

Megabreccia composed of fragments of sedimenary rocks represents an accumulation of boulders, blocks, and klippen of different lithologies of the sedimenary cover, rare gneiss fragment occurring in places, though. It varies considerably in composition in dependence on adherent bedrock lithologies indicating hence relatively short displacements of the target material. Close to the crater rim remnant formed by Cambrian rocks, the megabreccia consists of klippen of dolomite up to 1 km^2; other lithologies contribute <5%. Westward, at Tumul Taas hills, fragments of Permian and Carboniferous coaly aleurolite dominate over dolomite; subordinate dolerite and Mezozoic terrigenous rocks are common in addition. West of this area, dolerite clasts can dominate over other lithologies. Fields of ejected allogenic breccia are characterized by the predominance of Cretaceous rocks, all other target lithologies including shocked gneisses and even rare Triassic tuffs being represented as well, though.

The common size of blocks in this megabreccia is 2–40 m (except for dolomite klippen at the Kurdyagolakh Upland). These fragments are cemented by microbreccia, which contains an admixture of green and grey impact glass fragments (up to 15%). In the borehole sections, continuous microbreccia intervals reach more than 95 m in places.

Microbreccia occurs locally filling in sags in the roof of impactite bodies; it is no more than 10 m thick there. These are more probably remnants of a destroyed microbreccia blanket.

Impactites form a relatively large, lens-like, meridionally elongated body within polymict allogenic megabreccia at the right side of Arylakh-Yuryage Creek. It is of 5.5 km long, up to 3 km wide, and more than 115 m thick. The base of the body plunges out northwestwards from altitudes of +111 to 0 m; its western part is overlain by the polymict breccia (Fig. 2.18). The most of the body (about 1.5 km^3) is composed of LT tagamite. The maximum (incomplete) thickness of the latter in

borehole sections is 86 m. Northward tagamite thins out and replaced by vitroclastic and lithovitroclastic suevite that peak 75 m thick.

LT-tagamite contains 25–45% of inclusions of cataclased and intensely shocked gneiss and, more rarely, dolomite, quartzitic sandstone, aleurolite, and dolerite. Close to its base, tagamite becomes breccia-like due to linear accummulations of clastic material. In addition, thin lenses of glass agglutinates are often observed both in the base and within tagamite. The breccia-like (taxitic) tagamite is up to 11 m thick; in places, it is replaced at the base of the body by vitroclastic suevite. However, commonly tagamite lies directly on allogenic megabreccia. This contact is uneven, but gently-dipping in general, while fluidal glass fragments in welded suevite are aligned much more steeply (up to 30°–40°).

Suevites develop mostly in the front (northern part) of the impactite body to replace tagamite in its strike. Small suevite or tagamite patches are mapped in the field of allogenic breccia. Commonly, they do not exceed 0.01 km^2 in area and 5–7 m thick; a small body of impactite (mostly suevite) of 21 m thick is opened by boreholes at Tumul-Taas hill, though.

The main structural features of the Arylakh-Yuryage area are the following.

1. The large impactite body represents an impact melt ejection mixed with the main mass of lithic breccia and forming due to dissemination of the melt a wide range of impactite varieties from massive ones (tagamite) to suevite dominated by sedimentary clasts.
2. The impactite body fixes a radial trench; in front of the latter, a remnant of the structural rim of 150–180 high composed of deformed Cambrian dolomite within a field of less disturbed Upper Paleozoic rocks occurs.
3. Polymict allogenic megabreccia dominated by fragments of crystalline rocks develops around impactite ejections while the main mass of breccias is composed mostly of sedimentary rock material.

2.2 Annular Trough and Peak Ring

2.2.1 Balagan-Yuryage Area

This area embraces the basin of upper and middle reaches of the Balagan-Yuryage River (a left tributary of the Daldyn River) in the southwestern sector of Popigai Crater where the structure of the annular trough and adjoining crater rim and annular uplift, as well as composition and relationships of the impact formations there were studied in detail. The area under consideration includes Balagan-Yuryage River valley following generally the axis of the annular trough and the contiguous watershed areas from the upstream of the Daldyn River at southwest to sources of the Balagannakh Creek (a tributary of the Parchanai River) at northeast (Fig. 2.1). This is a gently rolling plateau with the elevations of 100–150 m. In its northeastern part, crystalline rocks of the peak ring are exposed on the surface; and in the southwest, sedimentary

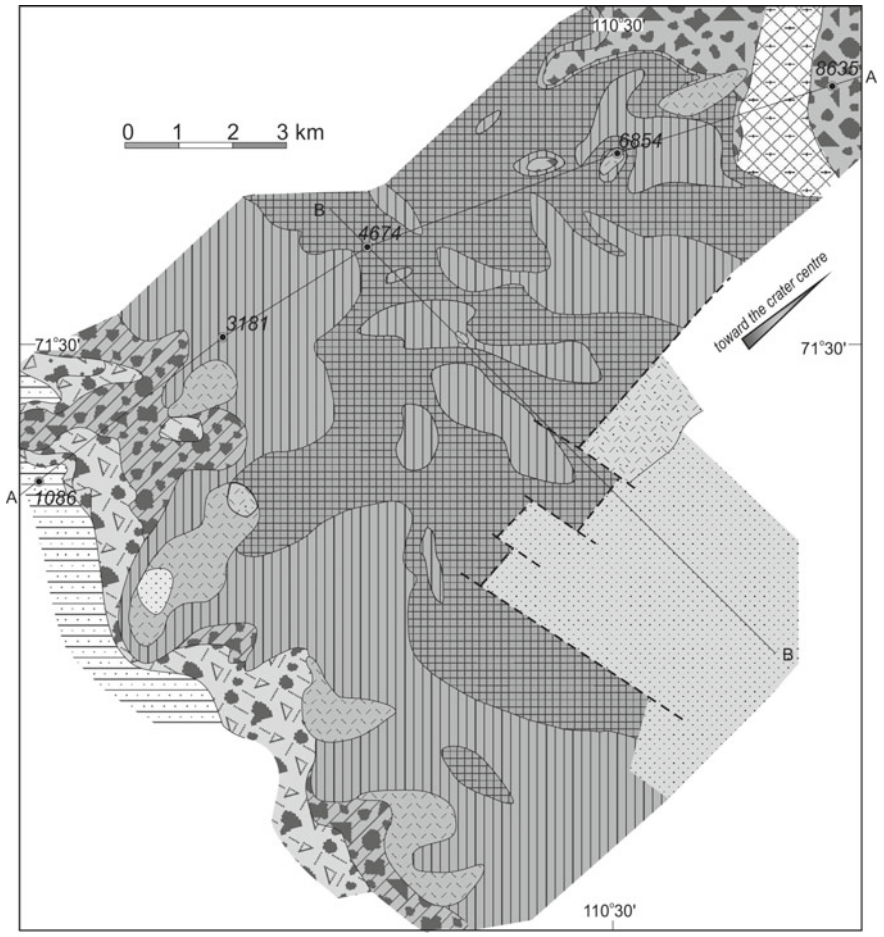

Fig. 2.19 Geological map of the Balagan-Yuryage River area at the elevation of +0 m. For legend, see Fig. 2.20. A crossed and a longitudinal sections through the annular trough shown at Figs. 2.20 (A-A) and 2.22 (B-B), correspondingly, are marked by solid lines. Also shown are drillholes, column of which are given in Fig. 2.21

rocks of the crater rim. Over the rest the territory, tagamites and suevites mainly occur; to a lesser extent, diverse allogenic breccias develop (Fig. 2.19). Quaternary deposits are widespread, particularly within flat valleys in the upper course of the Balagan-Yuryage River and in the Upper Daldyn Depression; in the latter, Pliocene-Quaternary deposits are up to 75 m thick. The area was studied in detail in the course of geological surveying, particularly, by means of numerous boreholes, which enable to reveal the structure of the annular trough, composition and relationships of the rocks filling it (Masaitis et al. 1999).

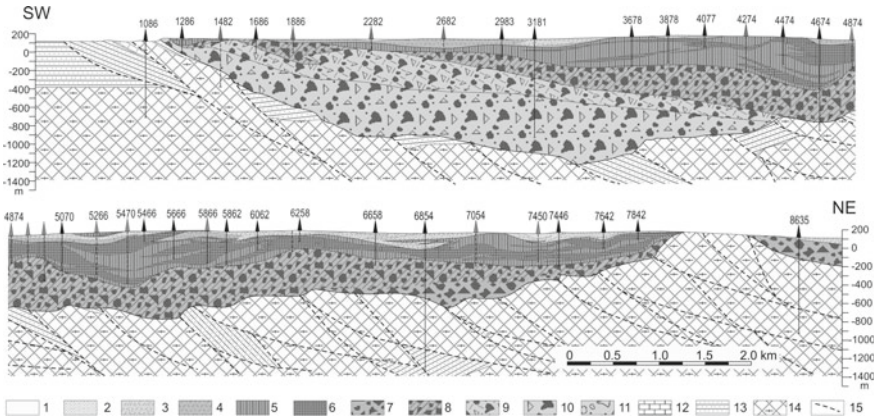

Fig. 2.20 Geological profile across the annular trough at the SW sector of the Popigai crater (Balagan-Yuryage area). Vertical and horizontal scales are equal. The location of the section is shown at the Fig. 2.19. 1—Quaternary deposits, 2—Polymict allogenic microbreccia, 3—Suevites containing mainly epiclasts of sedimentary target rocks; 4—Suevites containing mainly epiclasts of crystalline target rocks, 5—LT tagamite, 6—HT Tagamite, 7–11—Allogenic lithic breccia: 7—megabreccia and mesobreccia of crystalline target rocks, 8—the same megabreccia cemented by tagamite; 9—polymict mesobreccia composed of both crystalline and sedimentary target rock fragments cemented by suevites, 10—polymict mega- and mesobreccia cemented by coptoclastite, 11—allogenic megabreccia composed of sedimentary target rocks; 12–14—target rocks: 12—Cambrian carbonate rocks, 13—Mesoproterozoic quartzitic sandstone, 14—Archean to Paleoproterozoic crystalline basement rocks, 15—shockgenerated faulting

The width of the annular trough in the Balagan-Yuryage area is about 15 km; and of the peak ring, about 3 km (Fig. 2.20). The maximum depth of the trough filling in by impactite and allogenic breccia exceeds 1100 m. The steepness of the inner slope of peak ring adjacent to the central depression is of no more than 15°–20°, while of the outer one adjoining the annular trough, exceeds 30°–35°. The latter is shortly flattened toward the axis of the trough, its floor being slightly inclined to the southwest; however, further outward from the uplift, its surface is subsiding abruptly reaching its minimum hypsometric level (lower than −1000 m sea level) about 5–6 km from the outer edge of the trough. At the axial part of the trough, the depths of the latter reach 0.8–1.0 km only at lows of the crater floor. The outer slope of the trough is assumed to be about 25°–30° steep. In general, the surface of the trough floor is quite irregular, elevation variations reaching several dozens and even some hundreds of meters.

Crystalline rocks composing the floor of annular trough and peak ring can be regarded as parautochthonous formations; they make up large blocks to hundreds of meters across, slightly displaced relative to each other. Paraauthochthon (authigenic breccia), penetrated at peak ring by borehole 8635 in the interval of 230–1040 m (Fig. 2.21), is made up of such blocks of biotite-bipyroxene gneisses and plagiogneisses and subsidiary biotite-garnet plagiogneisses and charnockites injected locally by dolerites and gabbrodolerites. These rocks were deformed and subjected

to shock compression with amplitude up to 8–10 GPa [planar fissures in salite, and, less frequently, kinkbands in biotite plus one system of planar deformation features (PDF) in quartz]. Blocks are separated by cataclastic and mylonitization zones from several cm to several meters thick. Cataclastic zones are accompanied by slight alteration (mostly chloritization, carbonatization, and sulfidization). These zones often contain fine-clastic injection breccias up to 0.6 m thick. Veins of such breccias are traceable are observed down to the borehole face. Among the clastic material of the breccia veins there are diaplectic quartz fragments with 3–4 PDF systems, diaplectic glass after quartz and feldspar, in places fusion glass particles and minor fragments of mudstones. At the depth of 883–903 m, i.e. at about 850 m below the surface of the annular uplift, some thin tagamite injections were intersected. These are hyaline amydgaloidal tagamite, in places with fluidal structure. They either form intricate veinlets in friction breccias up to several dozens of centimeters thick or cement gneiss fragments, often plastically deformed. All inclusions in the tagamites are intensely shocked gneiss constituting up to 40 vol%.

On the floor of the ring trough, along with crystalline rocks, blocks of the Mesoproterozoic quartzitic sandstones occur in places. Borehole 6854 drilled 2.5 km east from the trough axis (Figs. 2.20 and 2.21) penetrated almost 1 km (from 291 to 1262 m) of authigenic breccia of crystalline rocks, similar to that described at peak ring, but noted for a smaller size of blocks and thicker cataclastic and crushing zones, and a more intense hydrothermal mineralization (predominantly saponite). Some impact melt (tagamite) veins up to 14 m in core occur extend down to 685 m. These are LT-tagamite with micro-ophitic texture and 5–7 vol% of lithic inclusions. Shock deformation features in rock-forming minerals (planar fissures in salite and biotite, appearance of the basal PDF system in quartz) indicate that the shock compression of rocks at the depth of 800–1000 m did not exceed 5–7 GPa. Further downward, the intensity of these deformations is reduced; here, the impact loading was not more than 3–5 GPa. At the depth of 1262–1520 m (borehole face), the block of Mesoproterozoic brecciated quartzitic sandstone was penetrated; they have a mortar structure ("gris") and are mainly transformed to rock flour.

In addition, the true crater floor is opened by the borehole 4674 at the axial portion of the annular trough (Figs. 2.20 and 2.21). This hole penetrated near its face (down of 827 m) a block of fissured and locally cataclased biotite-bipyroxene gneisses, subjected to compression not higher than 3–5 GPa.

Target rocks making up the outer edge of annular trough are Mesoproterozoic quartzite; locally, in subsided blocks, Lower Cambrian carbonate rocks (Fig. 2.20). A number of thrust sheets are revealed there, where older rocks (up to the Archean) occur over younger formations. These thrust sheets are up to 250 m thick and extend from hundreds of meters to the first kilometers. In particular, borehole 1086 (Fig. 2.21) located at 0.5 km outward from the brow of the trough, penetrated a block of intensely fractured biotite-amphibole gneiss in the interval of 6.0–125.7 m. Below it (from 125.7 to 508.5 m), a normal sequence of the sedimentary cover is opened. It includes 54 m of Cambrian variegated dolomites and mudstone and 328 m of Mesoproterozoic pink sandstone. The bedding of sedimentary rocks is gently (less than 10°) dipping towards the trough. This sedimentary sequence is underlain by crys-

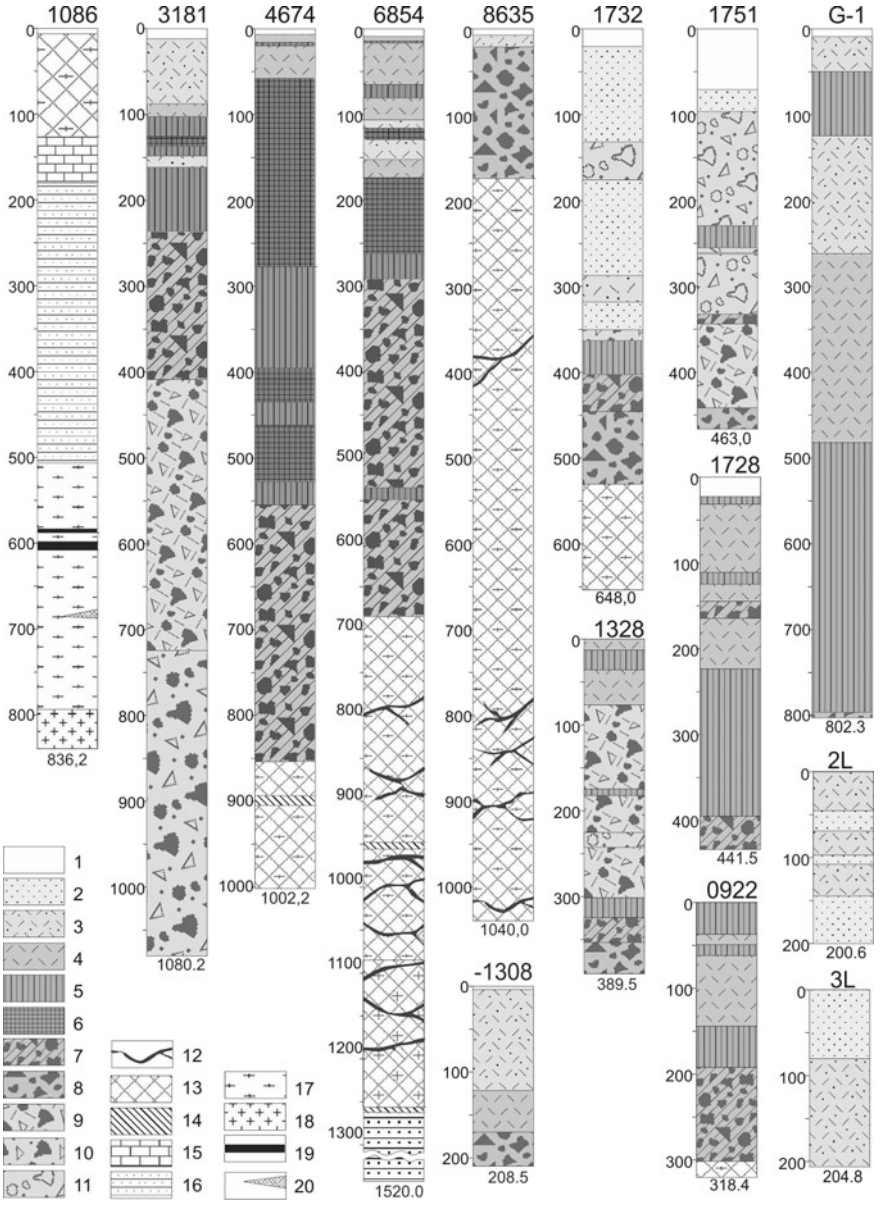
1086
3181
4674
6854
8635
1732
1751
G-1
836,2
1080.2
1002,2
1520.0
1040,0
648,0
463,0
802.3
1728
1328
2L
441.5
389.5
200.6
0922
-1308
3L
318.4
208.5
204.8
1
2
3
4
5
6
7
8
9
10
11
12
13
14
15
16
17
18
19
20

◄**Fig. 2.21** Geological columns of key boreholes from the Balagan-Yuryage area (boreholes 1086, 3181, 4674, 6854, 8635), from the Mayachika Upland area (boreholes 0922, −1716, 1328, 1728, 1732, 1751) and from the Daldyn River area (boreholes G-1, 2L and 3L). Location of the boreholes is shown at Figs. 2.1, 2.13, and 2.22. 1—Quaternary deposits, 2—Polymict allogenic microbreccia, 3—Suevites containing mainly clasts of sedimentary rocks; 4—Suevites containing mainly clasts of crystalline rocks and enriched by vitroclasts, 5—LT tagamite, 6—HT tagamite, 7–11—Allogenic lithic breccia: 7—megabreccia and mesobreccia of crystalline rocks cemented by tagamites, 8—megabreccia and mesobreccia of crystalline rocks; 9—polymict megabreccia and mesobreccia composed of fragments and blocks of crystalline and sedimentary rocks cemented by suevites, 10—polymict blocky breccia cemented by microbreccia, 11—allogenic mega- and mesobreccia composed of sedimentary rocks. 12—injection veins of polymict breccia with glass and veins of tagamites. 14–20—Target rocks: 13—Brecciated parautochthone, 14—Dolerite, 15—Cambrian carbonate, 16—Mesoproterozoic quartzite, 17–20—Archean to Paleoproterozoic gneisses: (17), gneiss-like hypersthene granite (18), mafics and ultramafics (19), calciphyre and marble (20)

talline basement rocks, but the contact seems to be not original (tectonic) because of both the base (lower 22 m) of sandstone and the top (23 m) of the crystalline basement are represented by intensely brecciated and in places cataclased rocks fixing of an upthrust zone. The basement rocks to the depth of 786 m are represented by migmatized and granitized biotite-bipyroxene, biotite-salite, and biotite-hypersthene gneisses with calciphyre and marble lenses to 4–6 m thick. Gneisses are locally marked by intense fissuring and cataclasis. Down of 786 m, the borehole penetrated granites and granite-gneisses containing lenses of mesocratic gneisses.

Due to a detailed study of borehole sections, the general occurrence pattern of various allogenic breccia and impactites filling the trough were revealed. The total thickness of impact-generated formations in the central part of the trough can reach 1.4 km; the opened thickness peaks 1080 m (Bh. 3181). The total ratio of the estimated volumes of allogenic lithic breccia, tagamite to suevite is 12:4:1. Close the peak ring and in the central part of the trough, the sequence is composed mainly of impactites, while near the outer edge, suevites and tagamites wedged out gradually, and allogenic lithic breccias prevail there. Generally, the impact fill of the trough is a sequence of alternating flat lenses and sheeted bodies with horizontal or gently undulating bedding. Allogenic breccias are confined to the lower part of the section, and tagamites and suevites, to the middle and upper parts.

At the bottom of the impact sequence, polymict allogenic breccia occurs. Its maximum thickness occurs in the deepest part of the trough where it reaches possibly 1 km; in borehole sections, it peaks 655 m (Borehole 3181; Figs. 2.20 and 2.21). The breccia is made of blocks, rubble, and debris of different target rocks up to 75 m thick in core. The distribution of fragments is irregular, continuous intervals (100 m or even more) lacking in large (>0.5 m) fragments are observed in places. Crystalline lithologies, commonly shocked (up to 15–20 GPa), predominate everywhere contributing about 2/3 of larger fragments. The latter are cemented by a thin-crushed (silty to psammitic in size) material of the same lithologies, but with the ratio of crystalline basement and sedimentary cover lithologies of about 1:1. The rest is represented almost exclusively by quartzitic sandstones; subordinate dolerites and minor carbonate rocks occur in addition. In the upper 200–250 m of the section, the content

of thin-crushed cement is markedly reduced, as well as the number of sedimentary rock fragments and blocks. Some impact glass fragments appear in the cement, so that the latter could be assigned by its lithological composition as a melt-free suevite. At different levels of the section, there are accumulations of crystalline rock blocks (to 100 m in core) occur.

The thickness of the polymict allogenic breccia lens decreases towards the outer slope of the trough. The surface of the polymict breccia uplifts steeply to the outer rim (updip). From other hand, this breccia is absent in the central part of the trough and on the inner slope of its deformed floor (Boreholes 4674 and 6854). Thus, it is assumed to wedge out both southwestwards and northeastwards.

The polymict megabreccia and parautochthon within the annular trough are overlain by megabreccia and debris-block breccia after crystalline rocks cemented by impactites. As contrasted to the polymict breccia, the crystalline megabreccia develops through the entire width of the annular trough. Its thickness varies from 60–80 m close to the outer slope of peak ring to 500–550 m in swells in the central part of the trough. The maximum penetrated thickness is 420 m (Borehole 6854). At 2–3-km-wide zone close to the crater rim, the megabreccia is reducing locally, so that in places impactites overlie directly the polymict breccia. This megabreccia is made up of blocks of different size (to several dozens of meters across), cemented by the finely crushed material of the same crystalline rocks, or by tagamites and suevites. Tagamite cement contributes about 13% to the total volume of crystalline megabreccia on average, although locally the amount may reach up to 50%. Certain tagamite bodies as thick as 55 m in core. The variations in the tagamite content within the megabreccia do not show significant correlation with occurrence parameters of the overlying tagamite sheet and can be caused surely by different factors. Some blocks are cut by veins of fine-clastic polymict breccia with glass.

There are certain differences in the lithological composition and structure of this breccia in the transverse section of the trough. Close to the outer slope of the ring uplift, blocks of intensely cataclastized biotite-bipyroxene, biotite-hypersthene, and biotite-garnet (including graphite-bearing) gneisses predominate; they show shock features corresponding to shock compression with the amplitude over 25–35 GPa. Tagamite cement constitutes not more than 10 vol%; it occurs mostly in the central portion of the vertical section of the megabreccia lens. In the central part of the ring trough (Borehole 4674), blocks are made up of rocks of the same composition, but slightly shocked (not more than 8–10 GPa); the amount of tagamite cement is increasing (to 20% or even more), in the deepest part of the trough megabreccias are often cemented by agglomerate suevites or agglomerate breccia with glass. Injection breccias are rarely found here.

On the inner slope of peak ring, megabreccia composed of crystalline blocks were penetrated by Borehole 8635 located approximately 1 km NE of the peak ring axis. This megabreccia is composed of blocks of 10–20 m in size of intensely deformed biotite-garnet (in places with graphite) and pyroxene gneisses and plagiogneisses, granite-gneisses, less frequently, other lithologies. The blocks are cemented by the same finely crushed material, often with impact glass, locally constituting 15–20 vol%. Cement of the breccia is recrystallized in places; besides, calcite, pyrite, zeo-

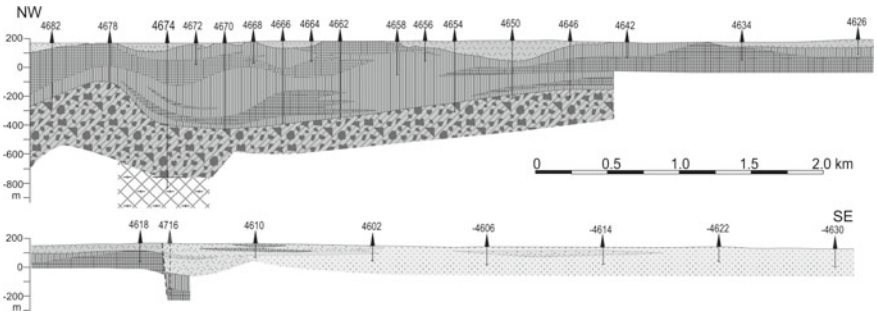

Fig. 2.22 Longitudinal geological section through the annular trough, the Balagan-Yuryage area. The section follows the drilling profile 46. For legend, see Fig. 2.20. The location of the section is shown at the Fig. 2.19

lites, and saponite develop there. Crystalline lithologies from blocks in the breccia show shock deformations corresponding to 25–35 GPa. The megabreccia is of 209 m thick in the borehole 8635 (depth interval 21–230 m). Inferred from drilling data, it is reduced along the peak ring axis both northwesterly and southeasterly.

Upward in the section, the crystalline megabreccia cemented by tagamites grades to a continuous, sheet-like body of tagamite. In the area considered, which occupies 4% of the total area of the annular trough, tagamite volume is estimated to be 22.5 km^3. This sheet spreads for 15 km from the annular uplift up to the outer edge of the annular trough in places (Fig. 2.19). Along the trough axis to the northwest and southeast it is traceable for approximately the same distance (Fig. 2.22).

The relief of the base (Fig. 2.23) and the roof (Fig. 2.24) of the tagamite sheet are significantly different. The base arises in a generally outward direction, but it has a more complicated relief in detail. The main features are several radial and near-radial trenches 1–3 km wide, separated by accumulations of large blocks of crystalline megabreccia that are uplifted locally to 450 m above the base of the tagamite sheet. These trenches could be traced to the outer margin of the annular trough and contain the bulk of the volume of tagamites.

The thickness of tagamite sheet is correlated entirely with the relief of its base (Fig. 2.23). However, thickening of the tagamite sheet occasionally results in a relative rising of its upper surface; moreover, this elevation was more significant before erosion. The roof of the tagamite sheet is characterized by a general sinking in centrifugal directions as well as by a combination of radial and concentrical elements of its structure (Fig. 2.24). The radial elements appear as chains of narrow (0.5–1.5 km) deep (up to 150 m and more) depressions that do not coincide with trenches excavated in the base of tagamite sheet near peak ring.

In the central part of the area under consideration that is corresponding to a deep excavation trench, the thickness of the tagamite sheet exceeds 600 m. Outside of this segment northwestward and southeastward, the thickness of tagamites diminishes but may still be about 150–200 m (Fig. 2.23). Further southeastwards, its thickness

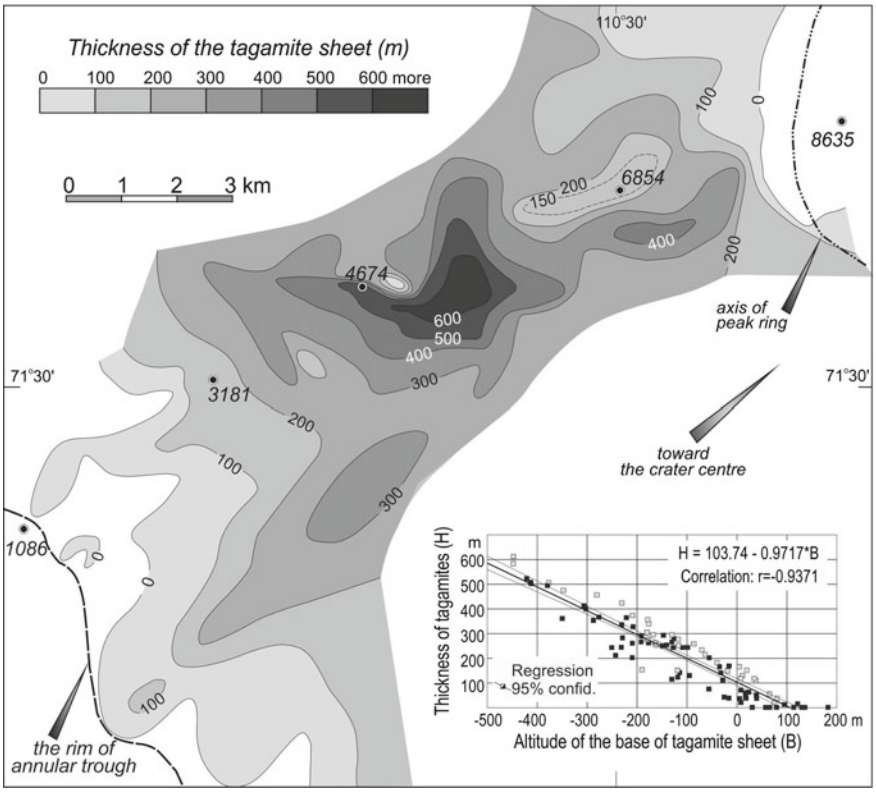

Fig. 2.23 Isopach map of the tagamite sheet, Balagan-Yuryage area. Contour interval, 100 m. Also shown are drillholes, column of which are given in Fig. 2.21. Diagram shows correlation of thickness of tagamites (black squares, true thickness; open squares, apparent thickness) and elevation of the base of the tagamite sheet. The diversion of open squares from the regression line to higher value of thickness shows that the initial thickness of tagamites in these places was greater before erosion

is markedly reduced, and in the Daldyn River valley it is not more than two dozens of meters.

The complex thick tagamite body is composed of a series of subhorizontal simple bodies, made up of two varieties, which, by a number of structural and petrological features are assigned to the high-temperature (HT) and low-temperature (LT) tagamites, respectively (see Chap. 4).

Inferred from abundant core study data, the LT variety contributes 58% to the total volume of the tagamite sheet and has a more uniform space distribution. The HT tagamites commonly cause an abrupt increase in sheet thickness and local elevation of the roof. In radial directions, HT tagamites wedge out much closer than LT-tagamites (Fig. 2.19). Although the LT/HT volume ratio, in general, increases in centrifugal direction (appropriate correlation coefficient $r = 0.63$), its correlation with the main appearance features (e.g., thickness, relief of the base and roof) of the tagamite

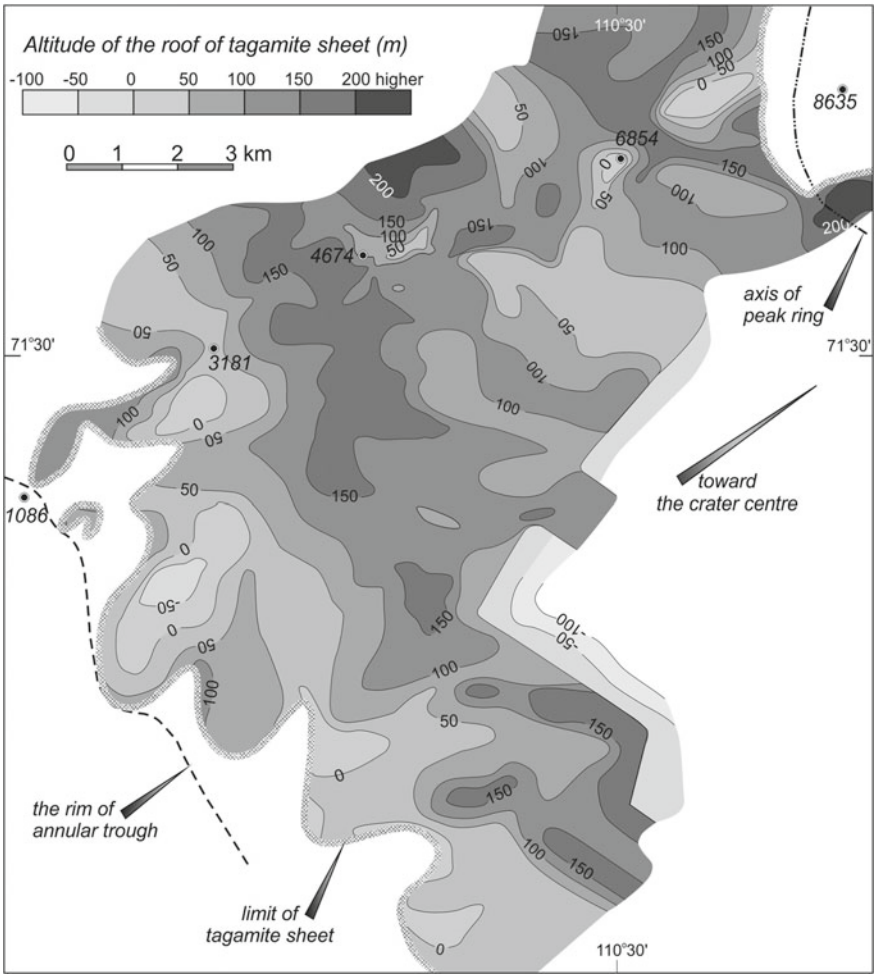

Fig. 2.24 Hypsometric map of the roof of the tagamite sheet, Balagan-Yuryage area. The eastern part of the sheet has subsided along the system of post-impact faults. Contour interval, 50 m. Also shown are drillholes, column of which are given in Fig. 2.21

sheet is insignificant. Consequently, the variability of tagamites originated before deposition of impact melt in the annular trough and is not related to post-impact processes.

The volumetric ratio of HT and LT tagamite varies spatially: in the thickest central part of the sheet, HT tagamites contribute 60–80% while on the flanks, LT tagamites predominate. In the generalized section of the composite body, upper and lower simple bodies of HT tagamites can be distinguished; these are separated by LT-tagamite up to 200–250 m thick; however, the latter is wedging out in places, and HT tagamite bodies are merged together (Fig. 2.25). In most cases, the upper HT tagamite

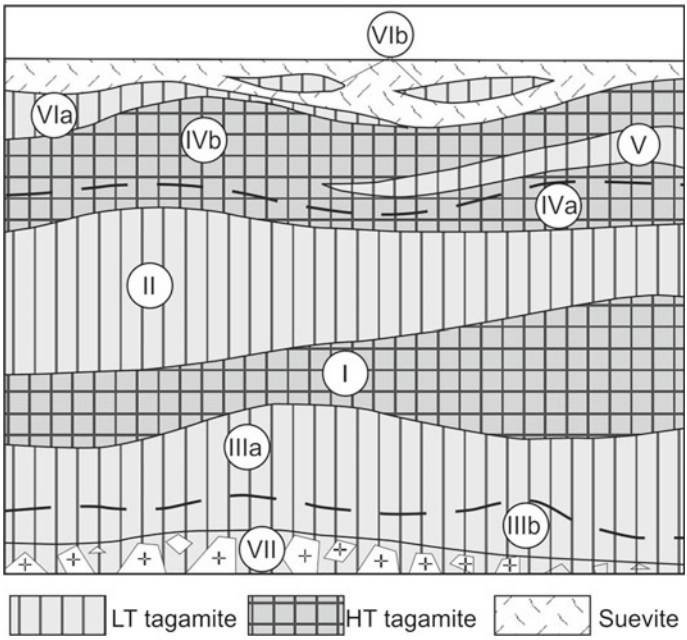

Fig. 2.25 A general model of inner structure of a thick tagamite sheet. Tagamite: I, II—holocrystalline; III—heterocrystalline (a—upper subzone, b—lower subzone); IV, V—holohyaline and hemicrystalline (a—upper subzone, b—lower subzone); VI—mainly holohyaline (a—at endocontacts of the tagamite sheet, b—small bodies in suevites); VII—mainly holohyaline in cement matter of megabreccia

body is overlain by a suevite sheet; however, in places LT tagamite lenses occur in its roof. Similar rocks occur as irregular lenses from the first metres to 60 m thick among suevites. At the same time, suevites also contain frequently HT tagamite lenses. In the central part of the upper sheeted body of HT tagamite, LT tagamite lenses to 10–70 m thick often occur. The lower HT tagamite body is of average thickness of 50–80 m; in the central part of the trough, it swells to 100–170 m with dactylic offsets. The lower LT tagamite body occurs at the base of the entire composite bed; its thickness is very variable, it ranging from 20 to 80 m. Downward in the section, it is gradually passing into tagamite cement of the megabreccia.

Noteworthy are the relationships between HT and LT tagamites, which are clearly seen in boreholes core, as well as in rock blocks exposed by mine working. Contacts between two varieties are also observed at natural exposures along the Daldyn River valley in the southern part of the area. In many cases, contacts between two tagamite varieties are abrupt, they being sinuous and irregular, though. Very frequently, transitions between the bodies are due to the increasing amount and size of the inclusions of one variety of tagamites in another. These inclusions are characterized by abrupt boundaries and also by variable size (from the first centimeters to dozens of centimeters and the first meters) and shape (see Chap. 4). In certain sites

where low-temperature alteration processes (montmorillonitization, limonitization, etc.) are superimposed, a contact can be revealed only in the course of thin sections study. The thickness of transition zones between HT and LT tagamite bodies where the above-mentioned mutual inclusions develop varies highly to reach 80–120 m in places. Orientation of the described inclusions is observed rarely, but in places one can see irregular lump-shaped inclusions of HT tagamite in LT tagamite orientating both in the flow plane and in plan pointing to the flow direction.

Both HT- and LT-tagamites contain inclusions of crystalline rock and their minerals; their content varies in the vertical section of the composite body. The content of large (more than 1–2 m) crystalline rock blocks in LT-tagamite is higher when compared with HT-tagamite; these inclusions are predominantly concentrated in swells of the sheeted body, confined to its base subsiding parts. As to minor inclusions, their content is clearly controlled by the position in the vertical section: in the upper part of the composite sheet, they contribute 15–20 vol%, but in the lower one, as few as 3–5%. Some other variations of the petrographic features of tagamites are also established; they are considered in detail below under Sect. 4.2.

The upper part of the crater fill in the Balagan-Yuryage River Basin is composed of suevites and microbreccias, which enclose lenticular or irregular tagamite bodies; the latter form lenses up to 44 m thick that contribute 6% of the suevite sequence. From other hand, in the upper part of tagamites (up to 100 m down in vertical section) suevite lenses up to 40 m thick occur rarely. The abundance of tagamite lenses in suevites decreases regularly outward from annular uplift; near the latter (at distances up to 4–5 km), alternating of relatively thin intervals of tagamites and suevites in the upper of impactite sequence is usual; further closer to the crater rim, such a picture is rare. Tagamite lenses in suevites are found in depressions of the roof of the sheet and decrease regularly outward from the annular uplift. In contrast, suevite bodies in the tagamite sheet appear in zones where its roof is uplifted; they occur mainly in the outer part of the annular trough.

Suevites overlie tagamites everywhere in the area with the exception the uppermost tagamite sheet (elevation above 50 m); they are inferred to have formed a continuous cover before erosion. The average thickness of preserved suevite cover 42 m, with a maximum of 196 m.

Despite erosion, the basic regularities of the inner structure of suevite cover are preserved. As a whole, both the base and the erosional top of this suevite sheet dip southwestward away from the peak ring to the edge of the annular trough; thus its thickness is mainly determined by the relief of the base, i.e., the roof of the tagamite sheet (Fig. 2.24).

The suevite blanket is inhomogeneous due to local variations in the composition of clastic constituents. Vitroclastic suevites sintered often near contacts, are resting directly on tagamites, often with gradual transitions via their ataxitic variety. In general, they pass up in the section into suevites, enriched in crystalline rocks clasts and then, the same with significant contribution of sedimentary rock fragments. The latter suevites comprise microbreccia lenses. The largest bodies of vitroclastic suevites are penetrated by boreholes in the southeastern and southwestern parts of the study area, where they form lenses or layers, extending up to 3–5 km long and up to

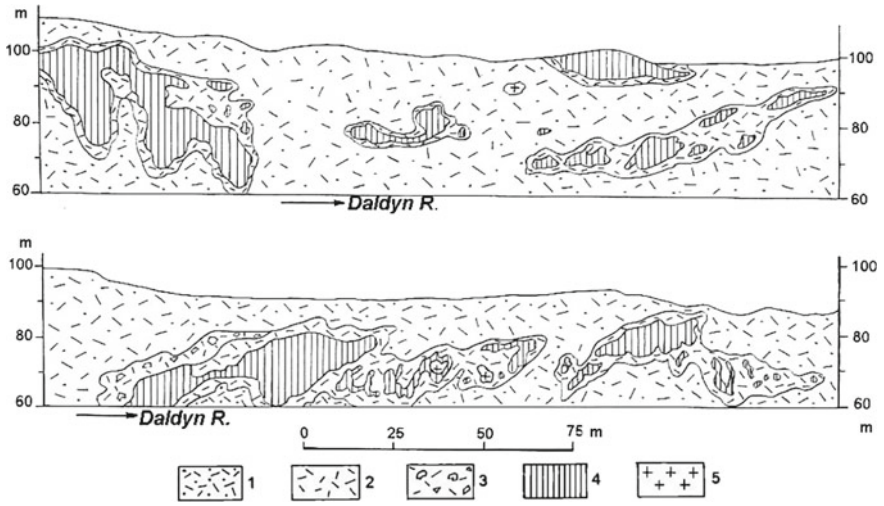

Fig. 2.26 Morphology and position of small tagamite bodies within suevites at the left bank of the Daldyn River, southeast of the Balagan-Yuryage area. 1—Suevite comprising mainly of clasts of sedimentary rocks and subordinate vitroclasts; 2—Suevite comprising mainly of predominant vitroclasts and clasts of crystalline rocks; 3—the latter enriched by lithic fragments; 4—HT tagamite; 5—gneiss in inclusions within impactites

148 m thick while in the upper course of the Balagan-Yuryage River, their thickness does not exceed 50 m; suevites are enriched by impact glass fragments there.

Vitrolithoclastic suevites are most widespread; they seem to overlie as a blanket all the other formations; their thickness reaches 165 m. They also comprise lenticular and irregularly-shaped tagamite bodies. Relationships between this suevite and tagamite are clearly seen at the exposures along the Daldyn River (Kygam stow), where both HT- and LT-tagamites are developed (Fig. 2.26). At contacts, ataxitic tagamites are commonly developed, passing into vitroclastic and then vitro-lithoclastic and other suevites. The character of contacts between microbreccia, vitro-lithoclastic suevites, and tagamites indicates that they were ejected and deposited practically simultaneously, being partly mixed during ejection.

Several boreholes located both on the slope of the central uplift and in the axial part of the trough penetrate within the suevite sequence under consideration an unit, which is noteworthy by a certain grading of the clastic material and a vague bedding, as well as by the presence of accretionary lapilli. The obscure bedding is expressed by the occurrence of layers of 10–50 cm thick distinguished by regular variations of grain size; the bedding is inclined under 30° in core. The distance between the most remote points where this unit was recorded is 9 km; in closely located boreholes on the uplift slope, this unit is correlated both by the depth (about 90–110 m) and by thickness (about 10–20 m). At the axial part of the annular trough, it occurs closer to the roof of the suevites (about 10 m dip) and peaks 60 m thick. At the same time, it cannot be clearly traced in all the contiguous boreholes; thus, this unit

is discontinuous. A similar suevite was also recorded in the downstream basin of the Daldyn River, as well as at the Chordu-Daldyn River valley and its tributary, Kychypkynaakh Creek.

The southeastern part of the Balagan River basin differs distinctly in its geologic structure from the region just described. A continuous field of microbreccia grading to suevites enriched by clasts of sedimentary rocks and containing lenses of small bodies of suevites and tagamites was mapped here (Figs. 2.19 and 2.22). Beneath a 228-m-thick microbreccia layer, tagamites were encountered in a drill hole at an elevation of 133 m. The occurrence of tagamite at this depth is probably the result of post impact downfaulting, with the amplitude more than 100 m. The southeastern block probably represents the uppermost part of the impact rock sequence that was removed by erosion elsewhere in the Balagan-Yuryage area.

The main structural features of the study area can be characterized as follows:

1. The peak ring has an asymmetric transverse profile; the steepness of the outer slope averages at about 35°; and that of the inner one, does not exceed 20°;
2. Rocks of the floor of the annular trough represent a parautochthon with relative centrifugal displacements of separate blocks amounting to several km;
3. Parautochthonous rocks of the peak ring are injected by fine clastic polymict breccias with glass as well as by tagamites;
4. Shock metamorphism grade of the coarse clastic material of parautochthon and allogenic breccias differs essentially, being much lower for the parautochthon;
5. The area is noteworthy for the occurrence of a voluminous impactite sheet dominated by tagamite, the maximum thickness of which is allowed by a radially orientated trench.
6. Inner structure of the impactite and breccia sequences, filling the annular trough, is composite; there are differences in relationships between the molten and crushed material, as well as clastic material of different size both through the vertical section and laterally.
7. Inner structure of the impactite body filling the annular trough, is composite; there are certain variations in relationships between the molten and crushed material, as well as in relationships between clastic material of different size both through the vertical section and laterally.
8. Allogenic breccias cemented by impactites that underlies the thick tagamite sheet is developed only in the annular trough;
9. The general flattening of lenticular and sheeted bodies of different rocks up the section is typical.

2.2.2 Mayachika Upland Area

The area includes the Mayachika-Kerikete Upland and adjacent lowland northwest of the upland. It is located in the northern sector of the impact structure on an area of 6 × 8 km (Fig. 2.1). This is an isolated group of hills with the relative

Fig. 2.27 The landscape of the Mayachika Upland. In the foreground, shocked gneisses are exposed on the surfacse. In the background, low hills composed of tagamite occur

elevation of about 150 m, standing apart against the swampy plain making up by Quaternary deposits. On the slopes and summits of hills, gneisses, impactites and different breccias are exposed, overlain by debris of the same rocks (Fig. 2.27). In the central part of the Upland, slightly extending northeastwards, crystalline rocks of the peak ring occur on the surface; on its slopes, they are covered by allogenic breccias and impactites (Fig. 2.28).

Geological mapping and abundant drilling evidence show that the surface of partly crushed and displaced crystalline rocks (parautochthon) traceable northwards for over 2 km along the dip, is subsiding irregularly to the annular trough axis at an angle of about 20°. However, locally, the steepness of the outer slope of the peak ring varies markedly from horizontal bedding on some areas to steeply inclined bedding (40°); locally, a reverse dip is observed. Possibly, there are bluffy escarpments to several dozen and, probably, the first hundreds of meters high, which is confirmed by comparison of sections of closely spaced boreholes (Fig. 2.29).

The inner slope of the peak ring is much gentler; from drilling data, its subsidence angle is estimated at 8°–10°. The boreholes drilled as close as 0.6–0.8 km from the uplift axis did not penetrate the basement at the depth below 200 m.

Archean gneisses projections are covered by breccias and impactites not only in the northwest and southeast, but also on the eastern and western slopes of the Upland, which indicates that generally the latter represents a large fragment of peak ring elevated in the process of the cratering and partly prepared by erosion afterwards.

Crystalline rocks of the uplift are characterized by the northwestern strike. They are composed mainly of leuco- or mesocratic biotite-garnet gneisses and plagiogneisses with graphite, as well as garnet-cordierite gneisses, locally migmatizied

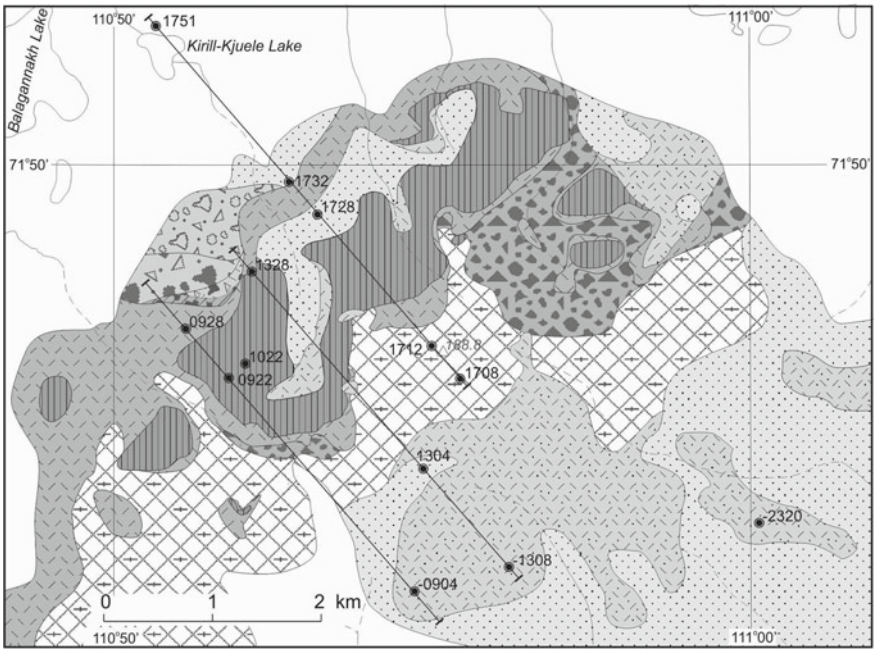

Fig. 2.28 Geological map of the Mayachika Upland area. For legend, see Fig. 2.20. Double circles mark key borehole sites, solid lines—drilling profiles 09, 13, and 17 (see Fig. 2.29) trending across the axis of peak ring

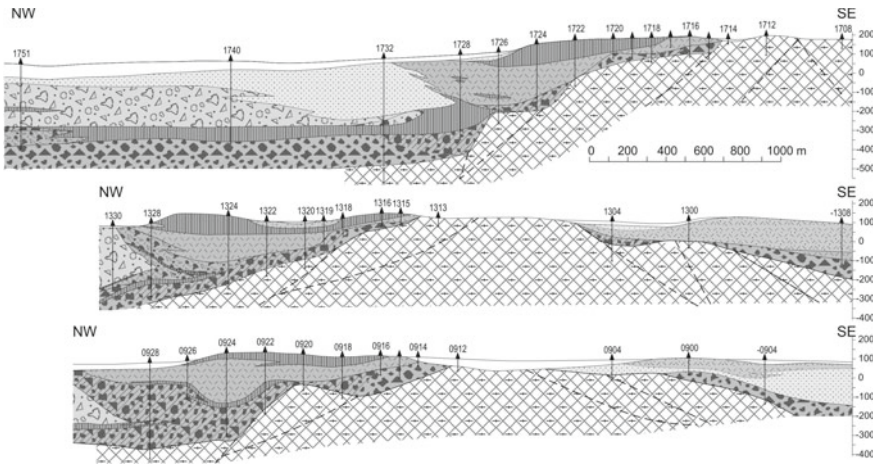

Fig. 2.29 Geological cross-sections through peak ring at the northwestern sector of the Popigai crater (Mayachika Upland area). For legend, see Fig. 2.20. The positions of the section are shown at the Fig. 2.28

(Boreholes 1708, 1712, Fig. 2.29). In the lower part of the outer slope of the peak ring, hypersthene and bipyroxene gneisses occur as thin bands and lenses among them (Borehole 1732 and others, Fig. 2.21). In addition, subordinate melanocratic varieties of biotite-garnet-cordierite gneisses, also containing sillimanite and spinel occur there. Graphite is recorded in different crystalline lithologies, but it is most common in biotite-garnet plagioclase-dominated gneiss. All these rocks are intensely deformed, cataclased and divided into separated blocks; their diameter might be evaluated at many dozens and the first hundreds of meters. Friction breccias develop frequently between such blocks. In the axial part of peak ring, boreholes also penetrated such brecciated rocks at the depth up to 80 m; further downward, more monolithic gneisses occur. Throughout the penetrated depth, crystalline rocks show indicative features of the shock compression of biotite and quartz with the amplitude up to 6–8 GPa (kink bands, planar fractures of 1–2 directions, basal system of PDF in quartz). Similar shock-metamorphic features are recorded in rocks of the outer slope of peak ring. At the same time, boreholes drilled north of the peak ring axis, at the distance slightly more than 2 km, penetrated hypersthene and bipyroxene gneisses and plagiogneisses, subjected to pressure not higher than 4–6 GPa (kink bands in biotite and quite rare PDF in quartz). All these crystalline rocks can be assigned to the authigenic breccia.

Allogenic megabreccias and debris-block breccias composed of gneiss fragments exclusively are resting directly on the deformed gneisses of the both outer and inner slopes of peak ring. On the inner slope, the breccias are covered by suevite; on the outer slope, they are traceable as a discontinuous belt up to 1.5 km wide. The thickness of the megabreccia is increasing outwards to peak 340 m on the outer slope at the distance of 2 km from the axis of peak ring (borehole 0928) and remains probably the same in the annular trough. On the inner slope, the opened thickness of the crystalline megabreccia does not exceed 30–40 m at the distance of 0.5–1.5 km from the axis of peak ring. Further toward the central depression, it diminishes. The upper surface of the crystalline megabreccia is irregular with local elevations up to 100–150 m.

Megabreccias are made up of rock debris, but predominantly of blocks of intensely deformed and cataclastic gneisses from first meters to tens and hundreds of meters across. The composition of blocks and fragments is more diverse as compared to the authigenic breccia; however, it is more important that they show a much higher level of shock transformations, which could have been caused by compression up to 25–35 GPa (PDF of 2–3 systems in quartz, appearance of diaplectic glass after quartz and plagioclase, etc.). Cataclastic rocks often contain thin irregular lenses and bands, in places plicated, of dark-coloured impact glass. Together with them, fragments of deformed sedimentary rocks, i.e. carbonate rocks, mudstones (including carbonaceous ones) occur on the outer slope of the peak ring in megabreccia, along with crystalline rock fragments. Here, megabreccias are locally cemented by tagamites; they are most characteristic of transition zones to the overlying sheeted bodies of these rocks, or are observed within frontal parts of such thick sheeted bodies. Such tagamite cement can contribute to 10% of the breccia volume; in some boreholes, continuous intervals of tagamite reach 5 m in core.

On the northwestern slope of peak ring, in its central part, megabreccia of crystalline rocks cemented by tagamites seems to be splitting northwards, covering a lenticular body of microbreccia up to 2 km across. Its maximum penetrated thickness is 336.5 m (Bh. 1732). Microbreccia is mainly composed of psammitic-silty material of disintegrated rocks, i.e. siltstones and sandstones, the latter forming in places large blocks enclosed into the clastic matrix. At the same time, microbreccia often contains small fragments and minor blocks of shock-metamorphosed gneisses and fragments of impact glass. Larger clastic material prevails in the lower part of this lenticular body. In the transition zone to the crystalline megabreccia, the abundance of the corresponding fragments in microbreccia increases, similarly to the content of impact glass, which forming in places lenticular accumulations up to 5 m thick. Rock lenses, which should already be assigned to lithovitroclastic suevites, can also be distinguished there.

The above-mentioned allogenic breccia composed mostly of disintegrated material of sedimentary rocks and comprising suevite lenses, can be traced further northwestwards up to the axis of the annular trough where it peaking 460 m thick (Borehole 1783 at 7.5 km northwest of the axis of the annular uplift). It is replaced gradually in strike by megabreccia of sedimentary rocks. Borehole 1751 (Fig. 2.21) drilled in 4 km from the peak ring axis, in the area of continuous occurrence of the Quaternary deposits (the latter amounting there 70 m), penetrated the sequence of allogenic megabreccia of 260 m thick that is composed of klippe and blocks of the Cretaceous coaly sandstone at the top and the Upper Paleozoic mudstone and sandstone at the bottom, the cementing microbreccia contributing about 50%, though. In the central part of the sequence, the breccia comprises minor tagamite bodies with shocked gneiss fragments. It is underlain by the polymict breccia cemented by vitroclastic suevite, and, in places, tagamite. This breccia is traced downward in the section for about 130 m. The above data, as well as the results of drilling of several shallow boreholes in this area show that allogenic breccias and suevites occur under the continuous cover of the Quaternary sediments north of the Mayachika Upland in the upper part of the sequences infilling the annular trough.

Lens-like and sheet-like bodies of tagamites, suevites, and fine-grained, glass-free allogenic breccia overlie the slopes of the Mayachika Upland, but their sequences on inner and outer slopes of the annular uplift are different (Fig. 2.29). The main mass of impact melt-rocks on the outer slope consists of a lenticular body of lithic-vitroclastic to vitroclastic suevites overlain by an upper tagamite sheet. Their summary thickness peaks 284 m (Bh. 1022); the volumetric ratio of suevite to tagamite being 2:1 on the average. These units lie in a semicircular depression between the outcropping parautochthonous basement of peak ring and the crystalline megabreccia whose roof forms a steep morphologic rise of 750 m/km. A line of the maximum thickness of the impactite body is aligned to the axis of the peak ring but it displaces for about 2 km northwestward of the latter. As the distribution of thickness of both suevites and tagamites at the outer slope of the annular uplift shows (Fig. 2.30), the placing of impact melt bodies is controlled by the relief of the top of the underlying crystalline megabreccia.

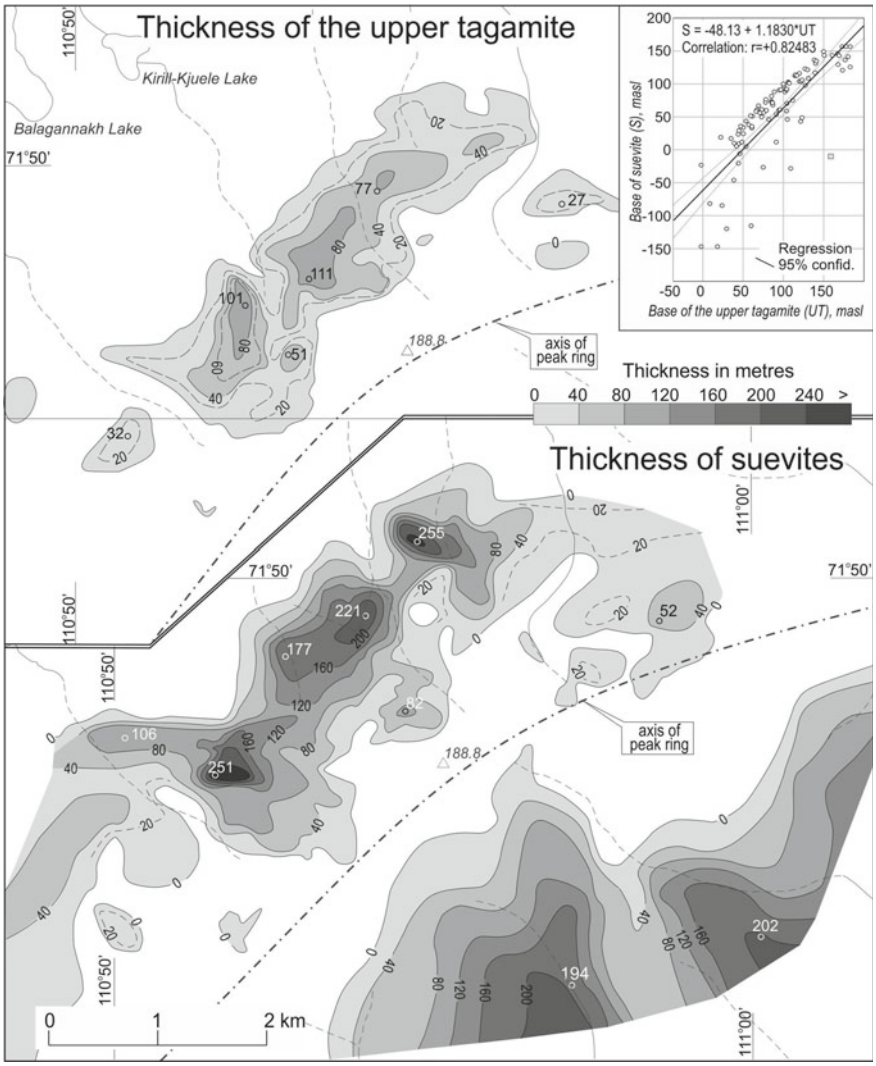

Fig. 2.30 Isopach map of the upper tagamite sheet (top) and of the suevite sheet (bottom) at slopes of the peak ring, Mayachika Upland area. Contour interval for main isopachs 40 m, for intermediate isopachs, 20 m. Peak thickness values (core data) are marked by white circles. At top right, a correlation diagram showing positive correlation (i.e. conformity) between base surfaces of suevite and tagamite sheets. The diversion of marks from the regression line to lower values of tagamite thickness shows that the initial thickness of the latter was greater before erosion; the removed tagamite thickness is estimated to range between 5 and 30 m

The suevites form a bowl-shaped body up to 2.3 km wide and about 8 km long; its base dips northwestward at angles of about 8°–15°. At northeastern and southern slopes of the Upland, the suevite body plunges under microbreccia or Quaternary

deposits. The maximum thicknesses of suevites (up to 252 m) are confined to the lower part of the uplift slope as far as 2.2 km from the uplift axis. High variability in thickness of suevites in a semicircular depression is caused by the uneven base reflecting an appropriate relief of the uplifted parautochthonous basement. Thus, the suevites are considered to fill in asperities of the top of the megabreccia. In turn, the variability of the thickness of the upper tagamite sheet is a result of its uneven original roof modified by recent erosion (Fig. 2.30).

The suevite sequence locally comprises thin (up to 20 m thick) tagamite sheet-like bodies traceable in adjacent boreholes for 500 m in places. Overall, suevites associating with tagamite sheets on the outer slope are vitroclastic, frequently welded, enriched in massive dark-coloured impact glass bombs and lumps. The thickness of such transitional horizons ranges from several dozens of cm to some meters. Tagamite is of brecciated structure (ataxitic) at contacts; thus, the latter are generally not sharp, transition takes place at a short distance, though.

Tagamite forms two thick sheeted bodies occurring at two hypsometric and stratigraphic levels. The upper body is cropping out on the northwestern slope of the Upland. It is subdivided by erosion into several fields. This body is of 0.8–1.3 km wide and up to 111 m thick (Fig. 2.30). Along the slope, it is traced for 5.5 km. As contrasted to the underlying suevite, it plunges northwestwards at a gentle angle (4°–5° on the whole); the base is relatively flat and do not correlate with the surface of the megabreccia.

The lower tagamite body is resting directly on the allogenic crystalline megabreccia, following the irregularities on its upper surface. On raise, it splits into two or three branches and then it is wedging out. Its thickness ranges from 20–70 to 100–150 m, it is traced for about 3 km along the uplift slope and for more than 4 km on dip towards the annular trough axis.

In addition to two major sheets, certain boreholes yield small, thin tagamite bodies among suevites, as well as among megabreccias after crystalline rocks and polymict breccias.

Tagamites forming sheeted bodies, contain inclusions of 0.5–2 cm or, less frequently, 5–15 cm in size, in places up to several meters, all these constituting not more than 5–10 vol%. These are predominantly different shocked and thermally metamorphosed crystalline rocks while dolerites, carbonaceous mudstones, quartzites and carbonate rocks are rare. Small (0.5–2 mm) clasts constitute from 5–10 to 20–25 vol% and are mainly made up of gneiss mineral fragments, including shocked ones. The matrix of tagamite is generally insignificantly crystallized; only within central parts of thicker bodies the rock is crystallized fully. Tagamite bodies are connected with both underlying and overlying rocks by gradual transitions via ataxitic tagamites and crystalline rock breccias cemented by tagamites.

Vitro-lithoclastic suevites and associated microbreccias crown the impact rock sequence on the outer slope of peak ring. They develop throughout the periphery of the Mayachika Upland on its slopes. Their thickness does not exceed 64 m. A significant contribution to the composition of these suevites is assigned by disintegrated material of diverse terrigenous rocks, predominantly of the Cretaceous. Microbreccia peaks 32 m thick; it is considered to represent the uppermost member of the sequence of

ejected and deposited material in this area because it occurs as sags in the roof of the upper tagamite body.

On the inner slope of the peak ring, the relief of the parautochthonous basement and the distribution of impact lithologies are less well confined due to the lack detailed data. Tagamites are absent there; suevites overlie directly on shocked gneisses or on the allogenic crystalline megabreccia. They are distinct from suevites described above and are represented mostly by a vitro-lithoclastic variety interlayred with microbreccia, the latter constituting about 25 vol%. The thickness of the suevites on the inner slope is increasing toward the central depression and peaks 202 m as close as 1.8 km from the annular uplift axis (Bh. −2320); the dip of its base is estimated to be about 10°.

The above data allow to outline the following conclusions concerning the structure of the Mayachika Upland area

1. The considered sector of the peak ring of crystalline rock is characterized by block structure of the parautochthonous authigenic breccia, and is noted for significant differences in surface elevations;
2. Crystalline rocks of peak ring underwent shock compression with the amplitude of not greater than 10 GPa;
3. The outer slope of the peak ring is steeper, than the inner one; the sequences of impact rocks overlying the authigenic breccia on both slopes differ considerably.
4. The parautochthon is overlain by the sequence of allogenic formations with crystalline rock megabreccias in the lower part, tagamites and suevites in the central part, and suevites and microbeccia in the upper one;
5. Away from the peak ring axis, towards the annular trough, tagamites and suevites enriched in impact glass seem to be replaced by the allogenic blocky and fine clastic breccias after sedimentary rocks and by suevites;
6. Two tagamites bodies separated by a thick suevite sheet develop at the outer slope of the annular uplift. The lower body is displaced relatively to the upper one for 0.5–1.0 km away from the axis of peak ring.
7. Upward in the impact rock section, there is a gradual flattening of the bedding of lenses and sheeted bodies of different allogenic breccias and impactites: the dispersion of hypsometry of the border surfaces decreases by a factor of four times from the bottom to top of the sequence. In addition, the axes of gravity mass for the upper units are displaced toward the crater center relative to the lower ones. Thus the centripetal tendency of this distribution exists.

2.3 Central Depression. Lower Daldyn Area

Basin of the lower course of the Daldyn River (Fig. 2.1) covers the central part of the Popigai hollow, which is a slightly rolling plain with absolute elevations of 40–60 m. The thickness of Quaternary deposits there reaches the first dozens of meters. Impactite and breccia exposures are on low uplands on the right bank of

the Daldyn River, and in the sources of the left tributaries of Daldyn River, i.e. the Parchanai and Balagannakh Creeks. Most of this area has no bedrock exposures; however, in its central part, several shallow boreholes were drilled (up to 200 m dip), which give an idea of the composition and structure of the upper horizons of impact rock sequences filling the central part of the crater. There are more data on areas adjoining to the inner western slope of peak ring (upper courses of the Parchanai and Balagannakh creeks) where suevites and tagamites are exposed on the surface of the Parchanai-Kerikete Upland and its southern extension. A deep borehole was drilled there (G-1, Fig. 2.21).

In the central part of the plain, the upper horizons of the crater fill judging by observations in borehole cores are composed of alternating suevite and microbreccia lenses of 10–80 m or more in thickness. This composite rock unit is of 160–170 m thick at least; however, on the watershed are with the Popigai River, it does not exceed 60–70 m thick. In the geometric centre of the crater (Borehole 5L), the thickness of an upper microbreccia lens is 150 m. Below the unit of alternating suevite and microbreccia, boreholes penetrate a continuous sequence of suevites, which are exposed within the above-mentioned uplands and comprise tagamite bodies.

Microbreccias penetrated by boreholes, are weakly cemented and comprise irregularly distributed angular fragments of various rocks (up to 10%) of 1–4 cm in size, as well as altered glass bombs. They comprise in places thin (up to 1 m) irregular suevite lenses filled with mineral clasts. Their contacts can be both abrupt and gradual. Suevites in this upper unit are commonly litho-vitroclastic, in certain cases they enclosing accretionary lapilli to 1 cm across, and in places, single glass bombs up to 20–30 cm across. One of the boreholes (Bh. 3L) at the depth of 131 m intersected a neptunian veinlet in suevites, made up of microbreccia material.

A more detailed inner structure of microbreccia units can be established from observations at one of the exposures on the right bank of the Daldyn River approximately 10 km upstream from the mouth of the Ulakhan-Yuryage Creek. These rocks are traceable here for approximately 300 m and are characterized by a distinct structure: flattened glass bombs, plate-shaped fragments and blocks of different rocks, suevite lenses up to 5–7 m thick are dipping northwards (350°–360°) at an angle of about 20°. Microbreccias contain abundant impact glass bombs of different size (from several cm to 1–2 m), in places ribbon-shaped and enclosing gneiss fragments; partly remolten and not completely homogenized crystalline rock blocks with a composite inner structure, in places zonal; fragments of different shocked rocks including those with shatter cones, as well as of intensely deformed rocks. Clastic material (its common size ranges from several cm to 0.5 m) is represented by lithologies of all formations of different age known in the vicinity of the impact crater, as well as of hypabyssal basic intrusions. Frequently, larger fragments and blocks (up to 5–8 m) of coal-bearing Cretaceous rocks occur, small pebbles, sideritized wood, as well as rock fragments with Cretaceous fauna. Characteristically, at contacts of bombs and impact glass lapilli (in places, the largest of them are slightly crystallized in the central parts; in places, they are porous and are impregnated with calcite). The microbreccias, which are cementing them, are commonly thermally metamorphosed and

compacted. The contribution of different fragments and blocks irregularly distributed in microbreccia is of about 10–15%.

The general idea of the structure of a deeper suevite and tagamite sequence is resulted from core observations in Borehole G-1 at the Parchanai Creek (Fig. 2.21), as well from some minor exposures. Down to about 60 m, the G-1 borehole penetrated suevites, in which the size and number of impact glass fragments and bombs to 20 cm across is increasing down in the section. A transition to massive tagamite, which is of about 60 m thick, is effected via a thin horizon of rather dense sintered suevites. Below, tagamite is again replaced by suevites by a gradual contact; a lower suevite sequence is of 360 m thick. These are mainly vitroclastic suevites with different rock fragments up to 20–30 cm across including both sedimentary rocks and shocked biotite-garnet and other gneisses. Further downward, massive tagamite was penetrated for 300 m. It contains not more than 5–10% crystalloclasts and fragments of altered crystalline rocks of 0.5–4.0 cm in size. In places, rare larger inclusions of these rocks including graphite-bearing gneisses occur. Irregular cavities in tagamites are filled in places with crystalline quartz; within thin fractures (located at 50°–60° to the core axis), zeolites and pyrrhotite develop. In the lower part of the tagamite body (below 760 m), there are isolated blocks of shocked gneisses up to 1–3 m across. The borehole had been stopped in one of them at the depth of 802.3 m; the contact surface is located at an angle of 30° to the core axis. Presumably, the appearance of numerous large inclusions is indicative of the proximity of the lower contact of the tagamite body; probably, the allogenic megabreccia is occurring in its base. Possibly, this breccia is, in its turn, resting on the crushed and shocked gneisses of the true crater bottom or, partly, on similar rocks in parautochthonous occurrence that form the inner slope of peak ring exposed on the surface at 5 km west of the borehole.

At some exposures on the Parchanai-Kerikete Upland, vitroclastic and vitrolithoclastic suevites are observed. They are distinguished by the relative abundance of glass fragments and other inclusions, their grain size, as well as colouring of rocks. The bleaching of the latter is connected commonly with an extensive development of smectites and other clay minerals, which are often accompanied by zeolites and calcite. In places, suevites comprise microbreccia lenses, blocks of molten shock-metamorphosed gneisses with zonal inner structure, and bombs of altered fluidal glass. Tagamites occur on the surface as submeridional ranges, the slopes of which are covered by talus of these rocks. At certain small exposures, suevites are predominantly recorded, in places they enclosing thin tagamite bodies, some of which may be injected into suevites.

Upstream of the confluence of two sources of Parchanai Creek, suevites serve as both roof and base of a small tagamite sheet traceable for 200–250 m; its thickness is of about 15–20 m. This layer passes into a subvertical body, subsiding under the water edge. Suevites are compacted at exocontact, and tagamites have a glassy character and contain cylindrical pores, normal to the contact surface. All these observations enable to presume that there are several injection tagamite bodies including steeply dipping ones. Possibly, the upper tagamite body penetrated by G-1 borehole is a subsurface extension of a discontinuous tagamite range, traceable meridionally for approximately 10 km.

Similar suevite and tagamite bodies, commonly poorly exposed, are recorded on gentle uplands at the watershed of the lower Daldyn and Popigai Rivers.

In general, formations of the crater fill in the central part of the crater are characterized by the following features:

1. Significant thickness, according to gravity data, probably reaching 2 km or more (see Sect. 1.4);
2. Three-membered structure of the crater fill: polymict allogenic megabreccia at the base; tagamite and suevite in the central part; suevite and microbreccia in the upper part;
3. Presence of injection tagamite bodies;
4. Features of relatively extensive low-temperature hydrothermal alteration of impactites and impact glass.

References

Danilin AI (1982) On characteristics of the inner structure of thick sequence of allogenic breccia and suevites in large astroblemes (in Russian). Meteoritika 40:102–106

Masaitis VL (ed) (1980) Geological map of the Popigai meteorite crater of 1:200 000 scale (in Russian). VSEGEI Press, Leningrad

Masaitis VL (2003) Obscure-bedded ejecta facies from the Popigai impact structure: lithological features and mode of origin. In: Koeberl C, Martinez-Ruiz FC (eds) Impact markers in the stratigraphic record. Springer, Berlin, pp 137–162

Masaitis VL, Mikhailov MS, Selivanovskaya TV (1975) The Popigai meteorite crater (in Russian). Nauka Press, Moscow, 124 pp

Masaitis VL, Danilin AN, Mashchak MS, Raikhlin AI, Selivanovskaya TV, Shadenkov EM (1980) The geology of astroblemes (in Russian). Nedra Press, Leningrad, 231 pp

Masaitis VL, Mashchak MS, Raikhlin AI, Selivanovskaya TV, Shafranovsky GI (1998) Diamond-bearing impactites of the Popigai astrobleme (in Russian). VSEGEI Press, St. Petersburg, 182 pp

Masaitis VL, Naumov MV, Mashchak MS (1999) Anatomy of the Popigai impact crater Russia. In: Dressler BO, Sharpton VL (eds) Large meteorite impacts and planetary evolution II. Geol Soc of America Spec Pap 339, pp 1–19

Masaitis VL, Mashchak MS, Naumov MV (2004) Popigai impact crater: guide of geological excursions. VSEGEI Press, St. Petersburg, 55 pp

Masaitis VL, Naumov MV, Mashchak MS (2005) Original diameter and depth of erosion of the Popigai impact crater Russia. In: Kenkmann T, Hörz F, Deutsch A (eds) Large meteorite impacts and planetary evolution III. Geol Soc of America Spec Pap 384, pp 131–140

Mashchak MS, Selivanovskaya TV (1988) Breccia and impactites at the southeastern rim of Popigai astrobleme (in Russian). Meteoritika 47:178–188

Chapter 3
Post-impact Geological Evolution Within the Crater and in Its Surroundings

Mikhail V. Naumov

After its rise, the Popigai crater was influenced by three main interrelated processes (1) tectonic deformation of the crater fill and host target rocks; (2) denudation of impact-generated and deformed target rocks; (3) deposition of late sediments.

3.1 Rupture Deformations of Target Rocks, Impact Breccias, and Impactites

The faulting within Popigai impact structure and in its surroundings caused to impact cratering was described briefly above. Extented faults and system of fissures, originated during successive stages of this process, immediately afterwards and long after, dissect the crater fill, remnants of ejecta blanket and the Precambrian, Paleozoic and Mesozoic target rocks. Not all of these ruptures may be distinguished according to the time of formation, e.g. belonging to any stage of cratering, or to post-impact tectonic deformation.

In general, three groups of fractures and faults differing by interrelation with bedrock, by succession of appearance, by kinematic parameters, and, in places, by shape may be outlined: (1) systems of syn-impact arched overthrusts and radial fissures appearing mainly in the platform sedimentary cover surrounding the crater, and displacements in crystalline basement in annular trough and peak ring as well as main radial and concentric faults; (2) post-impact faults and local fissures caused by recovery of the gravitational equilibrium inside the crater fill and underlying rocks; (3) proper post-impact tectonic faults occurred at the Late Cenozoic, some of them may be attributed to neotectonic movements.

The distinguishing of the proper post-impact deformation features from the patterns that belong to the regional tectonic framework on the one side and to the impact on the other side, is frequently ambiguous because of the post-impact movements

M. V. Naumov (✉)
A.P. Karpinsky Russian Geological Research Institute, Sredny prospekt, 74, 199106 Saint Petersburg, Russia
e-mail: m_naumov@mail.ru

V. L. Masaitis (ed.), *Popigai Impact Structure and its Diamond-Bearing Rocks*,
Impact Studies, https://doi.org/10.1007/978-3-319-77988-1_3

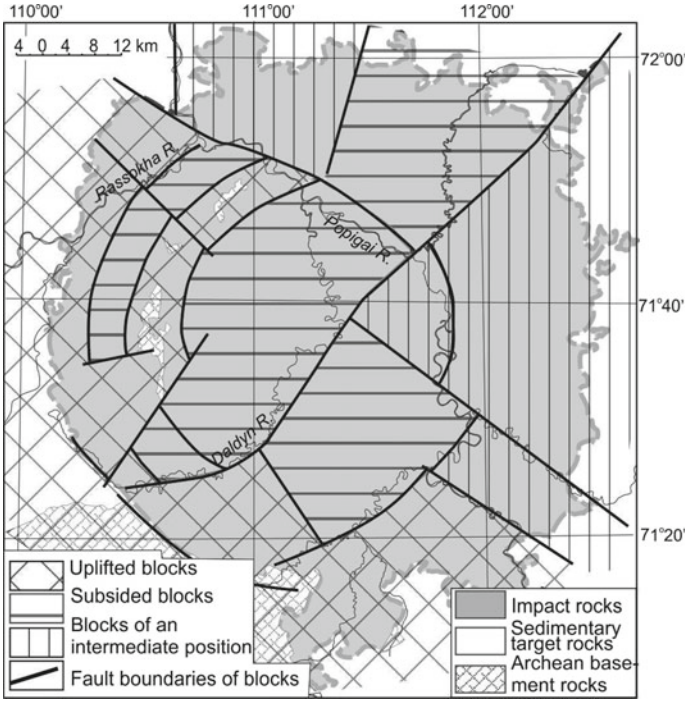

Fig. 3.1 Scheme of post-impact block structure of the Popigai crater (from Mashchak and Naumov 2005). The southern and western parts of the crater belong to the most elevated blocks. The central depression and some areas of the annular trough represent the most subsided blocks. The eastern and northern parts of the crater represent blocks of an intermediate position

exploit pre-impact fault systems, whereas a subsequent regional tectonism accentuates impact-related faults as well.

Inferred from topography and geological framework, the post-impact structure of the Popigai crater can be represented as a series of fault blocks (Mashchak and Naumov 2005). differing in extent and direction of vertical displacements (Fig. 3.1); Two groups of faults are distinguished: (1) radial and concentric faults, which have caused the present radial-concentric drainage pattern within the Popigai hollow, and (2) northwestward and south-westward oriented post-impact faults that have been caused by regional tectonics (a rise of the Anabar Shield) during the Neogene-Quaternary period (Novikov 1997). A typical radial fault zone is mapped at the southwestern sector of the crater (see Sect. 2.2.1). A maximum amplitude of vertical displacements estimated from sudden variations in thickness and altitude of post-impact sediments, reaches several hundred meters (Mashchak and Naumov 2005).

Apart from the block faulting, numerous smaller faults and fractures, which cut impact rocks, were found. These fractures are well-exposed on aerial photographs by lineaments of drainage pattern; by zones of abundant vegetation; by boundaries

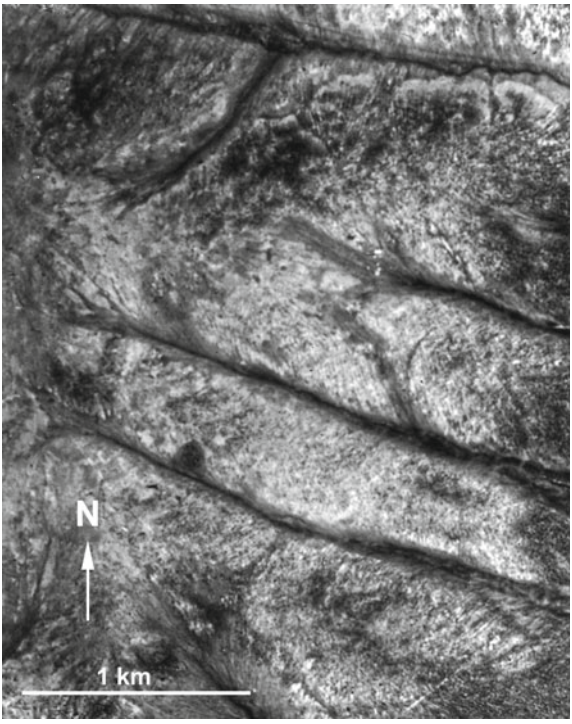

Fig. 3.2 Aerial photograph of a suevite field, showing well-exposed linear drainage pattern caused by faulting (the southern part of the crater, Chordu-Daldyn area)

between lithologies differing in colour and specific microrelief (Fig. 3.2). In some areas with thick sequences of lithic breccia, the density of faults and fractures is as much as 5–10 per 10 km^2. Individual faults don't exceed 5–6 km in length and show in places vertical or horizontal displacemens up to 10 m; however, tear fractures are predominant. A regular orientation pattern of fractures and faults has not been established.

Some observed ruptures caused by tension occurred in separate blocks. In a continuous outcrop on the right bank of the Chordu-Daldyn River, tagamites are cut by several clastic dikes, which are from 0.6 to 3.0 m thick and up to 30 m in length (Mashchak and Fedorova 1987). The dikes are of meridional orientation, their borders dip steeply westward. They are composed of psammitic-aleuritic material, which represents a product of disintegration and re-deposition of lithic microbreccias. The clastic components (10–15%) are from 0.5 to 20–25 cm across; they are represented by impact glass, carbonate rock, shale, coal, argillite, and rare crystalline rocks (including shocked ones). Any gradation or sorting are not observed. The groundmass is composed of fine fragments of minerals (quartz, feldspar) and clayey matrix.

It is of important to note that the neotectonic activity in the Popigai structure has not ceased up to today, for instance, the thickness of alluvial deposits in the Popigai River valley is determined by the recent displacements (Plotnikova 1990). In the

Popigai hollow some modern changes of riverbeds positions, shape of lakes etc. are resulted from the intense development of thermokarst.

3.2 Modification of the Crater Relief and the Neogene-Quaternary Sedimentation

The Popigai crater has been slightly modified by denudation and deposition during 35 Ma after its origin. The maximum depth of erosion is estimated to vary from about 100 m in the inner depression to 250–500 m at the southwestern rim of the crater. Denudation of the crater fill and ejecta blanket had been accompanied by accumulation of the products of their disintegration, and these processes repeated in time and again. Four periods of such modification can be distinguished (Fig. 3.3, Plotnikova 1990):

(1) Miocene to Early Pliocene. Inferred from paleogeographic reconstructions of the Anabar region, during Oligocene and Miocene both denudation of the upper part of the impact ejecta blanket and accumulation in lake basins (an over rim one in Oligocene and pit lake in Miocene) occurred. The strong erosion is supported by a warm, wet climate. The new-formed deposits were not thick and to the beginning of Pliocene were fully removed together with wast bank and most of the fall-out breccia and impactite bodies (Masaitis et al. 2005). More probably, some tagamite snouts were opened by erosion as early as in the end of Miocene because debris of this rock usually presents within Neogene-Quaternary deposits.
(2) Pliocene to Early Quaternary: local deposition of lake sediments (sands with gravel interbeds) under cool and dry climate. The topography of the Popigai hollow became very close to the actual image (Fig. 3.3d).
(3) Middle and Late Quaternary: repeated glaciations and formation of lake basins in the Popigai depression where sands, aleurites, gravels, and clays were deposited. The uplifting of the area at the end of Pleistocene caused a discharge of the lake northward along the Popigai valley.
(4) Holocene: formation of river valleys, alluvial, lacustrine-palustrine, eluvium, and eolian deposits.

The above reconstructions are based mostly on the evidences from modern relief and unconsolidated Neogene and Quaternary deposits. Distribution, composition, and age of these deposits were studied in detail using both surface exposures and numerous boreholes (unpublished reports of A.I. Raikhlin, M.I. Plotnikova, V.V. Chernoknizhnikov, and others).

The early crater lake deposits are not preserved in the Popigai. However, finds of re-deposited Paleogene diatoms in Quaternary deposits give a hint about possible occurrence of Eocene deposits, which could be removed during the long denudation period that lasted for 30 Myr. Accumulation processes in the crater recommence as late as in the end of Neogene. So, the most of the Popigai hollow is filled in by

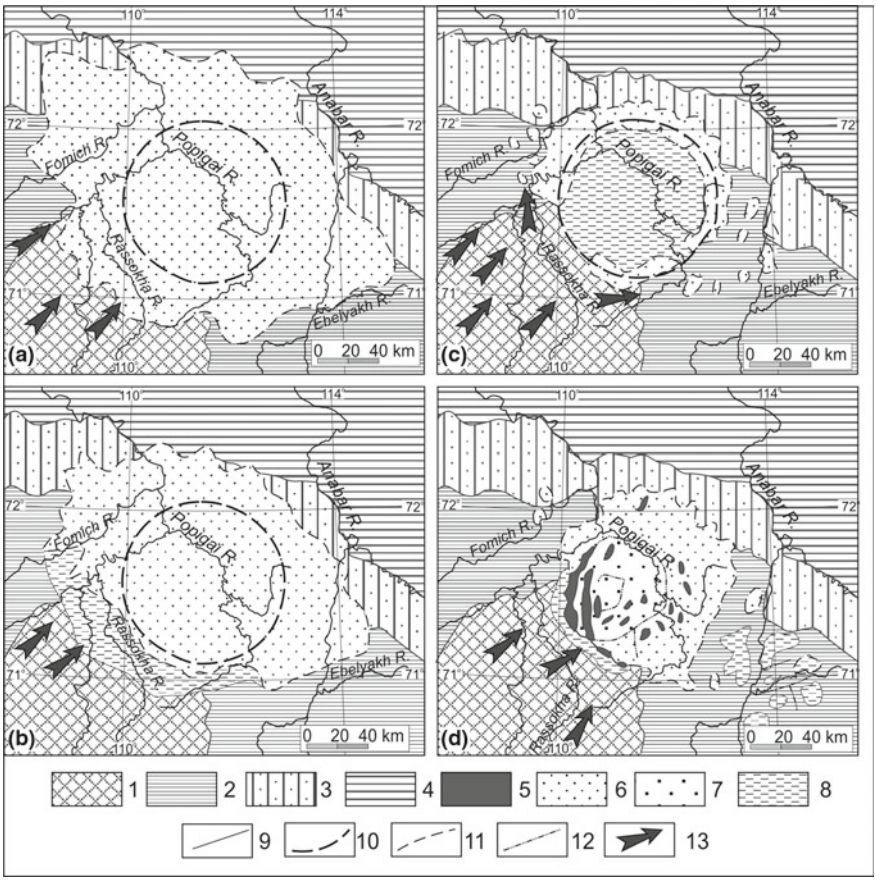

Fig. 3.3 Paleogeographic charts of the Popigai morphostructure. **a** in Oligocene; **b** in Late Oligocene–Early Miocene; **c** in Miocene, **d** in Late Pliocene–Early Quaternary (from Plotnikova 1990), Paleogeographic areas: 1—low-elevation denudation plateau on Early Precambrian crystalline rocks, 2—low-elevation structural-denudation plateau on Neoproterozoic and Cambrian sedimentary rocks, 3—low-elevation structural-denudation plateau on Upper Paleozoic rocks, 4—structural-denudation plain on Jurassic and Cretaceous sedimentary rocks, 5—denudation ridges on tagamite, 6—accumulative and denudation relief on suevite and lithic breccia, 7—lake and lake-alluvial plain, 8—lake basins, 9—assumed borders of paleogeographic areas, 10—outer border of annular trough, 11—assumed limit of impact-related rocks, 12—assumed paleo-river valleys, 13—assumed paleo-currents directions

Pliocene-Quaternary and Quaternary deposits of variable genetic types. The thickness of post-impact sediments is clearly controlled by the impact morphostructure, recent tectonics and composition of the bedrock contributing to a lesser extent (Plotnikova 1990). The maximum thickness of post-impact sediments occurs within radial trenches. It peakes 90–102 m in valleys of Dogoi and Arbangda rivers intersecting the eastern edge of the crater. In the annular trough, Pliocene and Quaternary deposits

Table 3.1 Stratigraphic chart of Neogene-Quaternary deposits in the Popigai depression

Series	Stage	Regional horizon	Genetic type	Lithology	Max. thickness, m
Holocene			Allivial; lacustrine-palustrine; eluvium, deluvium, kolluvium and solifluction; eolian	Loamy sand, sandy loam with peat interbeds, boulder and pebble gravels, clays, find sands (eolian)	20–22
Pleistocene	Upper	Sartan	Glacial and glaciofluvial	Sands, gravels, boulder gravels	1.5–2
		Kargin	Limnic, limnic-alluvial and glaciolimnic	Pebble gravels, brownish-yellow polymict sands, varved clay, aleurite	20
		Murukta	Glaciolimnic and limnic	Varved aleurite and clays with ice, sand, and peat lenses	40
	Middle	Kazantsev	Limnic-alluvial and alluvial	Cross-bedded grey sands with gravel interbeds	77
	Lower		Alluvial	Pebble conglomerate	4.3
Pliocene			Limnic-alluvial	Cross-bedded, pinkish-grey, quartz-feldspathic sands with gravel interbeds	32

peak 80 m thick. The moderate thickness (from 8–16 to 25–27 m) is a feature of the central depression.

The stratigraphic column of post-impact deposits is given in Table 3.1. The stratigraphic age of certain members is well-founded by spore-pollen assemblages (Vasilyeva 1989; Plotnikova 1990, unpublished data of Bobrov et al. 1990). The sketch map of distribution of Neogene-Quaternary deposits is shown on Fig. 3.4.

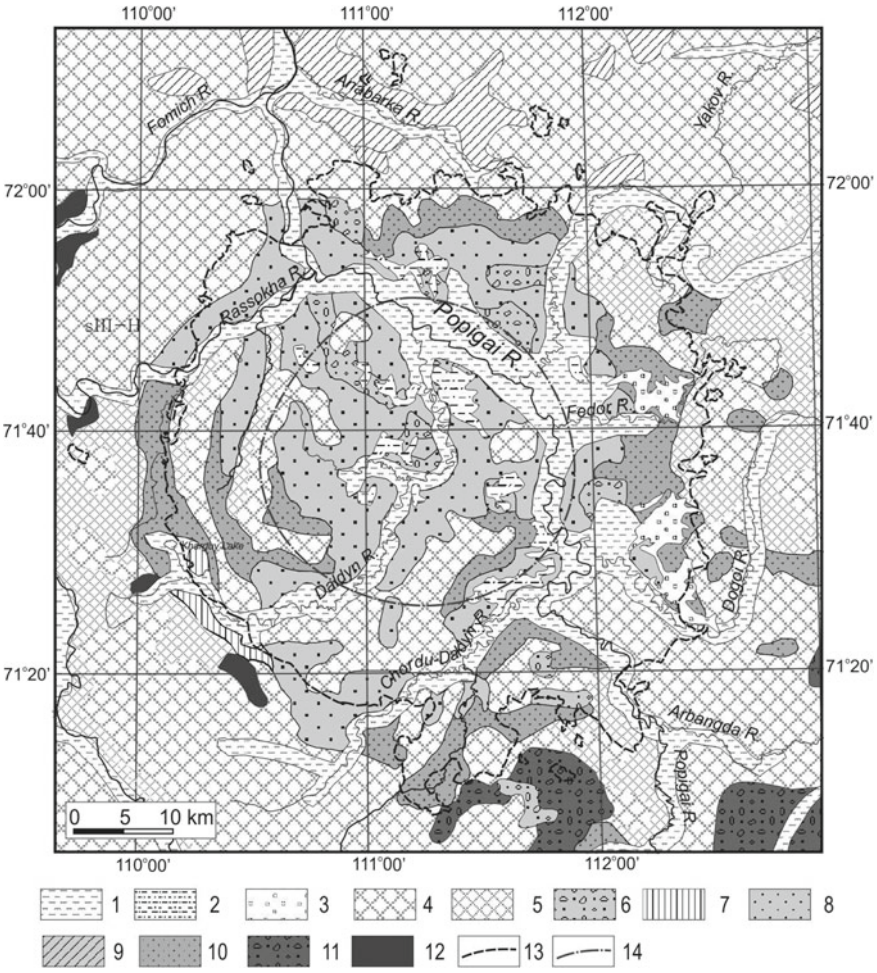

Fig. 3.4 Sketch map of Neogene-Quaternary deposits in the Popigai area. Compiled using Masaitis (1980), and data from unpublished Technical Reports prepared by M.I. Plotnikova, V.V. Chernoknizhnicov, A.I. Raikhlin, A.V. Matyushkov, and other reshearchers. 1–3—Holocene: alluvial sands, aleurite, and gravel (1), lacustrine-palustrine clays, loams, peat, and sands (2), eolian sands (3). 4–7—Upper Pleistocene to Holocene: eluvium, solifluction, and deserption scree and rock fields (4), solifluction and deluvial deposits (5), limnic sand, aleurite, clay, loam, gravel (6), glaciofluvial sands, gravels, boulder gravels of the Sartan glaciation (7). 8—Upper Pleistocene, Kargin horizon: limnic, limnic-alluvial and glaciolimnic sands with gravel interbeds, varved clay, aleurite. 9—Upper Pleistocene, Murukta horizon: limnic and glaciolimnic deposits. 10—Middle to Upper Pleistocene, Kazantsev horizon: limnic-alluvial and alluvial sands, varved aleurite and clays with ice and pit lenses. 11—Pliocene-Lower Quaternary: cross-bedded limnic-alluvial sands and gravels. 12—Pre-Pliocene lithologies, 13—border line of impact rock area, 14—axis of peak ring

Pliocene-Quaternary limnic-alluvial deposits occur in two positions: (1) they form rare outliers at the altitude of 230–295 m along the southern edge of the crater and

south of the crater rim; (2) at the base of thick Quaternary sequences filling in erosion depressions inside the crater at the altitude of 20–25 m. They are dominated by poorly sorted arkoses of 4–5 to 25–27 m thick, in places, boulder gravels occur at the base raising the thickness up to 32 m. In places, gravels contribute up to 90% of the sequence. The composition of pebbles and boulders is determined by the underlain bedrock. The contribution of impactite pebbles ranges from 0.8 to 55%.

Deposits of the Lower Pleistocene are observed in the only location—in the thickest Quaternary sequence (102 m) in the Dogoi River valley (the eastern edge of the impact structure). These are pebble conglomerate composed of pebbles of Proterozoic and Cambrian target rocks cemented by carbonate.

Limnic and alluvial deposits of the Middle to Upper Pleistocene are widespread through the eastern of the Popigai depression and eastward of its eastern edge (at the Popigai-Anabar interfluve) where they are as thick as 77 m (at Arbangda River). Commonly, its thickness is of 5–30 m. The deposits fill in structural and carst grooves and at the Popigai hollow, pebble gravels contribute considerably; they form interlayers up to 18–20 m thick and in places predominate in the sequence.

Upper Pleistocene glaciolimnic and limnic deposits of the Murukta horizon develop locally north of the Popigai depression while younger limnic, limnic-alluvial and glaciolimnic sediments of the Kargin horizon are facially replaced to one another both within the depression and on its edges filling in erosional hollows. At the bottom, pebble gravels develop, at the top, brownish-yellow polymictic sands with gravel interbeds, varved clay, aleurite.

At the base of the Holocene section, a thin layer of the glacial of the Sartan horizon occur locally in the southwestern part of the Popigai depression (the upstream of the Daldyn River).

The recent deposits are widespread through the depression and its surroundings. They include six formations: (1) alluvial covering all main valleys up to 7–8 km wide. Flood-plain deposits (loamy sand, sandy loam with peat interbeds, fine-grained sands up to 12 m of total thickness), channel deposits up to 17 m thick (boulder and pebble gravels in the western, pinkish-grey sands in the eastern), and cutoff deposits (bluish-grey clays and loams) can be distinguished. (2) Lacustrine-palustrine deposits—muddy sands, loams, peat—are of no more than 1–2 m thick but in the central depression of the crater peak locally 4–5 m. (3) Eluvium and solifluction deposits develop everywhere at interfluve plains; these are block (over gneisses, sandstone, dolomite) or rubble (over impactite) scree of 0.5–6 m thick. (4) Deluvium and solifluction deposits (2–5 m) develop at structural slopes of soft rocks (microbrecia, Pliocene-Quaternary sediments). (5) Deluvium and kolluvium deposits (up to 10 m), at structural slopes of solid rocks (impactite, target gneiss, dolomite, sandstone etc.). (6) Eolian fine sands (of 1–3 m thick) are widespread in the eastern part of the Popigai hollow (Allara-Tokulama and Kyukyur-Tokulama river basins) where they are appearing due to deflation of terraces composed of Middle to Late Quaternary sediments.

References

Masaitis VL (ed) (1980) Geological map of the Popigai meteorite crater of 1:200 000 scale (in Russian). VSEGEI Press, Leningrad

Masaitis VL, Naumov MV, Mashchak MS (2005) Original diameter and depth of erosion of the Popigai impact crater Russia. In: Kenkmann T, Hörz F, Deutsch A (eds) Large meteorite impacts and planetary evolution III. Geol Soc of America Spec Pap 384, pp 131–140

Mashchak MS, Fedorova IG (1987) Composition and conditions of formation of clastic dikes in tagamites of the Popigai astrobleme (in Russian). Meteoritika 46:124–127

Mashchak MS, Naumov MV (2005) Late modification-stage tectonic deformation of the Popigai impact structure Russia. In: Koeberl C, Henkel H (eds) Impact tectonics. Springer, Berlin, pp 191–210

Novikov IS (1997) Denudation periods and Cenozoic evolution of relief in the northwestern part of the Anabar anteclise (in Russian). Russ Geol Geophys 38:1465–1474

Plotnikova MI (1990) Essay on post-Oligocene history of the Popigai impact morphostructure (in Russian). Meteoritika 49:154–164

Vasilyeva MN (1989) State geological map of the USSR of 1:200 000 scale. Sheet R-49-V, VI. Explanatory notes (in Russian). Ministry of Geology of USSR, Moscow, 92 pp

Chapter 4
Petrography of Shock-Metamorphosed Crystalline Rocks and Impactites

Victor L. Masaitis, Anatoly I. Raikhlin, Tatjana V. Selivanovskaya, Mikhail S. Mashchak and Mikhail V. Naumov

4.1 Crystalline Target Rocks and Their Shock Metamorphic Features

Petrography of shock-metamorphosed rocks and impactites in the Popigai astrobleme was first characterized by the authors in a number of papers (Masaitis and Selivanovskaya 1972; Masaitis et al. 1971, 1972, 1975, 1980 etc.); they are also described in some publications of other researchers (Vishnevsky and Montanary 1999; Whitehead et al. 2002).

As noted above, various features of shock metamorphism are recorded in crystalline rocks of peak ring, and, partly, within the floor of the annular trough. Shock metamorphism is much more distinct in the clastic material comprised in allogenic lithic breccias, suevites, and tagamites. At the same time, in the two last-mentioned rock varieties, features of shock metamorphism of the therein-enclosed fragments and blocks are often vague due to the subsequent impact of high temperatures, as well as superimposed hydrothermal alterations. Sedimentary rocks occurring in allogenic breccias as blocks and fragments, display shock alteration, which is much weaker as compared to gneiss; it is mainly manifested as jointing, crushing, mortar structures, and shatter cones.

V. L. Masaitis (✉) · A. I. Raikhlin · T. V. Selivanovskaya · M. S. Mashchak · M. V. Naumov
A.P. Karpinsky Russian Geological Research Institute, Sredny prospekt, 74 199106 Saint Petersburg, Russia
e-mail: vcmsts@mail.ru; victor_masaitis@vsegei.ru

M. V. Naumov
e-mail: m_naumov@mail.ru

V. L. Masaitis (ed.), *Popigai Impact Structure and its Diamond-Bearing Rocks*,
Impact Studies, https://doi.org/10.1007/978-3-319-77988-1_4

4.1.1 Brief Characteristic of Gneisses

As shown above, the rocks making up the true bottom of the impact structure and studied mainly in its western part, are predominantly represented by high-alumina gneisses and plagiogneisses, often graphite-bearing (biotite-garnet, biotite-garnet-sillimanite, biotite-garnet-sillimanite-cordierite) and calcareous-silicate garnet-bearing gneisses and plagiogneisses (biotite-hypersthene, biotite-bipyroxene, and biotite-salite). There are also lenses of high-calcareous rocks (marbles, calci phyres, salite-scapolite rocks). Charnokites occur in migmatization and granitization zones. Allogenic lithic breccias and impactites contain crystalline rock fragments of all above varieties; however, shocked fragments are dominated by garnet-bearing gneisses and plagiogneisses. Only tagamites in the southeastern sector are noted for the predominance of pyroxene gneisses and plagiogneisses among crystalline rocks inclusions.

Gneisses and plagiogneisses are leuco-, meso-, and melanocratic rocks with the grain size of 0.5–2 mm and gneissic structure. Commonly, they are of the granoblastic texture combining with poikiloblastic texture. Garnet gneisses are frequently noted for the porphyroblastic texture; sillimanite gneisses, for the nematoblastic texture; and cordierite gneisses, for the symplectic one. The main rock-forming minerals are plagioclase (35–70%), quartz (10–35%), and biotite (2–17%). Orthoclase constitutes up to 30% of the gneiss volume; in granitized varieties, microcline develops. In pyroxene gneisses and plagiogneisses, hypersthene constitutes up to 25 vol%, while salite, up to 45 vol%. In melanocratic varieties, the summary content of pyroxenes reaches 80 vol% or even more. In biotite-garnet gneiss, garnet takes up about a half of the rock volume in places, and sillimanite in biotite-garnet-sillimanite gneiss, to 20 vol%. Cordierite in the corresponding rocks makes up their essential portion, i.e. up to 30–45%. High-alumina rocks also contain the first percents of graphite, spinel, and hypersthene. Calcic-silicate lithologies contain garnet and titanite. Tenths of a percent are made up by magnetite, ilmenite, pyrrhotite, apatite, zircon, rutile, monazite; in cordierite-bearing gneisses, chromite occurs in addition.

Plagioclase is represented by acid and intermediate andesine (Table 4.1), sericitized locally. In melanocratic plagiogneisses, it corresponds to the basic andesine $An_{46–48}$. There are poikiloblasts with quartz, hypersthene, and salite inclusions. Quartz occurs irregularly forming lenticular segregations aligned with banding. Alkali feldspar is represented by the orthoclase granoblasts with microperthite plagioclase growths (Table 3.1), corresponding by its composition to orthoclase-microperthite from pyroxene granulites (Dobretsov et al. 1971). Porphyroblasts of latticed microcline also occur on granitization areas.

Salite forms irregular or oblong prismatic grains of a light green colour. In crystalline schists, it is the main rock-forming mineral and is represented by poikiloblasts with frequent growths of basic plagioclase. It often localizes as bands along banding of the rock. The composition of salite (Table 4.1) is characterized by a high and stable magnesium content, a low iron content and a low CaO/(CaO+MgO+FeO) ratio, which corresponds to the intermediate salite-augite, characteristic of granulite

Table 4.1 Average compositions of main minerals from gneiss (EMP data)

Gneiss composition	SiO_2	TiO_2	Al_2O_3	FeO	MnO	MgO	CaO	Na_2O	K_2O	Total	n	FeO, mol%	MgO, mol%	CaO, mol%	Na_2O, mol%	K_2O, mol%
Plagioclase																
Bt+CPx+Opx	59.00	–	25.26	–	–	–	8.61	6.27	0.45	99.59	2	–	–	42	55	3
Bt+CPx	60.23	–	24.96	–	–	–	8.16	6.25	0.48	100.08	9	–	–	41	56	3
Bt+OPx and Bt+Grt+Opx	59.53	–	26.2	–	–	–	6.12	7.82	0.14	99.81	7	–	–	30	69	1
Bt+Grt	59.59	–	25.05	–	–	–	6.84	7.32	0.52	99.32	6	–	–	33	64	3
Bt+Grt+Sill and Bt+Grt+Sill+Cord	58.6	0.02	26	0.06	–	0.01	7.51	7.27	0.72	100.19	11	–	–	35	61	4
Orthoclase																
Bt+OPx and Bt+Grt+Opx	64.94	–	19.86	–	–	–	0.49	1.79	13.41	100.49	2	–	–	3	16	81
Bt+Grt+Sill and Bt+Grt+Sill+Cord	64.29	–	19.45	0.13	–	0.06	0.66	2.65	11.69	98.93	3	–	–	3	25	72
Salite																
Bt+CPx+Opx	51.37	0.69	1.38	11.4	0.24	14.3	19.96	–	–	99.34	10	18	41	41	–	–
Bt+CPx	52.35	0.46	1.2	8.36	0.18	14.58	22.86	–	–	99.99	9	13	41	46	–	–
Hypersthene																
Bt+CPx+Opx	51.79	0.25	3.94	19.76	0.38	23.22	0.83	–	–	100.17	7	32	66	2	–	–
Bt+OPx and Bt+Grt+Opx	50.4	0.11	2.83	25.97	0.38	19.8	0.17	–	–	99.66	3	42	57	1	–	–
Bt+Grt	49.34	0.23	5.29	24.92	0.22	19.79	0.18	–	–	99.97	8	41	58	1	–	–
Bt+Grt+Sill and Bt+Grt+Sill+Cord	50.19	0.44	4.33	24.52	0.27	19.93	0.22	0.06	0.12	100.08	7	41	58	1	–	–
Biotite																
Bt+CPx+Opx	37.15	4.65	14.65	18.28	0.16	13.04	0.32	0.18	9.15	97.58	6	44	56	–	–	–
Bt+OPx and Bt+Grt+Opx	36.35	5.49	16.03	15.73	0.05	13.65	0.41	–	8.96	96.67	11	40	60	–	–	–

(continued)

Table 4.1 (continued)

Gneiss composition	SiO_2	TiO_2	Al_2O_3	FeO	MnO	MgO	CaO	Na_2O	K_2O	Total	n	FeO, mol%	MgO, mol%	CaO, mol%	Na_2O, mol%	K_2O, mol%
Bt+Grt	36.44	6.9	15.53	14.46	0.03	13.86	0.54	–	9.21	96.97	4	37	63	–	–	–
Bt+Grt+Sill and Bt+Grt+Sill+Cord	36.75	5.97	15.61	13.62	0.04	14.58	0.28	–	9.17	96.02	11	34	66	–	–	–
Garnet																
Bt+OPx and Bt+Grt+Opx	36.8	0.03	22.6	32.53	0.52	6.52	–	–	–	100.01	9	71	26	3	–	–
Bt+Grt	38.59	0.02	22.17	28.26	0.65	8.62	–	–	–	99.57	8	62	34	4	–	–
Bt+Grt+Sill and Bt+Grt+Sill+Cord	38.16	0.04	22.45	29.62	0.49	8.27	–	–	–	100.73	9	64	32	5	–	–
Sillimanite																
Bt+Grt+Sill and Bt+Grt+Sill+Cord	34.65	–	62.66	0.58	–	0.24	0.14	0.57	0.5	99.34	16	–	–	–	–	–
Cordierite																
Bt+Grt+Sill and Bt+Grt+Sill+Cord	47.72	0.05	33.41	8.2	0.07	9.07	0.03	0.08	0.82	99.45	21	–	–	–	–	–
Spinel																
Bt+Grt+Sill and Bt+Grt+Sill+Cord	0.55	0.15	60.61	28.16	0.17	7.75	–	–	–	100.32[a]	14	–	–	–	–	–
Hornblende																
Bt+CPx+Opx	44.54	2.05	10.42	8.77	0.1	15.6	11.55	0.25	0.96	94.68[b]	4	24	76	–	–	–
Bastite																
Bt+OPx and Bt+Grt+Opx	38.37	0.19	8.15	25.42	0.26	12.64	1.24	–	0.05	86.32	2	–	–	–	–	–

n—Number of analyses. Total Fe as FeO

[a]Plus 2.93% Cr_2O_3 in analysis

[b]Plus 0.44% Cr_2O_3 in analysis 0.44%

complexes (Dobretsov et al. 1971). In the bipyroxene gneisses, composition of salite is noted for a marked reduction of iron content and increase of calcium content, along with a constantly high magnesium content, which is directly dependent on the composition of initial rocks. In granitization areas, salite is partly or fully replaced by the brown-green hastingsite hornblende (Table 4.1).

Hypersthene most often occurs as relatively large prisms with a sinuous outline. There are frequent poikilocrysts to 2–3 mm with plagioclase and quartz inclusions. The characteristic feature of the composition (Table 4.1) is a constantly high content of alumina, a low content of calcium, and magnesium to iron ratio, which is typical of the granulite complex of the Anabar Shield (Vishnevsky 1978). The observed differences in the content of iron, magnesium, and alumina are directly related to the concentration of these components in host rocks. Primarily hypersthenes from parageneses with spinel are noted for a high alumina content (6.13% Al_2O_3). The highest magnesium content (26.44%) is recorded in hypersthene from bipyroxene plagiogneisses. Along fissures and around the periphery of grains, and, in rare cases, totally, hypersthene is replaced by the finely structured serpentine-chlorite aggregate of a light brown colour, possibly, bastite (Table 4.1).

Biotite commonly occurs as bands in the rock and is represented by yellow-brown scales, oriented along banding. Its composition (Table 4.1) is characterized by a constantly high titanium content. In the rock series from calcareous-silicate to high-alumina, the content of titanium, alumina, and magnesium in biotite increases, and that of silica, iron, and manganese decreases. Such a change in the composition might be due not only to the composition of host rocks, but also to the increasing metamorphic grade; there occurs a reduction of Mn, Fe content and a simultaneous increase of Ti, Mg, Cr, and V amounts. Biotites in rocks of a low metamorphic grade are characterized by a higher Si content and a lower Al content as compared to biotites in rocks of the intermediate and high grades (Perchuk et al. 1985).

Garnet is represented by rounded, in places faced crystals or porphyry poikiloblasts up to 6–8 mm of the pyrope-almandine series (Table 4.1). Its composition varires insignificantly; it is characterized by a high-alumina and iron content and a rather low content of the grossular constituent. Such features are typical of garnets from granulite complexes (Vishnevsky 1978).

Sillimanite forms oblong colourless prisms with rounded edges and commonly with distinct transverse cleavage. Locally, certain individuals are replaced by the low-birefringent micaceous aggregate. This mineral is often intergrown with garnet. The composition of sillimanite (Table 4.1) is noted for the low silica content, increased alumina content, and an admixture of abundant constituents, which are more typical of kyanite.

Cordierite commonly forms large grains with a composite polysynthetically sectorial twinning. In places, pleochroic halos around small zircon, rutile, and monazite grains are observed. Often particularly in granitization areas, it is replaced by serpophite or talc-serpentine aggregate. The composition of cordierite (Table 4.1) is noted for a slightly elevated total content of iron and magnesium. It constantly contains small simplectite growths of brown-green spinel and, in places, chromite of

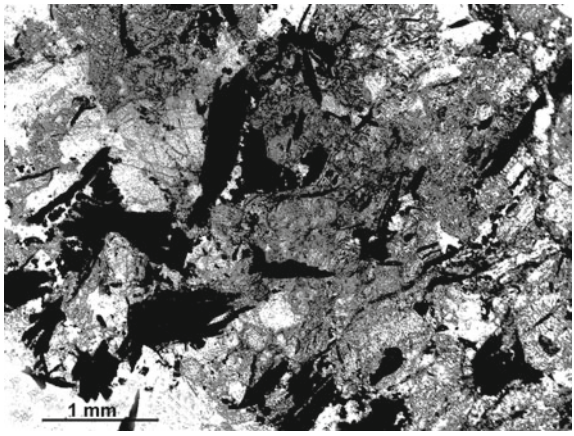

Fig. 4.1 Biotite-garnet-cordierite gneiss with numerous tabular grains of graphite (black). Microphotograph, parallel nicoles

different shape. By its composition (Table 4.1), spinel corresponds to magnesioferrite with chromium content of 1.3–4.1%.

Graphite prevails as oblong laminae with the sides ratio from 1:4 to 1:10 (Fig. 4.1). In rare instances, there occur relatively isometric plates. There were intergrowths of several differently oriented scales; in quartzitic gneisses graphite segregations reach several millimetres. The predominant size of the latter is 0.4–0.8 mm; however, there are also scales, which are up to 2 mm long. Graphite is mostly confined to the quartz-feldspar areas, where it mainly occurs as intergrowths in quartz and feldspars; in these cases, such segregations might be up to the first centimeters across. There are quartz and feldspar granoblasts, containing accumulations of differently oriented graphite scales. The highest graphite contents are characteristic of biotite-garnet-sillimanite-cordierite gneisses.

The compositions of the main rock-forming minerals (Table 4.1) and the observed parageneses from the abyssal (Hy+Cord+Ort, Sill+Gr+Bt, Gr+Hy+CPx) to the medium-depth (Sill+Gr+Cord+Ort) subfacies (Vishnevsky 1978; Bucher and Grapes 2011) indicate that gneisses and plagiogneisses formed under granulite facies of moderate and elevated pressures.

Marbles and calciphyres are medium-, more frequently coarse-grained rocks of yellow, cream, or greenish-grey colour with the prevailing heterogranoblastic texture and gneissoid, or, in places, massive structure. Monomineral marbles are rare; there are frequent mica, graphite, in places diopside scales. Most of calciphyres are composed of calcite (70–80%) and subsidiary diopside; in places, wollastonite, feldspars, and quartz occur in addition. There are calciphyres with a more diverse composition, where silicate minerals exceed the amount of calcite. Along with the constantly present calcite, feldspars and quartz, they also comprise different shares of diopside, wollastonite, scapolite, phlogopite, talc, serpentine, forsterite, or more often its replacement products, as well as spinel, titanite, and apatite.

Scapolite-salite rocks form lenses or separate bands among calciphyres or bipyroxene and salite plagiogneisses. There are inequigranular meso-melanocratic rocks of greenish-grey colour with diablastic or granoblastic texture and massive structure. They are made up of approximately equal amounts of salite and scapolite or scapolitized plagioclase, which are in intergrowth. Salite has a bright green colour, Inferred from its optical properties corresponds to of ferruginous diopside. Scapolite is represented by high-calcium meionite; and plagioclase, by andesine or labrador. The rock also constantly contains calcite as granoblasts and titanite as accumulations of small, often irregular grains; their content can reach 3–5%. Ore minerals and apatite are rare.

Gneissoid hypersthene granite (charnokites) are particularly widespread among pyroxene gneisses. These are medium- or coarse-grained inequigranular rocks of a brownish-yellow, less frequently yellowish-red colour. Their texture is granoblastic or blastocataclastic; less frequently allotriomorphic granular and porphyroid. The main rock volume is taken up by plagioclase, potassium feldspar and quartz, with the general predominance of plagioclase. Hypersthene, biotite, plus, in places, salite and hornblende do not exceed 15 vol%. Among the accesories, magnetite, pyrrhotite, allanite, and apatite are characteristic. Plagioclase is often represented by sericitized oligoclase or andesine; and alkali feldspar, by orthoclase, or, in migmatization zones, by microcline. Migmatites accompanying charnokites have a coarse crystalline texture and an irregular distribution of the constituent minerals, represented by quartz, microcline, and plagioclase in different proportions, with rare biotite scales and single magnetite and zircon grains.

4.1.2 Mineralogical Criteria of the Shock Metamorphic Parameters

Data on alteration of tectosilicates are commonly used as the basic criteria of the shock compression degree of crystalline rocks and the constituent minerals (Stöffler 1971; Val'ter and Ryabenko 1977; Ryabenko 1982; Basilevsky et al. 1983; Feldman 1990; Stöffler and Langenhorst 1994; Grieve et al. 1996; French and Koeberl 2010, etc.).

There were repeated attempts to determine the value of the loads applied with a very high precision, for example, to tenths of GPa. In this connection, it is necessary to make a few remarks. Firstly, the precise evaluations have certain sense only if the samples are taken from the autochthon or parautochthon (i.e. target rocks), which can allow to restore the zonation of the character of their attenuation in space, etc. Secondly, the differences in the initial temperature of rocks, subject to shock compression, which are difficult to access and which affect the intensity of alterations under the same load, should be taken into account. Thirdly, account should be taken of a significant dynamic inhomogeneity of rock masses, of a complex action of the stress waves on them, particularly in case of large-scale impact processes, influence

Table 4.2 Progressive shock metamorphism of crystalline feldspar-bearing rocks (Grieve et al. 1996)

Stage of shock metamorphism	Pressure, GPa	Post-shock temperature, °C	Shock-metamorphic effects in quartz and feldspars
0	<5 to 10	<100	Irregular fractures
Ia	5 to 10–20	100–170	Planar fractures and planar deformation features (PDF)
Iб	20–35	170–300	PDF, reduced refractive indexes, stishovite, traces of coesite
II	35–45	300–900	Diaplectic glasses, coesite and traces of stishovite
III	45–60	900–1200	Diaplectic glasses, homogeneous ("monomineral") fusion glass (e.g. lechatelierite), coesite
IV	60–100	1200–2500	Heterogeneous fusion glasses (complete melting of the rock)
V	>100	>2500	Volatilization

of fluid phases, etc. The last two circumstances, which are not easily registered precisely, can result in the shift of estimates, amounting to 5–10 GPa. In most cases, the use of the integral averaged estimates of the shock alteration parameters in rock volumes about $n \times 10^6$ to $n \times 10^8$ m^3 is commonly quite sufficient for the practical purposes.

Another feature of the shock wave alterations in rock masses, which is not always taken into account in the analysis of these processes, should be emphasized. These are the shear stresses, which are accompanying or directly following the rarefaction wave, and can result in brittle destruction of rocks even under a relatively weak shock compression; and in case of significant shock loads, to flow of the molten material. This leads to crushing, cataclasis, mixing of rock substance and, eventually, to generation of homogenized impact melt masses.

In the present section, the evaluations of the shock compression amplitude are given, proceeding from the main criteria, established using experimental evidence (Stöffler and Langenhorst 1994; Grieve et al. 1996) and generally presented in Table 4.2.

Though there are not distinct boundaries between the distinguished alteration stages, they should be considered within certain intervals of the shock loads, applied to the rocks and constituent minerals.

4.1.3 Weakly and Moderately Shock-Metamorphosed Rocks

Gneisses and other crystalline rocks, subject to weak (to 10–20 GPa) and moderate (20–35 GPa) shock loads, are characterized by different diaplectic altrerations, including brittle deformations of quartz and feldspars, to a lesser extent biotite and other rock-forming minerals. In cases, when shock compression is accompanied by shear stresses, impact cataclastites form, which have a breccia, banded or lenticular fluidal structure and are often made up of turned, displaced fragments of different size, separated by bands and lenses of cataclastic material.

Irregular jointing develops in quartz under weak alteration conditions and the displacement of certain parts of crystals occurs, resulting in mosaic attenuation and block character. Under a more intense impact, planar fractures (PF) become widespread and, mainly planar deformation features (PDF), their number in quartz grains ranging from one to 5–7 (Fig. 4.2). Their orientation relative to the crystallographic axis C can be used as a geobarometer (Grieve et al. 1996). Quartz crystals, where the number of PDF systems exceeds three and, particularly, if there are five or six systems are characterized by a noticeable change of some physical properties, including the decrease of the mean refractive index from 1.548 to 1.536 and below, and picnometric density from 2.65 to 2.635 and even 2.615 g/cm^3. Certain grains display slightly birefringent (to 0.002) or isotropic areas, in which PDF seem to be attenuating. Certain PDF systems are decorated by stishovite in the form of the finest (several mm) needles and laminae. Stishovite, clearly diagnosed by X-ray techniques (Vishnevsky et al. 1975), is mainly generated under loads of 12–20 GPa or more.

Plagioclase in rocks of the considered group is characterized by jointing, but, which is more typical, by the appearance of deformation lamellae; to a lesser extent, PDE (one or two systems, which are predominantly parallel to the albite twin systems). In plagioclases of the intermediate composition ($An_{27–35}$), the refractive index is decreased by 0.017–0.019; respectively, there is a density reduction from 2.66 to 2.62 g/cm^3. Often, plagioclase grains display certain spots and irregular isotropized areas, as well as partly or fully isotropized system of twins, with birefringence being

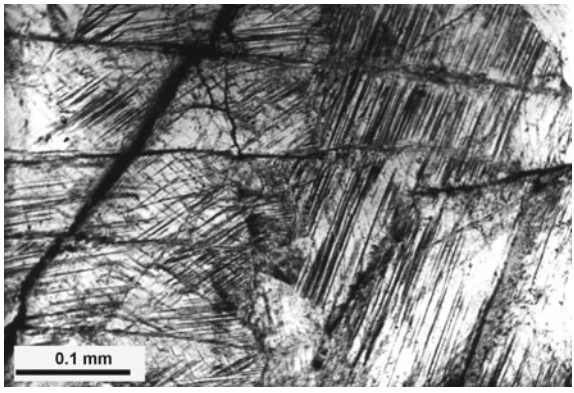

Fig. 4.2 Diaplectic quartz with several systems of planar deformation features. Microphotograph, parallel nicols

retained in the other system. The last-mentioned effects, judging by experimental evidence, point to a moderate shock compression to 35 GPa.

Alkali feldspars (orthoclase etc.) under weak and moderate shock compression are characterized by development of the deformation bands and one to three PDE systems; the refractive index is decreased by approximately 0.006–0.009; birefringence drops to 0.003–0.004 up to the partial isotropization; density decreases from 2.56–2.58 to 2.52 g/cm^3 (Raikhlin et al. 1979).

Biotite, altered under the above loads, is noted for the development of kink bands, as well as one to three PDF systems, oriented parallel to (111), (111), (112), (112), etc. In certain cases, the reduction of birefringence and loss of pleochroism are recorded.

Garnet bears almost no traces of alteration, except a slight jointing, which is enhanced in rocks, subject to moderate alterations under shock compression to 20–35 GPa. Grains are cut into microblocks by the network of irregular fissures; their transparency decreases, and the intensity of the colour increases, which asquires brownish hues.

Pyroxenes, similar to garnet, are resistant to the moderate shock compression. Hypersthene and salite, subject to loads below 30 GPa, are characterized by an irregular jointing, more pronounced in rocks, undergoing more intense alterations; in this case, crystals appear to be cut by abundant coarse fissures.

Other rock-forming minerals (sillimanite, cordierite, spinel and some others) do not reveal any noticeable mechanical and optical alterations within the considered shock load ranges.

4.1.4 Intensely Shock-Metamorphosed Rocks

Crystalline rocks, subject to intense shock compression, are noted for marked changes in the character of minerals, which are particularly pronounced in thin sections, as well as a certain reduction of density, increase of porosity, etc. Tectosilicates are commonly transformed to diaplectic glass, and a simultaneous dynamic action results in generation of cataclasites.

The main rock-forming minerals of gneisses, compressed to 35–45 GPa, can be characterized as follows.

Quartz transforms into diaplectic glass under the pressure above 35 GPa; glass has a brownish colour and the characteristic shagreen surface. In places, domains of low-birefringent quartz are discernible in it; and relics of the PDF systems are visible in transmitted light. A significant feature of the impact of high pressures is the transformation of a part of quartz and diaplectic quartz into coesite in the rocks under consideration (Masaitis et al. 1974). Coesite forms kidney-shaped accumulations, intersecting veins, and grain aggregates up to 100–200 mm and more (Fig. 4.3). It is colourless, or locally has a slightly brownish colour and is slightly birefringent: $2V = 57°–61°$, $Ng = 1.602 \pm 0.002$, $Np = 1.597 \pm 0.002$.

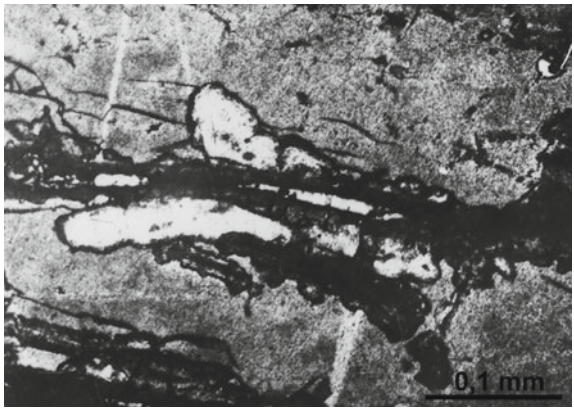

Fig. 4.3 Diaplectic glass after quartz. Kidney-shaped coesite aggregates (white) develop after the glass starting from walls of the cracks filled in by lechatelierite. Microphotograph, parallel nicols

Plagioclase in gneisses ($An_{27–35}$), subject to intense shock compression, transforms into diaplectic glass (maskelynite) with the refractive index of 1.525, though, in certain cases, vaguely outlined areas with a weak birefringence can be distinguished in its isotropic mass.

Orthoclase and orthoclase-perthite undergo alterations, similar to those of plagioclase, when subject to loads above 35 GPa. Disordered orthoclase represents an amorphous phase, retaining the shape of the initial crystal and with the refractive index of 1.518–1.520 and the density of 2.5–2.48 g/cm^3 (Raikhlin et al. 1979).

Biotite laminae are characterized by weakening or complete loss of pleochroism; there occurs a partial thermal decomposition with generation of fine-grained opaque aggregate accumulations of ilmenite, hypersthene, alkali feldspar, and glass.

In garnet, abundant fissures develop within the considered interval of alterations including planar fractures; it becomes opaque and asquires a brounish and dark grey colour at the expense of new phases, appearing in the course of its thermal decomposition, i.e. hypersthene, hercynite, and glass (Gnevushev et al. 1982; Kaminskaya et al. 1986; Kozlov et al. 1987; Feldman 1990). Locally, spots of non-decomposed garnet are preserved.

Pyroxene is noted for the slightly decreased birefringence, wavy extinction, appearance of planar fractures.

Cordierite in the considered group of crystalline rocks is transformed into colorless or brownish diaplectic glass, composition of which being given in Table 4.3.

Sillimanite, forming prismatic grains, is characterized by coarse transverse fracturing; its colouring is intensified in places.

Graphite, which is present in rocks, is also subjected to alteration and transforms to diamond; the specific features of this alteration are considered below, as well as under Chap. 6.

Table 4.3 Chemical composition of homogeneous ("momomineral") fusion glasses and products of their devitrification from vitrified gneisses ("protoimpactites")

Lithology	SiO_2	TiO_2	Al_2O_3	FeO	MnO	MgO	CaO	Na_2O	K_2O	Total	n
Glass after alkali feldspar											
– After orthoclase	63.96	0.05	19.86	0.18	–	0.23	0.78	1.67	13.09	99.82	4
	65.38	–	17.5	–	–	–	0.53	0.54	15.54	99.49	2
– After microcline-microperthite	63.74	–	22.34	–	–	–	0.51	3.82	8.29	98.7	1
Spherulitic aggregate after apoplagioclasic diaplectic glass, it corresponding to $An_{38–40}$ in composition	58.87	–	25.68	–	0.12	–	8.2	6.34	0.65	99.86	3
	58.32	–	26.49	–	–	–	8.54	6.21	0.36	99.92	2
Apoplagioclasic recrystallized glasses (of spherulitic texture), they corresponding to An_{30} in composition	58.38	–	26.11	–	–	–	6.35	7.85	1.08	99.77	3
	58.24	–	25.95	0.12	–	–	6.17	8.47	0.97	99.92	2
	60.75	–	25.51	0.08	–	–	6.96	7.72	0.16	101.18	2
Apocordieritic glass	49.45	0.05	34.41	5.15	0.14	10.9	0.02	–	0.02	100.14	4
	50.23	0.1	33.41	5.74	0.12	10.26	–	–	–	99.86	3
	48.23	–	34.82	5.41	–	9.07	–	–	–	97.53	2
Apobiotitic (?) glass	44.1	2.01	16.57	16.5	0.35	8.78	0.77	–	6.9	95.98	3
	38.56	1.12	16.63	20.27	0.42	14.12	1.42	–	3.45	95.99	3

Electron microprobe analysis, n—number of analyses

4.1.5 Very Intensely Shock-Metamorphosed Rocks

Gneisses subjected to very strong shock transformations, commonly above 45 GPa, are of utmost interest. If the rocks assigned to this group appearing to be enclosed into impactites as blocks and fragments and undergo additional heating, recrystallization of minerals and different glass results to essential changes in the rock habit and, in places, to an almost complete disappearance of the shock metamorphic features. This leads to significant difficulties in distinguishing the effects caused by the shock load proper (including the post-shock temperature) and resulting from subsequent annealing. In this sense, for analysing the shock effects proper, it would be preferable to study the fragments, subject to chilling or quick cooling after the pressure dropping.

Under shock compression above 45–50 GPa and residual temperature above 1,100°, there occurs a partial or complete melting of quartz, which after cooling solidifies to form quartz glass or lechatelierite with the refractive index 1.460–1.462. Lechatelierite often encloses rounded pores, has a fluidal texture resulting from the starting flow of the material. During slow cooling, lechatelierite recrystallizes, often forming cristobalite and α-quartz. The former is easily diagnosed by the characteristic ball-texture, while the latter commonly replaces cristobalite and also forms mosaic aggregate. Lechatelierite, partly transformed, often occurs in suevites and lithic microbreccias as minor independent bombs and fragments.

Under strong compression, plagioclase fusion glass appears (Table 4.3), it commonly being characterized by porosity and fluidal texture. Refractive indices of this glass (which is of oligoclase-andesine composition), are lower as compared to those of maskelynite (about 1.520–1.523). During plagioclase transition into fusion glass, the supply of potassium and silica, and the removal of calcium and, particularly, sodium occurs (Sazonova and Korotayeva 1989). Slow cooling leads to recrystallization of both fusion glass and maskelynite with generation of spherulitic and radially-fibrous aggregates of neogenetic plagioclase, which is commonly more high-temperature (Table 4.4).

Orthoclase transforms into monomineral fusion glass (Table 4.3) with porosity and fluidal texture. Its density falls to 2.35–2.27 g/cm^3; refractive index, to 1.502–1.505. Chemical changes show up as the increasing silica content, and to a lesser extent, aluminium and calcium contents, and an abrupt reduction of potassium (Sazonova and Korotayeva 1989). Similar to plagioclase fusion glass, these data point to a significant role of the volatile transport. Fusion glass after orthoclase during annealing undergoes recrystallization with generation of radially fibrous sanidine aggregates (Table 4.4).

Thereby, the main constituents of intensely compressed gneisses, i.e. quartz and feldspars, are, to a major degree, transformed into commonly vesicular fusion glass. The latter in most cases is similar by composition to mineral precursors and may be regarded as "monomineralic". Mixing of these melts along the differential moving of transforming rocks led to the appearance of "polymineralic" i.e. homogenized impact melt. Original rocks partly consisting of "monomineralic" glass, usually retain the initial structural and textural features. This allowed once calling them

Table 4.4 Representative EMP analyses of products of thermal alteration of some original minerals

Products of transformation	SiO_2	TiO_2	Al_2O_3	FeO	MnO	MgO	CaO	Na_2O	K_2O	Cr_2O_3	Total
After garnet											
– Ferrogortonolite	32.13	0.05	0.46	54.14	0.51	12.95	–	–	0.05	0.32	100.61
– Cordierite	39.87	0.04	36.83	9.58	0.25	8.63	0.27	–	0.6		96.07
– Hercynite, central part of a grain	–	–	65.88	22.57		8.89	–	–	–	1.9	99.24
– Hercynite, peripheral part of a grain	–	0.73	61.31	25.67	1.67	8.89	–	–	–	1.15	99.42
After feldspar											
– Sanidine spherulitic aggregate	70.3	–	19	–	–	–	–	2.28	10.2	–	101.78
After plagioclase											
– Andesine (An_{30}) spherulitic aggregate	58.38	–	26.11	–	–	–	6.35	7.85	1.08	–	99.77

"protoimpactites" (Masaitis 1983), unlike tagamites, which are also mainly made up of impact glass (however, totally homogenized) and have quite different textural and structural features. Though the term "protoimpactite" is not quite strict, it will be applied below when necessary. The chilled specimens of such rocks occur in vitroclastic and vitrolithoclastic suevites, which are relatively cool at the moment of deposition. Depending on the amount of glass, different protoimpactite varieties can be distinguished, containing 10–30, 30–80 and over 80% of products of the shock melting of mineral species.

In the first variety, an essential part of tectosilicates is molten, though there are areas of preserved diaplectic plagioclase glass, but to a major degree, diaplectic quartz. The general initial structure is not disturbed. Coloured minerals usually show shock deformations, and features of thermal decomposition, particularly biotite. With increasing melting degree against the background of the relict initial texture, lenticular banded areas appear, made up of porous fusion glass after orthoclase, and to a lesser extent, after plagioclase. Feldspar glass often encloses isometric, angular rounded particles of diaplectic glass and lechatelierite. Garnet retains the initial shape of grains; however, it is transformed into the black mass of decomposition products. Biotite appears as brownish semitransparent isotropic substance (Table 4.3). In certain cases, cordierite fusion glass is recorded (Table 4.3). In protoimpactites, characterized by the maximum melting degree, salic constituents are fully molten, and dark-coloured minerals are completely altered as noted above, and cut into blocks subsided into monomineral fusion glass. Locally, areas of mixing of such glass occur, which might be joined by the substance of molten cordierite or coloured minerals. Garnet and pyroxenes are transformed into opaque structureless masses, commonly recrystallized. Detailed research shows that after garnet, hercynite, ferrogortonolite, hypersthene, and cordierite can form in different proportions (Table 4.4), as well as glass. (Masaitis 1978). Recrystallization commonly proceeds under the actions of heat of the surrounding rocks or melt. Biotite is transformed into pink-brown glass, whith encloses very small idiomorphic spinel crystals. Commonly, quartz and feldspar glass are also recrystallized with generation of mosaic or granoblastic quartz, plagioclase microlites and spherulites, high-temperature feldspar, respectively.

In certain cases, differential movements of this molten material result in generation of fluidal structures; porphyroblasts of altered garnet are deformed and extended. Along certain planes, where such movements were most intense, thin veinlets, minor spots of black glass corresponding in its composition to the mixture of all the initial constituents and essentially representing the initial generation phase of large masses of impact melt, form in rocks. Evaluations of shock loads and temperatures, under which the above alterations occur and protoimpactites appear, are, respectively, within 45–60 GPa and 900°–1300°, or, less frequently, more.

Gneiss fragments containing initial graphite transformed in impact diamonds to a certain degree, often occur as inclusions in suevites and tagamites. In addition to shock alterations, they are commonly strongly recrystallized. Such inclusions were studied, especially to establish the character of parasteresis association of the transformation products of rock-forming minerals and evaluating the parameters of graphite transformation to diamond.

The main coloured minerals presented in the described group of graphite- and diamond-bearing gneisses, are garnet, biotite, and, less frequently, sillimanite, all these constituting 20% of the rock volume or more. All of them are, to a major extent, altered, apart from quartz and feldspars, the shock alteration products of which being represented by fine-grained aggregate accumulations of new-formed minerals. At the same time, in certain cases, when the protoimpactites underwent quick chilling, they are totally made up of fresh pumiceous monomineral glass after quartz and feldspars. In places, the latter are subject to mixing to a minor extent and enclose opaque palimpsest porphyroblasts of garnet transformed (inferred from X-ray patterns) into the mixture of very small (to 10 mkm) hypersthene and hercynite grains.

These rocks enclose in places diamonds, which were recorded in them not only by studying of the residues of their termochemical decomposition, but also by direct observations in petrographic thin sections under the microscope (Fig. 4.4). Relatively larger diamond particles are disintegrated during preparation of thin sections (they in places leave distinct scratches on the surface of the rock section), but flat tabular grains less than 0.03 mm thick are preserved. In some cases, several small diamond grains can be seen simultaneously within the thin section. They are enclosed into the recrystallized diaplectic glass or fusion glass fragments of predominantly plagioclase composition, diamonds also occur among recrystallization products of quartz glass, as well as within altered garnet in places. Such rocks also commonly contain, apart from diamond, laminae and scales of shock-metamorphosed graphite.

All these observations, as well as the reconstructions of the state of tectosilicates altered in the shock wave prior to their annealing in the intensely heated environment, show that the crystalline rocks, in which impact diamonds occur, were subject to the shock load of about 40–60 GPa. The possible lower limit of the evaluation of pressure, at which graphite starts to transform to diamond, is indicated by the presence of the latter in gneisses, where only plagioclase is fully transformed to maskelynite (about 35 GPa). In most cases, diamonds and shock-metamorphosed graphite, which commonly coexists with them, are associated with diaplectic glass and melting glass

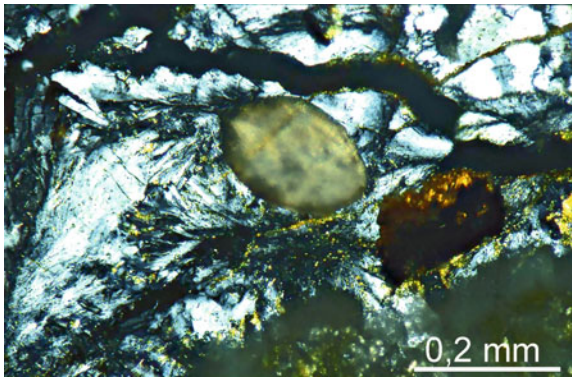

Fig. 4.4 A hexagonal, tablet-shaped apographitic paracrystal of impact diamond (in centre) within recrystallized quartz-feldspar matrix of an intensely shocked gneiss. Diameter of the diamond 170 μm. Microphotograph, crossed nicols

both after feldspar and after quartz. These gneisses, possibly, belong to the III and, partly, to the IV shock metamorphic grades.

4.2 Tagamites

4.2.1 Mineral Composition and Texture

Tagamites of the Popigai impact structure are characterized in a number of publications (Masaitis et al. 1975, 1980, 1983; Selivanovskaya 1977, 1987; Masaitis 1983, 1994; Raikhlin et al. 1983, 1987; Mashchak and Selivanovskaya 1988; Vishnevsky and Montanary 1999; Whitehead et al. 2002, etc.). They are massive, less frequently porous or ataxic rocks of aphanitic image, that have almost black, dark grey, grey-lilac or light grey colour. They are made up of glassy or, to a certain extent, crystallized matrix, into which the fragments mainly of crystalline rocks and their minerals are subsided (Fig. 4.5). Relatively larger inclusions (from the first cm to several metres) commonly contribute no more than 3–5% and are regularly distributed, there are some areas where blocks constitute 40% of tagamite volume or more. Minor inclusions (tenths of a mm—the first centimetres) take up from 5–10 to 25–30% and often form shlieren-like and band-like accumulations. Porous tagamites contain to 15–20% or more rounded or ellipsoid-like oblong pores from 1–2 to 5–8 mm across, or, less frequently, larger; in places, there are caverns to 5–8 cm. Tagamite matrix is holohyaline, hemicrystalline or holocrystalline; it contains plagioclase, orthopyroxene, lesser amounts of other minerals, as well as glassy or crystallized groundmass.

Fig. 4.5 LT tagamite with numerous inclusions of gneisses (light-colored), which are shocked to a variable degree and annealed. Mayachika Upland, borehole 1726, depth 42–48 m. Core diameter is 57 mm. The scale on the figure is in cm

Inclusions in tagamites are represented by diverse crystalline (to 90%) and sedimentary (to 10%) target rocks (lithoclasts) and their minerals (crystalloclasts). Crystalline rocks are dominated by biotite-garnet, biotite-pyroxene, bipyroxene and other gneisses and plagiogneisses (including shock metamorphosed ones); dolerites and some other rocks are less frequent. Among the sedimentary rocks, quartzites, siltstones, sandstones, shales, coaly mudstones, limestones, and dolomites are frequent. Crystalloclasts, formed due to destruction of all these rocks, represented by quartz and feldspars (prevail); garnet (almandine), hypersthene, salite, ilmenite, magnetite. Hornblende, sillimanite, and other minerals are rare. There are also graphite and impact diamonds. The heavy fraction of tagamites is dominated by pyroxene (mainly hypersthene); almandine, ilmenite, magnetite and pyrrhotite spherules, and limonite occur; there are minor amounts of sillimanite, zircon, apatite, rutile, mullite, kyanite, epidote, titanite, hornblende, biotite, rarely other sulphides (pyrite, sphalerite, galena, chalcopyrite), as well as moissanite. The structures and mineral composition of rock inclusions from tagamites (as well as from suevites) carry many expressive features of their transformation and interrelation with host impactite (Masaitis 1976).

For the purpose of subdivision of tagamites, primarily microscopic textural features are used, reflecting the temperature regime of impact melt generation and its cooling. Proceeding from these features, tagamites are classified under the high-temperature (HT) and low-temperature (LT) varieties, forming from the impact melt fractions with different initial temperature. As noted above, the bodies, made up of these varieties, are often in complex geological relationships; peculiar heterotaxial tagamites form, they made up of areas, spots, blocks, etc., of both varieties, commonly with abrupt contacts between them (Figs. 4.6 and 4.7).

Petromagnetic studies revealed significant differences between HT- and LT-tagamites, resulting from the domain structure of ferromagnetic substance in these rocks (Gorshkov and Starunov 1981, etc.). HT-tagamites mainly contain finely dispersed grains of ferromagnetic pyrrhotite in supermagnetic state, whereas in LT-tagamites, this mineral is represented by multi- and uni-domain grains. Results of measurements on natural residual magnetization (I_n) and magnetic susceptibility (κ) demonstrated that I_n of HT-tagamites is 1–2 orders lower than that of LT-tagamites, whereas κ value for these rocks is of the same order (Fig. 4.8); these features are not caused by alteration processes, but are due to the generation and crystallization regime of different impact melt fractions.

4.2.2 Low-Temperature Tagamites

These rocks occur ubiquitously within the Popigai structure; they form bodies of different size and shape. LT-tagamites were studied in most detail within the Majachika Upland and in the Balagan-Yuryage River Basin, as well as in some areas in the southern, northeastern, and northern sectors of the impact structure.

Most of holohyaline tagamites are represented by significantly altered glass (from 70 to 90%), which has massive, fluidal, breccia-like ataxitic structure and contains

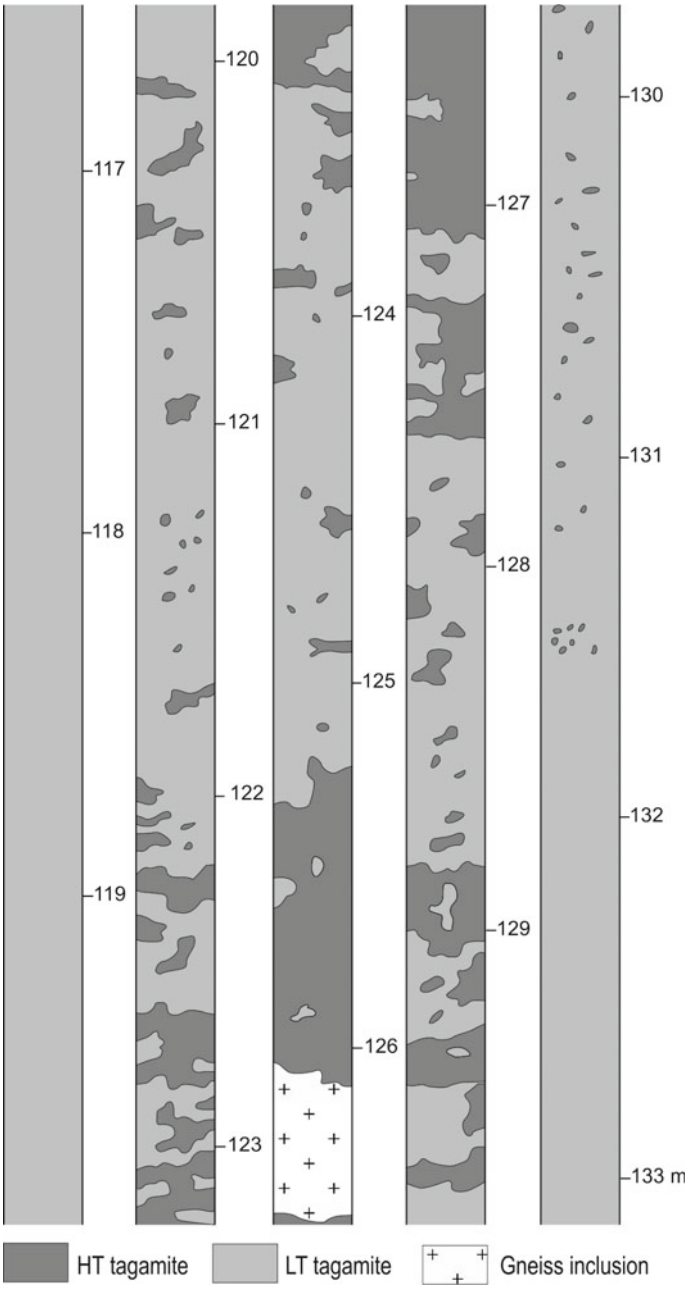

Fig. 4.6 Mode of interrelations between HT and LT tagamites forming irregular lumps and patches inside the first one. Sketch of core of borehole 4274, depth 117–133 m, Balagan-Yuryage area

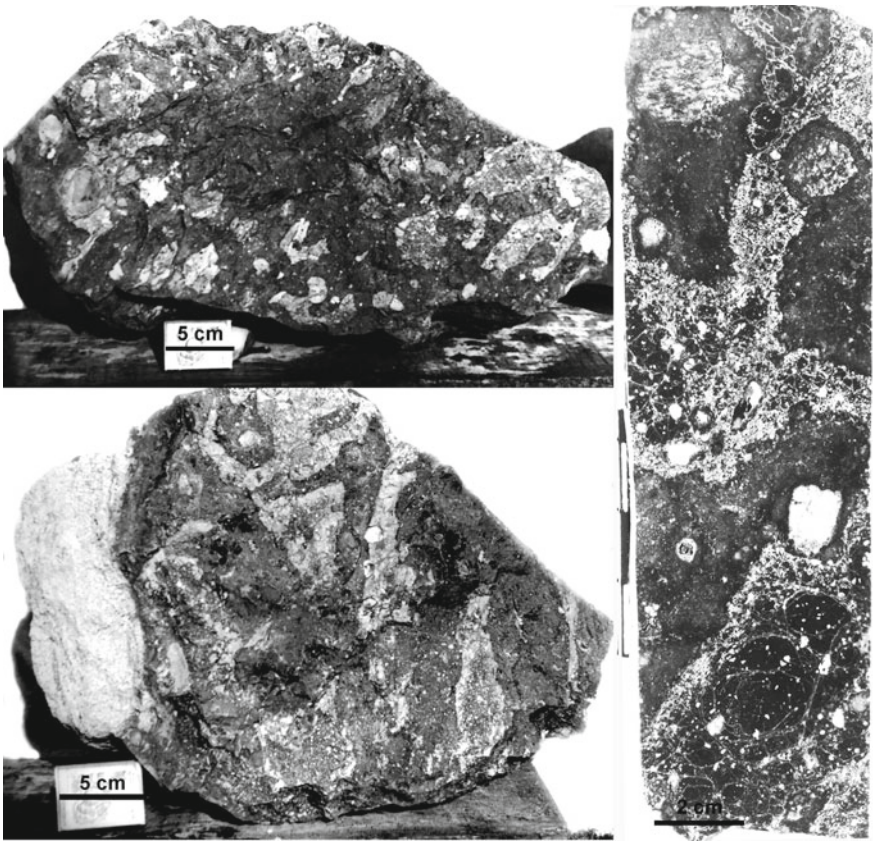

Fig. 4.7 Interrelation of HT tagamite (light fields) and LT tagamites (dark fields) demonstrating a heterotaxitic texture. At left—rock specimens, at right—core (borehole 4274). Balagan-Yuryage area

about 25–30% minor inclusions. These rocks are characteristics of the marginal parts of large bodies and also form small isolated bodies. The glassy matrix is brownish or brownish-grey under the microscope, which is commonly caused by its alteration. The greatest contribution into the general content of clasts of all fractions (60–70% of the total volume of clasts) is made by microinclusions (less than 0.5 cm) and, to a lesser extent (about 10%) fragments of the fraction of 3–5 cm (Fig. 4.9). Crystalloclasts mostly display no features of significant shock alterations, there are inclusions of monomineral fusion glass and partly crystallized diaplectic glas, though.

Hemicrystalline tagamites are characterized by a partial crystallization of the matrix glass, they contain to 10–15% rock and mineral fragments. These rocks occur in the inner parts of sheeted bodies, they also make up minor independent bodies. Hemicrystalline tagamites with microlitic and cryptocrystalline texture of the groundmass can be distinguished. The former are characterized by development of

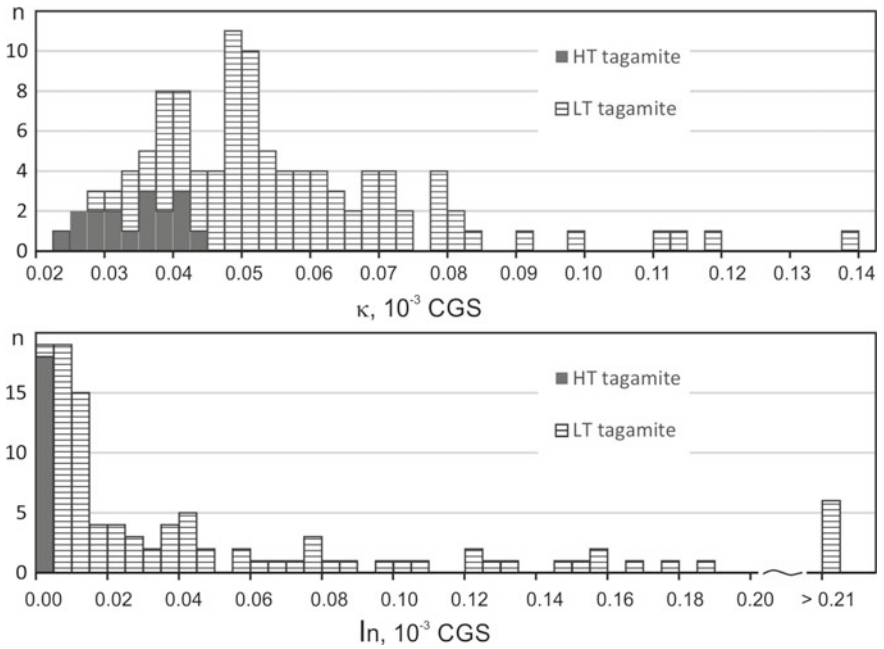

Fig. 4.8 Hystograms of magnetic susceptibility (κ) and natural remanent magnetization (I_n) for HT and LT tagamites. "n" is number of samples

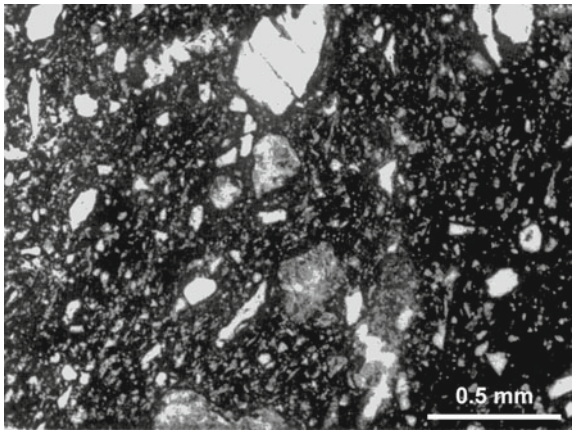

Fig. 4.9 LT tagamite with a holohyaline texture of the matrix comprising numerous inclusions of diaplectic quartz and feldspar, some of them in parallel arrangement. Microphotograph, parallel nicols

small (0.01–0.02 mm, less frequently larger) prisms of orthopyroxene in the glassy, mostly altered opaque matrix (Table 4.5) and microlites of acicular and prismatic andesine-labradorite (Table 4.6); the content of plagioclase is approximately @at 1.5 times higher, than that of pyroxene. Residual glass in the considered rocks is enriched in silica, and to a lesser extent, in alkalies (Table 4.7). Quartz and feldspar clasts often

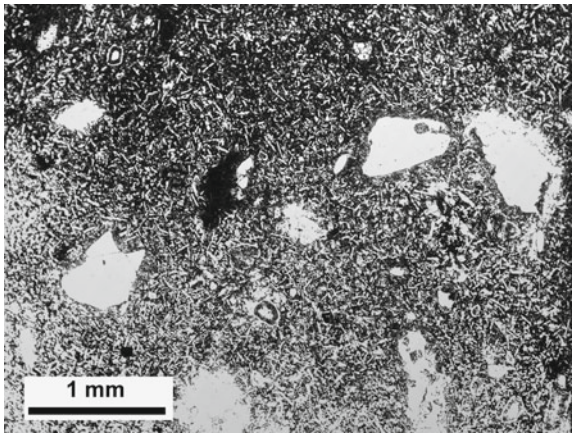

Fig. 4.10 LT tagamite with a micro-ophitic texture composing of plagioclase laths (light gray), hypersthene prisms replaced by biotite (dark grey), an opaque mineral, and minor glass. Minor quartz fragments are partly fused and enveloped by thin reaction rims Microphotograph, parallel nicols

bear traces of shock metamorphism, as well as recrystallization; their contours are vague. Hemicrystalline tagamites, which form cement of megabreccia, are characterized by hyalopilitic or pilotaxitic texture; acicular plagioclase microlites peaking 0.1–0.2 mm long in places, can constitute up to 40% of the rock volume. Small isometric hypersthene crystals occur in interstices together with non-crystallized semitransparent basis.

Hemicrystalline tagamites with cryptocrystalline texture are commonly characterized by irregularly mottled structure, which is due to crystallization in the basis of the finest hundredths and thousandths of a mm) isometric quartz and cristobalite grains and their accumulations. Plagioclase microlites, enclosed within this basis, are represented by labradorite, frequently zonal and more acid in the marginal part of the grains; pyroxene is represented by hypersthene, which also displays zonation (the centre, Fs_{40}; margins, Fs_{60}, where titanium content also increases).

Holocrystalline tagamites, occurring in the central parts of thick sheeted bodies, contain not more than 5–10% minor inclusions. The matrix (to 90%) is made up of the aggregate of andesine-labrador ($An_{50–54}$) and hypersthene ($Fs_{40–45}$) microlites and prisms of 0.02–0.1 mm in size, which determining microophitic, micro-pismatic-granular, and micropanallotriomorphic granular texture (Fig. 4.10). There are minor amounts (fractions of a %) of cordierite plates, sanidine, biotite lamelae, ilmenite needles, and magnetite (Table 4.6). Interstitial glass (Table 4.7) is, as a rule, devitrified, has a cryptofelsitic texture resulting from the development of the finest quartz and trydimite grains, along with biotite and sanidine. Relationship of the clasts with the matrix has a distinct reactionary character and shows up as partial melting of quartz, around which a rim of minor hypersthene crystals forms, making up accumulations in the groundmass in places (Fig. 4.11). Inclusions of quartz and diaplectic glass are commonly recrystallized.

All low-temperature tagamites are characterized by extensive development of secondary minerals, i.e. smectites, chlorite, zeolites, calcite, less frequently, quartz. They fill pores and caverns, replace the minerals of inclusions and microlites from

Table 4.5 Average compositions (wt%) of pyroxenes from tagamites (EMP analyses)

Pyroxenes from tagamite	SiO_2	TiO_2	Al_2O_3	FeO	MnO	MgO	CaO	Total	Fs	En	Wo	n
Hypersthene microlites in groundmass												
LT tagamite	51.54	0.51	1.34	25.14	0.44	19.71	1.05	99.73	41	57	2	4
HT tagamite. the thick sheet from the southwestern sector	51.02	0.53	2.34	25.46	0.26	19.72	0.52	99.85	42	57	1	22
Small bodies from the southern sector	53.24	0.47	1.42	19.73	0.3	22.39	2.08	99.63	32	64	4	15
Pyroxene microlites from reaction rims enveloping quartz clasts												
Hypersthene												
HT tagamite. the thick sheet from the southwestern sector	50.59	0.34	2.06	26.26	0.27	19.62	0.36	99.5	42	57	1	16
Small bodies from the southern sector	52.68	0.31	0.58	20.88	0.28	21.92	2.96	99.61	33	61	6	17
Augite												
Small bodies from the southern sector	51.95	0.73	0.61	12.03	0.18	14.78	19.27	99.55	19	42	39	24
Pigeonite												
Small bodies from the southern sector	52.83	0.28	0.16	21.59	0.3	20.85	3.84	99.85	34	59	7	34
Reaction rims around pyroxene clasts												
Hypersthene												
HT tagamite. the thick sheet from the southwestern sector	51.94	0.32	0.87	21.62	0.32	20.91	3.71	99.69	34	59	7	3
Small bodies from the southern sector	52.94	0.3	0.66	20.2	0.25	22.51	2.74	99.6	32	63	5	21
Salite												
Small bodies from the southern sector	52.84	0.27	0.55	19.4	0.39	21.66	3.75	98.86	31	61	8	4

n—Number of analyses

Table 4.6 Average compositions (wt%) of minerals from tagamite matrix as measured by EMP analyses

Mineral	Plagioclase			Sanidine			Cordierite		Ilmenite			Biotite
Tagamite	LT	HT_1	HT_2	LT	HT_1	HT_2	HT_1	HT_2	LT	HT_1	HT_2	LT
SiO_2	54.22	52.25	53.78	66.03	67.90	67.33	49.13	48.32	–	–	–	38.74
TiO_2	0.04	0.05	–	0.25	0.25	–	0.10	–	53.03	53.00	56.15	4.59
Al_2O_3	28.59	28.29	28.47	17.94	19.51	17.55	32.68	33.38	–	–	–	13.36
FeO	0.23	0.22	–	0.18	0.20	–	7.56	7.68	42.95	42.92	38.52	15.76
MnO	–	0.01	–	–	–	–	0.04	0.04	0.49	0.45	0.28	–
MgO	0.02	0.05	–	–	–	–	9.61	9.69	3.51	3.63	4.02	16.21
CaO	11.33	11.24	12.54	0.94	0.94	0.39	0.01	–	–	–	–	0.31
Na_2O	5.01	4.79	4.17	3.25	3.35	2.89	0.05	–	–	–	–	1.03
K_2O	0.58	0.48	0.26	8.56	8.96	11.72	0.28	0.50	–	–	–	8.53
Total	100.02	97.38	99.22	97.15	101.11	99.88	99.46	99.61	100.06[a]	100.00	99.30[b]	98.53
Ab	43	42	37	34		26						
An	54	55	61	6		3						
Ort	3	3	2	60		71						
n	10	15	16	3	3	4	8	3	6	5	8	2

Electron microprobe analysis, n—number of repeated analyses

[a]Plus 0.08% Cr_2O_3 in analysis

[b]Plus 0.33% Cr_2O_3 in analysis

LT—Low-temperature tagamites; HT—High-temperature tagamites: the thick sheet from the southwestern sector of Popigai (HT_1) and small bodies from the southern sector of the impact structure (HT_2)

Table 4.7 Average compositions (wt%) of residual glass from tagamites and buchites as measured by EMP analysis

Residual glass from	SiO_2	TiO_2	Al_2O_3	FeO	MnO	MgO	CaO	Na_2O	K_2O	Total	n
LT tagamite	80.93	0.93	12.53	1.03	–	0.05	–	0.12	4.13	99.72	2
HT tagamite											
The thick sheet in the SW sector of the Popigai structure	77.05	0.86	12.08	1.39	0.01	0.18	0.5	0.95	4.05	97.07	20
Small bodies from the SW sector	75.46	0.76	11.6	0.62	0.03	0.08	0.51	1.72	7.01	97.79	13
Small bodies from the southern sector	74.67	1.26	11.69	1.81	0.02	0.05	0.87	1.86	5.68	97.91	17
Spheroids in HT tagamite of the thick tagamite sheets	73.98	0.61	11.77	1.51	0.01	0.07	0.59	2	5.38	95.92	18
Buchite hosted by HT tagamite (thick sheets)	74.16	0.49	12.75	1.82	0.02	0.12	0.67	1.48	4.83	96.34	28

n—Number of analyses

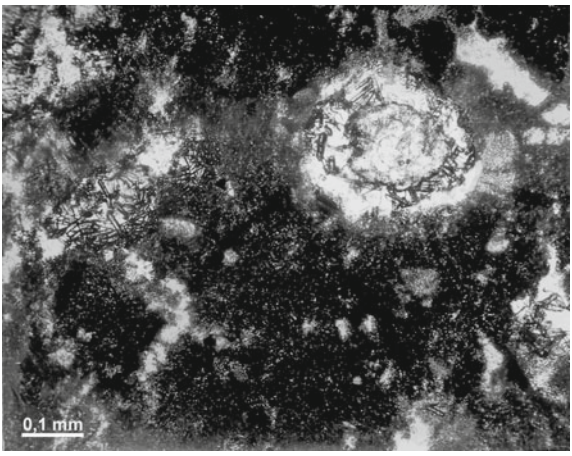

Fig. 4.11 HT tagamite with cryptocrystalline texture of the groundmass. Quartz clasts are surrounded by narrow reaction rims of hypersthene microlites and residual glass. Microphotograph, parallel nicols

reaction rims, and also develop as spots and irregular areas. In places, there are thin stringers made up of quartz, calcite, zeolite aggregates with participation of pyrite.

LT-tagamites are generally characterized by a comparatively low value of low-temperature water losses (0.8–1.5%), its volatilization occurring at temperature to 250°. DTA curves clearly display the effects, typical of smectite.

4.2.3 High-Temperature Tagamites

High-temperature tagamites were discovered within a composite sheeted body in the Balagan-Yuryage River Basin. They were also recorded on the surface in several places in the southern sector of the impact structure (Kysym River Basin, the Upper Chordu-Daldyn River, and the Kygam area in the upper course of Daldyn River), where they form relatively small sheeted and irregular bodies, in places in complicatred relationships with the low-temperature tagamites (Figs. 4.6 and 4.7). Among the considered rocks, tagamites with holohyaline and hemicrystalline texture of the matrix can be distinguished. The former are characteristic for the near-roof parts of thick sheets; they also make up minor bodies. Rocks contain from 10–15 to 25–30% of frequently irregularly distributed inclusions, predominantly of quartz and feldspar clasts, which have abrupt boundaries, or, less frequently, shock-metamorphosed and partly molten with generation of a very thin (thousandths of a mm) rim of coloured glass, in places in combination with the finest pyroxene grains. The glassy matrix is rather homogeneous, despite a certain degree of alteration (in this case it is brown and opaque) or devitrification, in places, there are areas of fresh semitransparent glass (Fig. 4.10). Generally, these rocks look more fresh than their low-temperature equivalents. The analysis of derivatograms shows, that in the HT-tagamites the loss

of low-temperature water is significant (2–3%) and occurs within a broad range of temperatures (60–600 °C).

Hemicrystalline tagamites, predominantly occurring within thick sheeted bodies, are easily diagnosed even from the outward appearance displaying a greasy lustre and a darker colour. Inclusions in these rocks constitute 2–5%; these are almost exclusively crystalline rocks and their minerals, though sedimentary ones are also occur in places. Quartz and plagioclase crystalloclasts often bear features of intense shock alterations and recrystallization.

The matrix of these rocks has a microlithic, or, less frequently, intersertal texture. The matrix is composed of colourless or light-coloured residual glass and microlites. Glass constitutes 10–20 to 30–40% of the volume and has the refractive index of n = 1486–1502; its composition is given in Table 4.7. It is enriched in silica and potassium. Often, perlitic jointing and the finest crystallites of trichite type are observed there. In the most entirely crystallized rocks, glass is partly transformed into the aggregate of sanidine (Table 4.6) and quartz. Prismatic plagioclase and hypersthene microlites (their quantitative ratios being evaluated on the average as 1.5:1) have the mean size of 0.02–0.03 mm, the maximum ones are of 0.08–0.1 mm. Besides, cordierite plates, ilmenite laminae, magnetite and pyrrhotite also occur, the latter forming spherules in places. Hypersthene in tagamites of the large sheeted bodies has the average composition Fs_{42} (Table 4.5); in places, it displays zonation: the central parts of microlites are more magnesian; the marginal ones, more ferruginous. In hypersthene microlites from minor bodies, where it is less ferruginous (Fs_{32}), the role of wollastonite constituent is increased; however, this hypersthene is poorer in alumina. There are also relatively more ferruginous and magnesian varieties, also differing in the content of alumina. Proceeding from the optical properties of hypersthene ($2V = -60° \ldots -74°$) and its composition variations, it might be inferred, that hypersthene microlites from tagamites of the small bodies are the least ordered ones and crystallized under an abrupt change in the temperature regime as compared to large bodies (Mashchak et al. 1992).

Plagioclase in high-temperature tagamites is represented by labradorite $An_{55–60}$ (Table 4.6), in places also with normal zonation. Cordierite more often occurs near contacts with gneiss inclusions; its plates are characterized by the sectorial and polysynthetic twins and inclusions (Table 4.6). Ilmenite often forms thin hexagonal, slightly translucent laminae (Table 4.6).

The most pronounced petrographic characteristic of the considered rocks are the features of intense interactions of the matrix with inclusions of rocks and minerals. Clasts of molten or recrystallized quartz are surrounded by relatively broad (up to 0.2–0.5 mm) zonal reaction rims, made up of pyroxene prisms (on the average, about 0.06–0.07 mm, in places up to 0.15 mm) and surrounding glass. In the large sheeted bodies these rims are composed exclusively of hypersthene, which has the composition Fs_{42} (Table 4.5). Commonly, in places of the entierly absorbed inclusions, aggregate accumulations of relatively large hypersthene prisms remain. Such accumulations can constitute 5–7% of the rock volume; in places, their amount is 10–15% (Fig. 4.12); their size reaches 0.2–0.5 mm.

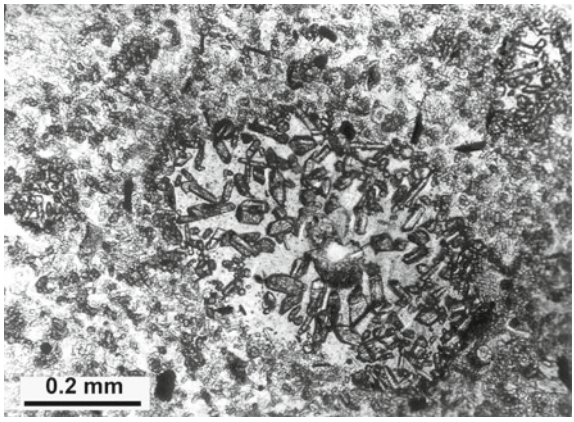

Fig. 4.12 HT tagamite with a hemicrystalline texture. Microlites of hypersthene (dark grey), plagioclase (light grey) are immersed in the transparent glass (grey). In the center—aggregate of large hypersthene prisms and residual glass, which appeared on the site of the engulfed fragment of quartz. Microphotograph, nicols are parallel

In tagamites from minor bodies, the composition and ratios of minerals in reaction rims around quartz clasts are more complicated. These rims can be made up of pigeonite and augite, around which hypersthene also develops (Table 4.5). Ferrosilite constituent and alumina content in the latter are lower than in tagamites from larger bodies; there is also a much higher content of the wollastonite constituent. All these differences point to the heteromorphism phenomena during crystallization caused by different cooling conditions of the melts, which generally had the same composition (Mashchak et al. 1992).

Plagioclase clasts inclusions in tagamites have a cribrate habit ("chess texture"), which is resulted from their selective melting and generation of glass with n = 1.527. Often, regeneration rims form around clasts; usually, they are of a more basic composition. Similar regeneration rims are observed around clasts of orthpyroxene and clinopyroxene originated from various gneisses. Iron and aluminium content in the neogenetic rim decrease, whereas the content of the wollastonite constituent grows as compared to the composition of the nucleus preserved (Table 4.5). Pigeonite rims are observed around salite (augite) inclusions in rocks from minor bodies (Table 4.5).

Noteworthy are the phenomena of pyrometamorphic melting of gneiss inclusions in high-temperature tagamites of the thick sheeted bodies in the Balagan-Yuryage River Basin. These inclusions are of 10–20 cm across. They were recorded frequently at depths from several dozens of meters to 500 m or more from this roof; they also occur elsewhere. Glass and the therein contained microlites constitute 50% of these inclusions; they result from crystallization of the pyrometamorhpic melt. Taking into account their predominantly quartz-feldspar composition, these pyrometamorphosed rocks can be called buchites.

Buchites have a diatectic texture resulting from generation of the pyrometamorphic melt at the boundaries of the corroded quartz and feldspar grains, in which the relics of non-molten initial gneiss minerals seem to be floating (Fig. 4.13). These primary minerals commonly bear traces of shock metamorphism and shock melting, as well as the subsequent thermal action of the surrounding impact homogenized melt.

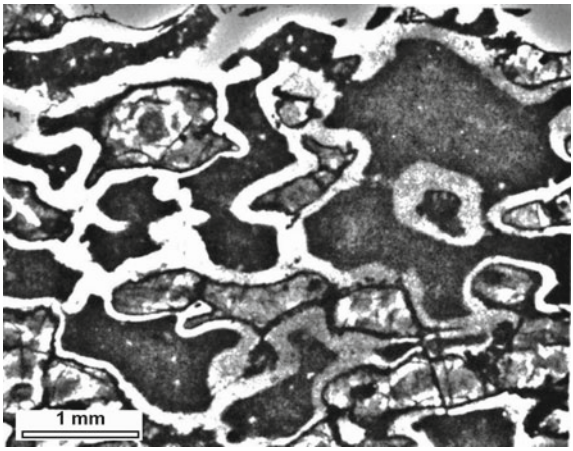

Fig. 4.13 Buchite (shock-metamorphosed leucocratic gneiss underwent to pyrometamorphic fusion). The diathectic texture formed by partly recrystallized plagioclase (dark areas), recrystallized diaplectic quartz surrounded by tiny hypersthene rims (grey), and eutectic glass, caused by fusion on the borders of plagioclase and quartz (bright areas). Microphotograph, parallel nicols

The corresponding alterations of these minerals were characterized in the chapter 4.1.3. Pyrometamorphic melt in buchites comprises hypersthene microlites (Fs_{49} with variable alumina contents (0.3–4.3%) and elevated concentraion of TiO_2); hypersthene commonly forms rims around quartz and its recrystallization products. Less frequently, plagioclase ($An_{45–55}$) microlites occur. Anorthoclase was recorded in certain instances; in places, cordierite and ilmenite laminae also develop. The volumetric content of microlites in the melt varies from the first to per cents 10%; the rest of melt is made up of coloured glass. The pores in it are often filled by zeolites, smectites, chlorite, etc. The glass is essentially enriched in silica and alkalies (Table 4.7).

Observations on the well core show that at high degree of pyrometamorphic melting of crystalline rock inclusions in tagamites, buchites disintegrate into the constituent relic minerals and the pyrometamorphic anatectic melt. In this case, the latter does not mix with matrix impact melt of tagamites and localizes as small (to 1 mm) spheroids concentrated on areas of the first tens of cm^3 (Masaitis and Raikhlin 1985). At such areas, the composition and textural features of different spheroids are similar. At the same time, the composition of spheroids, which are spaced significantly and occur at different depths, is different. Spheroids are composed of glass, which encloses a certain amount of hypersthene, plagioclase, anorthoclase, tridymite, ilmenite microlites; in places, they are recrystallized into the quartz-feldspar aggregate (Fig. 4.14).

Comparison of the residual glass composition in buchites and spheroids demonstrates their similarity (Table 4.7), whereas glass of spheroids differs markedly from residual glass of tagamites by a lower silica, higher alkalies, an essential predominance of potassium, over sodium, and the two times higher Fe/Mg ratio. Glass in

Fig. 4.14 The spheroid of pyrometamorphic glass in HT tagamite. Microlites of plagioclase, hypersthene, ilmenite are visible in the partially crystallized glass, which in places shows trachytoid texture. Microphotograph, parallel nicols

buchites also display similar features. All these observations generally point to the immiscibility of the matrix impact melt, by crystallization of which tagamites originate, and the pyrometamorphic melt, generated at a later stage of formation of the former. At the same time, melting products of inclusions, captured by the impact melt at the earlier stage of ejection, were practically completely absorbed by it.

As noted above, the thick tagamite sheet in the Balagan-Yuryage River area is made up of the series of simple bodies, formed by LT- and HT-tagamite. Tracing of changes in the petrographic features of tagamites through the section of this composite body, conducted in the course of detailed studies on core, revealed a certain pattern (Raikhlin et al. 1983, 1987). In the central part of the composite body (Figs. 4.15 and 4.16), similar to the central parts of simple bodies, of a significant thickness (over 70–100 m), at the depth of 200–300 m and below, rocks with the moderately and well crystallized matrix and a comparatively small number of inclusions are observed (hemicrystalline and holocrystalline mioclastic tagamites with a small number of inclusions). Towards the roof and the base of the composite body the matrix crystallization degree is gradually decreasing; the size of microlites decreases, while the number of inclusions increases. Near the base and the roof, tagamites with non-crystallized or slightly crystallized matrix and a great number of inclusions (to 25–30% of the rock volume) occur.

A gradual transition from slightly crystallized to moderately and well crystallized rocks indicates that the composite body was cooling as a single whole. This is also confirmed by the lack of chilled contacts between HT- and LT-tagamites, features of their mixing, along with a simultaneous immiscibility, etc. Data on the distribution of inclusions throughout the section of the composite body show that at the depth of 200–300 m, the boundary between the rocks differing in their content, is drawn: down in the section, the number of inclusions decreases abruptly. This might indicate

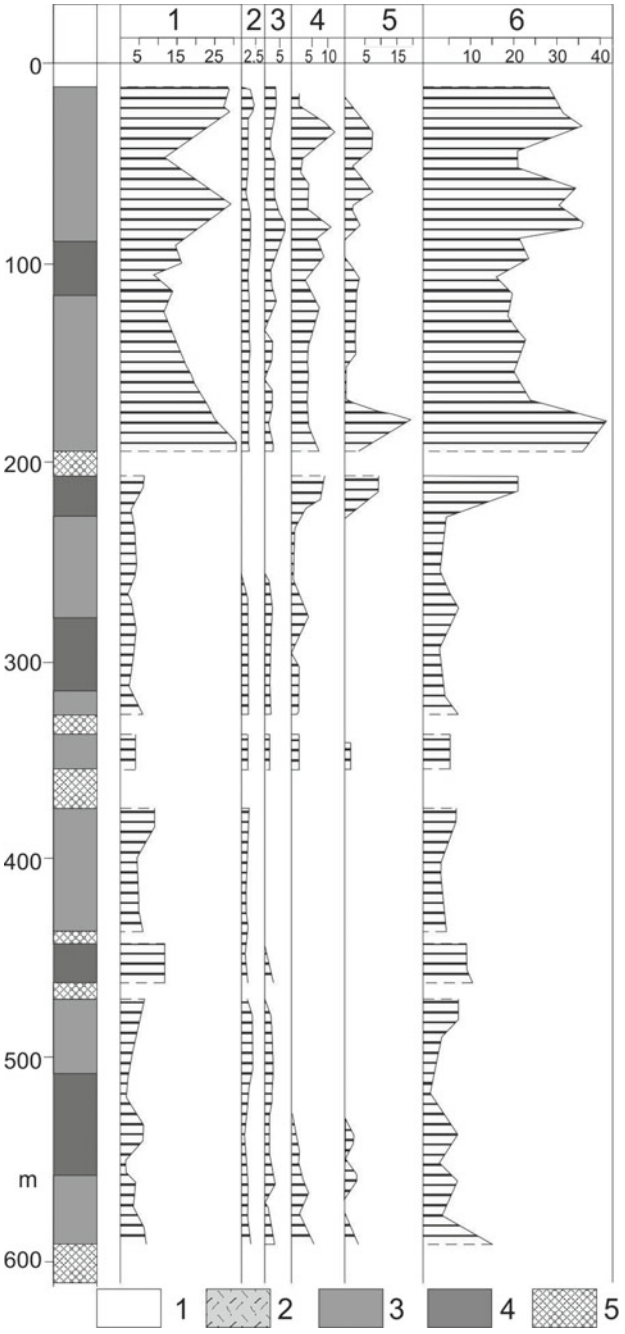

Fig. 4.15 The granulometry of fragments in tagamites from borehole 4670 (Balagan-Yuryage area, see Fig. 2.22). 1—Quaternary deposits, 2—Suevite, 3—LT tagamite, 4—HT tagamite, 5—Crystalline rock inclusions. Fractions of clasts (%), numbers above the columns: 1—<0.5 cm, 2—0.5–1 cm, 3—1–3 cm, 4—3–5 cm, 5—5–10 cm, 6—total amount of debris <0.5 to 10 cm

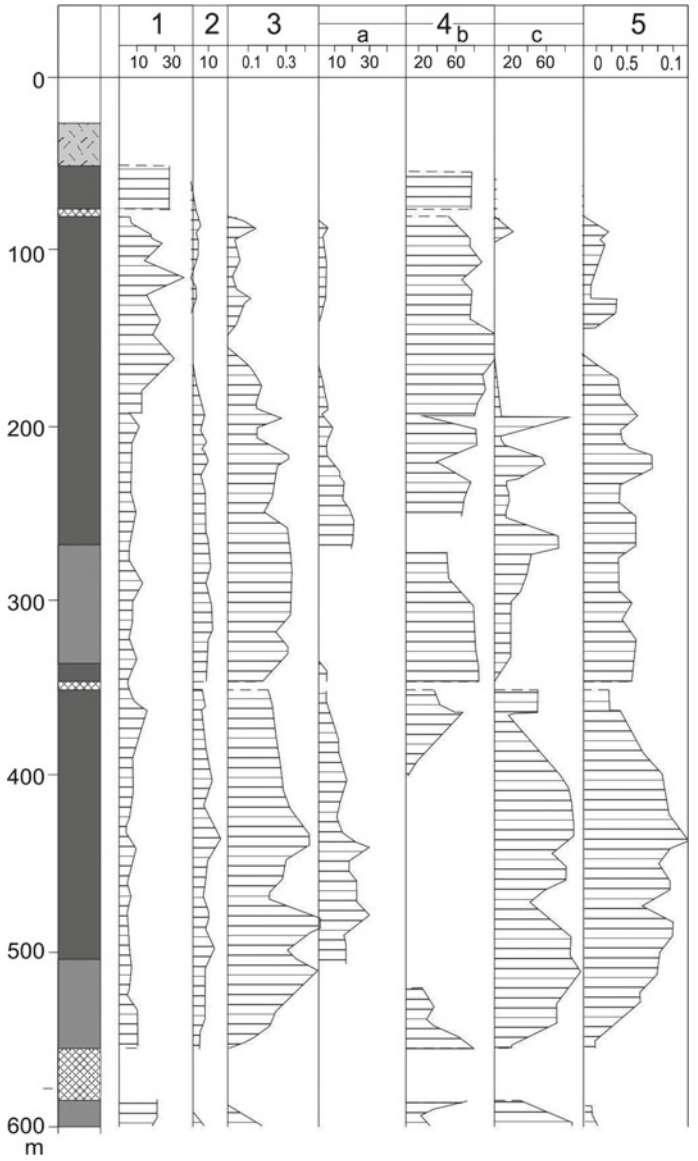

Fig. 4.16 Petrographic characteristic of tagamites from the borehole 4666 (Balagan-Yuryage area, see Fig. 2.22). For lithological legend, see Fig. 4.15. Petrographic characteristics (figures above the columns): 1—inclusions <0.5 cm (vol%); 2—amount of pyroxene accumulations (vol%); 3—size of pyroxene aggregates (mm); 4—matrix composition (vol%): a—residual glass, b—basis of a cryptocrystalline structure, c—microlites; 5—the maximum length (mm) of pyroxene microlites in reaction rims

that tagamites occurring above and below of this boundary formed from different melt fractions, distinguished by the extent of inclusion trapping.

4.3 Suevites

4.3.1 Composition, Structure and Texture

Suevites of Popigai structure made up of fragments, bombs, and lumps of impact glass of different size (vitroclasts) and target rock fragments (lithoclacts), cemented by the same finely crushed (less than 0.1 mm) material, partly lithified by sintering or other processes (Engelhardt et al. 1969; Masaitis et al. 1975, 1980; Selivanovskaya et al. 1990; Masaitis 1999, 2005; Stöffler et al. 1977, 2013; French 1998; etc.). Suevites, as a rule, lack in bedding and characterized by poor sorting of clastic material (Fig. 4.17). The size of vitro- and lithoclasts ranges from millimetres to 0.5–1.0 m, less frequently more (bombs and blocks). The crushed lithic material of crystalline and sedimentary rocks, represented by crystalloclasts and rounded mineral grains, have the same size, about 0.1–2.0 mm, less frequently more. In some cases the volume of this fine-grained material in lithovitroclastic suevites may be significant, up to 30%. This glassy material may be partly transformed into mixture of various alteration minerals. Suevites differ by a number of lithological and petrographic features: ratio of vitroclasts, lithoclasts and fine-grained material as well as by their grain size and cementation character (Masaitis et al. 1975, 1978, 1983, 1992; Raikhlin and Selivanovskaya 1979; Vishnevsky 1992, etc.).

Depending on the ratio between the main constituents, making up suevites, i.e. impact glass fragments, (vitroclasts) and rock fragments (lithoclasts), three families of these rocks are distinguished: vitroclastic (70–90% glass), lithovitroclastic (40–70% glass) and vitrolithoclastic (10–40% glass).

Suevites with the prevailing size of fragments of 0.1–2.0 mm are assigned to ash; suevites 2.0–50 mm, to lapilli; ones and >50 mm, to agglomerate and block suevites, similar to volcanic tuffs (Petrographic code 2009). If the fragments of a certain size occur approximately equally, ash-lapilli or lapilli-agglomerate suevites can be distinguished. In the generalized section of the crater fill (Raikhlin 1996), ash, less frequently lapilli, vitrolithoclastic suevites, and, to a lesser extent, vitroclastic suevites make up its upper part where abundant lithic microbreccia lenses, often with gradual transitions to vitrolithoclastic suevites, are observed. Lithovitroclastic and vitroclastic suevites are widespread in the lower part of the section, where they are closely associated with tagamite bodies and are connected with them by gradual transitions. The main lithological features of suevites in the generalized section are given in Table 4.8.

The content and ratio of certain constituents of suevites in different sectors of the impact structure were evaluated selectively using the quantitative calculation of plots covered by fragments of certain rocks and vitroclasts exceeding 0.5 cm in

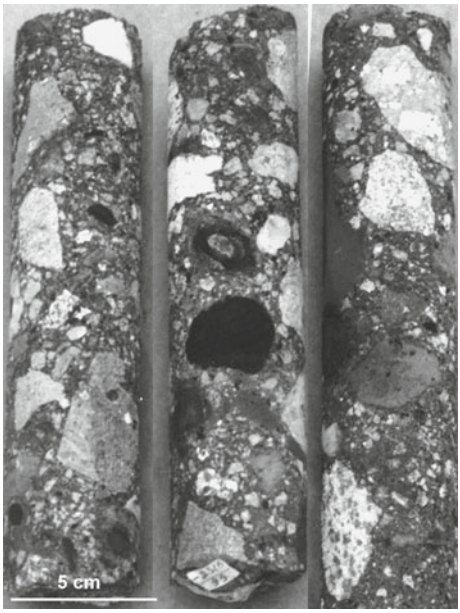

Fig. 4.17 The core of vitrolithoclastic suevite with numerous fragments of shocked gneiss (white), quartzite (grey), siltstone (dark grey and black). Automorphic and xenomorphic glass lapilli (dark gray) are distributed unevenly in the groundmass. Core of borehole −2516, depth 99–101 m, eastern slope of the Mayachika Upland. Core diameter 46 mm

size, directly at some exposures (areas of 0.5–1.0 m^2) and from core of a number of boreholes (areas of 0.3 m^2); in addition, the distribution of clastic materials in

Table 4.8 Principal lithological features of suevite from the upper and lower parts of the general sequence

Lithological feature	Upper part of the general sequence	Lower parts of the general sequence
Lithological composition	Lithovitroclastic, vitrolithoclastic (clasts of sedimentary rocks are predominant) suevite	Lithovitroclastic, rarely—vitrolithoclastic (clasts of crystalline rocks are predominant) suevite
Predominant particle-size distribution	Ash, rarely lapilli	Lapilli, rarely agglomerate
Predominant clast lithology	Sedimentary cover rocks	Crystalline basement rocks
Shape of vitroclasts	Mainly xenomorphic	Aurhomorphic and xenomorphic
Alteration of vitroclasts	Vitroclasts are mostly fresh or weakly altered	Vitroclasts are recrystallized to some extent, altered frequently
Cementation degree	Poorly or moderately cemented	Highly cemented
Inner structure of the sequence	Uniform with some fine-grained lithic breccia lenses	Not uniform, with lenses of tagamite and transitions to ataxitic tagamite

Fig. 4.18 The core of lithovitroclastic suevite. The xenomorphic lapilli-sized gneiss fragments (light), as well as fragments of argillites and siltstones (dark grey) are cemented by groundmass of fine-grained glass particles. Mayachika Upland, borehole 1726, depth 123.7–137.6 m. Core diameter 46 mm

fractions <0.5 cm has been studied in large petrographic thin sections. The calculation results are given in Table 4.9. As it seen from the table, suevites in the lower part of the section are enriched in glass, particularly in the NW and SW sectors (Buordakh and Balagan-Yuryage River sections). Lithoclasts of lapilli and agglomerate size prevail here; and among the lithoclasts, crystalline rock fragments of 0.5–20 cm or more across dominate. The cementing mass exceeds 10% of the rock volume in rare cases. In suevites of the upper part of the section, glass content is lower (predominantly less than 50%); most of the clastic material has ash, less frequently lapilli size (<0.5 cm); a rather high content of the cementing matrix (over 20%) is characteristic.

4.3.2 Suevites Enriched by Lithoclasts

Suevites, in which sedimentary rock fragments and fine-grained material prevails, are predominantly represented by moderately and slightly cemented ash-sized, less frequently, lapilli-sized vitrolithoclastic varieties of grey, greenish-grey, and brownish-grey colour (Fig. 4.18). Ratio between the lithoclasts, vitroclasts and cementing mass is wide-ranging. Among the sedimentary rock fragments, which commonly constitute 7–10 to 20–30% or more of the suevite volume, the Permian and Cretaceous siltstones, mudstones, and sandstones, the Cambrian limestones and dolomites, the Mesoproterozoic quartzite, the Cretaceous coalified wood, etc., prevail. Characteristically, these rock fragments are predominantly less than 0.5 cm in size; most of them are disintegrated into the fraction of psammitic size (0.1–0.2 mm or, less frequently, more).

Table 4.9 Lithology of suevites from certain sectors of the Popigai impact structure

No.	Position in the impact structure	Position in the general section	Suevite varieties	Number of lithological stations	Fraction of clastics (%)					
					>0.5 cm			0.1 mm–0.5 cm		<0.1 mm
					Impact glass	Crystalline rocks	Sedimentary rocks	Impact glass	Litho- and crystallo-clasts	Matrix
1	NW sector, outer zone of deformation (Buordakh Creek)	Lower part	Lapilli-agglomerate and agglometate; crystal-vitroclastic, litho-vitroclastic, and vitroclastic, incl. welded	8 (expo-sures)	47.7	16.3	5.3	14.7	11.7	4.3
2	N sector, outer zone of deformation (Arylakh-Yuryage area)	Lower part	Lapilli-agglomerate, litho-vitroclastic	4 (cores)	12.4	14.6	2.1	28.4	33.3	9.2
3	NE sector, outer zone of deformation (Tongulakh area)	Lower part	Lapilli, rarely agglomerate; crystal-litho-vitroclastic and litho-vitroclastic	2 (cores)	12.7	10.2	0.5	26.8	38.3	11.5

(continued)

Table 4.9 (continued)

No.	Position in the impact structure	Position in the general section	Suevite varieties	Number of lithological stations	Fraction of clastics (%)					
					>0.5 cm			0.1 mm–0.5 cm		<0.1 mm
					Impact glass	Crystalline rocks	Sedimentary rocks	Impact glass	Litho- and crystallo-clasts	Matrix
4	SW sector, annular trough (Balagan-Yuryage area)	Lower part	Lapilli, crystal-litho-vitroclastic and vitroclastic (incl. welded)	4 (cores)	22.3	4.8	0.3	47.2	16.0	9.4
5	SW sector, annular trough and the outer slope of the annular uplift (Balagan-Yuryage area)	Upper part	Dusty, rarely dusty-lapilli; litho-vitroclastic and vitro-lithoclastic	10 (cores)	8.0	3.2	1[a]	39.5	26.3	22.0
6	NW sector, the inner slope of the peak ring (Mayachika Upland area)	Upper part	Dusty and dusty-lapilli; litho-vitroclastic and vitro-lithoclastic	14 (cores)	11.6	2.0	0.8[a]	20.5	42.8	22.3

[a]Epiclasts of sedimentary rocks occur mostly in the fraction of <0.5 cm because of these suevites are commonly dusty

Fine-grained material (10–20% of the volume or more) is mainly represented by fragments of quartz, plagioclase, microcline grains, which often have a rounded, or, less frequently, angular shape. There are commonly no shock features, except brittle deformations (jointing, crushing). The source of these grains were incoherent sediments. Shock effects are observed only in crystalloclasts (0.2–2.0 mm, less frequently larger) of quartz, feldspars, biotite, garnet, their content commonly being not high (to several %).

Crystalline rock fragments, which are of subsidiary significance (1–5% of the volume, or, less frequently, more), are represented by gneisses of different composition, subject to the shock of predominantly low and moderate intensity; shock vitrified gneisses are less frequent. In places, large (to 5–10 cm or more) crystalline rock fragments are coated by rims (to 0.5–1.0 cm wide) of dark grey impact glass.

The predominant size of sedimentary and crystalline rock fragments is 0.2–10 mm, less frequently 2–3 cm or more. Some blocks are several dozens of cm to 1 m across.

Vitroclasts are composed of both fresh impact glass of different colour and porous, pumiceous glass, which is altered to a great extent. Fresh and altered glass fragments can occur simultaneously. The size of their fragments ranges within 0.5–2.0 mm, less frequently 5–10 mm or more; certain glass bombs are to 10–15 cm across or more. A detailed description of glass is given below.

The groundmass of described suevites, which commonly amounts to 15–20% of the rock volume or more, is mainly composed of finest (<0.1 mm) mineral fragments, a small amount (the first %) of glass particles and alteration clay minerals, calcite, limonite, zeolites, etc. Cement matter is porous or, less frequently, basal.

Vitrolithoclastic suevites contain in places the accumulations of accretionary lapilli (Balagan-Yuryage, Parchanai, Chordu-Daldyn Rivers, etc.). They appear as rounded zonal masses of 1–1.5 cm across, constituting 20–30% of the rock volume and made up of tiny mineral fragments (70–80%) and glass (10–15%) of silty and psammitic size, cemented by the same psammitic material.

Suevites, dominated by crystalline rock fragments and characteristic of the lower part of the crater fill (Table 4.8), are penetrated by numerous boreholes in Mayachika Upland and Balagan-Yuryage River areas, where they are widespread. They are also exposed in northwestern, western, and southwestern sectors of the impact structure (basins of Buordakh, Kybyttygas, Parchanai, creeks etc.). These are dense rocks characterized by the dark brownish-grey and dark greenish-grey colour. By the grain size of the clastic material, they are mainly assigned to the lapilli, lapilli-agglomerate, less frequently, to agglomerate varieties (Fig. 4.19). Clasts are predominantly represented by crystalline rock fragments (15–30% of the rock volume or more) and fragments of the constituent minerals, contributing more than 10–15%. The size of the fragments is from the first mm to 3–5 cm, less frequently more. Their shape is similar to isometric, often angular. They are commonly characterized by moderate and intense degree of shock alterations. Subsidiary amounts (1–3% or more) of sedimentary rock fragments occur, as well as their destruction products.

Crystalloclasts, as noted above, are represented by disintegrated gneiss fragments, often bearing shock metamorphic features (diaplectic minerals and glass, frequently recrystallized). Xenomorphic and authomorphic vitroclasts have a massive or flu-

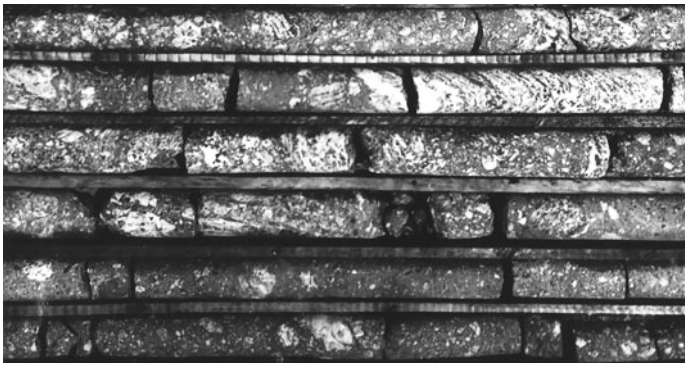

Fig. 4.19 Allogenic crystalline breccia cemented by suevite (dark). Light-colored patches are fragments of shocked crystalline rocks. The core of borehole 1751, depth 422.6–430.7 m. Mayachika Upland area. Core diameter is 46 mm

idal structure, sinuous, less frequently vague boundaries. Impact glass often forms authomorphic lumps, varves (Fladen), and bombs from fractions of a cm to several dozens centimeters and even 0.7–1.0 m in size.

Cementing mass of a pore character represents a mixture of the finest (less than 0.1 mm) ash particles and mineral fragments. Cement content varies from the first % to 7–10%, or, less frequently, more. In glass-enriched suevites the groundmass is partly recrystallized. Montmorillonite, chlorite, calcite and other alteration minerals arose after this material.

4.3.3 Suevites Enriched by Vitroclasts

Vitroclastic suevites predominantly develop in the lower part of the general impactite and impact breccia section (Table 4.8). They are penetated by boreholes in the annular trough and on slopes of the peak ring in the northwestern and southwestern sectors of the structure (Mayachika Upland, Balagan-Yuryage River Basin); they are also exposed at Buordakh, Kybbyttygas, Parchanai creeks and some other areas. These rocks predominantly occur in close association with lithovitroclastic suevites and often occur together with tagamite bodies.

Vitroclastic suevites are dense, dark brownish-grey rocks with a massive structure and lapilli, lapilli-agglomerate and agglomerate size of fragments (Fig. 4.20). Vitroclasts often have a fluidal structure; they are authomorphic or xenomorphic, and contain to 5–10% or more of crystalloclasts. Impact glasses often form sinuous bands, figured lumps and bombs, in places with a “ropy” surface, from fractions of a cm to 10–15 cm or more. Clasts of sedimentary and crystalline rocks constitute from 3–5% to 15–25% of the volume of these suevites; the latter rocks prevail and are characterized by a rather high level of shock and thermal alteration.

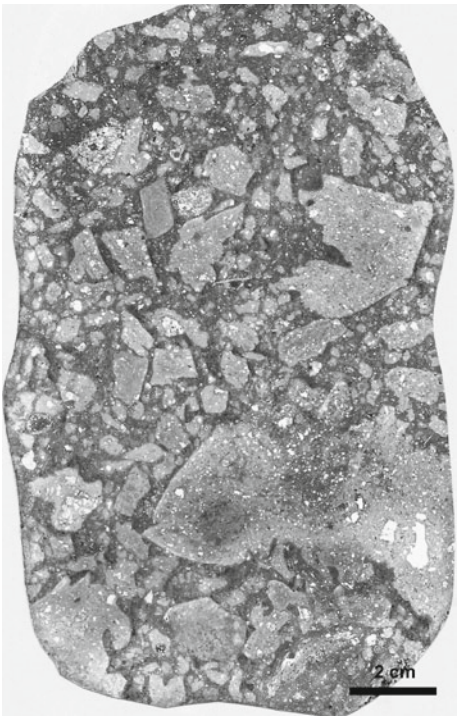

Fig. 4.20 Vitroclastic sintered lapilli-agglomerate suevite. Fragments of devitrified glass (grey) are filled with fine angular quartz and feldspars fragments. The dense groundmass consists of clastic glassy material. The rock specimen, Sogdoku Upland area

The cement of vitroclastic and sintered suevites that constitutes to 7–10%, is dominated by the finest ash glass particles. Close to lenses and, particularly, thick tagamite bodies, this cement is partly or fully recrystallized. Small (<0.5 cm) clasts of crystalline rocks also undergo intense recrystallization. Alteration and secondary minerals, i.e. montmorillonite, chlorite, calcite, zeolites, and limonite, develop after the cementing mass. Impact diamonds also frequently occur in suevites (particularly in vitroclastic ones).

4.3.4 Impact Glass from Suevites and Lithic Microbreccias

Among impact polymineral glass occurring as bombs and fragments in suevites and lithic microbreccias, two varieties can be distinguished: (1) fresh and (2) devitrified.

Fresh or slightly altered glass of a tar-black and dark green (“chrysolite”) colour is most characteristic of vitrolithoclastic suevites. Tar-black glass has a glassy lustre on the fresh fracture, it is semitransparent in thin section. Its structure is massive, less frequently fluidal, the texture is holohyaline; there is a slight porosity (Fig. 4.21). In thin sections, these are light brown or cream-coloured transparent glass with the refractive index ranging within 1.541–1.546, less frequently, to 1.553. The inclusions

making up to 1–3 vol.%, are represented by the finest (hundredths and tenths of a mm) quartz and feldspar fragments, as well as ilmenite, magnetite, and sulfide spherules. As irreguarly shaped patches, monomineral fusion glasses, in the first place lechatelierite, occur. Slightly altered glass fragments display a zonal colouring, from brown and yellowish-brown to light brown and cream of variable intensity; contours of these zones often repeat the boundaries of fragments (Fig. 4.22). The central part of the fragments is often characterized by microspherulitic texture; and the marginal part, by cryptocrystalline texture. Secondary alterations mainly show up as the development of montmorillonite in pores and marginal parts of glass fragments.

In vitrolithoclastic suevites forming lenses in microdreccias or gradual transitions to the latter, the most distributed are fragments of fresh glass of a dark green ("chrysolite") colour, which most frequently occur in microbreccia. They form both xenomorphic fragments 0.5–5 mm in size, and authomorphic bombs, lapilli from 0.3–0.5 to 1–3 cm in size. Under the microscope, these glass is transparent, colourless or slightly coloured to yellow-greenish. The refractive index n = 1.532–1.534. They are characterized by holohyaline texture and massive, locally porous and, in places, fluidal structure. The inclusions, i.e. diaplectic quartz and feldspars, diaplectic and monomineral glasss, are rare (up to 1–3%). Often, ilmenite spherules occur, and less frequently, magnetite spherules up to fractions of a mm across; there are also pyrrhotite and troilite spherules. An alteration show up as the development of smectites along the boundaries of fragments and pore walls.

The results of studies of the chemical composition of impact glass are given in Chap. 5. Features of their microstructure were investigated using different spectroscopic techniques (Raikhlin et al. 1981, 1982, 1986, 1987, 1991; Kozlov and Raikhlin, 1989; Reshetnyak and Raikhlin 1988). According to IR-spectroscopy, fresh glass is noted for vague spectra, a great width of maxima, slightly pronounces bands corresponding to crystalline phases, which points to the absence of the long-range order, i.e. products of glass crystallization or secondary alteration. Data of

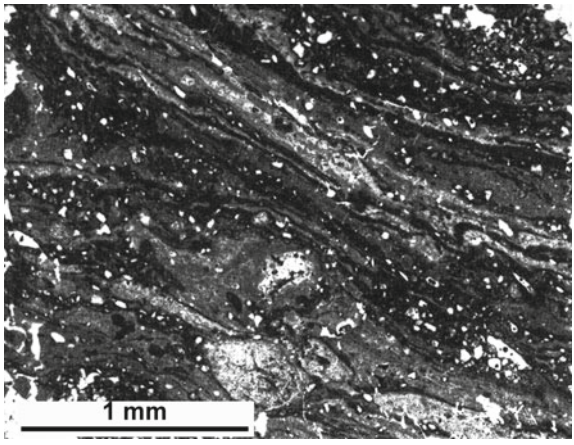

Fig. 4.21 Impact heterotaxitic glass with fluidal structure that forms the bomb in the suevite. The bands and lenses of the semi-transparent glass (gray) with a small number of inclusions alternate with lenses and strips of opaque glass (black) enriched by fragments of diaplectic quartz and plagioclase. Microphotograph, nicols are parallel

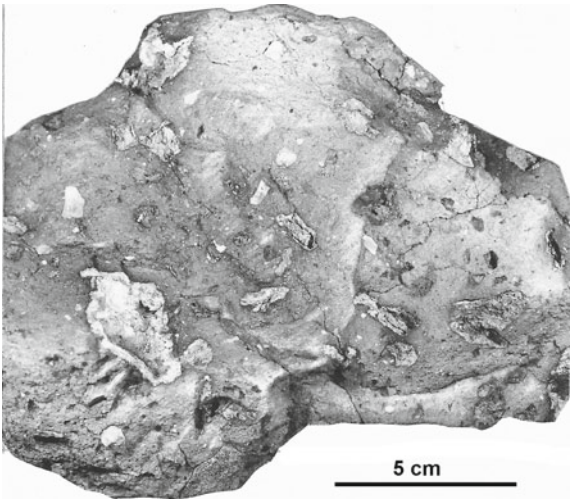

Fig. 4.22 Microbreccia with xenomorphic lappili-sized inclusions of impact glass (white). Lapilli are completely altered and transformed into secondary aggregate of clay minerals

IR-spectroscopy point to an almost complete lack of water in the structure of fresh glass, which is confirmed by a weak absorption within 3000–3600 cm^{-1} range. Very low water content is also attested by the results of thermal and microchemical analyses.

A characteristic feature of the chemical composition of impact glass (see Chap. 5) is a high reduction degree of iron, which is confirmed by Mössbauer spectroscopy and EPR. The analysis of NGR spectra demonstrates that only bivalent iron in tetrahedral and octahedral coordination is present in fresh glass. A similar, markedly broadened asymmetric doublet, pointing to the absence of structures with long-range order bonds in glass, is also characteristic of tektites. EPR tecnique was applied to study the occurrence of ferrous iron in the structure of glass. A low absolute content of Fe^{3+} (0.001–0.01%) determines an abruptly reducing environment of generation of the glass. Ranges of the contents of different forms of iron are similar for tektites and chilled green glass from suevites and microbreccia of the Popigai structure. Fe^{3+} in the structure of the impact glass from Popigai being the lowest.

Structural features of the aluminosilicate glass framework are revealed in Raman dispersion and IR-reflection spectra. The appearance of a low-frequency shoulder about 950 cm^{-1} in Raman spectra is associated with depolymerization of the glass network and the growing concentration of non-bridge oxygen bonds in its structure, partly frozen under the abruptly chilled cooling environment.

Qualitatively similar conclusions were also obtain from IR-reflection spectra. Tar-black and, particularly, green glass, are characterized by the highest defectiveness of the microstructure (local framework deformations, a high concentration of non-bridge oxygen bonds). There, similar to tektites (moldavites and indochinites), non-equilibrium disturbances of the glass network are most expressed. Glass is characterized by the minimum size of micro-inhomogeneities, revealed from low-angle X-ray dispersion spectra.

Characteristic features of fresh glass considered pointing to the high temperature of the initial melt and its quick chilling are: (1) holohyaline texture, lack of crystallization products and reaction rims around inclusions; (2) small number of inclusions (less than 1–3%); (3) presence among the inclusions of molten diaplectic quartz, lechatelierite, ilmenite, magnetite, and sulphide spherules, as well as native iron aggregations (Vishnevsky 1975); (4) lack of unbound oxygen in fluid inclusions and a high CO/CO_2 ratio in them, exceeding 1 (Dolgov et al. 1975); (5) a marked predominance of bivalent iron as compared to trivalent one, along with a low water content; (6) a high textural-structural and chemical homogeneity.

The spectroscopic and other studies conducted on fresh glass demonstrated that this glass formed under an abruptly reducing environment during quick chilling of strongly overheated impact melts. We consider them as a high-temperature impact glass, unlike glass of other varieties altered to a variable degree that is described below and is assigned to relatively low-temperature formations.

Devitrified, highly altered glass fragments, often occurring in suevites, are grey and brounish-grey, have a xenomorphic shape and vary in size from fractions of a mm to 0.5–1.0 cm, or, less frequently, more. The glass is dull, opaque, its structure is massive or, less frequently, fluidal, locally porous and vesicular; the texture is cryptocrystalline. Inclusions of mineral fragments, mainly quartz and feldspars, constitute from 3–5 to 10–15%. Among the alteration minerals, particularly developed in porous and pumiceous glass, illite, limonite, zeolites, clay minerals, and carbonates occur. Crystalloclasts often bear traces of high shock loads (diaplectic glass, monomineral melt glass, mostly recrystallized). They are irregularly distributed in the glass matrix; in places, they form shlieren-like accumulations. In slightly porous and porous glass, oblong pores and inclusions form chains empasizing the fluidal structure, which points to the plastic state of glass during transportation.

Along with relatively homogenous dark-coloured glass ($n = 1.551–1.565$) characterized by holohyaline or cryptocrystalline texture and massive, slightly porous structure, greenish- and brownish-grey, light brown and brownish, slightly porous, porous, and vesicular non-homogenized - heterogeneous glass particles are widespread; The refractive index of this glass varies from 1.54 to 1.72. The glass fragments are mostly devitrified. In vitroclastic and, particularly, sintered suevites, glass is crystallized to a certain extent; its texture is hypohyaline, spherulitic, hyalopilitic. Microcrystals are represented by globospherites, globulites, and cumulites. Alteration is common including the appearance of chlorite, limonite, smectites, etc. The most intensely devitrified glass acquires dark grey or black colouring.

Vitrolithoclastic suevites and, to a lesser extent, other varietes, contain light-coloured (light grey, yellowish-grey) xenomorphic porous and vesicular glass ($n = 1.540–1.560$, commonly 1.550) containing from 3–5 to 10–15% of mineral inclusions. Fluidal structure or plication are not recorded in them. There are altered glass fragments, the number of alteration mineral is the same that in above glass.

The study of magnetic properties of impact glass (Gorshkov and Starunov 1981; Raikhlin et al. 1983; Starunov et al. 1984) confirms the distinguishing of two contrasting groups among them. Ferromagnetics from high-temperature varieties (fresh dark green and tar-black glass) are represented mainly by dispersed particles in a super-

magnetic state, similar to those in high-temperature tagamites, whereas in glass of other varieties, which are assigned to the low-temperature formations, by multidomain particles with a minor amount of unidomain particles, which is also typical of ferromagnetics from low-temperature tagamites.

Impact diamonds are also present in impact glass particles.

4.4 Hydrothermal Alteration of Impactites and Impact Breccias

Although alteration minerals are present almost in all impact lithologies from different parts of the impact structure, the post-impact hydrothermal mineralization in the Popigai structure is characterized by the low intensity. It is developed mainly in tagamites, suevites, and impact glass while within allogenic breccia and, especially, in parauthochtonous rocks of the peak ring and crater edge, it is much rarer. The distribution of hydrothermal altered rocks is irregular on the crater area. It depends on location of massifs of highly heated rocks, permeability of their surrounding and water supply penetrating mostly from the surface. Most probably, there appeared numerous limited circulation cells, especially under the floor of small lakes, which sporadically arose on the surface. So, the hydrothermal mineralization is characterized by the relatively wide compositional difference of minerals due to the variation of crystallization environment.

Various alteration minerals are typical especially for suevite. Hydrous phyllosilicates locally replace impact glass, but much more frequently occupy pores and fissures. Calcite, zeolites (predominantly mordenite), minor sulphides (mostly pyrite), quartz, cristobalite, and opal are common hydrothermal minerals in vugs and amygdules. From interrelations between minerals infilling cavities, the following generalized order of the mineral formation is established: silica modifications (quartz, cristobalite, opal), hydrous phyllosilicates (smectites and chlorites), zeolites–calcite–pyrite (Naumov 2002).

The spatial distribution of post-impact hydrothermal mineral assemblages across the whole structure indicate that some of their associations are characteristic for certain structural elements of the crater or for certain parts of vertical section. Cristobalite and mordenite, together with saponite and mixed-layered phyllosilicates, dominate among alteration phases in tagamites, whereas in underlying crystalline megabreccia and in the uppermost suevite filling the central depression, calcite, quartz, pyrite, and low-silica zeolites are prevailing.

In microbreccias and suevites of the upper part of the crater fill dioctahedral smectites (beidellite or montmorillonite) dominate, whereas in lithovitroclasic and vitroclastic suevites of the middle part, Ca-saponites ($d_{001} = 14.7–15.3$ Å), mixed-layered chlorite-saponites, and Fe-chlorites are developed; these data indicate the increase of Fe and Mg contents and the decrease of Si, Al, Na, and K contents in clay minerals downward in the vertical section (Fig. 4.23). However, in thick tagamite sheets both

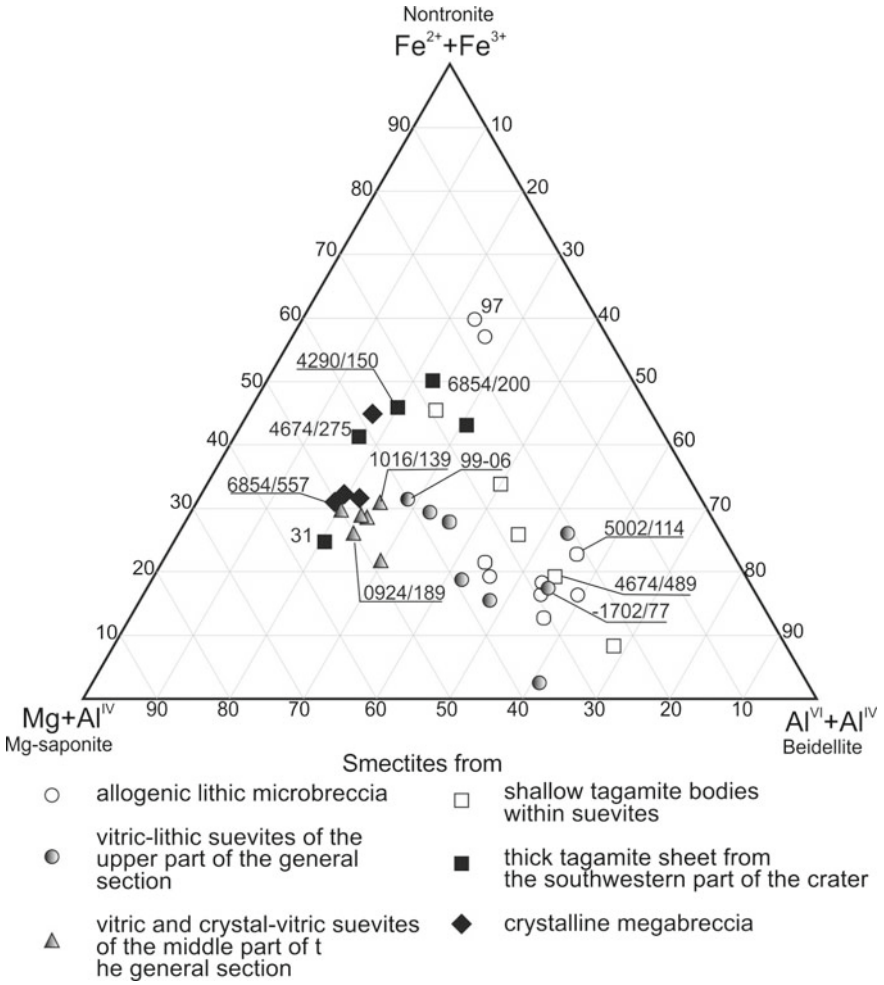

Fig. 4.23 Ternary $Fe^{2+}Fe^{3+}$-$MgAl^{IV}$-$Al^{VI}Al^{IV}$ diagram for alteration smectites, which replace impact glass and fill cavities in different impact lithologies from the Popigai crater (results of 36 electron microprobe analyses are used; see Naumov 2002)

trioctahedral and dioctahedral (both montmorillonite and beidellite) smectites occur often together. This indicates that local compositional variations of solutions, which reflect a local inhomogeneity, are more significant than temperature gradients within a thick impact rock sequence.

Thus, a general trend for variations of clay minerals composition from high-aluminia varieties (beidellite) to Mg–Fe varieties (saponite) from top to bottom in a generalized crater fill sequence is established. The diversity of conditions of hydrothermal alteration is manifested also in the wide range of zeolite compositions. Two zeolitic associations are distinguished (Naumov 2001): (1) mordenite associ-

ated with cristobalite, and, in rare cases, with minor chabazite, occurs in cavities of tagamite and suevite bodies, as well as in cataclasites within the polymict megabreccia; (2) stilbite, Na-chabazite, and, more rarely, heulandite, together with calcite, form zonal veins and geodes within the deep-seated breccia of crystalline rocks and tagamite sheets (predominantly in their near-bottom parts enriched in rock clasts), and in vitrolithoclastic suevites of the upper part of the general sequence. All zeolite species are enriched by silica relatively their stoichiometric formulae (Naumov 2001).

Epigenetic sulfides formed during the hydrothermal circulation are represented by the major pyrite and subordinate chalcopyrite and sphalerite. Pyrite (associated with calcite and zeolite) forms veins in tagamites and aggregate pseudomorphs after fragments of carbonaceous shale, argillite, siderite, and others in suevites and allogenic breccia. The youngest pyrite generation is developed in subvertical joints in tagamites. The pyrite is enriched in Ag, As, and Zn and depleted in Ni, Cu, and Co as compared with syngenetic sulfides. Some pyrites contain up to 1.4% Ni and up to 0.3% Co (Naumov et al. 2004). The sulfur isotope composition of epigenetic sulfides varies within a narrow range (from −0.7 to 3.2‰ CDT) to correspond the same values for target metamorphic rock.

Three main features of the hydrothermal mineralization are: (a) occurrence of low-temperature minerals alone; (b) the spatial distribution between different impact lithologies, which have a definite location within crater; a decrease of the Al^{IV} content from the base to top of thick tagamite bodies is the main alteration trend of compositions of both clay minerals and zeolites. It shows the decrease of temperature and of pH of the mineral-forming solutions in this direction; (c) some common features (e.g., enrichment in silica of hydrothermal minerals, higher Fe content in Mg–Fe phyllosilicates) of the chemical composition.

In geochemical aspect, the hydrothermal alteration in the Popigai is expressed in the concentration of weak basic elements and the depletion of alkali and of high-valency amphoteric elements, which precipitate in cavities as zeolites (Naumov 2005). The extent of chemical alteration of impact rocks under post-impact hydrothermal circulation is determined by the intensity of interactions between hydrothermal solutions and substrate, i.e. the amount of available water.

Inferred from the composition of hydrothermal mineralization, physical-chemical parameters of the impact-induced hot-water circulation system are modelled to be the followings. (a) The superficial meteoric and ground water, products of dehydration and degassing of minerals under shock are the sources for hot-water solutions. (b) Shocked target rocks are sources for the mineral components of hot-water solutions. No evidence of any deep heat and mass addition in the post-impact hydrothermal activity is found. (c) Fluid temperatures vary from ambient to 350–400 °C; (d) high rates of filtration (10^{-4}–10^{-3} ms^{-1}) are assumed by analogy with a modern Pauzhetka hydrothermal system (Rychagov et al. 1994); this is indicated by intense development of high-aluminia smectites. (e) In general, the succession of mineral crystallization confirm the uniform regressive course of the hydrothermal process.

The chemical parameters of the mineral formation vary within a narrow interval of pH and correspond to weakly alkaline and near-neutral environments ($pH = 6 \div 8$).

This feature is very close to composition of host rocks, which consist mainly of shock-disordered aluminosilicates and fusion glass. The intense leaching of this material providing the above-mentioned properties of solutions. The common presence of sulfides together with rare occurrence of iron oxides, indicates that the solutions maintained Eh values of >-0.5 V (for neutral environment) during the course of the hydrothermal process.

References

Basilevsky AT, Ivanov BA, Florensky KP, Yakovlev OI, Feldman VL, Granovsky LB (1983) Impact craters on the Moon and planets (in Russian). Nauka Press, Moscow, 200 pp

Bucher K, Grapes R (2011) Petrogenesis of metamorphic rocks. Springer, Berlin, 428 pp

Dobretsov NL, Kochkin YN, Krivenko AP, Kutolin VA (1971) Rock-forming pyroxenes (in Russian). Nauka Press, Moscow, 454 pp

Dolgov YA, Vishnevsky SA, Shugurova NA (1975) Gas inclusions in impactites. In: Thermobarometry and genetic mineralogy (in Russian). Nauka Press, Novosibirsk, pp 129–140

Engelhardt W, Stöffler D, Schneider W (1969) Petrologische Untersuchungen in Ries. Geol Bavarica 61:229–295

Feldman VI (1990) Petrology of impactites (in Russian). Moscow University Press, Moscow, 299 pp

French BM (1998) Traces of catastrophe. A handbook of shock-metamorphic effects in terrestrial meteorite impact structures. LPI Contribution No. 954. Houston, 120 pp

French BM, Koeberl C (2010) The convincing identification of terrestrial meteorite impact structures: what works, what doesn't and why. Earth-Sci Rev 98:123–170

Gnevushev MA, Krasavina TN, Kuznetsova LG (1982) Shock-enhanced transformation of garnet (in Russian). Mineral Zbornik 36(2):27–31

Gorshkov ES, Starunov VA (1981) Magnetic criteria of coptogenesis [abs] (in Russian). All-Union Meteorite Conference XVIII. Moscow, p 64

Grieve RAF, Langenhorst F, Stöffler D (1996) Shock metamorphism of quartz in nature and experiment: II. Significance in geoscience. Meteorit Planet Sci 31:6–35

Kaminskaya TN, Kamentsev IE, Orlova JV (1986) Garnets from shocked rocks (in Russian). Mineral Zh 8(3):8–17

Kozlov VS, Raikhlin AI (1989) Valence-coordinational state of iron ions in impact glasses from the Popigai meteorite crater (in Russian). Meteoritika 48:193–201

Kozlov VS, Kaminskaya TN, Orlova JV (1987) Study of shocked garnet with Mössbauer specrtoscopy (in Russian). Meteoritika 46:142–148

Masaitis VL (1978) High-temperature metamorphism and melting in impact craters. In: Problems of petrology of Earth crust and upper mantle (in Russian). Nauka Press, Novosibirsk, pp 188–194

Masaitis VL (ed) (1983) Textures and structures of impact breccias and impactites (in Russian). Nauka Press, Leningrad, 159 pp

Masaitis VL (1994) Impactites from Popigai crater. In: Dressler BO, Grieve RAF, Sharpton VL (eds) Large meteorites and planetary evolution I. Geological Society of America Spec Pap 293, pp 153–162

Masaitis VL (1999) Impact structures of northeastern Eurasia: the territory of Russia and adjacent countries. Meteorit Planet Sci 34:691–711

Masaitis VL (2005) Morphological, structural and lithological records of terrestrial impacts: an overview. Aust J Earth Sci 52:509–528

Masaitis VL, Raikhlin AI (1985) Immiscibility of impact and pyrometamorhic melts (in Russian). Meteoritika 44:159–163

Masaitis VL, Selivanovskaya TV (1972) Shocked rocks and impactites of the Popigai meteorite crater (in Russian). Zap Vses Mineral O-va 100(4):385–393

Masaitis VL, Mikhailov MS, Selivanovskaya TV (1971) The Popigai meteorite crater (in Russian). Soviet Geol 6:143–147

Masaitis VL, Mikhailov MS, Selivanovskaya TV (1972) The Popigai meteorite crater in Northern Siberia (in Russian). Meteoritika 31:74–78

Masaitis VL, Raikhlin AI, Reshetnyak NB, Selivanovskaya TV, Shitov VA (1974) Coesite from the Popigai crater (the first find in the USSR) (in Russian). Zap Vses Mineral O-va 103(1):122–127

Masaitis VL, Mikhailov MS, Selivanovskaya TV (1975) The Popigai meteorite crater (in Russian). Nauka Press, Moscow, 124 pp

Masaitis VL, Raikhlin AI, Selivanovskaya TV (1978) Principal criteria for classification and nomenclature of explosion breccia and impactites (in Russian). Lithologija i poleznye iskopaemye 1:125–133

Masaitis VL, Danilin AN, Mashchak MS, Raikhlin AI, Selivanovskaya TV, Shadenkov EM (1980) The geology of astroblemes (in Russian). Nedra Press, Leningrad, 231 pp

Masaitis VL, Mashchak MS, Selivanovskaya TV, Danilin AI (1983) New data on the inner structure and origin of the Popigai depression. In: Marcov FV (ed) Explanatory notes to Geological map of the USSR of 1:1 000 000 scale (new series), sheet R-48-(50) (in Russian). Nedra Press, Moscow, pp 180–190

Masaitis VL, Raikhlin AI, Selivanovskaya TV (1992) Impactites and impact breccia. In: Classification and nomenclature of metamorphic rocks (in Russian). Nauka Press, Novosibirsk, pp 168–187

Mashchak MS, Selivanovskaya TV (1988) Breccia and impactites at the southeastern rim of Popigai astrobleme (in Russian). Meteoritika 47:178–188

Mashchak MS, Orlova JV, Selivanovskaya TV (1992) Pyroxenes from tagamites of Popigai astrobleme [abs]. Russian-American microsymposium on planetology 16th. Moscow, pp 49–50

Naumov MV (2001) Zeolites in impact craters. In: Galarneau A, Di Renzo F, Fajula F, Vedrin J (eds) Zeolites and mesoporous materials at the dawn of the 21st century. Studies in Surface Science and Cathalysis 135, pp 41–48

Naumov MV (2002) Impact-generated hydrothermal systems: data from Popigai, Kara, and Puchezh-Katunki impact structures. In: Plado J, Pesonen LJ (eds) Meteorite impact structures in precambrian shields (impact studies 2). Springer, Berlin, pp 117–171

Naumov MV (2005) Principal features of impact-generated hydrothermal circulation systems: mineralogical and geochemical evidence. Geofluids 5(3):165–184

Naumov MV, Lyakhnitskaya VD, Yakovleva OA (2004) Sulfide Mineralization in the Popigai Impact Structure. Trans (Dokl) Russ Acad Sci, Earth Sci Sect 399A(9):1283–1289

Perchuk LL, Aranovich LY, Podlessky KK, Lavrent'eva IV, Gerasimov VY, Fed'kin VV, Kitsul VI, Karsakov LP, Berdnikov NV (1985) Precambrian granulites of the Aldan shield, eastern Siberia. J. Mefamorph Geol 3:265–310

Petrographic Code (2009) Magmatic, metamorphic, metasomatic, and impact rocks, 3rd edn (in Russian). VSEGEI Press, St. Petersburg, 128 pp

Raikhlin AI (1996) Suevite from the Popigai crater: inner structure and mode of origin. Sol Syst Res 30(1):11–15

Raikhlin AI, Selivanovskaya TV (1979) Breccia and impactites from explosion meteorite craters and astroblemes (in Russian). Meteorite impact structure on surfaces of planets. Nauka Press, Moscow, pp 65–81

Raikhlin AI, Kamentzev IE, Kuznetsova LG, Orlova JV, Samusina IA (1979) Modification of structural state of alkali feldspars under shock metamorphism (in Russian). Zap Vses Mineral O-va 108(4):466–471

Raikhlin AI, Danilin AN, Kozlov VS, Reshetnyak NB (1981) Chilling products of superheated impact melts from some astroblemes of the USSR territory [abs]. Lunar Planet Sci Conf XII, Houston, pp 860–862

Raikhlin AI, Danilin AN, Maslov VA (1982) Composition and microstructure features of chilled impact glasses from astroblemes at the USSR territory [abs]. Lunar Planet Sci Conf XIII, Houston, pp 636–637

Raikhlin AI, Danilin AI, Gorshkov ES, Starunov VA (1983) On contrast tagamite varieties from Popigai and Boltysh astroblemes (in Russian). Meteoritika 42:144–148

Raikhlin AI, Kirikov AD, Kozlov VS (1986) Fe^{3+} in impact glasses and tektites (in Russian). Trans (Dokl) Acad Sci USSR 287:422–424

Raikhlin AI, Reshetnyak NB, Golubkov VV (1987) Microstructure of impact glasses and tektites from IR-reflectance and low-angle X-ray dispersion (in Russian). Meteoritika 46:136–141

Raikhlin AI, Reshetnyak NB, Kozlov VS, Kirikov DA (1991) Complex spectrometric study of impact glasses and tektites (in Russian) [abs]. Int workshop on planetology XIV, Moscow, pp 34–35

Reshetnyak NB, Raikhlin AI (1988) Raman spectra of impact glasses and tektites [abs]. Lunar Planet Sci Conf XIX, Houston, pp 974–975

Ryabenko VA (ed) (1982) The geology and petrology of explosion meteorite craters (in Russian). Naukova Dumka Press, Kiev, 228 pp

Rychagov SN, Glavatskikh SF, Goncharenko OP (1994) Thermal regime of secondary mineral formation and structure of temperature field in interior of Baransky volcano (Iturup Island) (in Russian). Volcanologija i seismologija 6:96–112

Sazonova LV, Korotayeva NN (1989) Signatures of morphology and chemical composition of feldspars from impact melt rocks of Boltysh astrobleme (in Russian). Meteoritika 48:183–193

Selivanovskaya TV (1977) Petrographic types of tagamites of the Popigai meteorite crater (in Russian). Meteoritika 36:131–134

Selivanovskaya TV (1987) Crystal fractionation of impact melts (in Russian). Meteoritika 46:128–135

Selivanovskaya TV, Mashchak MS, Masaitis VL (1990) Impact breccias and impactites of the Kara and Ust-Kara astroblemes (in Russian). In: Masaitis VL (ed) Impact craters on Mesozoic-Cenozoic boundary. Nauka Press, Leningrad, pp 55–96

Starunov VA, Gorshkov ES, Raikhlin AI, Maslov VA (1984) Magnetic properties of impact glasses and suevites (in Russian) [abs]. All-Union Meteorite Conference XIX, Moscow, pp 132–133

Stöffler D (1971) Progressive metamorphism and classification of shocked and brecciated crystalline rocks at impact craters. J Geophys Res 76:5541–5551

Stöffler D, Langenhorst F (1994) Shock metamorphism of quartz in nature and experiment: I. Basic observation and theory. Meteoritics 29:155–181

Stöffler D, Ewald U, Ostertag R, Reimold WU (1977) Research drilling Nördlingen 1973 (Ries): composition and texture of polymict impact breccias. Geol Bavaria 75:163–189

Stöffler D, Artemieva NA, Wünnemann K, Reimold WU, Jacob J, Hansen BK, Summerson IAT (2013) Ries crater suevite revised—observations and modeling. Part I: Observations. Meteorit Planet Sci 48:515–589

Val'ter AA, Ryabenko VA (1977) Explosion craters in the Ukraine shield (in Russian). Naukova Dumka Press, Kiev, 154 pp

Vishnevsky SA (1975) Some ore minerals from impact glasses of the Popigai structure (in Russian). In: Methodology and methods of geological and geophysical research in Siberia. Nauka Press, Novosibirsk, pp 105–115

Vishnevsky AN (1978) Metamorphic complexes of Anabar crystalline shield (in Russian). Transactions of Arctic Geol Inst 184, Leningrad, 213 pp

Vishnevsky SA (1992) Suevites from the Popigai astrobleme: some paradoxes and apparent secondary interrelations (in Russian). Siberian Branch of Acad Sci of USSR Inst of Geol and Geophys Adv 7, Novosibirsk, 53 pp

Vishnevsky S, Montanary A (1999) Popigai impact structure (Arctic Siberia Russia) geology, petrology, geochemistry, and geochronology of glass-bearing impactites. In: Dressler BO, Sharpton VL (eds) Large meteorite impacts and planetary evolution II. Geol Soc of America Spec Pap 339, pp 19–50

Vishnevsky SA, Dolgov YA, Kovaleva LT, Pal'chik NA (1975) Stishovite from the Popigai structure rocks (in Russian). Russ Geol Geophys 10:156–159
Whitehead J, Grieve RAF, Spray JG (2002) Mineralogy and petrology of melt rocks from the Popigai impact structure, Siberia. Meteorit Planet Sci 37:623–647

Chapter 5
Petrochemistry and Geochemistry of Impactites and Target Crystalline Rocks

Anatoly I. Raikhlin and Victor L. Masaitis

5.1 Main and Trace Components and Isotopic Composition of Some Elements

As was shown by studies of tagamites and impact glass from suevites over the area of the Popigai impact structure, their bulk chemical composition is rather similar (Masaitis et al. 1975; Raikhlin and Mashchak 1977; etc.). This points to a high homogenization degree of the distribution of major elements throughout the entire impact melt volume. Biotite-garnet gneisses, which are widespread in the Khapchan series of Early Precambrian in the Anabar Shield, are most close to tagamites (Table 5.1). Despite the similarity in the contents of rock-forming oxides, the character of distribution of associations of lithophile and siderophile elements and the intensity of correlational links between elements within the associations differ markedly in tagamites and gneisses. In tagamites, the breakage of these correlations occurs; there is an abrupt change in the character of traditional lithophile and siderophile associations. Petrochemical data do not revealed any noticeable contamination of tagamites by sedimentary material from the target, and data of minor element abundance (Table 5.2) confirm this fact (Whitehead et al. 2002).

The average composition of tagamites through whole impact structure determined by numerous silicate analyses, does not differ from the composition of these rocks either within separate localities or from deep horizons (Table 5.1), there are certain insignificant variations, though. Limited sampling of impactite at some scanty areas on the surface showed similar results (Vishnevsky and Montanary 1999; Whitehead et al. 2002; Tagle and Claeys 2005).

The use of the non-polynomial trend analysis (see, e.g., Davis 1986) to reveal the character of changes in the composition of tagamites within the impact structure demonstrate generally that the distribution of a number of components in these rocks follows certain patterns (Masaitis et al. 1980; Masaitis 1994). Silica, magnesium, and

A. I. Raikhlin · V. L. Masaitis (✉)
A.P. Karpinsky Russian Geological Research Institute, Sredny prospekt, 74, 199106 Saint Petersburg, Russia
e-mail: vcmsts@mail.ru; victor_masaitis@vsegei.ru

V. L. Masaitis (ed.), *Popigai Impact Structure and its Diamond-Bearing Rocks*,
Impact Studies, https://doi.org/10.1007/978-3-319-77988-1_5

Table 5.1 Average chemical compositions of impacites and gneisses

Impactites and gneisses		SiO_2	TiO_2	Al_2O_3	Fe_2O_3	FeO	MnO	MgO	CaO	Na_2O	K_2O	P_2O_5	L.O.I.	Total	n
Tagamite															
Averaged for the Popigai structure	$\bar{X}$	63.17	0.74	14.54	2.29	4.68	0.06	3.38	3.70	2.29	2.71	0.08	2.04	99.68	163
	S	2.53	0.00	0.37	2.11	3.87	0.90	0.26	0.53	0.10	0.04	0.00			
LT tagamite, Mayachika Upland	$\bar{X}$	62.16	0.77	14.91	2.36	4.36	0.07	3.37	3.28	2.36	2.69	0.09	2.76	99.18	40
	S	1.50	0.03	0.49	1.29	1.78	0.01	0.44	0.52	0.34	0.27	0.09	1.03		
LT tagamite, Balagan-Yuryage River area	$\bar{X}$	62.57	0.75	14.98	1.54	5.69	0.06	3.91	4.15	2.40	2.76	0.13	1.20	100.14	71
	S	1.10	0.07	3.85	0.72	1.04	0.02	0.44	0.59	0.30	0.11	0.02	0.31		
HT tagamite, Balagan-Yuryage River area	$\bar{X}$	61.30	0.74	14.91	0.96	6.24	0.06	4.09	4.18	2.59	2.66	0.13	1.74	99.60	30
	S	0.91	0.02	0.27	0.43	0.96	0.01	0.32	0.64	0.29	0.13	0.02	0.80		
HT tagamite, Chordu-Daldyn River area	$\bar{X}$	63.61	0.71	14.82	1.99	3.84	0.08	3.14	3.86	2.59	3.07	0.10	2.27	100.08	18
	S	1.29	0.05	0.54	0.72	0.81	0.01	0.36	0.35	0.72	0.37	0.03	0.83		

(continued)

Table 5.1 (continued)

Impactites and gneisses		SiO_2	TiO_2	Al_2O_3	Fe_2O_3	FeO	MnO	MgO	CaO	Na_2O	K_2O	P_2O_5	L.O.I.	Total	n
Suevite															
Averaged for the Popigai structure	$\bar{X}$	65.41	0.63	13.11	3.34	2.75	0.08	2.77	2.60	1.83	2.73	0.07	3.97	99.29	58
	S	6.58	0.07	3.14	2.84	4.95	0.01	0.44	0.93	0.25	0.09	0.01			
Balagan-Yuryage River area	$\bar{X}$	65.69	0.68	13.78	2.98	4.18	0.07	3.34	2.97	1.76	2.66	0.11	2.21	100.43	22
	S	1.73	0.15	0.90	0.90	1.90	0.01	0.29	0.62	0.34	0.20	0.05	0.71		
Gneisses															
Weighed averaged composition of Khapchan series gneisses of the Anabar Shield	$\bar{X}$	63.14	0.59	15.02	2.20	4.29	0.08	3.06	3.77	3.02	2.39	0.08	1.98	99.62	122
Biotite-garnet gneisses composing the peak ring (Mayachika Upland and SW sector of the impact structure)	$\bar{X}$	63.44	0.77	15.47	1.77	5.31	0.07	3.20	3.00	2.57	2.47	0.09	1.65	99.81	45
	S	2.69	0.16	1.45	1.25	1.77	0.03	0.69	1.00	0.48	0.86	0.07	0.97		

Table 5.2 Minor element abundance in tagamites from the southwestern part of the Popigai impact structure (Balagan-Yuryage area) (from Whitehead et al. 2002)

Element	$\bar{X}$	S	Element	$\bar{X}$	S	Element	$\bar{X}$	S
Cr	141	9	Cs	0.85	0.26	La	53	4
Ni	62	11	Sr	224	12	Ce	108	8
Co	18	1	Tl	0.43	0.06	Pr	12	1
Sc	15	1	Ga	17	1	Nd	45	3
V	99	5	Ta	0.6	0	Sm	7.3	0.5
Cu	57	29	Nb	12	1	Eu	1.4	0.1
Pb	20	7	Hf	6.4	0.4	Gd	5.8	0.3
Zn	83	16	Zr	254	17	Tb	0.89	0.05
Sn	3.1	3.5	Y	34	1	Dy	5.3	0.3
Mo	2.4	1.4	Th	14	1	Ho	1.2	1.1
S	1564	548	U	1.7	0.2	Er	3	0.2
Sb	0.8	0.9	F	764	116	Tm	0.48	0.03
Ag	0.1	0.3	Cl	162	86	Yb	3.3	0.2
Rb	85	7	Be	1	0.1	Lu	0.49	0.03

$\bar{X}$—Mean value (from 37 analyses), S—standard deviation

sodium show a concentric distribution (Fig. 5.1), whereas ferric iron and alumina display a banded plan, parallel to the strike of gneiss sequences of the Anabar shield. The first type of distribution is due most likely to certain differences of rock composition in the vertical section of the melting zone, and to ejection of corresponding melt portions to different distances from the center. The second type of distribution is caused apparently by a slightly lesser homogenization degree of the melt fractions ejected along the strike of crystalline rock strata of a certain composition.

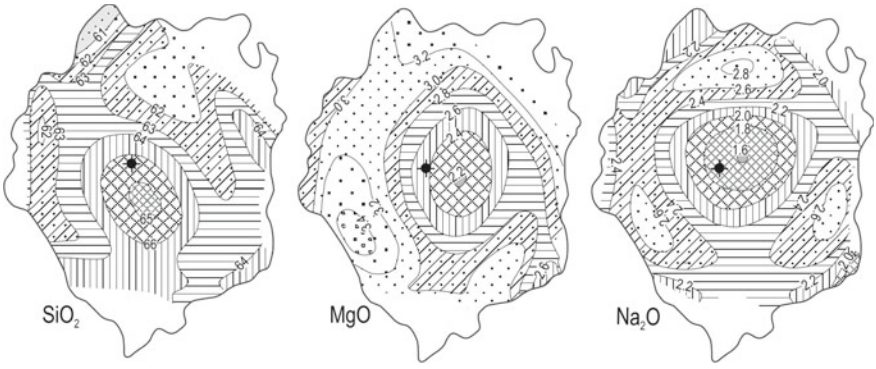

Fig. 5.1 Flow charts for the distribution of SiO_2, MgO, Na_2O (wt%) in tagamite through the Popigai impact structure. Non-polynomial trend analysis, 163 samples. The point shows the center of the crater

The detailed study throughout the 600-m-thick composite tagamite sheet in the Balagan-Yuryage River Basin also shows no essential changes in the chemical composition of these rocks. This points to the absence of significant processes of component redistribution during melt cooling and crystallization even in very thick bodies. At the same time, minor variations indicating the crystallization fractionation are recorded (Selivanovskaya 1987). As it was demonstrated above, some inhomogeneity in structure may be caused by the variation of melting parameters. The chemical compositions of LT- and HT tagamites in the Balagan-Yuryage River area are close (Table 5.1), though a statistical test of great number of analyses of LT and HT tagamites using Student's t-criterion reveals differences in SiO_2, Fe_2O_3, FeO, K_2O and L.O.I contents in these varieties (Table 5.3). The thermal analyses (DTA) of HT- and LT-tagamites showed that the first ones have a significant (2–3%) loss of water at the 60–600 °C, while in the second ones, this process takes place less than 250 °C, and the weight of water lost is 0.8–1.5%. All these features are regarded to the variation of initial temperatures of original impact melts.

Compositions of fresh glass fragments from suevites and microbreccia were studied using microprobe and by means of microchemical analyses, which showed similar results (Table 5.4). Both green and black glass fragments are generally similar and correspond to the average composition of tagamites. At the same time, green glass, as well as HT tagamite, is noted for the high reduction degree of iron. Noteworthy is a low content of alkalis in black glass, as well as differences in K/Na ratios in these two groups of glass. The Na content is approximately two times lower in black glass, and that of K is markedly increased. These differences have not yet been clearly interpreted.

Table 5.3 Values of the t-criterion when compositions of LT tagamite (n = 71) and HT tagamite (n = 30) being compared

Component	t-criterion
SiO_2	**5.89**
TiO_2	0.81
Al_2O_3	1.38
Fe_2O_3	**4.29**
FeO	**2.96**
MnO	0
MgO	2.66
CaO	2.49
Na_2O	0.35
K_2O	**5.58**
P_2O_5	1.95
L.O.I.	**11.5**

Underlined are significant values of t-criterions exceeding 2.67 at a confidence level of 99%
n—Number of analyses

Table 5.4 Average compositions of impact glass

Impact glass variety	Green glass from vitro-lithoclastic suevite and microbreccia				Dark glass from litho-vitroclastic and vitroclastic suevites			
Method of analysis	EMP data		XRF data		EMP data		XRF data	
	$\bar{X}$	S	$\bar{X}$	S	$\bar{X}$	S	$\bar{X}$	S
SiO_2	63.11	0.96	63.52	1.73	63.36	0.85	62.64	1.77
TiO_2	0.96	0.07	0.83	0.11	0.97	0.13	0.84	0.08
Al_2O_3	16.87	0.51	15.55	1.08	15.88	0.79	15.18	0.61
Fe_2O_3	–	–	1.09	0.65	–	–	1.70	0.79
FeO	–	–	5.95	0.67	–	–	5.37	0.73
FeO[a]	6.80	0.27	–	–	6.82	0.21		
MnO	0.09	0.03	0.08	0.02	0.08	0.03	0.09	0.02
MgO	3.33	0.24	3.47	0.35	3.49	0.36	3.50	0.22
CaO	3.72	0.18	3.69	0.70	3.74	0.68	3.38	0.43
Na_2O	2.21	0.10	2.35	0.25	1.03	0.45	1.35	0.32
K_2O	2.84	0.07	2.66	0.29	3.37	0.35	2.95	0.60
L.O.I.			0.49				2.23	
Total	99.93		99.68		98.74		99.23	
K_2O/Na_2O	1.29		1.13		3.24		2.19	
FeO/Fe_2O_3			5.45				3.17	
n	86		11		86		15	

[a]All Fe as FeO
n—Number of repeated analyses, $\bar{X}$—mean value, S—standard deviation

As is shown above, in the course of low-temperature hydrothermal circulation, impact glass, particularly their porous varieties, are altered; their water content and iron oxidation degree increasing markedly, and there is an essential change in the contents of most of the components.

Along with the general similarity between the bulk composition of suevites and tagamites the composition of suevites more essential fluctuates, which is connected with the presence of a great number of different sedimentary rock fragments in rocks (Table 5.1).

The study of REE distribution in tagamites and impact glass revealed the negative europeum anomaly and the rock enrichment in light REE (Masaitis 1994; Whitehead et al. 2002). A similar character of distribution is also established for single gneiss samples. This feature points to the belonging of corresponding precursor rocks to the lower crustal formations (Taylor and McLennan 1985).

Special researches of isotopic ratios of Rb/Sr and Sm/Nd in tagamites showed their correspondence to those in gneisses (Raikhlin et al. 1984; Hölker et al. 1997; Kettrup et al. 2003). As well, it points to the significant homogenization of melted substance. The tagamites have present day $^{86}Sr/^{87}Sr$ ratios between 0.7191 and 0.7369. Their Sr

model ages T^{Sr}_{UR} range from 1.9 to 2.3 Ga. The $^{143}Nd/^{144}Nd$ ratios of tagamites and impact glass cluster between 0.5113 and 0.5115. The Nd model ages T^{Nd}_{CHUR} range from 1.9 to 2.1 Ga.

Any comparison of the impact melt and target crystalline rocks composition account should be taken of the fact, that the melting zone cannot be adequately characterized by samples of these rocks, taken within basement outcrops on the surface or from wells penetrate the crater floor. Reconstruction of the initial composition of the melting zone, which disappeared completely during ejection, is always conditional, particularly in case of significant extent of melting and unhomogenous character of the substrate, where formations of different composition and, in places, of different age could be enclosed.

5.2 Projectile Matter Contamination

Study of the content and distribution of nickel, chromium, cobalt, and iridium in tagamites and impact glass and their comparison with the relevant values for gneisses enabled to reveal the remnants of the projectile in solidification products of impact melt (Masaitis and Raikhlin 1986, 1989). Ni, Co, Cr concentrations in tagamites are 1.5–3.0 times higher than in biotite-garnet gneisses with features of weak impact alterations (Table 5.5). Even greater differences in Ni content are recorded in tagamites compared with gneisses, not affected by shock metamorphism, where contamination by the projectile's substance is ruled out or minimized. In the latter, nickel content is 14 mcg/g (average of 18 samples).

Nickel distribution in tagamites is irregular; tagamites occurring in the lower part of the impactite sequence in the southwestern and northwestern sectors are most enriched in this element. Markedly elevated concentrations (to 630–730 mcg/g) are revealed here in thin lenses and veinlets of impact glass in intensely cataclased gneisses. Distribution of iridium in tagamites is also irregular (the analyses were performed using INA technique by I.G.Kapustkina, Vernadsky institute, RAS). Its average content is 0.072 ng/g (12 samples). Throughout the section of the thick sheeted tagamite body, its concentrations vary markedly. The background Ir content

Table 5.5 Average content of Ni, Co, and Cr (μg/g) in tagamites and shocked gneisses

Element	Ni			Co			Cr		
Lithology	$\bar{X}$	S	n	$\bar{X}$	S	n	$\bar{X}$	S	n
Shocked gneiss	27	17	41	13	5.2	41	80	44	32
Tagamite	85	31	85	19	3.7	83	110	18	79
Input into tagamite	58			6			30		

$\bar{X}$—Mean value, S—standard deviation, n—number of analyses

in non-contaminated gneisses is 0.007 ng/g; thus, the melt was enriched in this element by about one order. At the same time, glass veins in large blocks from megabreccia cemented by tagamites, are even more enriched in iridium. There, the contents of 5.0 and 5.7 ng/g of this element are, correspondingly, recorded in two samples. A highly homogenous distribution of the supplied meteorite substance in tagamites, along with the above-demonstrated homogenous character of these rocks in terms of petrogenic and trace elements indicates that the trapping of the projectile substance occurred after melt homogenization to the full extent. Most likely, this could occur as the absorption of minor clasts, which were the condensation centers of evaporated matter of the projectile in the transit crater.

Ratios between the supplied meteorite components, i.e. Ni, Co, and Cr, established in tagamites and glass of the Popigai structure, are similar to those of the common chondrites of L type. Using the above data and the information on the contents of nickel (1.3%) and iridium (500×10^{-7}%) in common chondrites, the share of the cosmic substance supplied both to tagamites and to impact glass veins in gneisses, which are most enriched in this element, can be evaluated (Table 5.6). Supply of the projectile substance to the impact melt, forming tagamites, is about 0.01–0.5%; and to small melt portions, at the expense of which glass veins formed in gneisses, 1.0–4.5% (Masaitis and Raikhlin 1989). Such a significant supply of dispersed substance of the impacting bodies (of, presumably, chondritic composition) into impactites is also known in some other impact structures of the world. For example, for the Brent crater, it is approximately evaluated at 1% and for the West Clearwater crater, at about 6% (Palme 1982).

Analogous results of the evaluation of the composition of the impacted body and the introduction of its substance into the impact melt, based on a study of the distribution of PGE in tagamites and gneisses, are given by Tagle and Claeys (2005). The content of PGE in tagamites exceeds that in gneisses by a factor of 3–14 and melt contamination by the impactor from 0.1 to 0.45% by weight, on average about 0.2%. A similar level of contamination is established for a number of impact craters (Koeberl 1998). Ratios of Ru/Rh versus Pt/Pd or Ru/Rh versus Pd/Ir confirmed the correctness of determining the composition of the projectile as an ordinary chondrite, most likely L-chondrite (Tagle and Claeys 2005).

Table 5.6 Estimate (wt%) of chondrite substance infused into impactites

Element	Abundance in chondrite	Input of the element into		Input of chondrite substance	
		Tagamite	Glass veinlets	Tagamite	Glass veinlets
Ni	1.3	72×10^{-4}	592×10^{-4}	0.55	4.55
Ir	0.5×10^{-4}	0.057×10^{-7}	5.34×10^{-7}	0.01	1.07

References

Davis JC (1986) Statistics and data analysis in geology, 2nd edn. Wiley, New York, 625 pp
Hölker T, Deutsch A, Masaitis VL (1997) Nd-Sr isotope signatures of impactites from the Popigai impact crater (Russia) [abs]. Lunar Planet Sci Conf XXVIII, Houston, pp 583–584
Kettrup B, Deutsch A, Masaitis VL (2003) Homogenous impact melts produced by a heterogeneous target? Sr-Nd isotopic evidence from the Popigai crater, Russia. Geochim Cosmochim Acta 67:733–750
Koeberl C (1998) Identification of meteoritic components in impactites. In: Grady MM, Hutchison R, McCall GJH, Rothery DA (eds) Meteorites: flux with time and impact effects. Geol Soc London Spec Publ 140:133–153
Masaitis VL (1994) Impactites from Popigai crater. In: Dressler BO, Grieve RAF, Sharpton VL (eds) Large meteorites and planetary evolution I. Geological Society of America Spec Pap 293, pp 153–162
Masaitis VL, Raikhlin AI (1986) The Popigai crater formed by the impact of an ordinary chondrite (in Russian). Trans (Dokl) Acad Sci USSR 286:1476–1478
Masaitis VL, Raikhlin AI (1989) The cosmic projectile matter in different types of rocks from impact craters (in Russian). Meteoritika 48:161–167
Masaitis VL, Mikhailov MS, Selivanovskaya TV (1975) The Popigai meteorite crater (in Russian). Nauka Press, Moscow, 124 pp
Masaitis VL, Danilin AN, Mashchak MS, Raikhlin AI, Selivanovskaya TV, Shadenkov EM (1980) The geology of astroblemes (in Russian). Nedra Press, Leningrad, 231 pp
Palme H (1982) Identification of projectiles of large terrestrial impact craters and some implication for the interpretation of Ir-rich Cretaceous/Tertiary boundary layers. Geol Soc Am Spec Pap 190:223–233
Raikhlin AI, Mashchak MS (1977) Petrochemical correlation of impactites of Popigai crater and its bed crystalline rocks (in Russian). Meteoritika 36:140–145
Raikhlin AI, Shergina YP, Murina GA (1984) Isotope composition of strontium: new evidences for impact origin of the Popigai structure (in Russian). Trans (Dokl) Acad Sci USSR 275:1153–1156
Selivanovskaya TV (1987) Crystal fractionation of impact melts (in Russian). Meteoritika 46:128–135
Tagle R, Clayes P (2005) An ordinary chondrite as the impactor of the Popigai crater, Siberia. Geochimica et Cosmochimica Acta 69:2877–2889
Taylor SR, McLennan SM (1985) The continental crust: its composition and evolution; an examination of the geochemical record preserved in sedimentary rocks. Blackwell, Oxford, UK, 312 pp
Vishnevsky S, Montanary A (1999) Popigai impact structure (Arctic Siberia Russia) geology, petrology, geochemistry, and geochronology of glass-bearing impactites In: Dressler BO, Sharpton VL (eds) Large meteorite impacts and planetary evolution II. Geol Soc of America Spec Pap 339, pp 19–50
Whitehead J, Grieve RAF, Spray JG (2002) Mineralogy and petrology of melt rocks from the Popigai impact structure, Siberia. Meteorit Planet Sci 37:623–647

Chapter 6
Impact Diamonds from Shocked Crystalline Rocks and Impactites

Georgy I. Shafranovsky

6.1 Principal Characteristics

In the 1960s, so-called "shaly" placer diamonds were discovered in sandy deposits of Ukraine, the source of these diamonds was unknown. It has been suggested that these are cosmogenic diamonds analogous to those encountered in some types of meteorites (Kashkarov and Polkanov 1964; Polkanov 1967; Sohor et al. 1973). After the finds of similar diamonds in the impact rocks of the Popigai impact structure it was determined that they were formed due to impact from graphite contained in terrestrial rocks (Masaitis et al. 1972). Subsequently, such diamonds were found in a number of impact structures of Russia, Ukraine, Germany, Finland and Canada (Rost et al. 1978; Val'ter et al. 1992; Masaitis et al. 1995, 1997, 1998, 1999a, b; Langenhorst et al. 1999 etc.). In 1970–1990s impact diamonds from Popigai structure were investigated in the laboratories of the All-Union (now Russian) Geological Research Institute (Leningrad), Central Research Geological Prospecting Institute (Moscow), All-Union Research Institute of Diamond Raw Materials (Moscow), Institute of Geology and Geophysics (Novosibirsk), Institute of Geochemistry and Physics of Minerals (Kyiv), Institute of Mineral Resources (Simferopol), All-Union Institute of Technique of Prospecting (Leningrad), in some other laboratories, and also in Institute of Planetology of Muenster University (Muenster, Germany), Institute of Max Plank (Mainz, Germany), Bavarian Geoinstitute (University of Bayreith, Germany), in the Vienna University (Austria), and in a number of other scientific centers. Principal results of undertaken studies are published (Masaitis et al. 1972, 1990, 1995; Vishnevsky and Pal'chik 1975; Vishnevsky et al. 1975; Rumyantsev et al. 1980; Shafranovsky 1985; Gnevushev et al. 1986; Val'ter et al. 1992; Masaitis 2013, Shumilova et al. 2014; Kis et al. 2016, etc.).

G. I. Shafranovsky (✉)
A.P. Karpinsky Russian Geological Research Institute, Sredny prospekt, 74, 199106 Saint Petersburg, Russia

V. L. Masaitis (ed.), *Popigai Impact Structure and its Diamond-Bearing Rocks*,
Impact Studies, https://doi.org/10.1007/978-3-319-77988-1_6

Table 6.1 Main characteristics of impact diamonds

Shape	Paracrystals, slaty plates, massive and irregular grains
Dimension	0.007–10 mm, mode 0.2–2 mm
Color	White, yellow, grey, brown, black
Phase composition	Diamond, lonsdaleite, graphite, chaoite, fullerene-like carbon, amorphous carbon, a super-hard carbon phase (?)
Inner fabric	Polycrystalline, composed of nanocrystals 0.2–0.5 nm, structural arranged
$\delta^{13}C$, ‰ PDB	−15 to −20
Micro-impurity elements	Si, Ca, Ti, Al, Na (total up to 0.1%)
Mineral inclusions	Quartz, aluminosilicates, glass
Refraction index, n	2.113–2.436
Birefringence	0.027–0.044
Density, g/cm^3	3.2846–3.612
EPR spectra defects g = 2 cm^{-3}	1017–1019
C-center, cm^{-3}	Absent
UF luminescence spectra (3500–4000 Å)	Yellow-orange luminescence, band series in the field 650–780 nm
Raman spectroscopy	Diffuse main peak 1332.5 cm^{-1}
Electric resistance, Ohm	Light-colored >1012, dark-colored −105 to 106
Magnetic susceptibility, cm^3/g	0.40×10^{-6}
Thermal conductivity (large fractions)	150–600 W/(m K)

The features of impact diamonds that distinguish them from widely known diamonds from kimberlites and lamproites are their appearance, polycrystalline structure, phase composition and a number of other properties caused by the presence of a number of allotropic forms of carbon and their combinations (Table 6.1).

6.2 Morphology

As noted above, impact diamonds occur in shock-metamorphosed gneisses and impactites; in addition, they are found in places in lithic breccias containing impact glass. Authigenic impact diamonds locate in situ at the place of their origin and are enclosed in shocked graphite-bearing rocks subjected to intense and rather intense shock metamorphism. In these rocks diamonds occur together with silicate and other rock-forming shocked minerals as well as with different kind of impact glass. Allothigenic impact diamonds are enclosed into glassy or crystalline groundmass

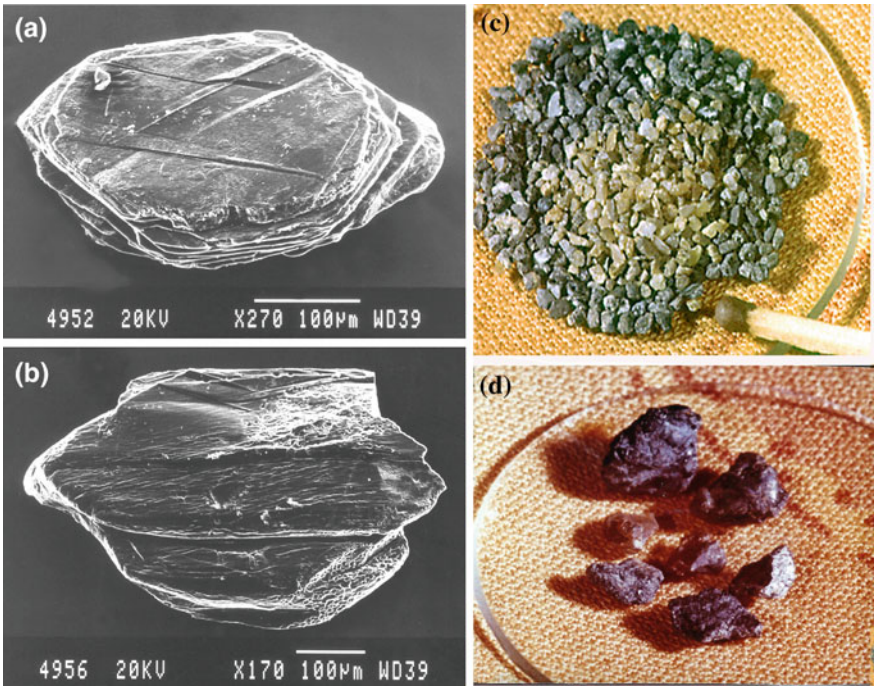

Fig. 6.1 Morphology of authigenic impact diamonds. **a**, **b** SEM images of paracrystals (0.3 and 1 mm in size respectively) extracted from shocked gneiss, **c** fragments (of about 0.5 mm in size) extracted from tagamites (a match for scale), **d** large rounded grains from placers. SEM images at Fig. 6.1, 6.2, and 6.4 are kindly provided by Dr. Falco Langenhorst (now Jena University, Germany)

of tagamite, impact glass fragments, comprised into suevites or lithic breccias. The last rocks can also comprise authigenic diamonds, however in this case, diamonds are again comprised into shock-metamorphosed gneiss fragments, which are a constituent part of tagamites and suevites.

Authigenic diamonds, to a major extent, retain the features of morphology and inner structure inherited from the initial crystalline graphite (Figs. 6.1 and 6.2), whereas allothigenic diamonds bear features of interaction with the intensely heated environment, acquiring morphological characteristics, which are not typical for initial graphite. Specific conditions of impact diamonds formation consisiting in the solide-phase transition from graphite and subsequent interaction with the melt, determine their constitution and physical properties. The mineralogical features inherited from the initial substance, as well as the newly acquired ones, can be distinguished. Since impact diamonds are polycrystalline aggregates of cubic and hexagonal hyperbaric carbon phases, at the same time, having the inherited shape of graphite crystals, they can be regarded as paracrystals, and their crystallographic elements, as para-faces, para-edges, etc.

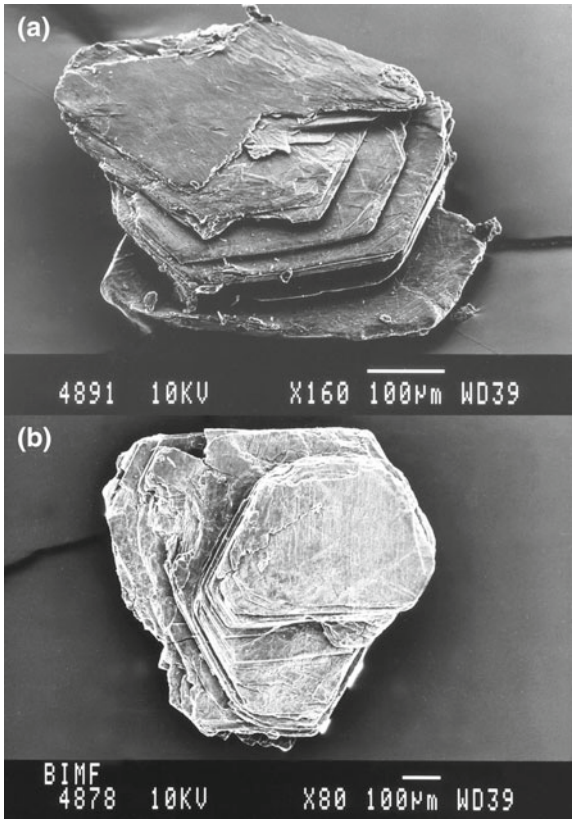

Fig. 6.2 SEM images of graphite crystals extracted from shocked gneiss: **a** tabular, **b** isometric, with unidirectional twin shading on the face (0001). Principal crystallographic features of such crystals are usually inherited by impact diamonds due to martensite transition

The size of impact diamonds grains extracted from the bedrock, ranges from 0.02 to 1.5–2.0 mm; in placers forming during destruction of diamondiferous rocks, diamonds to 8–10 mm across were found. The true size distribution of diamonds in non destructed hard rocks may be only roughly evaluated. The restricted tests showed that diamonds extracted by thermochemical decomposition from tagamite samples crushed to −8 mm mostly concentrate in fractions −0.5 + 0.2 mm (63 weight %) and −1 + 0.5 mm (23%), whereas fractions +3, −3 + 1 and less than 0.2 mm represent 8 and 6% accordingly.

The habit of impact diamonds is, in many cases, similar to the initial graphite—there are flattened plates, their basal planes retaining striation due to twinning typical of graphite, and lateral planes being step-like. There are parallel intergrowths, traditional for graphite, and non-classical Veselovsky's twins. In addition to grains retaining the habit of initial graphite crystals, there are numerous irregular aggregates, as well as grains bounded by natural surfaces, but not displaying the inherited faces. Irregular partly rounded grains more often occur in placer deposits.

Comparative analysis of the morphology of impact diamonds and graphite from the same gneiss samples reveals both similarity in the size of these minerals, but

also some differences. Similar distributions of lengths and widths are recorded in graphite and diamond, both facet objects and grains. One should also note a slightly lower value of the length mode, particularly in impact diamond paracrystals, as compared to similar data for graphite. It allows presuming graphite response to volume reduction with transition to the impact diamond. Size-width distribution of allothigenic diamonds extracted from the tagamite samples shows that it is similar to that of authigenic diamonds.

Data on goniometry of impact diamonds are based or measurements of 40 well-faced paracrystals, their size not exceeding 0.25 mm. One of the main criteria for selecting impact diamonds for measurements was a complete extinction of the object in polarized light. As it was shown by X-ray studies, well-structured varieties are distinguished, in which the fabrics coincide with crystallographic elements of cubic diamond crystals and crystalloptical axes, that is very important for interpreting goniometric data.

In the previous works (Shafranovsky 1985; Kvasnitza 1985) it was noted that impact diamonds mainly display the "pinacoid-prismatic" habitus, inherited from graphite; therefore, when the faces of impact diamonds being described, symbols typical of hexagonal crystals are used. The measurements demonstrated the inherited character of the oblique belt of faces of impact diamonds in relation to dipyramidal graphite faces, unlike a clearly newly acquired feature of alteration of the vertical belt. In graphite crystals, irrespectively to the shock metamorphism degree, the vertical belt is composed of two prisms: the unit habit prism $\{10\bar{1}0\}$ ($\varphi = 0°$, $\rho = 90°$) and the prism of the second $\{11\bar{2}0\}$ ($\varphi = 30°$, $\rho = 90°$) type, their faces alternating at 30°. For impact diamonds polar distances of parafaces of the unit and second prisms mainly differ from 60°.

In all measured paracrystals, there is a distinct pattern: opposite angles of both prisms are equal. A connection is revealed between the measured vertical "forms" and the habit of paracrystals, showing up the location of the largest angle from the vertical belt of the unit prism [$(\bar{1}010)$:$(\bar{1}100)$; $(10\bar{1}0)$:$(\bar{1}100)$]. The angle along the impact diamond elongation can be designated as α, its value ranges from 88 to 61° ($\Delta = 27°$). Polar distances of the other two angles, β, middle [$(0\bar{1}10)$:$(\bar{1}100)$; $(01\bar{1}0)$:$(10\bar{1}0)$] and γ, the smallest [$(0\bar{1}10)$:$(1\bar{1}00)$; $(01\bar{1}0)$:$(10\bar{1}0)$] are always less than α, i.e. β from 73 to 49°, and γ from 53 to 23°.

Values of α, β, γ angles of impact diamonds are diverse; their comparison with the corresponding graphite angles reveals that deviation of parafaces from the vertical belt of both paraprisms is given by three combinations of displacements from the position of faces in graphite crystals clockwise and counter-clockwise. This points to rotation mechanism of some morphological elements in case of graphite-impact diamond polymorphism. It should also be noted, that the presence or lack of other polymorphic carbon phases (lonsdaleite, graphite) does not affect the rotation degree of the vertical belt of parafaces. Most likely, this is the response of material to changes in volume during polymorphism.

Parafaces of the oblique belt of impact diamonds have an inherited character from graphite faces. For impact diamonds, 57 crystal forms were found, also occurring on graphite crystals (Kvasnitza et al. 1988). Parapyramidal faces of both the first

and the second prisms, coincide with ρ of graphite dipyramids. The most frequent dipyramids from the zone of habitus prism are recorded with $\rho = 72^\circ\ 32'$ $\{10\bar{1}1\}$, $\rho = 5^\circ\ 11'$ $\{1.0.\bar{1}.35\}$, $\rho = 68^\circ\ 31'$ $\{40\bar{4}5\}$; and para-pyramids of the second paraprism are characterized by low values $\rho = 20^\circ\ 09'$ $\{1.1.\bar{2}.15\}$, $\rho = 15^\circ\ 23'$ $\{1.1.\bar{2}.20\}$; however, most often paraface $\rho = 6^\circ\ 17'$ $\{1.1.\bar{2}.50\}$ occurs.

Summarizing up the analysis, it should be noted that parafaces of the unit prism are responsible for the habit, as well as for the appearance of step-like striation (growth layers) inherited from graphite. Paraprisms of second-order determine the trends of impact diamonds jointing, as well as macrotwinning striation inherited from graphite.

In addition to twinning striation inherited from graphite and from both partly inherited and new-formed fissures, basal parafaces of impact diamonds can bear traces of induction surfaces of intergrowth with other minerals, inherited from graphite and showing up as hollows. Due to the plasticity of graphite, its joint growth with other minerals can results in bending of crystals that is inherited by successive diamonds.

Allothigenic impact diamonds occurring in impactites (tagamites, etc.) have a specific rare-pitted surface relief, which results from oxidizing processes occurring at high temperatures. Due to this, characteristic features of impact diamonds from tagamites and impact glass, in addition to a dull character of surfaces are also rounded para-edges, para-faces, and para-apices; the degree of roundedness affects the habit of impact diamonds, brinding it to the extreme ellipsoidal forms—ovaloids, spheres, discs. Elements of the crystallographic forms become vague, twinning steps smooth out, and composition faces are etched up to generation of throughgoing "cuts". Intense corrosion can eventually result in generation of seemingly "corroded" diamond particles, locally reminding of lace (Fig. 6.3). Under great magnifications, the dulness of surfaces of paracrystals and grains has a character of a honeycomb relief (Fig. 6.4) revealing a fine-grained (crystallite) structure of impact diamonds, cut along fissures and twin boundaries (Rumyantsev et al. 1980). The thin secondary graphite film appears over this surface as the result of graphitization. Crystallites showing up on basal para-faces of diamonds, have hexagonal contours and an oblong-flattened habit; their mean size is 10×7 μm, characteristic elongation 1.4. Yellow diamonds display these parameters; crystallites of white and colourless varieties have a slightly larger size (15×9 μm), forms of such crystallites are more isometric (a/b = 1.3). SEM study of surface of impact diamonds in some cases reveal more complicated microsculptural three-dimentional features, composed of numerous very thin plates (about 1 μm and less) which lie one over another and intergrowth with columnar nanocrystallites perpendicular to them (Kis et al. 2016).

6.3 Phase Composition and Microtexture

Studies of impact diamonds establish their polycrystalline composition and structured character. They are composed by ordered crystallites about 10^{-5} cm across. X-ray diffraction analysis and Raman spectra (Masaitis et al. 1990) also demonstrate

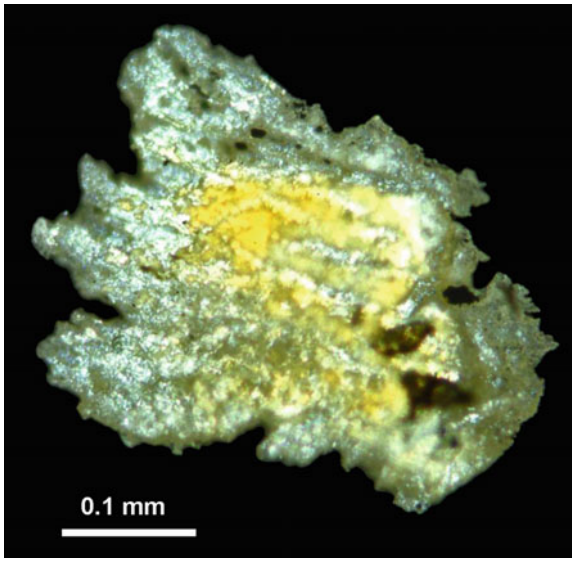

Fig. 6.3 An intensely corroded grain of impact diamond that is lace-like at the edges. The size of the grain is 0.25 mm across. Crossed nicols

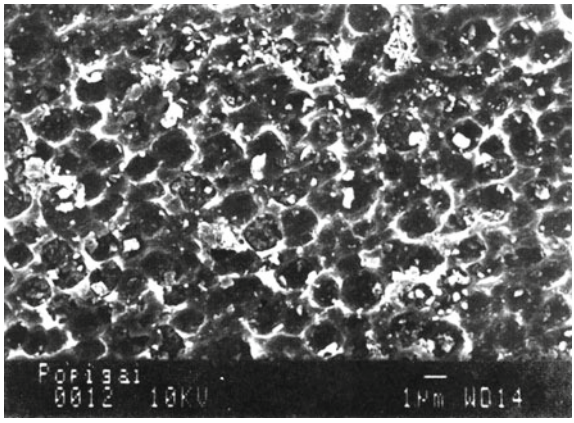

Fig. 6.4 The honeycomb relief on etched surface of allothigenic impact diamond combined with the graphite coating (upper right). SEM image

that they are subdivided into diamonds composed exclusively of the cubic phase, and diamonds, also containing the hexagonal phase, i.e. lonsdaleite. Besides, the former and the latter also often enclose a certain amount of both primary and new-formed graphite and some other carbon allotropic forms. The basis of impact diamonds is the cubic phase (parameter $a_0 = 3.56$ Å), having a polycrystalline character, which is confirmed by a marked broadening of 111 and 110 peaks in Debye-Scherrer powder photographs, as well as by the presence of twins registered in Lauhe patterns (Fig. 6.5). Besides stucturing of two orders is revealed, its presence being recorded in samples with complete extinction, thus connecting the inner structure with the outer morphology of paracrystals.

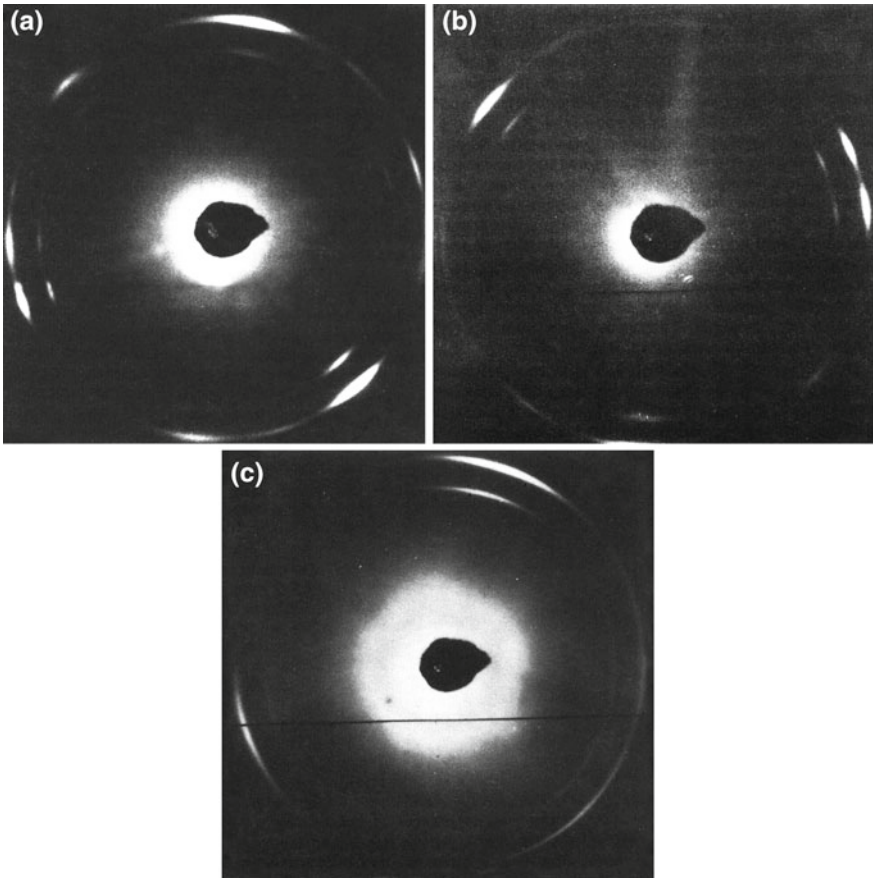

Fig. 6.5 Laue-photographs of impact diamonds containing lonsdaleite (six signals from {111} indicate a twinning character of its texture). Laue-photographs: **a** of the basal plane (0001); **b** paraface (0110); **c** paraface (2110)

The first direction of the structure is observed along the basal plane of the sample, where crystallites twinned along 111′ (the twinning is marked by stroke "′" after the index form) (Fig. 6.5) occur as layers. That is the pinacoid of initial graphite {0001} is passing into twinned crystallite lattice {111}′.

The second direction of structure connects the face of the prism $\{10\bar{1}0\}$ of graphite with $\{11\bar{2}\}'$ of diamond (more precisely, $\{10\bar{1}1\}$ of graphite with {111} of diamond (Fig. 6.5a, b) or the face $\{11\bar{2}0\}$ of graphite with {110}′ of diamond (Fig. 6.5c). Such an association is observed irrespective of the presence of other structural phases of carbon. Most widespread are diamonds containing from the first % to 40% lonsdaleite (Kvasnitza 1985; Rumyantsev et al. 1980; Kaminsky et al. 1985), and the latter intergrowths regularly with the cubic phase (Kurdyumov et al. 1979; Gorgotskaya et al. 1989). The orientation pattern of crystalline phases of carbon in natu-

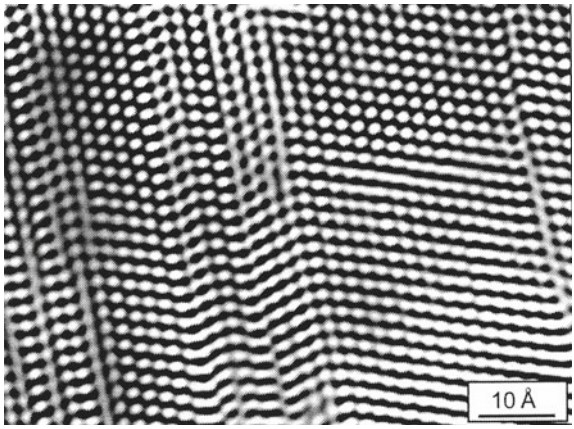

Fig. 6.6 Fourier-transformed and filtered HRTEM image of impact diamond. In this view along the [110] the diamond crystal shows numerous stalking faults and microtwins. Bright dots represent the channels in the diamond structure (Langenhorst 2003)

ral processes of polymorph transition graphite—impact diamond are illustrated by Table 6.2. Comparison of the pattern of nets of the corresponding faces of carbon polymorphs, where shows of epitaxis induced by graphite transformation into diamond by twinning and generation of lonsdaleite are recorded, demonstrates that such features can be easily explained. Noteworthy is the coincidence in orientations of hexagonal lonsdaleite and graphite phases in the impact diamond where the six-fold axes are superimposed on double axes with crystallographically similar intergrowths of non-classical graphite twins (Shafranovsky 1981). HRTEM study of entirely cubic impact diamonds and lonsdaleite-bearing diamonds reveals a high density (up to 5 per 10 Å) of linear-plane defects (stacking faults), as well as microtwins (Langenhorst 2003; Fig. 6.6).

It can not be ruled out that lonsdaleite does not exist as an independent phase, forming individuals separated by structurally non-conjugated separation surfaces from cubic one, and the corresponding x-ray characteristics are a consequence of the high density of such defects (Koeberl et al. 1997).

Raman spectroscopy of impact diamonds (Reshetnyak and Ezersky 1990; Bouldeulle et al. 1999) detects variations of the spectra at different points, which indicates that nanometer domain structure or inhomogeneities in the local relationships with sp^3—diamond character. The most characteristic is a broad Raman peak with a maximum 1330–1335 cm^{-1} with FWHM 19–23 cm^{-1}. A shift towards lower wavelengths in comparison with kimberlite diamonds may be due to the annealing, of different point or the more common defects, and the broadening of the peak may be caused by residual stress. The presence of amorphous carbon is identified by the presence of a peak 1600 cm^{-1}. At some points was revealed vitreous carbon (or nanocrystalline graphite).

Total imperfectness of impact diamonds and its nature were studied using the EPR technique (Suchardjevskiy et al. 1992). The specific feature of the research conducted was the use of RE-1380 spectrometer in Q-range at frequency of 37,100 MHz. Spectra were obtained at room temperature; to eliminate the effect of paramagnetic centres

of atmospheric air, photographing was performed in gaseous nitrogen atmosphere. Separate samples with distinct paracrystallographic outlines, were used as the objects of study, which allowed determining their orientation relative to the vector trend of the polarizing magnetic field. Overall, 150 EPR spectra were obtained on 25 impact diamond grains, characterized from X-ray research data and differing in colour and density. The results obtained enable to make the following assumptions on the defect structure of impact diamonds.

Study of angular dependence of the behavior of a package of low-resolution lines in the area of g-factor 2.0032, which is recorded for all studied samples, enables to conclude that they represent intergrowths of microcrystals where the direction of the prevailing orientation is parallel to axis L_3 of some cubic phase crystallites. Since the volume of the studied specimens did not exceed 0.5 mm^3, and EPR spectra of the centers in different directions corresponded to the powder spectra, it might be concluded that the size of certain crystallites does not exceed 25 μm. Besides, it was ascertained that the described package of lines in the area of g-factor 2.0032 is a superposition at least of two lines belonging to different paramagnetic defects. Due to their different physical nature and the type of crystal sites occupied, these electronic defects have a different ability to interact with electromagnetic SHF field. One of the observed centers practically does not experience saturation in electromagnetic field to 1 mW, whereas the intensity and width of the second one start displaying the dependence on the power of SHF field even at its values of about 0.05 mW, and is saturated at 0.1 mW. Electronic defect, which is not dependent on the power of the SHF field, correlates with the content of lonsdaleite, the presence and amount of which being determined from X-ray data.

Of utmost interest is the search of paramagnetic nitrogen in impact diamonds, its EPR spectrum being composed of 3 lines of superfine structure (SFS), resulting from interaction of non-paired spin density with magnetic moment of the atomic nucleus N and has the value of g-factor 2.0025. It is ascertained that the entire material investigated does not contain paramagnetic defects, associated with entering of atomic nitrogen into the lattice. At the same time, on the surfaces of paracrystals and irregular grains of impact diamonds thin crust or film formed of small diamonds of cuboctahedron habitus with nanocrystalline structure are found in places. They are composed of nitrogen-containing cubic phase (Val'ter et al. 1992; Shumilova et al. 2014). Paramagnetic nitrogen was observed only in the above mentioned thin crust cuboctahedron diamond, growing on basal parafaces of paracrystals and surfaces of irregular grains. Cuboctahedron crust probably is the result of condensation of diamond from the gas phase at lower pressure by the CVD mechanism. In addition, principal allotropic carbon forms, described above, rare chaoite finds were established in some rock samples together with graphite and diamond (Vishnevsky and Pal'chik 1975).

Infrared spectroscopy of the samples detected the presence of intense absorption bands around 655 and 2385 cm^{-1}, characteristic of CO_2, which are offset from their position at normal pressure to meet carbon dioxide under pressure of about 5 GPa (Koeberl et al. 1997). Impact diamonds can contain inclusions of quartz and aluminosilicates. Diamond powder contains Si, Ca, Mg, Al, Ti, Fe, and Na as much

as 0.05–0.1% in total. The study of impurity elements detects the similarity of their distribution with that of the original graphite, rare earths—with their distribution in gneisses (Koeberl et al. 1997).

In addition to the above-mentioned carbon phases established in impact diamonds, the HRTEM method has recently revealed multilayer fullerene-like carbon nanostructures with a diameter of 5–10 nm. The mode of their origin is not clear. It is proposed that the formation of onion-like carbon in impact diamonds is connected with high pressure graphite transformation or post-pressure stress cooling, which partly provides back transformation of diamond nanocrystallites to sp^2 carbon statement. However, possible relict origin of fullerene-like carbon from the impacted initial sedimentary rocks with fullerenes and fullerene-like substances, like shungite or coal, could not be excluded (Shumilova et al. 2014).

To confirm this idea, detailed investigation of the geological background is needed. The sedimentary part of the Popigai target is composed of five stratigraphic levels of sedimentary rocks enriched in carbonaceous material like coals and bitumenes with Proterozoic-Cretaceous and Pliocene-Quarternary ages. Earlier it was supposed that the sedimentary part of the target was too soft and its carbon-bearing material simply dispersed or burned, so could not take part in diamond-forming process due to high dynamic compressibility of host rocks (Masaitis et al. 1990). No any strongly shocked and melted sedimentary rocks were found among the Popigai impactites. At the same time, the presence of sedimentary rock fragments with coals and even some relicts of coalificated wood within the suevite was reported (Kiryushina 1959; Masaitis et al. 1975, 1998; Vishnevsky 1994, see also Chap. 2). Diamond formation from sedimentary carbonaceous material is known from diamond-bearing Kara impact structure where diamonds were formed directly from coal (Ezersky 1986). To judge of part of Popigai impact diamond grains (e.g. the irregular shaped nontextured ones) have been formed from poorly ordered non-graphitic carbonaceous material, a detailed study of the amorphous component and the nanostructure of the nanodiamond grains are necessary.

Nanotwinned nanodiamond crystals embedded in a native amorphous carbon matrix have been imaged by HRTEM from Popigai impact diamond as well. This analysis proves that the native amorphous carbon of the grains contains small amount of oxygen, while the nanodiamond seems to be oxygen free. The bonding texture of the amorphous carbon is dominated by sp^2 bonded carbon. Based on nanostructural features, such as non-uniform crystal size and twin thickness, and on the presence of oxygen-bearing native amorphous carbon, it may be supposed that the nontextured impact diamonds can be formed from poorly ordered (probably organic) carboniferous material of sedimentary origin and/or have been undergone a non-uniform degree of HPHT transformation including a pyrolysis stage (Kis et al. 2016).

In general, impact diamonds are a complicated constitutional mineralogical system (Masaitis et al. 1990), they may be presented as consisting from the structural elements of four levels. The first level lays down the subindividuals cubic nanocrystalline diamond (forming a counterpart in microcrystallite) and subindividuals nanocrystalline lonsdaleite (the dimension of ~0.2–0.5 nm), the second one, a separate microcrystallites formed by subindividuals of these two phases (the dimen-

Table 6.2 Correlation of orientations of morphological and structural elements and indicatrix axes of diamond paracrystals

Morphological elements of graphite	Structural elements		Indicatrix axes
	Cubic phase	Hexagonal phase	
0001	$\{111\}'$	$10\bar{1}0$	Nm
$10\bar{1}0$	$\{11\bar{2}\}'$	$11\bar{2}0$	Ng
$11\bar{2}0$	$\{110\}'$	0001	Np

sion of ~1–2 μm), the third one, conditional two-dimensional system microcrystallites with the texture; and finally, the fourth one in turn two-dimensional elements in the transition to three-dimensional structure, which is ordered or unordered and can be represented by paracrystals from 0.1 to 2–3 mm in diameter. Paracrystal may be complicated by the block structure. It is possible that further investigation of impact diamonds will bring many other data on their nanotexture, taken into account the presence of other allotropic forms of carbon.

6.4 Physical Properties

Despite their polycrystalline construction, impact diamonds are transparent and have unique crystal optical properties. Well-formed diamonds, i.e. diamonds with high ordering, showing up the presence of two structural directions, imitate single crystals of the lower systems in their crystal optical properties. They display birefringence in crossed nicols, its value ranging from 0.002 to 0.044, averaging at 0.0035–0.0040 (Gnevushev et al. 1986; Bochek et al. 1984). Birefringence of impact diamonds is a typomorphic feature. It results from their composite defect structure. Refractive index values of impact diamonds generally range from 2.436 to 2.113; there is a tendency towards the increase of refractive index from dark-coloured grains to light-coloured ones (Fig. 6.7a, b).

Orthoscopic studies of para-face {0001} demonstrate conoscopic pattern, characteristic of biaxial mineral—two vague hyperbolas, quickly going away, when the microscopic stage is turned beyond the field of vision. The optical sign determined by a hypsum plane is negative.

In crossed nicols, under rotation of polarizer, a double extinction of diamonds along $\{01\bar{1}0\}$ and $\{\bar{2}110\}$ is observed coinciding with Ng and Np. In paracrystals, Np axis is commonly parallel to elongation, and Nm axis is aligned to {0001}. Taking into account the above X-ray data, it is possible to connect the construction of twinned para-faces with crystallooptical characteristics of impact diamonds, as well as with their morphology. It should be noted that optical crystallography data are independent on the presence or lack of lonsdaleite phase (Table 6.2).

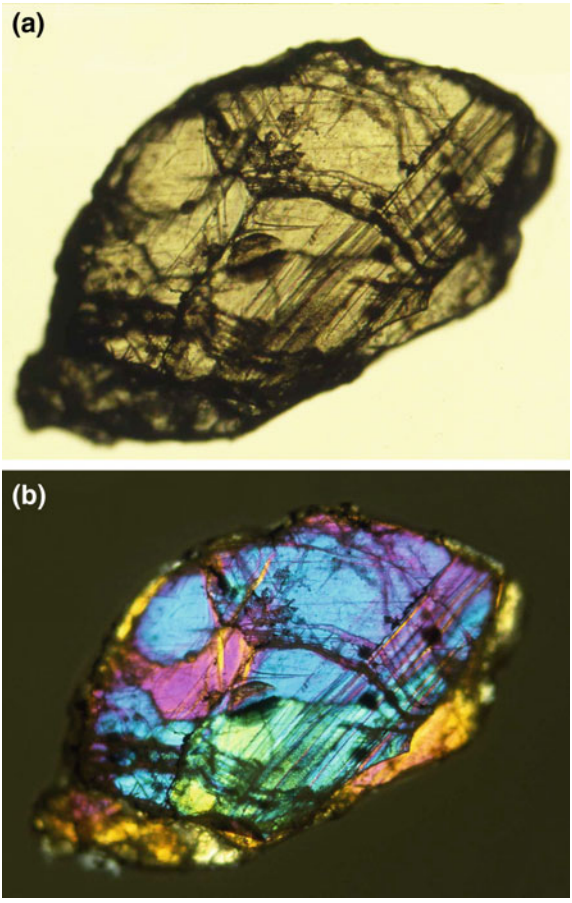

Fig. 6.7 A transparent impact diamond with twinning striations, nicols are parallel (**a**). The paracrystal shows the strong birefringence under crossed nicols (**b**). The diamond is 180 μm across

The above morphological, textural, and crystallooptical data provide grounds for distinguishing the unit layer in impact diamonds, its constitution and physical properties, most likely, corresponding to an individual crystallite. However, it should be noted, that well-constructed objects are extremely rare (6%); much more frequent are impact diamonds, in which the unit layers are unordered that results in undulatory extinction (80%). There are also isotropic impact diamonds; this is connected with the rotation angles of superimposed unit layers. Thus, diamonds, which do not display complete extinction (12%), are composed of two unit layers, their basal planes coinciding, and the optical indicatrix axes make up 45°; at the angle of 90°, impact diamond is not anti-reflecting (2%). Interference colors are dependent on the thickness of diamonds; brightly coloured are ridge-shaped microtwins, and relief projections; lows in the grain relief also reduce the interference colours relative to the background.

Table 6.3 Distribution (in %) of diamonds of different color in shocked target rocks and impactites

Colour	Shocked gneisses	HT tagamite	LT tagamite	Suevite	Allogenic microbreccia
Colorless and white	6	6.1	6.0	16.3	34.8
Yellow	15	28.0	30.1	57.9	38.0
Light brown	14	27.5	35.9	13.1	3.0
Dark brown	13	15.6	7.5	3.9	6.0
Grey	1	6.3	6.5	2.2	0.0
Black	51	16.5	14.0	6.6	18.2
Ratio of light-colored versus dark-colored diamonds	0.5	1.6	2.6	6.9	3.1

The group of dark-coloured diamonds is visually characterized by the presence of graphite. In particular, in dark brown diamonds, the amount of graphite can reach 50%; the black type comprises opaque diamonds, containing mosaic grains. In thin translucent plates, shiny black diamonds produce a dichroic pattern with a single polarizer, and for paracrystals there is an increase in color along Np, and attenuation along Ng, indicating a density of cracks along the Np direction through which graphitization took place. These inclusions lower the brilliance of diamonds, unlike fine-grained graphite, which gives the diamond a glassy sheen. Gray impact diamonds in their color are due to microfracturing, underlined by graphite, usually block mosaic grains. Development of unidirectional jointing, commonly along the boundaries of twins, impacts a silver colour, a moire fabric, and acicular jointing; such grains are extremely rare.

Data on the percentage of impact diamonds of different colour extracted from certain rock types presents on the Table 6.3. It should be borne in mind that in microbreccia diamonds occur in chilled glass fragments. In tagamites, diamonds of light-coloured group predominantly occur, though high melt temperatures, which affected diamonds, should have resulted in graphitization, i.e. increase of the number of grey-coloured grains, particularly in case of high-temperature tagamites. However, the intense oxidizing processes, most likely, destroyed graphite traces, thus causing clarification of the material. Authigenic diamonds from gneisses are characterized, contrariwise, by a relatively high content of dark diamonds, which can be accounted for by a low degree of development of the oxidizing processes and preservation of both relict inclusions of primary graphite, and graphite shells of diamond grains.

The density of diamonds ranges from 3.2846 to 3.6127 g/cm^3, it decreases with the increase in the number of defects and graphite content. The latter mineral, found in shock-metamorphosed gneisses along with diamonds, is also heterogeneous in density (2.20–2.58 g/cm^3), which is accordingly due to variations in defectiveness (Shafranovsky 1985). A wider range of density variation, as compared to the data on kimberlite diamonds, is due to the constitutional features of impact diamonds:

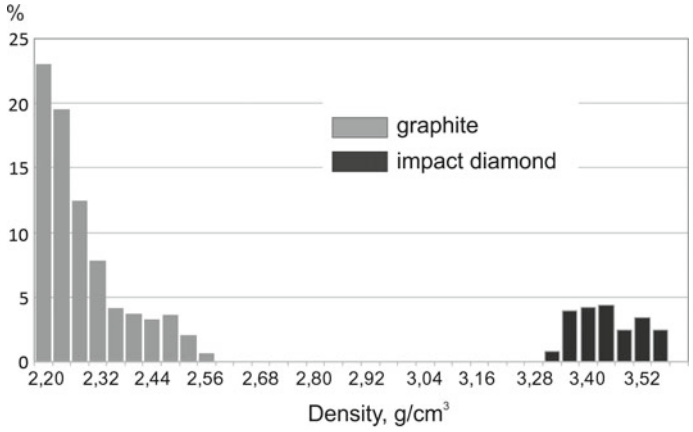

Fig. 6.8 The hystogram of distribution of density of graphite (left) and diamond (right) grains extracted from intensely shocked gneiss specimens

their polyphase character but mainly their polycrystalline texture. A dependence is observed between the density and color of impact diamonds. E.g., the percentage of dark diamonds among the low-density varieties is essentially higher, than that of the light-colored ones, the amount of which is markedly increasing with growing weight of the material. At the same time, throughout the entire density range, diamonds of a black color are present, and all ranges of density values, starting with 3.3845 g/cm^3, are noted for the constant presence of colorless, white, and yellow diamonds. Therefore, even homogenous grains of yellow color, without fissures visible under the microscope, mosaic pattern and inclusions (among them graphite), have the density of 3.3845 g/cm^3; and among black grains, containing graphite and, generally, noted for lower density values, there are grains with the density of 3.61 g/cm^3. This is accounted for by different number of defects in monochromatic impact diamonds, which was recorded when the material was studied by means of electron paramagnetic resonance (EPR) technique, its results are given below.

Of interest is the complete density-wise distribution of crystalline carbon minerals extracted from one diamond-bearing gneiss sample (Fig. 6.8). Noteworthy is a broken character of distribution, falling into two unequal parts: graphite (80%), taking up the interval from 2.2 to 2.58 g/cm^3 and diamond (20%), occurring within the range 3.34–3.55 g/cm^3.

Density-wise distribution of graphite has an asymmetric character with the mode (24%), close to the standard interval of graphite density (2.21–2.26 g/cm^3). There are also other peaks, but they are weakly expressed. Study of the chemical composition and X-ray textural features of graphites with different density demonstrated that, similar to impact diamonds, a change in the density of graphites subjected to impact depends mainly on the amount of defects in them. A great amount of defects shows up in a marked broadening of X-ray peaks of high-density graphite and shows up as a strong unidirectional twinning (commonly parallel to crystal elongation) as

dense striation complicating the pinacoid face of graphite. Besides, such graphite is brittle and disintegrates, losing cleavage along (0001) characteristic of graphite. The hardness of such grains measured by micro-hardness gauge PMT-3 reaches 71.1–131.5 g/cm^3, whereas low-density graphite has hardness values 4.9 g/cm^3, close to the standard value of 5.5 g/cm^3.

Impact diamonds (with the exception of black ones) have yellow-orange luminescence in ultraviolet rays (excitation by the region of 3500–4000 Å), which is also probably caused by texttural defects. In colorless diamonds, a series of emission bands corresponding to the N3 and H3 centers appear. Impact diamonds almost do not luminescent in X-rays and do not show thermoluminescence (Polkanov 2009).

The strength of impact diamonds is about 24–34 (breaking load in newtons for grain class 0.1–0.3 mm), the larger and light colored grains have greater strength (Polkanov 2006). The uniaxial compression strength for large diamonds from placers is up to several hundred newtons per grain. The hardness of light-colored impact diamonds is comparable to the hardness of kimberlite and synthetic diamonds, but in some cases exceeds it. With increasing hexagonal phase content, the hardness decreases, although theoretically the hardness of lonsdaleite should be one and a half times higher than the hardness of the diamond. Investigations of individual samples made it possible to establish the presence in the impact diamonds of lamellar inclusions of the superhigh-hardness carbon phase (El Goresy et al. 2003). Raman spectroscopy revealed two broad absorption bands inherent in this phase, ~1390 and ~1600 cm^{-1}. The nature of these inclusions has not been clarified. It is possible that they represent some high-density polymorphic phases of carbon, which arose from an even denser metastable phase. It is noteworthy that such a super-hard carbon phase was also detected in one of the samples of ureilite stone meteorites where diamonds also appeared under impact compression of graphite (Ferroir et al. 2010).

The electrical resistivity of most light-colored impact diamonds is higher than 1012 O/m and decreases with strong light irradiation (photoconductivity effect). In dark grains with finely dispersed graphite, the electrical resistance is reduced to 105–106 O/m. The diamonds are practically non-magnetic, the specific magnetic susceptibility $\kappa = -0.40 \times 10^{-6}$ cm^3/g (Polkanov 2006). The thermal stability of impact diamonds is lower than of kimberlite diamonds; the beginning of the exoeffect is at 720–770 °C, the peak, at 880–930 °C and the end, at 990–1080 °C.

6.5 Isotope Composition

Impact diamonds from the Popigai impact structure are characterized by the following fluctuation limits of δ^{13}C: from −9.9 to −31.5‰ PDB (Galimov 1984; Galimov et al. 1978, 1980; Vishnevsky et al. 1974; Ivanovskaya 1982; the author's data) (Fig. 6.9a, b). Study of isotope compositions of impact diamonds and coexisting carbon minerals and carbonaceous substance from different impact craters shows that they mainly inherit the isotope composition of initial substrate. Isotope composition of apographitic impact diamonds is similar to that of initial graphite (Vishnevsky et al.

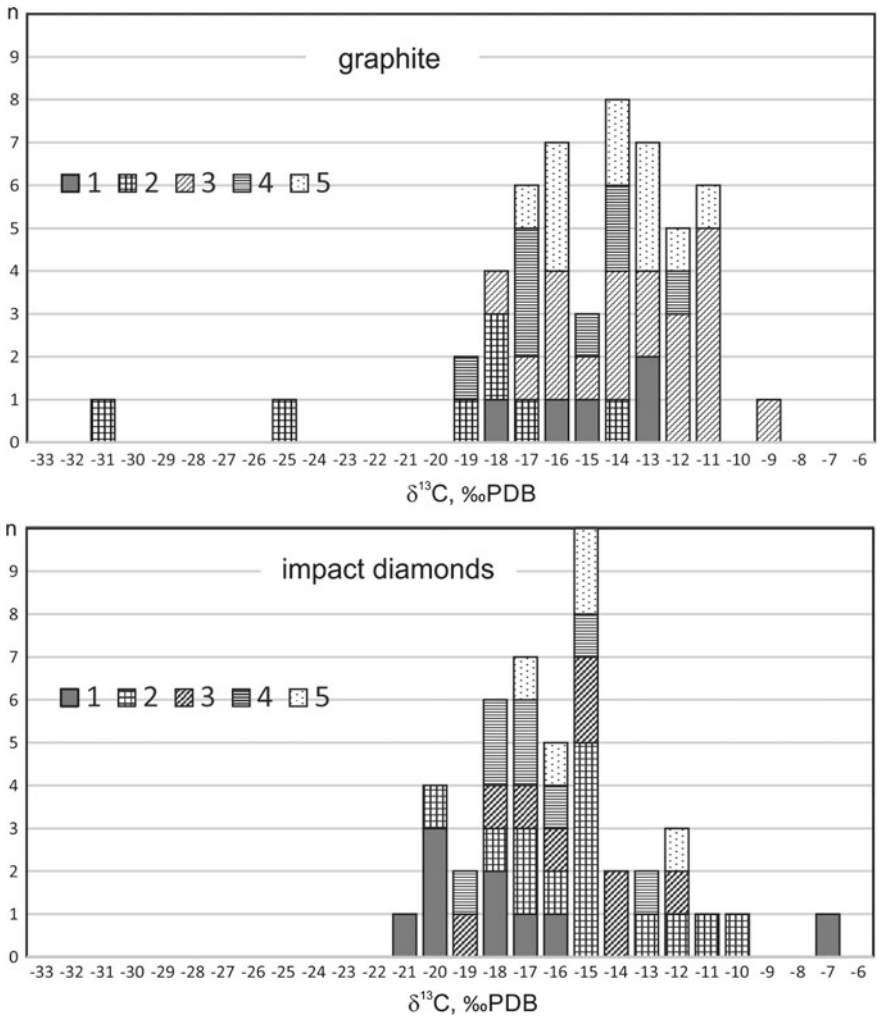

Fig. 6.9 Diagrams of the carbon isotopic composition for graphite and impact diamonds. Compiled from the data of (1) Vishnevsky et al. (1974), (2) unpublished data of G. Shafranovsky, (3) Galimov et al. (1978, 1980), (4) Gritsyk et al. (1988); (5) Ivanovskaya (1982)

1974), and that of apocoaly diamonds, to the composition of initial coal (Ezersky 1986). However, no complete coincidence of $\delta^{13}C$ values is observed, which, possibly, points to a slight fractionation of carbon isotopes in the course of transformation of initial material into diamond. Therefore, impact diamonds are inheriting not only morphological characteristics, but also geochemical features of initial material, including its isotope composition. In the considered case, this is mostly graphite of the Archean crystalline rocks.

References

Bochek LI, Nadezhdina-Bondarenko ED, Rumyantsev GS (1984) Reflection spectra and index of refraction of lonsdaleite-bearing diamonds (in Russian). Trans (Dokl) Acad Sci USSR 279:186–188

Bouldeulle M, Koeberl C, Langenhorst F, Masaitis V (1999) Diamond-graphite phase transitions in impact diamonds from the Popigai structure (Russia). Eur Union Geosci 10:636

El Goresy A, Dubrovinsky LS, Gillet P, Mostefaoui S, Graup G, Drakopulos M, Simionovici AS, Swamy V, Masaitis VL (2003) A new natural super-hard, transparent polymorph of carbon from the Popigai impact crater, Russia. CR Geosci 335:889–898

Ezersky VA (1986) High-pressure polymorphs formed under shock transformation of coal (in Russian). Zap Vses Mineral O-va 115(1):26–33

Ferroir T, Dubrovinsky L, El Goresy A, Simonovici A, Nakamura T, Gillet P (2010) Carbon polymorphism in shocked meteorites: evidence for new natural ultrahard phases. Earth Planet Sci Lett 290:150–154

Galimov EM (1984) $^{13}C/^{12}C$ in diamonds: vertical zonation of diamond generation in lithosphere (in Russian). In: Transactions of 27th Int. Geol. Congress, vol. 11: Geochemistry and cosmochemistry: Nauka Press, Moscow, pp 110–123

Galimov EM, Kaminsky FV, Ivanovskaya IN (1978) The studies of carbon composition in diamonds from Urals, Timan, Sayans, Ukraine, and other regions (in Russian). Geochimija 3:340–349

Galimov EM, Ivanovskaya IN, Klyuev YA (1980) Isotope composition and crystal structure signatures of natural polycrystals of lonsdaleite-bearing diamonds (in Russian). Geochimija 4:533–539

Gnevushev MA, Zilbershtein AH, Krasheninnikova GE (1986) Birefringence of diamonds from shock-metamorphosed rocks (in Russian). Zap Vses Mineral O-va 115(4):442–445

Gorgotskaya LI, Kvasnitsa VN, Nadezhdina-Bondarenko ED (1989) Orientation relations between graphite, lonsdaleite, and diamond under natural transformations in shock waves (in Russian). Mineral Zh 11(1):26–33

Gritsyk VV, D'yakov FG, Poberezhsky VA (1988) On the isotope composition of carbon from different diamantiferous provinces in the world (in Russian). Mineral Zbornik 42(1):68–70

Ivanovskaya IN (1982) Isotope composition of diamonds from meteorite craters as an indicator of their carbon source (in Russian) [abs]. 9th All-Union Symposium on Geochemistry of stable isotopes, vol. 1, Moscow, pp 123–126

Kaminsky FV, Blinova GK, Galimov EM, Gurkina GA, Klyuev YA, Kodina LA, Koptil VI, Krivonos VF, Frolova LN, Chrenov AY (1985) Polycrystalline aggregates of diamond with lonsdaleite from Yakutian placer deposits (in Russian). Mineral Zh 7(7):27–36

Kashkarov IF, Polkanov YA (1964) A finding of diamonds in titanium-zirconium sands (in Russian). Trans (Dokl) Acad Sci USSR 157:1129–1130

Kiryushina MT (1959) On appearamce of Meso-Cenozzoic volcanic activity at the north of Siberian Platform (in Russian). Proc USSR Acad Sci, Geol Ser 1:57–69

Kis VK, Shumilova TG, Masaitis VL (2016) HRTEM study of Popigai impact diamond: heterogeneous diamond nanostructures in native amorphous carbon matrix. Phys Chem Miner 43:661–670

Koeberl C, Masaitis VL, Shafranovsky GI, Gilmour I, Langenhorst F, Schrauder M (1997) Diamonds from the Popigai impact structure, Russia. Geology 25:967–970

Kurdyumov AV, Pilinkevitch AN (1979) Phase transformations of carbon and boron nitride (in Russian). Naukova Dumka Press, Kiev, 188 pp

Kvasnitza VN (1985) Small diamonds (in Russian). Naukova Dumka Press, Kiev, 216 pp

Kvasnitza VN, Krochuk VM, Melnikov VS, Yatsenko VG (1988) Crystallomorphology of graphite from magmatic rocks of the Ukrainian Shield (in Russian). Mineral Zh 10(5):68–76

Langenhorst F (2003) Nanostructures in ultrahigh-pressure coesite and diamond: a genetic fingerprint. Mitt Österr Miner Ges 148:401–412

Langenhorst F, Shafranovsky GI, Masaitis VL, Koivisto M (1999) Discovery of impact diamonds in a Fennoscandinavian crater: evidence for their genesis by solid-state transformation. Geology 27:747–750

Masaitis VL (2013) Impact diamonds of the Popigai astrobleme: main properties and practical use. Geol Ore Deposits 55(8):607–612
Masaitis VL, Futergendler SI, Gnevushev MA (1972) Diamonds in impactites of the Popigai meteorite crater (in Russian). Zap Vses Mineral O-va 101(1):108–113
Masaitis VL, Mikhailov MS, Selivanovskaya TV (1975) The Popigai meteorite crater (in Russian). Nauka Press, Moscow, 124 pp
Masaitis VL, Shafranovsky GI, Yezersky VA, Reshetnyak NB (1990) Impact diamonds from ureilites and impactites (in Russian). Meteoritika 49:180–196
Masaitis VL, Shafranovsky GI, Fedorova IG (1995) Apographite impact diamonds from Ries and Popigai astroblemes (in Russian). Zap Vses Mineral O-va 124(4):12–19
Masaitis VL, Shafranovsky GI, Grieve RAF, Peredery V, Balmasov EL, Fedorova IG (1997) Diamonds from suevites of the Sudbury impact structure (in Russian). Zap Vses Mineral O-va 126(4):1–6
Masaitis VL, Mashchak MS, Raikhlin AI, Selivanovskaya TV, Shafranovsky GI (1998) Diamond-bearing impactites of the Popigai astrobleme (in Russian). VSEGEI Press, St. Petersburg, 182 pp
Masaitis VL, Shafranovsky GI, Fedorova IG, Koivisto M, Korhonen YV, Elo S, Langenhorst F (1999a) Impact diamonds from suevites of the Lappajarvi astrobleme. Zap Vses Mineral O-va 128(5):25–33
Masaitis VL, Shafranovsky GI, Grieve RAF, Peredery VW, Balmasov EL, Fedorova IG, Langenhorst F, Therriault A (1999b) The first find of impact diamonds in the Sudbury structure, Ontario, Canada. In: Dressler BO, Sharpton VL (eds) Large meteorite impacts and planetary evolution II. Geological Society of America Special Paper 339, pp 317–322
Polkanov YA (1967) On a meteorite substance from Tertiary deposits in Ukraine (in Russian). Geophys Astron Inf Bull 11:227–229
Polkanov YA (2006) Cosmogenic diamonds in the Earth's crust: "aliens" and "natives" (in Russian). In: 2nd International Conference on Forecasting and Prospecting for Bedrock and Placer diamond deposits. Kiev, Ukraine, pp 281–288
Polkanov YA (2009) Small diamonds from sandy sediments (in Russian). SPD Baranovsky A.E. Publishing, Simpheropol, 228 pp
Reshetnyak NB, Ezersky VA (1990) Raman scaterring in natural diamonds (in Russian). Mineral J 12(5):3–9
Rost B, Dolgov YA, Vishnevsky SA (1978) Gases in inclusions of impact glasses from Ries crater (West Germany) and the find of high-pressure carbon polymorphes (in Russian). Trans (Dokl) Acad Sci USSR 241:695–698
Rumyantsev GS, Nadezhdina-Bondarenko ED, Malinovsky YA (1980) On lonsdaleite-bearing polycrystalline diamonds (in Russian). CNIGRI Trans 153:3–19
Shafranovsky GI (1981) New graphite twins (in Russian). Zap Vses Mineral O-va 110(6):716–720
Shafranovsky GI (1985) Crystallomorphology of paramorphs of diamond after graphite (in Russian). Zap Vses Mineral O-va 114(1):30–34
Shumilova TG, Kis VK, Masaitis VL, Isaenko SI, Makeev BA (2014) Onion-like carbon in impact diamonds from Popigai astrobleme. Eur J Mineral 26:267–277
Sohor MI, Polkanov YA, Eremenko GK (1973) A finding of a hexagonal polymorphic diamond modification in a placer (in Russian). Trans (Dokl) Acad Sci USSR 209:933–936
Suchardjevskiy SM, Shafranovsky GI, Balmasov EL (1992) The EPR study of impact diamonds from astroblemes [abs]. Lunar Planetary Sci Conf. XXIII, Houston, pp 1381–1382
Val'ter AA, Yeremenko AA, Kvasnitza VN, Polkanov YA (1992) Shock-generated carbon minerals (in Russian). Naukova Dumka Press, Kiev, 171 pp
Vishnevsky SA (1994) Suevitic megabreccia: a new of explosion airfall deposits in Popigai astrobleme. Siberian Branch of Acad Sci of USSR, Inst of Geol and Geophys Adv 11, Novosibirsk, 66 pp
Vishnevsky SA, Pal'chik NA (1975) Graphite from the Popigai structure rocks: its destruction and transformation to another carbon phases (in Russian). Russ Geol Geophys 1:67–75

Vishnevsky SA, Doilnitsyn EF, Dolgov YA, Pertseva AP (1974) Isotope composition of carbon in graphite and diamond from shock-metamorphic rocks of the Popigai structure [abs] (in Russian). All-Union symposium on geochemistry of stable isotopes 5th, pt. 2, Novosibirsk, pp 160–161
Vishnevsky SA, Dolgov YA, Kovaleva LT, Pal'chik NA (1975) Stishovite from the Popigai structure rocks (in Russian). Russ Geol Geophys 10:156–159

Chapter 7
General Patterns of Impact Diamond Distribution

Victor L. Masaitis, Tatjana V. Selivanovskaya, Anatoly I. Raikhlin and Valery T. Kirichenko

7.1 Sampling Methods

Diamond presence in impactites has been recorded throughout the area of the occurrence of the latter in the impact structure. For this purpose, the point sampling of bedrock exposures and residual and talus deposits has been conducted, especially in the course of diamond drilling exploration. In certain cases, large-volume samples weighing many tons were concentrated and diamonds were extracted from concentrates. Processing of point and core samples after their crushing and quartering was mainly performed by the thermochemical decomposition of their silicate part and extraction of different carbon phases from residues; however, other techniques were also applied (floatation, gravitational methods, etc.). A small size of impact diamond grains and their relative high concentration in impactites allowed using samples from 100 to 500 g, in certain cases, larger ones. The reliability of the results obtained was repeatedly checked, as well as the reproducibility of the analyses. At the same time, it was ascertained that in case of initial rock crushing during sample preparation, losses of diamonds occur, according up to 25% of their weight. Core sampling confirmed the results of surface rock sampling; only in one case the differences of the estimates exceeds 50%. Accounting of the irregular character of sampling, different losses, etc., enabled to ascertain that the accuracy of definition of the mean contents of diamonds in impactites throughout the impact structure is ±5–10%.

Selective sampling was also conducted on shock-metamorphosed gneiss inclusions in impactites. Determination of the diamond presence character of these graphite-bearing rocks is of great interest, since they are the initial substrate, subject to melting, due to which diamondiferous impactites appeared. In most cases, gneisses enclosed into the impactites are non-diamondiferous or contain single diamonds

V. L. Masaitis (✉) · T. V. Selivanovskaya · A. I. Raikhlin · V. T. Kirichenko
A.P. Karpinsky Russian Geological Research Institute, Sredny prospekt, 74, 199106 Saint Petersburg, Russia
e-mail: vcmsts@mail.ru; victor_masaitis@vsegei.ru

V. L. Masaitis (ed.), *Popigai Impact Structure and its Diamond-Bearing Rocks*,
Impact Studies, https://doi.org/10.1007/978-3-319-77988-1_7

grains; their presence, determined by the analyses, could rather be regarded as a laboratory background. At the same time, certain samples, particularly those where graphite scale inclusions might be revealed by visual inspection, have a rather high diamond content. It exceeds not only the background diamond content in tagamites and suevites in the crater, but is also higher than the average diamond content in these rocks at areas with a higher diamond presence, reaching the hurricane concentrations of hundreds of carats per ton. It is interesting to note that such samples of high-diamondiferous gneisses were found within the latter areas. These inclusions of high-diamondiferous gneisses mainly belonging to the biotite-garnet species.

7.2 Distribution of Diamonds Throughout the Impact Structure

The diamonds prospecting was made by pick sampling on the surface with a sample weight of 2–4 kg. Its effectiveness is confirmed by comparing the results of prospecting with the results of subsequent exploration work (Simonov et al. 2004). Throughout the crater area 2590 prospecting samples were selected and analyzed, including 1610 from tagamites, and 980 from suevites. The average sampling density for tagamites was 5.9–5.2 tests per km^2, for suevites—4.8–1.0 tests per km^2. The highly diamond-bearing impactites are exposed on area of 46 (tagamites) and 38 km^2 (suevites), moderately and low-diamond bearing on 260 and 796 km^2, respectively. The average content in low-diamond bearing impactites (background content) is 2.6 ct/t in tagamites and 2.3 c/t in suevites; in highly diamond-bearing—14.6 ct/t in tagamites and 10.2 ct/t in suevites (Masaitis et al. 2013).

Areas with a relatively high and moderate content it is approximated by the Gaussian curve with the mode, 3 or more times exceeding the background values. For areas with a relatively low diamond content, the distribution is asymmetric with the maximum in the area of the background concentration values; in places the distribution curve is bimodal with the small second maximum.

Evaluation of the ratios of diamond contents in tagamites and suevites developed within limited areas from the first square kilometers to the first tens of square kilometers in size demonstrated their clearly expressed positive correlation. For 34 such areas (their configuration was, in most cases, determined by the distribution of impactite exposures or by the outlines of areas with relatively homogenous concentrations of diamonds), the correlation coefficient was $r = +0.906$. The critical value of the coefficient at 99% significance level is evaluated at 0.435. If the entire occurrence area of impactites in the impact structure is subdivided into geometric areas, limited by radii with angles of 20° between them and concentric circles with the radius spacing of 6 km (59 areas), the correlation of diamond contents in tagamites and suevites is evaluated by the coefficient $r = +0.402$ while its critical value of 0.353.

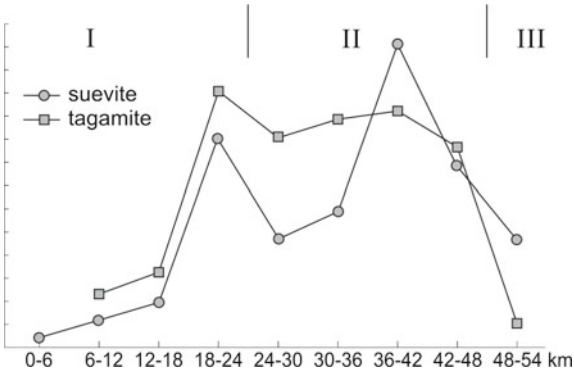

Fig. 7.1 The distribution of relative concentrations of diamonds in Central (I), Ring (II) and Peripheral (III) zones of the Popigai impact structure. Horizontal axis—distance from the center of the crater

Central symmetry of the impact structure generally allows approaching the analysis of diamond distribution inhomogeneities, using this procedure. It should be remembered, that the entire occurrence area of impactites was covered by a more or less regular sampling. Plotting of histograms, showing the distribution of diamond concentrations within certain concenters in accordance with the above-mentioned subdivision (Fig. 7.1) demonstrated that within the impact structure and around it, three zones can be distinquished, differing markedly in the mean level of diamond concentration in impactites: Central ($r = 0–18$ km), Ring ($r = 18–48$ km), and Peripheral ($r > 48$ km).

The Central zone comprises the central part of the Popigai structure, where the Quaternary deposits are widespread on the surface, and impactite exposures are rare and represented, as well as in rare boreholes, by predominantly lithovitroclastic and vitroclastic suevites enriched with sedimentary debris. These rocks are characterized by a generally low level of diamond contents.

In the Ring zone, the main zones of impactite occurence both on the surface and at depth occur. Structurally, it covers the area of peak ring and its slopes, the annular trough, including its outer slope, as well as the outer crater terrace, including relics of the crater outer rim in the northwestern sector. Diamond contents in suevites and tagamites are variable there; however, on the average, they are approximately three times higher than in the Central zone. In the Ring zone, all areas noted for the highest diamond presence occur.

Discrete areas, where the relics of ejecta blanket preserved from erosion occur, can be assigned to the Peripheral zone. This zone includes separate tagamite and suevite patches of small size.

It should be borne in mind that the averaged value of diamond contents in each of the concentric zones, for which the evaluation was conducted, gives only the general information on the relevant unhomogeneites in diamond distribution depending on the distance from the centre of the structure.

The analysis of azimuthal inhomogeneities gives a more vivid illustration of diamond distribution within the impact structure (Fig. 7.2). The evaluation of diamond contents in suevites and tagamites by sectors, covering 20° of the arc, enabled to reveal

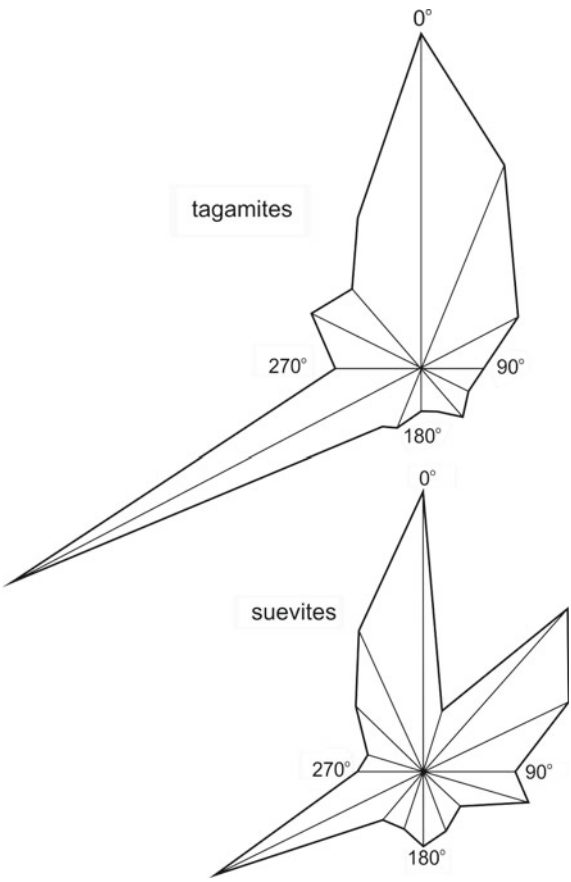

Fig. 7.2 Azimuthal heterogeneity of diamond concentrations in tagamites and suevites. It displays a ray-like distribution and the strong positive correlation between diamond contents in both types of impactites

their marked differences along certain rays, which coincide for both rock types. The highest diamond contents are recorded in tagamites and suevites occurring within the southwestern, northern, and, partly, northeastern sectors. It is noteworthy that these ray inhomogeneities are traced within the adjacent three or four concentric zones of about 6 km wide. Revealing of such azimuthal inhomogeneities in diamond distribution is extremely important for understanding the processes of their formation.

In order to rule out the effect of the factor of "geometric splitting" on the analysed dependences of diamond contents of the mutual location of sampling sites, including the location relative to the center of the structure, the non-polynomial trend-analysis was used. Maps of the trend surfaces of diamond concentrations were compiled (maps of the general trend) within 95% reliability and the maps, showing isolines of trend surfaces with 0% reliability and significance threshold equalling 1. About 1800 determinations of diamond contents in suevite and tagamite samples were used to compile the above maps; their sampling sites in a rectangular coordinates system

were taken from detailed topographic maps. To compile the maps of trend surfaces, a computer-aided procedure, based on specific programs, was applied.

The essence of trend-analysis consists in distinguishing and description of different constituents in the changeability of areal variables, aimed at the interpretation or interpolation between the irregularly located sampling sites. In this case, reliability is interpreted as the degree of agreement of the selected regression surface with the sampling data. A high degree of reliability (95%) gives the most general trend of changes in the selected parameter; with decreasing reliability (0%), its local features are displayed. Isolines of the trend surface constructed with 0% reliability, signify that the deviation of the surface from each specific value of diamond content in a definite sampling site, is zero. In the map compiled with 95% reliability, trend surfaces are only by 5% deviating from a certain average level and are reflecting the leading tendency of general diamond distribution within the crater. This map smoothes the details, giving only the general picture.

In the maps (Fig. 7.3) it is seen that the central part of the area of impactite occurrence is noted for low diamond concentrations which increase towards the periphery. Maxima areas, coinciding in both maps, are distinguished in the northern and southwestern sectors; and in case of suevites, the northeastern maximum is also distinguished, the banded zone of the north-west striking minima is also seen. Symmetry elements of trend surfaces have a central and banded character, reminding of the corresponding inhomogeneities in the distribution of petrogenetic elements, characterized above under Chap. 5. Thus, the concentric zonal and azimuthal inhomogeneities of diamond distribution within the astrobleme are generally revealed using this method.

7.3 Correlation of Diamond Content with the Composition of Impactites

Primarily the attempt was made with a view to determining a possible correlation of diamond presence in tagamites and suevites with their chemical composition. For this purpose, samples of these rocks were selected, in which, along with the content of diamonds that of the main elements was also measured. Subsequent correlational analysis demonstrated the following results (Table 7.1).

A strong and significant positive correlation is established between diamond contents in both types of impactites, and the concentration of phosphorus pentoxide in them. A significant positive association with magnesia content was revealed for suevites; for tagamites, it is slightly lower than the significance level. Silica content is characterized by a strong negative correlation with concentrations of diamonds in suevites; for tagamites, it is also negative, but below the significance level. Generally, it might be stated, that diamond content is slightly higher in impactites, enriched in P_2O_5, MgO, CaO and SiO_2-depleted.

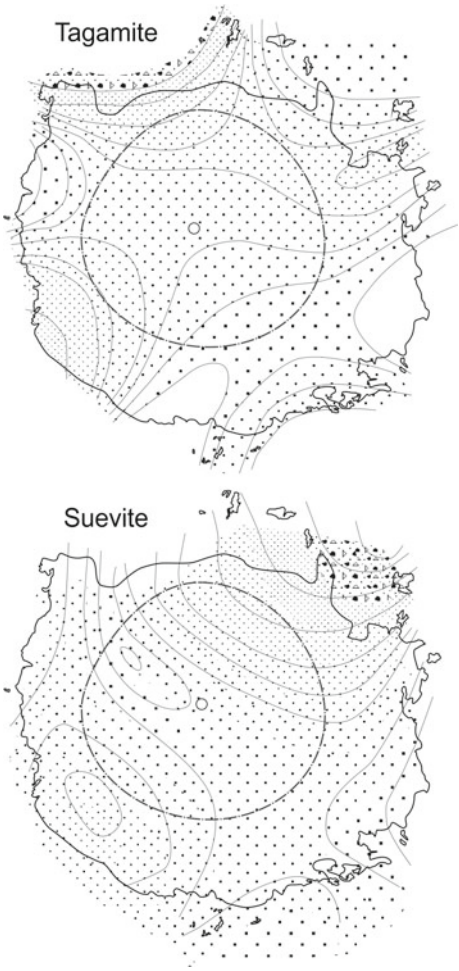

Fig. 7.3 Distribution of tagamites and suevites with variable diamond content within the Popigai crater (results of non-polynomial trend analysis). Density of hatching shows the relative content of diamonds. The axis of the peak ring is shown by dashed line. The solid line marks the outer border of diamond-bearing rock area

If account is taken of the fact that gneisses were initial material for generation of the diamondiferous impact melt, the above features of chemistry are more characteristic of relatively more melanocratic and commonly slightly enriched in apatite varieties. Study on gneiss inclusions in impactites and allogenic breccias shows that the inclusions, which are enriched by garnet, biotite, and, in places, orthopyroxene, often also contain appreciable amounts of graphite impregnations.

It should be emphasized that distinct positive correlation between diamond and phosphorus pentoxide contents is recorded only for the impact structure as a whole. When local areas being considered, the correlation is not manifested, although the attempts were taken to reveal such dependence for certain large impactite bodies and their associations.

Table 7.1 Correlation coefficients between major elements contents and diamond grade in impactites

Element	Tagamites	Suevites
SiO_2	−0.173	−0.394[a]
TiO_2	+0.124	+0.204
Al_2O_3	+0.028	+0.058
Fe_2O_3	+0.134	+0.153
FeO	−0.123	−0.015
MnO	+0.185	−0.048
MgO	+0.185	+0.391[a]
CaO	+0.195	+0.092
Na_2O	+0.107	−0.079
K_2O	−0.116	+0.169
P_2O_5	+0.410[a]	+0.549[a]
n	163	58
Threshold value	0.210	0.333

[a]Siginificant correlation
n—Number of analyses

Though no special study of correlations between graphite and apatite in crystalline rocks has been conducted, a strong positive correlation of their main constituent elements, phosphorus and carbon in impact melting products of these rocks (which generally ensues from the comparison of chemical composition of tagamites and gneisses), enables to assume an association of these elements in the initial substance, which served as a substrate for metamorphic rock generation as far back as the Precambrian. The bond of phosphorus and carbon is characteristic of most of sedimentary carbonaceous formations (Sozinov and Sidorenko 1976; Sidorenko et al. 1981). In the case under consideration, high-alumina gneisses (biotite-garnet etc.) were initially, possibly, pelites containing scattered carbonaceous matter, most likely of biogenic origin. Biogenic carbon and phosphorus were initially associated in the living material, its remains being enclosed in silts and clays, subjected later to high-grade granulite facies metamorphism. Carbon and phosphorus formed independent minerals, i.e. apatite and graphite; however, no significant migration of element occurred. A close association between carbon and phosphorus also showed up during subsequent alteration of crystalline rocks to the impact melt.

The primary biogenic nature of carbon is confirmed by the specific features of its lightened isotope composition. As shown above, isotope composition of graphite in crystalline rocks and impact diamonds of the Popigai structure is $\delta^{13}C = -12$ to $-19‰$. According to some researchers, the association of apatite and graphite, characterized by enrichment in a light carbon isotope discovered in Archean crystalline rocks in southwestern Greenland, also points to the biogenic origin of carbon and phosphorus contained in them (Mojzsis et al. 1996).

Since the main carrier of impact diamonds is the glassy or partly crystallized impactite matrix (making up the main tissue in tagamites or fragments of different

size in suevites), apparently, a relative increase of the role of this material in the composition affects the degree of diamond presence. An essential (in terms of volume) admixture of the fragments of non-diamondiferous rocks involves a relatively low diamond content in suevites as compared to tagamites, which has already been noted. Essentially, the same reason, i.e. presence of a minor amount of impact glass fragments (up to 7–10%) also results in a low diamond content of microbreccia, which is recorded in certain cases.

Certain suevite varieties differing by the abundance of vitroclastic material (and, respectively, the amount of non-diamondiferous rock fragments), also display essentially different diamond contents. Thorough sampling at some areas where different varieties occur simultaneously, demonstrated that, for instance, vitrolithoclastic and lithovitroclastic suevites are approximately two times poorer in diamonds than vitroclastic suevites. The sintered vitroclastic suevites are most enriched in impact glass fragments. Tagamites occuring together with the latter, have the same diamond content as these sintered suevites.

More complicated is the effect of composition of rock inclusions on diamond content in tagamites. The capture of high-diamondiferous shock-metamorphosed crystalline rock fragments disintegrated to a certain extent, can doubtless result in increasing diamond concentration. Such a possibility is indirectly confined by the predominance of biotite-garnet and biotite-garnet-hypersthene gneisses and plagiogneisses in high-diamondiferous tagamites localized within the southwestern part of the impact structure. Tagamites in this area are characterized by an elevated content of minor clasts of orthopyroxene which is typical of such rocks. At the same time, in the relatively low-diamondiferous tagamites of the southeastern sector, the occurred inclusion are dominated by bipyroxene gneisses.

An increased number of inclusions, occurring in tagamites (that are in most cases represented by low-diamondiferous or non-diamondiferous crystalline rocks and their mineral fragments), results in depletion of diamond concentrations, similar to that in suevites. On the other hand, the capture of relatively cool clastic material favours a quicker melt cooling, temperature drop, and a preservation of a significant part of diamonds from burnup. The analysis of connection between number of minor (0.5 cm) inclusions and diamond content in tagamites, conducted using borehole core material, showed that the positive correlation between these parameters is commonly retained as long as the amount of the inclusions captured does not exceed 20–25% of the volume. With the increasing amount of this material, diamond content in term of total rock volume is dropping. Diamond content in the chilled tagamite matrix can even increase in this case, which is again due to quick chilling of the diamondiferous melt. This issue will be considered in more detail below, when local inhomogeneities of diamond distribution in certain impactite bodies are characterized.

Comparison of HT- and LT-tagamites was investigated in detail in the southwestern sector of the crater, mainly using the borehole core sampling results. Statistical processing of these data showed that LT-tagamites on the average approximately two times richer in diamonds, than HT-tagamites; these differerences are significant.

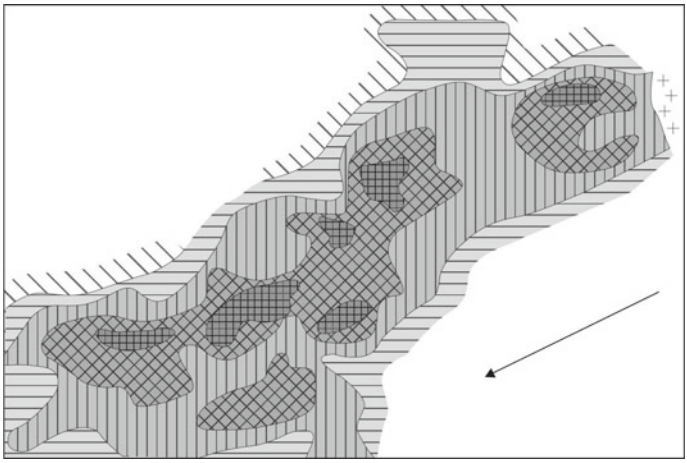

Fig. 7.4 Diamond contents over the area of a thick tagamite sheet. Crosses show gneisses of peak ring. The arrow shows a direction outward from the crater's centre. The intensity of the hatching reflects the relative concentrations of diamonds in tagamites

7.4 Diamond Distribution Within Sheet-like Tagamite Bodies

Local inhomogeneities of diamond distribution were the subject of a special research conducted using the material of borehole drilling. Inhomogeneities resulting from the above-mentioned radial character of diamond distribution and regarded as the primary ones, were revealed. Inhomogeneities caused by differences of the initial temperatures of certain impact melt fractions, can also be assigned to the primary ones. Secondary inhomogeneities are those, associated with cooling conditions of the diamondiferous melt at placement sites. The extent of local inhomogeneities is determined by tens and hundreds of meters; less frequently, the first kilometers; and in a number of cases, also by the first meters.

The character of inhomogeneities of diamond distribution in tagamites within the above-mentioned southwestern radius with the elevated concentrations is illustrated in Fig. 7.4. Seemingly, a patchy, irregular distribution of diamonds (these inhomogeneities are 500–1000 m across) is, at the same time, noted for a definite order. In the axial part of the radius, their content is higher in both in HT- and LT-tagamites; on the flanks it is reduced, respectively. A certain gradient in the change of concentrations transverse to the axis of the direction radius can be outlined.

A definite dependence of diamond concentrations on the geological position in the composite tagamite body is illustrated by Fig. 7.5. Elevated diamond contents are characteristic of the near-contact zones of this body, as well as of certain simple lenticular and sheeted bodies within it, differing by their belonging to definite varieties.

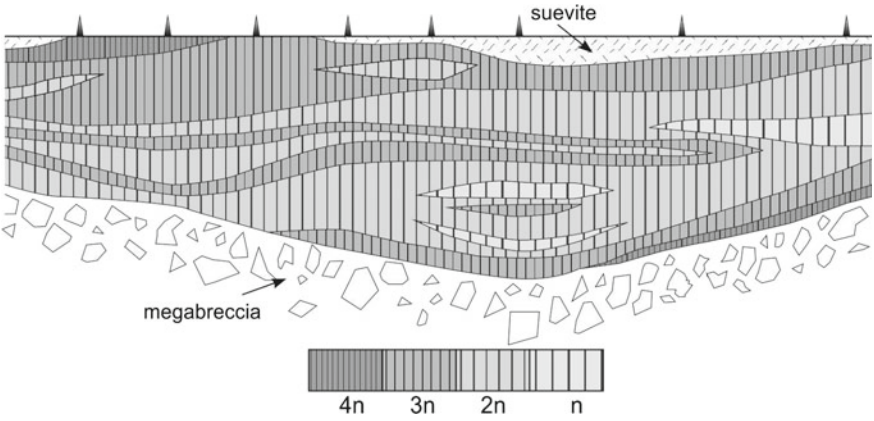

Fig. 7.5 Diamond contents in a generalized vertical section of the tagamite sheet. The chilled margins are enriched in diamonds. Density of striations corresponds to variations in diamond content

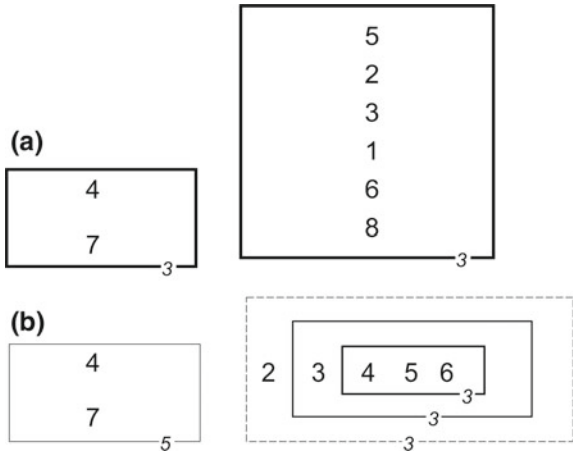

Fig. 7.6 Diagrams of reiterated correlation of diamond contents (9) and petrographic features (1–8) in tagamites (see Table 7.2). **a** LT tagamites (n = 290), **b** HT tagamites (n = 153). The line thickness corresponds to the order of correlation links. *n* is an conventional value used for comparison of diamond contents

Comparison of the results of detailed petrographic observations куздфсув ин ЭакщьЭ borehole sections with sampling results enabled to outline a definite association of certain petrographic features of tagamites with diamond contents in them. For this purpose, a number of such rock features was quantitatively evaluated (the size of hypersthene microlites in reaction rims around quartz clasts, the size of these microlites and their content in the matrix, amount of basis with cryptocrystalline structure, diameter of aggregate accumulations of hypersthene and their number, number of clasts less than 0.5 cm across, volume of residue glass in the basis, Fig. 4.16). Then different statistical methods were used to correlate the relevant evaluations with diamond contents in the rocks (Fig. 7.6).

Primarily, one should note the uniform trend of changes in the diamond content in tagamites and the content of clasts less than 0.5 cm across in them. Larger fragments,

generally accounting for not more than 5–10%, do not have any significant effect on diamond concentration. This regularity shows up most distinctly within extensive vertical intervals at the depth of the first hundreds of meters.

A clear positive correlation is revealed between the diamond content and the volume of cryptocrystalline tagamite basis, especially in moderately and slightly crystallized HT-tagamites in the upper part of the composite sheeted body. Most distinct is the character of changes in diamond contents and slightly crystallized basis in tagamites cementing the megabreccia, as well as near the contacts with large gneiss blocks, where, on the one hand, the role of the basis with a cryptocrystalline structure increases abruptly, and on the other hand, there are very high and even hurricane diamond contents.

A negative correlation is also established between the number of hypersthene accumulations occurring on place of the absorbed quartz clasts, and diamond contents in tagamites. Such accumulations are typical of the most well crystallized HT-tagamites in the central parts of rather thick simple bodies occurring at great depths. A clear negative correlation between diamond content in tagamites and the prevailing size of hypersthene microlites (along the long axis) absorbed into residual glass, is also typical. The lowermost diamond content is typical for HT-tagamites occurring at the depths of 400–500 m and containing microlites to 0.5 mm in size. The size of hypersthene microlites in reaction rims around quartz clasts also displays a nrgative correlation with diamond contents. A similar dependence, but a much less expressed is also revealed between diamond contents and amount of microlites in the matrix. For instance, in HT-tagamites of the lower part of the section of the thick sheet in the above interval, microlite amount make up to 80% of the rock and, as noted above, diamond concentrations are very low here. In a thick (50–100 m) LT-tagamite body, increase of the number of microlites downward in the section from 10 to 20% near the contact to 80–90% in the central part is accompanied by the significant decrease of the diamond content. In tagamites, which form cement of megabreccia, where microlites account for the first percent of the rock volume, the content of diamonds can be very high.

Correlation analysis of the quantitative evaluations of the size and number of hypersthene aggregates, as well as the size of microlites in reaction rims and, to a lesser extent, in the tagamite matrix and diamond content, in tagamites, demonstrated the significance of negative values of paired correlation at 0.01 significance level (Table 7.2). The strongest positive correlations with diamond contents are recorded for such parameters, as number of inclusions, and volume of the basis with cryptocrystalline texture. The results obtained using the multiple correlation technique (Fig. 7.6), as well as cluster and factor analysis, generally, as well agreed with the correlation analysis results.

Dependence of the diamond content on the rock fabrics can be easily explained from cooling and crystallization conditions of the diamondiferous impact melt. Quick cooling resulting in generation of the cryptocrystalline texture of the basis, including that caused by the capture of a great number of cool inclusions at the last stages of radial displacement of the impact melt, favours the preservation of diamonds in a rapidly cooling rocks. Contrarywise, a relatively long-term cooling resulting in the

Table 7.2 Correlation coefficients between some quantitative estimated petrographic parameters and diamond grade in tagamite

Tagamites	LT tagamite		HT tagamite		
	Central body (II)	Total	Upper body (IV)	Lowest body (I)	Total
Petrographic features of tagamite					
1. Size of microlites in reaction rims	−0.467	−0.482	−0.221	−0.156	−0.283
2. Size of microlites in the groundmass	−0.179	−0.469	−0.243	−0.231	−0.297
3. Microlite content in matrix	−0.128	−0.121	−0.316	−0.295	−0.397
4. Content of cryptocrys-talline groundmass	0.124	0.122	0.358	0.358	0.437
5. Size (across) of hypersthene accumulations	−0.537	−0.514	−0.45	−0.354	−0.480
6. Content of hypersthene accumulations	−0.248	−0.420	−0.35	−0.227	−0.397
7. Content of inclusions of less than 0.5 cm in size	0.222	0.415	0.317	0.169	0.359
8. Content of the residual glass in the basis	–	–	−0.412	−0.304	−0.427
Threshold values of correlation coefficients for significance levels					
0.01	0.316	0.205	0.177	0.225	0.150
0.05	0.245	0.158	0.136	0.213	0.115
Number of analyses	62	153	207	83	290

Numbers of tagamite bodies—see Fig. 2.26

absorption of clasts, development of hypersthene accumulations in their place, the full appearance of reaction rims and crystallization, leads to diamond burnup under a high temperature still retained.

7.5 Detrital Diamonds

As mentioned above, polycrystalline diamonds of the type under consideration were initially recorded in modern placers of the Ebelyakh region together with kimberlite-type diamonds 100–150 km south-east of the Popigai hollow (Chumak and Bartoshinsky 1968; Kaminsky et al. 1985; Grakhanov 2005). Their bedrock source ceased to be an enigma after discovery of diamondiferous impactites and comparison of the properties of relevant occurrences in detrital deposits, on the one hand, and tagamites and suevites, on the other hand. Nevertheless, during a long-term period of time, some researchers considered polycrystalline diamonds from placers of the Ebelyakh region as "carbonado with lonsdaleite" or "polycrystalline diamonds of the IX type", which caused a certain misunderstanding. Presently, it is definitely ascertained that the source of placer polycrystalline diamonds in areas adjoining the Popigai structure, are the rocks associated with it, similar to placers exactly within the structure and the surrounding area.

The main placer-forming source of impact diamonds in the Popigai area are the rocks most easily disintegrated during destruction on the surface. Such rocks are mostly lithic microbreccias despite their diamond content is minimal as compared to suevites and tagamites. Microbreccias prevail in the upper horizons of crater fill. They also composed a significant volume of the now almost fully eroded ejecta blanket. Reconstructions show that the upper part of the crater fill and the significant part of the ejection cover were eroded during 10–16 mln. year by approximately the Early Miocene. In Pliocene—Early Quaternary time, erosion exposed the near-roof parts of thick sheeted impactite bodies (Plotnikova 1990). The depth of erosion varies in the different crater sectors and concentric zones from 50–100 to 300 m (Masaitis et al. 2005). According to the evaluation, the total amount of diamonds released from this unconsolidated material, almost two times exceeds the total diamond release from suevites and almost four times, from tagamites.

An essential source of replenishment for the placers were also suevites due to a higher content of diamonds, as well as their significant share in the volume of the eroded material (about one-fourth of the microbreccia volume).

As it was shown in Sect. 4.4, low-temperature hydrothermal transformations of impact glass fragments constituting a significant part of the impactite bulk lead to sharp changes in their strength and resistance to the action of physical agents of destruction under the conditions of the earth's surface. The main importance in this case is the development of clay minerals of the smectite group, as well as various zeolites. These minerals amount to 10–20% of the total volume of hydrothermal new-forming matter. Such transformations are most typical for thick strata of suevites, characterized by higher porosity and permeability for percolating waters. In addition,

these rocks were hotter than, for example, microbreccia. The destruction of suevites and, to a lesser extent, microbreccia, ensures the supply of most of the diamonds in the placer. For the same reason, suevite (especially, weakly cemented varieties of the upper part of the general section of the crater fill) are preferable for working in the case of development of diamond mining in the future.

A more complicated issue is that of the impact diamonds discovered in placers at a significant distance from the Popigai impact structure. They are, most likely, the remnants of the thin discontinuous cover of remote ejections generated by the impact event and fully destroyed by erosion. This is particularly confirmed by a gradual decrease of impact diamond contents, when they are traced in placers from the Popigai structure southwestward to the Ebelyakh River Basin for the distance of 100–150 km, where they make up only a minor admixture to diamond placers of a kimberlite type (Grakhanov 2005).

There is scattered information on the occurrences of polycrystalline diamonds in alluvium, which are more remote from the Popigai structure, to 300–500 km, particularly, in the Khorbosuonka River Basin (a tributary of the lower course of Olenek River), and in some other places. These data are noteworthy and, doubtless, require a refinement. Of course, it is necessary to get proofs that the above occurrences are associated with the Popigai crater, but not with any other, as yet non-established a impact body.

As mentioned above, dust particles of the ejection cloud (including impact diamonds of the corresponding size) could be transported by the atmospheric flows to distances of many thousands and even tens of thousands of kilometers, similar to shock-metamorphosed quartz particles, ejected during impact crater formation at the Maastrichtian/Danian boundary. In this sense, detailed lithological and mineralogical-geochemical study should be conducted on the Upper Eocene sedimentary sequences in some regions of the world, which can enclose thin interbeds comprising dust-like particles of impact diamonds from the Popigai crater.

7.6 Indigenous and Placer Diamond Deposits and Their Resources

As already mentioned above, impact diamonds in the rocks of the Popigai structure were first discovered in 1971, and in the following two years special prospecting conducted by geologists of several organizations (VSEGEI, Krasnoyarsk Geological Survey, to a lesser extent, the Amakinskaya Expedition of the Yakutian Geological Administration and the Institute of Geology and Geophysics of Siberian Branch of the Academy of Sciences of the USSR) showed that the distribution of diamonds in impactites is ubiquitous. In 1974, the Polar Exploration Enterprise began detailed exploration works in the Popigai structure, as well as preliminary prospecting in some other areas.The extensive prospecting resulted in discoveries of several indigenous (in impact rocks) and secondary (in recent placers) diamond deposits, which were

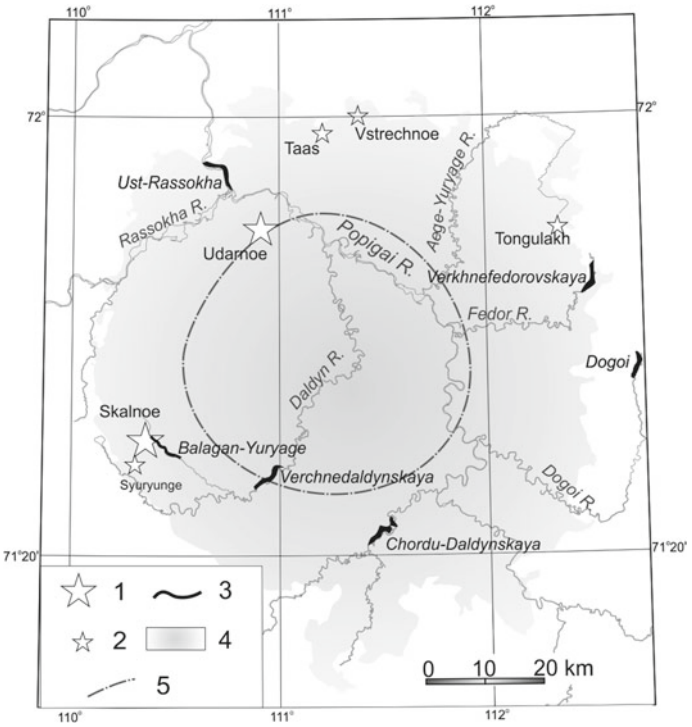

Fig. 7.7 Impact diamond deposits in the Popigai area (modified from Masaitis et al. 2013). 1—Large indigenous diamond deposits with proved resources, 2—Small indigenous diamond deposits estimated tentatively, 3—Large diamond alluvial placers estimated tentatively, 4—Area of the continuous distribution of impactites and impact breccias, 5—Axis of peak ring

explored and developed (Masaitis and Simonov 2004; Masaitis et al. 2013). One of the areas with sharply increased diamond content is Mayachika-Kerikete Upland (the Udarnoe deposit), another one is the basin of the Balagan-Yurjage River (the Skalnoe deposit). In addition, a number of areas with a slight excess of diamond content above the background were discovered. Several placer deposits were explored as well (Fig. 7.7).

The Udarnoe deposit occupies an area of 8.3 km^2, its length from the southwest to the northeast is about 6 km, the width is from 0.8 to 2.2 km. It locates at the outer slope of peak ring in the northwestern sector of the impact structure (see Sect. 2.2.2). There, primarily biotite-garnet and other gneisses are developed, overlapping with allogenic megabreccias and impactites, plunging to the northwest and southeast. On the surface, separate bodies of tagamites and suevites, which are actually ore bodies, form the tops of small hills. The inner structure of these bodies and their interrelations, studied to a depth of 300–500 m, are described in Chap. 2 (see Fig. 2.29).

Tagamite occurs as two sheet-like bodies from first dozens to 110 m thick; less frequently, as smaller lenticular bodies in suevites. Close to the floor of the sheets, impact melt forms in places as if the cement of the allogenic crystalline megabrechia. The largest subhorizontal tagamite body has a length of more than 3.8 km, a width of 0.25–1.25 km. Its thickness is most significant in the central part, where it exceeds 100 m. It is referred to the upper tagamite ore horizon.

Suevites form a thick bowl-like body covered with tagamite of the upper horizon. Its average thickness is 63 m, it increases from south to north peaking 252 m. In the same direction, suevites are replaced by allogenic lithic microbreccia. The suevite body is regarded as a suevite ore horizon. The suevite horizon is underlain by tagamite, which do not outcropped on the surface. They form the so-called lower tagamite ore horizon. It is not developed everywhere, at certain areas the suevites lie directly on either authigenic breccia or allogenic megabreccia. The latter ore horizon consists of several separate bodies. The largest of them has a length of about 3 km, a width of 0.3–0.7 km, an average thickness of 52 m (maximum 167 m).

The eluvial-deluvial formations with an average thickness of 3.8 m (maximum up to 17.8 m) are represented by the intermittent cover of clayey rock debris and colluvial placer of impactite debris that also contain diamonds.

Thus, three horizons are distinguished as ore bodies, however, they are not made of the same lithology. For example, in the upper tagamite horizon, about 4% is constituted by suevites, while in the suevite horizon, small layered bodies and lenses of tagamites are enclosed. In the lower tagamite horizon, small lenses of suevites also occur, plus large blocks of gneisses are enclosed. Such a subdivision of the entire productive stratum into the horizons makes it possible to simplify the separation of ore blocks in the calculation of reserves.

In total, the explored area of the productive stratum is 7.66 km^2, its average thickness is 97.7 m (maximum 369 m), it increasing from the southeast to northwest. In total, 226 wells with a total length of 23,318 m were drilled in the Udarnoye deposit, including 12,666 m along the productive stratum, and 10,652 m in the enclosing rocks. The deposit was drilled to a depth of 395 m by vertical core wells through a network of 200 × 200 and 400 × 400 m. On a pilot basis, as well as to determine an optimal size and density of the well network, a local area had been drilled with a 100 × 100 m net. Mining operations were carried out in an insignificant amount to obtain technological samples and to control the testing of the core.

The core was tested sectionally, the section size was 2–4 m, but it could be reduced to 0.5 m depending on the petrographic composition of rocks. The total length of the sampled core was 13,988 m, and the number of samples was 6051, 5162 of which were analyzed. From the pits traversed along the axis of individual wells, furrow samples were taken from intervals of depth corresponding to the intervals of core samples.

The diamond content in the ore horizons is illustrated in Table 7.3. The average content in the general reserve counting system was 7.6 ct/t.

To calculate the reserves for the deposit taking into account its geological features, the following conditions were adopted: the minimum industrial content of diamonds in the counting block is 5.5 c/t; the minimum thickness of the ore body and the

Table 7.3 The content of diamonds in the ore horizons of the Udarnoe deposit

Ore horizon	Average diamond content, ct/t						
	By samples		By wells		By blocks		In general
	From	To	From	To	From	To	
Upper tagamite	0	72.00	3.21	21.64	5.54	13.46	8.96
Suevite	0	125.16	2.20	14.95	2.63	10.85	6.60
Lower tagamite	0.1	34.26	4.23	14.08	4.24	13.52	10.21

Table 7.4 The reserves of the Udarnoe deposit

Category of reserves[a]	Coefficient of ore content	Coefficient of ore content, ct/t	Reserves, mln. carat
B	0.99	9.15	1648.43
C_1	0.98	7.49	3680.75
$B + C_1$	0.98	7.94	5329.18
C_2	0.95	7.96	5427.05
$B + C_1 + C_2$	0.97	7.95	10,756.23

[a]*Note* The categories of mineral reserves adopted in Russia can be compared with the categories of mineral reserves of the USA Mining Bureau as follows: $A + B + C_1$—probable, indicated, $A + B$—measured, proved, $C_2 + P_1$—inferred, possible, P_2—hypothetical

maximum thickness of the empty rocks included in the reserves calculation is 4 m. Empty rocks with a thickness of more than 4 m were excluded from the calculation using the ore mineralization coefficient.

Based on the results of exploration work, the contour of the project operating quarry was determined, the results of the reserves calculation according to which are given in Table 7.4.

The Skalnoe deposit is located in the southwestern sector of the crater, in the upstream of the Balagan-Yuryage River (see Sect. 2.2.1), and occupies a section of 13×6.5 km with a total area of about 85 km^2. Its outline is determined by the results of sampling, since diamond-bearing impactites are also distributed outside it. The deposit embraces the southwestern slope of peak ring, but lies mostly within annular trough. In the axial part of the peak ring, shock-metamorphosed and cataclased gneisses of authigenic breccia are exposed on the surface. They plunge at an angle of about 30° to the southwest and are opened by a number of wells at a depth of up to 900 m.

The boreholes drilled at the southwestern margin of the deposit, did not open the gneiss base of the crater. The latter is overlapped there by allogenic polymict mega- and mesobreccia, which in the lower part is cemented by suevites, and by tagamites in the upper part. This megabreccia is composed of blocks of crystalline rocks enclosed in tagamite matrix; it underlies everywhere the main body of coherent tagamites. It

is outcropping on the surface on the slope of the peak ring in the northeastern part of the deposit (Fig. 2.20). A composite thick, sub-horizontal tagamite sheet (it is up to 600 m in the axial part, average thickness is about 300 m), is characterized by the highest diamond contents. It is regarded as an ore tagamite horizon and comes to the surface in the upper part of the Balagan-Yuryage river basin. The tagamite horizon is opened within the deposit by all provided wells. Its pinching was observed only on the southwestern flank where its thickness diminishes in north-west and south-east directions. In the western part of the deposit, irregular bodies and lenses of suevites up to 100–150 m thick appear in the roof of the tagamite sheet. They are connected with tagamites by gradual transitions through taxitic varieties. The ore suevite horizon is regarded as an independent body. At the southeastern flank of the deposit, both ore horizons are overlapped by lithic microbreccia.

The floor of the tagamite body is generally gently undulating. Several subhorizontal subordinate bodies are distinguished within it, they being distinguished by a number of petrographic features, as well as by magnetic properties, so that they are considered as products of either high-temperature or low-temperature impact melts. Low-temperature varieties are characterized by higher diamond content compared to high-temperature ones. The distribution of diamonds in them is considered in detail above (Fig. 7.5).

In suevites of the upper ore horizon, whose thickness is 50–60 m on the average, two varieties are distinguished: vitroclastic and vitrolithoclastic. On the flanks of the deposit, the suevites are covered by microbreccia with an average thickness of 30 m (maximum 97 m). In places, the latter occur in suevites as irregular lenses no more than 10–20 m thick. The content of diamond in impactites varies in different parts of the deposit, both laterally and in vertical section. According to the sampling on the surface carried out during prospecting, the average content of diamonds in tagamites is 17.3 ct/t, while in suevites, 11.5 ct/t, correspondingly. Sampling of the core showed that the content of diamonds in the corresponding main types of impactites is 19.7 and 13.7 c/t, correspondingly. Exploration work allowed to determine the possible contour of the quarry of the first stage of mining where the average content in the tagamites was 23.23 c/t, that is almost 3 times higher than this value in the Udarnoe deposit. In general, tagamites in comparison with suevites are more highly diamond-bearing. The diamond content in low-temperature tagamites is on average twice as high as in the high-temperature ones. The content of diamond in suevites correlates with the volume of impact glass particles within them. For example, in the sintered vitroclastic suevites, the content of diamonds is almost three times higher than in vitrolithoclastic ones. It has been statistically established that the marginal parts of the thick sheet-like tagamite body are enriched with diamonds, both near the roof and, to a lesser extent, near the floor. The thickness of the diamond-enriched upper zone of the composite tagamite sheet is 50–200 m. This zone is near the surface, so the richest ores are available for open development.

An uneven distribution of diamonds in impactites of the crater as a whole is caused, as noted above, by the primary enrichment of individual jets or rays diverging from the center of the impact structure. The Skalnoye deposit embraces such a band of northeastern strike and of about 2.5 km wide. On its axis, the content of diamonds in

tagamites is maximum peaking 25–30 ct/t (in individual samples up to 40–110 ct/t), on the flanks the content falling down to 7–8 c/t or less. Within the band, the amount of diamonds in suevites is also increasing.

The exploration of the Skalnoye deposit was carried out by vertical wells. At first, the network was 1600 × 400 or 800 × 400 m, then it was thickened to 400 × 400 and was brought to 400 × 200 and 200 × 200 m in places. The depth of the wells was determined by the need to intersect all ore horizons to reach their base. The latter was penetrated to a depth of 400–500 m. The deepest well drilled east of the axial part of the annual trough reached 1520 m dip. With the thickening of the well network in the diamond-rich part of the deposit, their depths were only 100–150 m, in order to open the rich part of the ore horizon.

Sampling of cores, their processing and analysis were carried out according to the schemes approved at the Udarnoe deposit. The reserves calculated separately for two ore horizons (upper suevite and lower tagamite), as well as for the quarry of the first stage of the mining, were carried out under the same conditions as for the Udarnoe deposit. The calculation showed that the reserves of impact diamonds as a whole for the Skalnoe deposit in the B + C_1 category were 94,675.1 million carats, in the C_2 category—161,429.5 million carats. Based on the results of the work carried out at the Skalnoe deposit and a number of special studies, a geological and economic assessment of the development of the deposit was made, with several options for its output works.

More reasonably, than for the Udarnoe deposit, the technology of beneficiation and extraction of diamonds has been developed following the processing of 1200 tons of ore at an experimental factory in Mirny, Yakutia. 12,700 carats of impact diamonds obtained after the benefication, were tested in various tools. In order to improve the technology of ore processing and further experiments on the use of impact diamonds in industry in 1980–1981, the construction of an experimental operating factory was started in the Khatanga settlement, 300 km west of the deposits, where more than 5000 t of ore were then processed to produce a concentrate. Later, its development and extraction of raw materials were carried out in the Institute of Mineral Resources (Simferopol). After the processing of the concentrate, more than 100,000 carats of diamonds were sent for additional research.

The Vstrechnoe area is located in the north-north-eastern sector of the Popigai crater (Arylakh-Yuryage area—see Sect. 2.1.4), in the outer zone of distribution of allogenic megabreccia and impactites. The latter are developed within a meridional band of about 7 km long and 4 km wide on average. Tagamites in the eastern part of the area form a sheet-like body of 4 × 0.7–1.5 km in size; some tagamite patches were also found in western and southern parts of the area within impact breccias. The apparent thickness of the tagamite body peaks 86 m. Suevites are distributed in the north of the site, where they form on the surface a 2.5 × 0.5–1 km field stretched in the latitudinal direction (Fig. 2.18). According to the results of the prospecting of the tagamites (36 samples), the average diamond content in them is 7.8 ct/t that, taking into account the parameters of the ore body, made it possible to estimate the projected resources of the site at 5.7 billion carats. With additional prospecting and evaluation work, 10 wells of about 100 m of an average depth were drilled and the

core was tested. As a result, reserves of impact diamonds of category C_2 at the site were estimated at 14.45 billion carats.

The Tongulakh area is located on the northeastern flank of the Popigai crater (see Sect. 2.1.3) where carbonate deposits of the middle Cambrian outcropped on the surface. They are overlapped by allogenic megabreccia, which is covered by an erosion remnant of litho-vitroclastic suevites, which occupies an area of about 11 km^2. The site is the only prospecting area in the crater, where exclusively suevite with increased diamond content are developed while tagamite are absent (Fig. 2.15). During the testing of 21 samples, the average content of diamonds was determined to be 5.3 c/t. The exploration and evaluation works carried out at the site (9 wells with depth up to 100 m), including testing, allowed to estimate the reserves of impact diamonds of category C_2 at 3920 million carats.

In other prospective areas of the Popigai structure (e.g., Taas and Syuryunge occurrences), only prospecting were carried out with the sampling of impactites on the surface. Their forecast reserves can be estimated only approximately, but undoubtedly they make the first hundreds of millions carats.

Placers of impact diamonds are widespread in the Popigai area. The assessment of the prospects of alluvial diamond placers and the conditions for the formation of placers is based on the results of geomorphological studies and reconnaissance and prospecting sampling carried out by the Polar Exploration Enterprise and VSEGEI. The diamond content in alluvial deposits on the area of the Popigai hollow is established for, in fact, all river systems (an average content is 0.45 ct/m^3, in individual samples it reaches 3–5 ct/m^3), diamondiferous also are glaciofluvial (average content 0.108 ct/m^3), lacustrine-alluvial (average content 0.1375 ct/m^3) and eluvial-deluvial formations (an average content 0.078 ct/m^3). Along with impact diamonds in small- and large-volume samples from alluvium, kimberlite diamonds are found in places. Impact diamonds found in size fractions $-4 + 2$ and $-2 + 1$ mm, and their weight is about 75% of the total weight of diamonds of all classes. The average weight of one grain from placers is 1.5 mg.

The highest concentrations of impact diamonds in eluvial-deluvial sediments (in individual samples from 26 to 166 ct/m^3) were detected in the area of the indigenous deposits Udarnoe and Skalnoe, and they were also noted in the Middle-Upper Quaternary lacustrine-alluvial sediments in the southern part of the crater (1026 ct/m^3), where the largest diamond weighing 162.9 mg has been found. Prospecting and exploration works on the alluvium of the middle course of the Dogoy River, as well as along the Balagan-Yuryage River, revealed increased concentrations of impact diamonds of large classes. At the Dogoy placer, deep shafts (up to 20 m) and a number of wells have been drilled. The methods of work, the parameters of the mine workings network were borrowed from the experience of exploration of placer deposits of kimberlite diamonds on the Ebeliakh River located at 100 km to the east (Grakhanov et al. 2007). The width of the Dogoy riverbed together with flood plain and lower terrace is from 0.5 to 1.5 km, the thickness of stream channel pebble-bed is up to 10–15 m, the length of the placer more than 2 km. In samples from this placer deposit (total volume is of 129 m^3), several large diamonds of 8–10 mm in size and weighing more than 2 carats were found, while average diamond contents

were commonly 1–2, in places up to 3 ct/m^3. It should be noted that along with the impact diamonds in the placers, kimberlite diamonds of high quality were also found. Their content is 3–5% of the total diamond content. In the central part of this placer, the reserves for category C_2 were calculated; they amount to 12.4 million carats. On the flanks of the placer and at deep levels of productive beds, estimated resources are of 76.4 million carats.

A large residual placer in eluvial-deluvial formations represented by gravelitic clays and sandy loam, was found on the area of the Skalnoe deposit. The thickness of the placer varies from 1–2 to 10 m. The average content of diamonds based on the results of testing of 220 wells is 5.6 ct/t, some samples showed much higher content, though. Diamonds are contained in a free state; their concentration is up to 20 ct/t. In the alluvial deposits of streams draining this area of the huge indigenous deposit, the content of diamonds up to 30 ct/m^3 has been established for single samples. The maximum size of a diamond found in alluvium is 9 × 5.5 mm. In eluvial-deluvial deposits, diamonds of class −5 + 3 mm are encountered.

A rich alluvial placer is confined to the Balagan-Yuryage riverbed, draining the Skalnoe deposit. Its length is more than 6 km with the width of the channel from the floodplain to several hundred meters. Some samples show a diamond content of more than 1.5 ct/m^3.

The Verkhnedaldynskaya riverbed placer occurs at the Daldyn River in the southern sector, downstream of the mouth of Balagan-Yuryage River. It is of about 10 km long and up to 0.4 km wide; the thickness of alluvium is from 5 to 8–10 m. Individual samples show diamond content up to 1.6 ct/m^3, and in one well, even 5 ct/m^3. At the same time, 61% of the weight content of diamonds there are diamonds of the class −4 + 2 mm.

In conclusion, it should be noted that syngenetic impact diamonds represent a new type of mineral raw materials, and any experience of industrial exploration of impact diamonds deposits has not been obtained yet. The diamond deposits revealed in the Popigai are highly different from well-known diamond deposits hosted by kimberlite and lamproite (Masaitis 1989, 1994; Grieve and Masaitis 1994). At the same time, principal features of alluvial placer deposits of impact diamonds did not significantly different from that of kimberlitic diamonds.

7.7 Industrial Applications of Impact Diamonds

In general, the Popigai impact structure of the scattered diamonds in impactites, along with the identified indigenous deposits and occurrences, as well as alluvial and other placers, can be considered as a special metallogenic region, the potential of which is due to influence of combination of terrestrial and cosmic factors. The conducted geological survey showed that the total geological reserves of impact technical diamonds are several times higher than the world predicted resources of kimberlite diamonds, and their content in ores is higher than the richest kimberlite

types (Simonov et al. 2004; Masaitis et al. 2013). Impact diamonds are a new kind of mineral raw material that can be used in the industry.

Tests of technical properties of impact diamonds (abrasive, strength, electrical, thermal properties, etc.) were carried out in the 1970s and 1980s in a number of research institutes in the USSR, as well as in experimental production sites. As a result, a number of specific properties have been identified, which make it possible to judge the possibilities of their industrial use, primarily as abrasive materials. Several batches of raw materials weighing several tens of thousands of carats were tested for various types of testing, including 15,000 t of ore extracted from the Skalnoye deposit at the concentrator in the Khatanga settlement. The diamonds were divided into several varieties depending on the color, the shape of the grains, the sizes, etc. The material obtained from both impactites and placers, has been studied. It was found that with the use of special tool designs, the selection of operating modes, the effectiveness of the use of impact diamonds can reach kimberlite ones, and thus it is expedient to replace a number of synthetic diamond with a new type of natural raw material. The results of these tests are partially published (Goncharov and Chernoknizhnikov 2001; Simonov et al. 2004; Polkanov 2006; see also Val'ter et al. 1999).

Tests for uniaxial compression showed high strength of large granulometric classes of diamonds (>2 mm). The abrasive properties of light-colored varieties are 1.5–2 times higher than in kimberlite and synthetic diamonds. It was shown the suitability of impact diamonds for the creation of a wide range of cutting and other tools based on them, including for the processing of natural stones, reinforced concrete, hard alloys, steels, ceramics, glass, for the production of drilling tools, cutters for various needs, drills for the construction industry, ruling pencils, filers, tools for processing precious stones, cutting elements of saws, cutting, grinding, polishing wheels and pills, tools for rolling diamond discs. It is possible to compact impact diamonds with the subsequent manufacture of various tools from compacts. Impact diamonds can replace synthetic diamonds in tools and scarce tungsten-containing hard alloys. Data on the high efficiency of a number of abrasive tools made on the basis of impact diamonds have been obtained. A number of tools (drill bits, bits, drills, tools for processing precious stones, etc.) showed high performance, including exceeding the performance of a similar tool made from kimberlite diamonds. At the same time, the methods used for the manufacture of such tools require the consideration of the specificity of impact diamonds, in particular, the preliminary preparation of the material, the selection of binders, the manufacturing technology and the determination of the optimum operating conditions for tools and products. Diamonds extracted from placers have higher mechanical properties (hardness, strength etc.), as well as larger size, which significantly expands their application areas, in addition to using them as abrasives (Naumenko 2004).

The results of experiments on the use of impact diamonds in other fields of technology are not sufficiently representative. Work in this topic performed earlier in the majority on old equipment, was of a limited number. It has been established that impact diamonds are resistant to chemical, thermal, and radiation effects. The diamonds proved to be suitable for the manufacture of resistors with more optimal

properties compared to products made from kimberlite monocrystals. The development of the method of creating a resistive layer on the surface of impact diamond makes it possible to use them in the electronics industry. Resistive layers with different ohmic resistance were created. It is shown that from polished plates of polycrystals it is possible to fabricate resistors using micro-solderers as heaters in the tips, microheaters, thermoelements. Impact diamonds are promising for use in the manufacture of thermal insulators with high electrical insulation properties and with high thermal stability. High thermal conductivity of diamonds makes it possible to use them in the electronics industry as heat sinks. Thermal conductivity of diamonds of large fractions is 150–600 W/(m K). Compacts made in the form of sintered tablets were tested as substrates for electronic circuits. There are data indicating that impact diamonds can be used to create ionizing radiation detectors, temperature detectors, high-speed integrated circuits for computer technology

However, in general, various properties of impact diamonds and the application of this new type of mineral raw materials have not been studied enough. It is possible that further research will reveal new opportunities for its industrial use.

References

Chumak MA, Bartoshinsky ZV (1968) (in Russian), In: Geolog Yakutii newspaper No. 27(556): 1

Goncharov MM, Chernoknizhnikov VV (2001) Impact diamonds in Taymyr autonomic district and their industrial significance (in Russian). In: Samoilov AG (ed) Essays on findings of mineral deposits in the Taymyr Peninsula. Siberian Branch of Russian Academy of Science Publishing, Novosibirsk, pp 257–259

Grakhanov SA (2005) New data on distribution of lonsdaleite-bearing diamonds in the northeastern of Siberian platform. Trans (Dokl) Russ Acad Sci 405:779–782

Grakhanov SA, Shatalov VI, Shtyrov VA, Kychkin VR, Suleimanov AM (2007) Diamond placers of Russia (in Russian). Geo Press, Novosibirsk, 457 pp

Grieve RAF, Masaitis VL (1994) The economic potential of terrestrial impact craters. Int Geol Rev 36:105–151

Kaminsky FV, Blinova GK, Galimov EM, Gurkina GA, Klyuev YA, Kodina LA, Koptil VI, Krivonos VF, Frolova LN, Chrenov AY (1985) Polycrystalline aggregates of diamond with lonsdaleite from Yakutian placer deposits (in Russian). Mineral Zh 7(7):27–36

Masaitis VL (1989) Mineragenetic systems of impact craters (in Russian). Geol Rudnykh Mestorozhdeny 3:3–17

Masaitis VL (1994) Impactites from Popigai crater. In: Dressler BO, Grieve RAF, Sharpton VL (eds) Large meteorites and planetary evolution I. Geological Society of America Spec Pap 293, pp 153–162

Masaitis VL, Simonov ON (2004) Unique deposits of industrial diamonds in Popigai area (in Russian). Mineral commodities of the Taymyr autonomic district and prospective of its exploration. VSEGEI Press, St. Petersburg, pp 156–161

Masaitis VL, Naumov MV, Mashchak MS (2005) Original diameter and depth of erosion of the Popigai impact crater Russia. In: Kenkmann T, Hörz F, Deutsch A (eds) Large meteorite impacts and planetary evolution III. Geol Soc of America Spec Pap 384, pp 131–140

Masaitis VL, Kirichenko VT, Mashchak MS, Fedorova IG (2013) Primary deposits and placers of impact diamonds at the Popigai area (Northern Siberia) (in Russian). Regionalnaya geologija i metallogenija 54:89–98

Mojzsis SJ, Arrenius G, McKeegan KD, Harrison TM, Nutman AP, Friend CRL (1996) Evidence for life on Earth before 3800 million years ago. Nature 384(6604):55–59

Naumenko NG (2004) Prospective for diamond bearing placers in Popigai area (in Russian). Mineral commodities of the Taymyr autonomic district and prospective of its exploration. VSEGEI Press, St. Petersburg, pp 178–181

Plotnikova MI (1990) Essay on post-Oligocene history of the Popigai impact morphostructure (in Russian). Meteoritika 49:154–164

Polkanov YA (2006) Cosmogenic diamonds in the Earth's crust: "aliens" and "natives" (in Russian). In: 2nd International Conference on Forecasting and Prospecting for Bedrock and Placer diamond deposits. Kiev, Ukraine, pp 281–288

Sidorenko AV, Sidorenko SA, Sozinov NA (1981) Carbonaceous formations of Precambrian and their metal-bearing (in Russian). In: Problems of sedimentary geology of Precambrian. Nauka Press, Moscow, pp 9–17

Simonov ON, Masaitis VL, Mashchak MS, Goncharov MM (2004) Efficiency of forecast and prospecting for diamonds in Popigai astrobleme: a retrospective overview (in Russian). The efficiency of forecast and prospecting of diamond deposits: the past, now, and future. VSEGEI Press, St. Petersburg, pp 323–326

Sozinov NA, Sidorenko SA (1976) On formation types of carbonaceous shales of Precambrian and Phanerozoic (in Russian). Trans (Dokl) Acad Sci USSR 227:684–687

Val'ter AA, Gursky DS, Eremenko GK (1999) Impact diamonds—a new kind of mineral raw in Ukraine. Mineralnye resursy Ukrainy 3:16–22

Chapter 8
Origin of Diamond-Bearing Impactites

Victor L. Masaitis

8.1 Reconstruction of the Impact Event

The catastrophic collision of a cosmic body may be considered from two aspects: (a) the damage caused on the Earth surface directly around the point of impact and in the surrounding area, and far beyond it in the global scale, and (b) the formation a crater depression, transformation of upper part of crystalline basement and sedimentary cover, origin of the wide number of impactite and impact breccia varieties.

Paleogeographical reconstruction shows that the territory of central North Siberia where the Popigai impact event occurred at the end of Eocene was characterized by a relatively flat relief. It was covered by forest vegetation of transitive type from subtropical to moderate thermophilic (Krasheninnikov and Ahmetjev 1996). The energy of the impact may be evaluated to be $E = 2 \times 10^7$ Mt TNT, the peak pressure at the compression stage, as $P = 6.24 \times 10^{11}$ Pa, and the seismic magnitude at the point of impact, as 8.3–9.5 (Melosh 1989; Ivanov 2005). The shock wave was spreading in the target while the ballistic wave, in the atmosphere where the giant fireball was ascending.

The zone of the complete destruction of target rocks had a radius of about 50 km. It may be divided roughly into three subzones: evaporation (R ~ 9.5 km), melting (R ~ 11.3 km), and intensive deformation (R = 50 km). The ballistic ejecta, seismic wave, thermal radiation caused by fireball heating, blast wave in the atmosphere, and high-velocity wind were responsible for the principal damage on the Earth surface outside the area of complete destruction. Several zones of damage, which decreased with distance from the impact point, may be distinguished. The approximate radius of various types of damage which influenced on the environment mostly in combination may be reconstructed by means of evaluated energy of impact (Collins et al. 2005;

V. L. Masaitis (✉)
A.P. Karpinsky Russian Geological Research Institute, Sredny prospekt, 74, 199106 Saint Petersburg, Russia
e-mail: vcmsts@mail.ru; victor_masaitis@vsegei.ru

V. L. Masaitis (ed.), *Popigai Impact Structure and its Diamond-Bearing Rocks*,
Impact Studies, https://doi.org/10.1007/978-3-319-77988-1_8

Ivanov 2005; Masaitis 2010), and local environmental conditions. The near crater zone of local destruction and severe damage (R ~ 1500 km) had embraced the central and northern parts of the Eastern Siberia, partially northeast of Western Siberia, northwest of Verkhoyansk range, and a part of the Arctic ocean. This zone consists of three concentric subzones characterized by different intensity of damage. At the distance of about 100 km from the impact point the intensive ground displacement, very strong air blast, incineration due to fireball radiation, base surge and ejecta fallout occurred. The remnants of ejecta blanket are preserved now at the distance 70–80 km from the crater center, but ballistic ejecta originally had extended up to 500 km, where its thickness was only some centimeters or more. The evaluation of maximal distance of ballistic transportation of impact melt bombs and droplets is in agreement with distribution of impact diamonds scattered in the river beds far from the crater (Fig. 8.1), and caused by destruction of these diamond-bearing bomb's (Grakhanov et al. 2007).

The outer limits of influence of thermal radiation caused wild fire and strong burn is considered as far as 1500 km from the impact point. The radius of zone of moderate or light short-term damage of biotic systems may extend still further; it embraced northern Eurasia and the significant part of adjoining Arctic Ocean down to modern northern coasts of Greenland and Canadian archipelago. The deforested land of this zone producing by violent storm probably propagated to the distance about 2000 km, and area of slight damage of the vegetation caused by storm and strong gale at the distance up to 2500 km. Some disturbances caused by seismic-generated tsunami and gale may occur on the shores of an internal shallow seas and Arctic ocean coasts up to 3000 km. The influence of global long-term factors of defeat are studied insufficiently. It is known that considerable biotic change at the end of Eocene did not occur. The reconstruction shows that global cold snap (on 4–5°) and biotic changes took place on the Eocene/Oligocene boundary, it is considered as the result of common climatic change, but this snap probably may strengthen due to darkening of atmosphere with dust clouds. In the part of Siberia under review the change of the forest vegetation species occurred, they become less thermophilic, the flowering plants and fern allies were undergone more significant extinction (Krasheninnikov and Ahmetjev 1996). However, the probable contribution of the Popigai event consequence to these processes is not clear. In general, the intensive and moderate damage areas caused by this event captured about 5.5% of the Earth surface.

Nevertheless, the influence of the Popigai event may be traced at the distance more than 15,000 km using the distribution of the dust particles carried by atmospheric or gas currents and apparently extended all over the Earth. As mentioned in Chap. 2 the ejected material was also found in deep-seated South ocean sediments of corresponding age.

Popigai impact event was not the only one at the end of the Eocene. Close by time the Cheasapeake Bay impact structure about 90 km located at the Atlantic coast of the USA across has been formed (Poag 1996; Poag et al. 2004; Gohn et al. 2009). Impact event occur 35.2–35.5 Ma ago, which is confirmed by geological dates of thick (to 60 m) interbed of specific breccias with shock-metamorhosed quartz, occurring in contiguous parts of the continent and on shelf as well as shock-metamorphosed

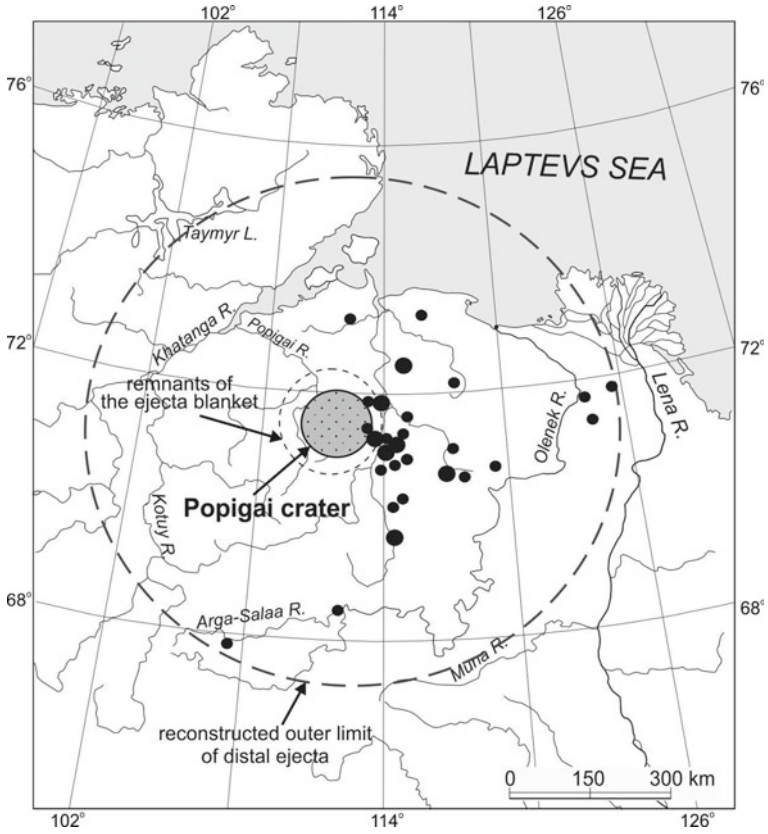

Fig. 8.1 Locations of placer impact diamonds in Quaternary deposits around Popigai crater showing a former distribution of eroded distant ejecta from the Popigai (author's unpublished data plus data from Vishnevsky et al. 1997; Grakhanov et al. 2007). Locations of impact diamond finding are shown by full circles; larger circles mark placers where amount of impact diamonds extracted exceeds 1000 mg (Grakhanov 2005)

material, revealed in the oceanic shelf section, 150 km from the New Jersey State coast and dated at 35.2 ± 0.3 Ma (Poag and Aubry 1995). Considence of the age of the Cheasapeake crater with that of the North American tektites, as well as the similarity of their Rb–Sr and Sm–Nd isotopic characteristics to those of target rocks of the Cheasapeake crater make the latter quite a probable source of the strewn field of these tektites (Poag et al. 2004).

Close by time large-scale impact events 34–35 million years ago violates the general statistical regularity in the frequency of collision of the crater-forming bodies. According to the estimated frequency such events should occur approximately once in 100 million years (Ivanov 2005). However, there are other impact structures that have arisen around the same time. East of the Chesapeake crater on ocean shelf the Toms Canyon depression with a diameter of 22 km was detected. It was considered to

be an impact crater that occurred simultaneously with the Chesapeake. In addition, in the Eastern part of the North American continent there are two known impact crater—Mistastin, with diameter of 28 km and Wanapitei, with diameter of 7.5 km, which arose, respectively, 36 and 37.2 million years ago. Finally, within the Canadian Arctic there is the Houghton crater with diameter of 40 km dated about 39 Ma (Sherlock et al. 2005). Thus, five or six impact events took place throughout 4–5 million years. It should be noted, firstly, that not all of the craters, which could occur during this time interval have been preserved from erosion, probably only large ones, 1998, and, secondly, part of the cosmic bodies might fall in the oceans. If powerful impacts followed at short time intervals after each other, they would undoubtedly cause not only local changes in the environment, but could lead to a long dusty atmosphere and to a cooling of the climate that occurred at the end of the Eocene.

8.2 Processes Within Melt- and Rock-Forming Systems

Diamond-bearing and diamondiferous impactites, occurring in the Popigai impact structure formed due to presence of carbonaceous substance in target rocks and a significant impact energy, resulting both in its transition to hyperbaric phases, and in melting of these rocks.

The scheme of such a process in the 3D space, taking into account an irregular distribution of carbonaceous substances, zonation of shock metamorphism and centrifugal displacement of impact melt during crater formation was first developed for diamondiferous impactites of the Popigai crater in 1974 and was later published (Masaitis 1984, 1993, 1998)

The general succession of crater-forming stages is characterized in many publications, the most complete characteristic being given by Melosh (1989). Commonly, three stages overlapping in time are distinguished:

(1) Contact and compression, during which the impacting cosmic body is decelerated in the target rock sequence;
(2) Excavation and formation of the transient crater;
(3) Modification when the transient crater is filled with the crushed and melted material and changes its morphology due to the movements of the floor and flanks of the structure.

All these stages, even in the case of formation of large craters, succeed each other very quickly (some hundreds seconds). However, several subsequent processes (cooling, lithification, isostatic leveling, hydrothermal activity etc.) can continue for a rather long period (to several hundreds of thousands of years and more), therefore it would be reasonably to subdivide the modification stage into the early and late ones.

The computer simulation of the Popigai structure origin (Ivanov 2005) showed that, taking into account its morphology and parameter, diameter of impactor at its accepted speed of 15 km/s, may be of about 8 km, and the impact energy 8×10^{22} J.

That insignificantly differs from our more early estimation (1.7×10^{23} J, see Masaitis 1984). According to calculations, on the stage of compression the transient crater could attain a depth of about 18 km after 20 s the colliding body touched the surface. The bottom of transient cavity was occupied by impact melt in a radius about 30–40 km, its thickness could reach 200 m or hardly more. On the stage of modification during the following 90 s the bottom of transient cavity uplifted above its initial level up to 6 km, the inner board of this cavity sink. The originated melt flowed down from a rising "hill", the diameter of which could reach about 40 km. To the 200-th s the "hill" settled, and the annular wave of heated and crushed rocks spread on the bottom. In the presented model this annular wave overlapped part of the melt flowed from the "hill", then this wave stopped, and formed the observed annular uplift or peak ring with a diameter of 45 km. Accordingly, the annular trough formed on the periphery of the transient crater due to sinking of its outer board.

The author rightly suggests caution to treat the results of calculations on the detailed model of the crater profile, which may not accurately describe the behavior of large masses of fragmented rocks (Ivanov 2005). Indeed, consideration of the mode of occurrence and relationships of the bodies of impactites, authigenic and allogenic breccias (including timing) in the NE-SW profile boreholes with a length of about 35 km and crossing peak ring, annular trough and a facing board of the impact structure (Fig. 2.20), detects the following inconsistencies:

(a) Authigenic breccias of the peak ring were subjected to shock compression with an amplitude of no more than 8–10 GPa and therefore this material initially could not be previously located in the center of the crater. Thus, these breccias do not constitute a "ring wave" that had moved from the inner part of the crater. Besides, there are no signs of burial of the melt beneath the thrust of transformed rocks of "ring wave", suspected by the model. Moreover, it should be taken in mind, that peak ring elevates above the bottom of the central depression at two kilometers. It is very doubtful that this is the result from speading of the wave of breccia from the center.

(b) The structure of the basement of the annular trough (displaced parautochtonous material) indicates that composed rocks, including a centrifugal thrust scales, do not originally represent the initial side of the transient crater. Such thrusts are observed now on the outer edge of the annular trough and outside on the outer ring terrace. Such centrifugal thrusts damped there with the distance from the annular trough. Kinematical pictures for the emergence of this type of displacement of target rocks inside the annular trough and out of it are the same.

(c) The internal structure of sequences of impactites and megabreccias filling the annular trough, in general, has the features of inverted stratigraphy. At the base are allogenic lithic megabreccias, consisting of fragments of sedimentary rocks, up of the section they are changed by polymict megabreccias of sedimentary and crystalline rocks, which, in turn, is overlain by megabreccias of the latter, cementing with molten material. They overlap by thick sheet of solidified melt ejected from the crater interior. All these patterns are close to the structure of the

overturned flap on the outer edge of the small impact crater formed in layered target.

Thus, geological data are in good agreement with conception that the peak ring is a relic of the elevated outer edge of the transient cavity, and the annular trough, filled with breccias and molten material is the compensated sink for the rise of the crater bottom. It is more probable that the material comprising the peak ring was not transported from the inner part of the transient cavity. This rises a problem to specify widespread models of crater collapse that presume annular trough and peak ring emerging at the modification stage of cratering due to the combination of collapse of the outer wall of the transient cavity and uplifting of its floor in the crater center and subsequent outward spreading of gravitationally unstable rock material (e.g., Morgan et al. 2000, 2016; Vermeesch and Morgan 2004; Ivanov 2005).

The main features of the movement of the shocked substance during cratering (stages of compression, excavation and, partly, early modification) are clear from Fig. 8.2.

Simulation of a deep structure based on the analysis of gravity and magnetic data, taking into account geological data and petrophysical properties of rocks (Pilkington et al. 2002) indicates the absence of a noticeable central uplift of the true bottom. Its transverse profile with a significant (about 2 km) elevation of the peak ring, above the level of the midpoint of the crater, at the same time being 22–23 km away from its center, also supports these views.

Petrogenesis of diamond-bearing impactites starts from impact melt formation and ends in cooling of various geological bodies, which were formed by participation of this melt. The reliability of the reconstruction of these processes is determined, on the one hand, by the completeness of geological-petrographic and mineralogical observations; and, on the other hand, by a certain degree of elaboration of theory of the processes considered. All these processes occur with large masses of mineral substances with directed rapid changes in its phase composition, aggregate state, thermodynamic parameters, and kinematics. The totality of these masses and the conditions for their transformation can be considered as complex interconnected petrological systems, among which there are conventionally three basic, sequentially evolving—initial, transitional and final ones.

The initial system represents by different target rocks, including graphite-bearing ones, transformed by the passing shock wave to the substances with different aggregate state. Transitional system embraces altered substance of initial rocks, which is in the state of disintegration, differential movements, flow, mixing, ejection and deposition. The final produced system is in fact, impact breccias and impactites in the process of equalization of the parameters of the state with atmosphere and surrounding rock massifs, partly water saturated.

It should be emphasized, that these petrological systems are generally open; the first two are, in most cases, noted for the extremely unbalanced character of the processes, abrupt kinetic changes; and the first one is, besides, characterized by remarkably quick increase of entropy and enthalpy due to the energy pulse received. In the

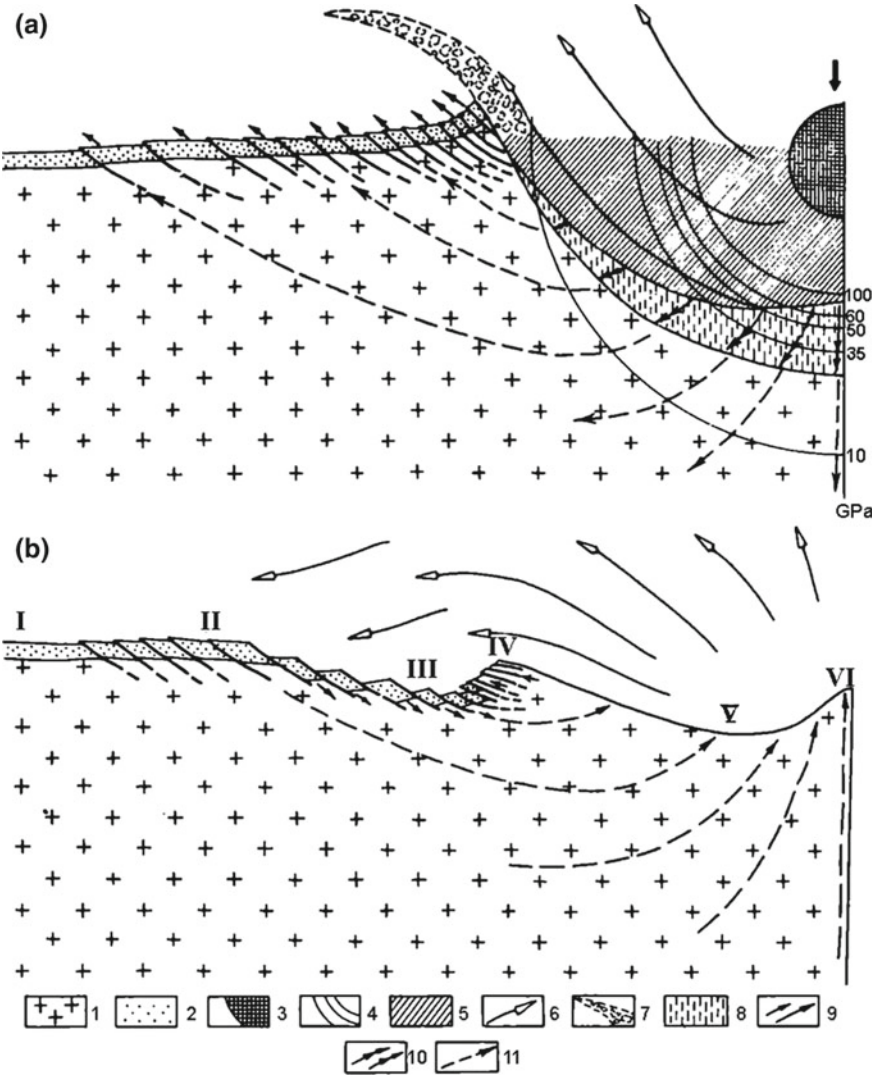

Fig. 8.2 The scheme of displacements of deformed and shocked rocks during different stages of cratering of the Popigai structure. **a** excavation stage, **b** early modification stage. 1—Crystalline basement, 2—sedimentary cover, 3—impactor, 4—isobars of the shock wave, calculated on the model of point-like explosion in an unbounded medium, 5—excavation cavity, 6—displacement of crushed and melted rocks from the excavation cavity, 7—ejecta curtain, 8—zone of flowage in the transient cavity, 9—displacement of deformed rocks and blocks, 10—plastic flow, 11—deep sliding and elastic rebound. I—Undisturbed or slightly disturbed zone, II—external structural rim, III—annular trough, IV—peak ring, V and VI—inner unevenness of crater bottom. Fire ball and some other types of ejecta are not shown

final system, due to cooling and crystallization, the structural ordering increases, and heat content drops.

Petrological processes of melt and rock formation in each system are regulated by intense and extensive factors, which are also affecting the generation and preservation of impact diamonds in them. The leading intense factors for the initial system are the pressure in the shock wave, propagating from the impact point and gradually attenuating, duration of compression, temperature level and mass velocity beyond the shock front. In transitional system, among intense factors are the pressure in the jets of the ejected substance, its temperature, velocity, angle of ejection, and the duration of transportation. In the final system, these are lithostatic pressure in rock sequences, their temperature, duration of equalization of parameters, composition, temperature and pressure of migrating fluids.

Extensive factors in all the three systems characterize the chemical and phase-mineral composition of substance, including its structure (constitutional and geometric), as well as physical properties (density, porosity, viscosity and the associated properties), content of volatiles and fluid-saturation. One should emphasize the gradient character of all the three systems, which shows up, particularly in variations of both intense, and, to a lesser extend, extensive factors of melt and rock formation.

The factors, determining the possibility of formation of certain modes of diamond distribution and preservation, can be considered within the same approach. An extensive factor is the occurrence of graphite in target rocks and its properties, character of graphite distribution, textural-structural features of rocks, enclosing it, and the presence of fluids. Among the intense factors are pressure in the shock wave, duration of compression, temperature beyond the compression front, extent of material mixing, determined by the pulse and trajectory, duration of cooling, and the regime of fluids. All these factors can be evaluated as favourable or unfavourable in terms of the influence on the formation of the largest diamond concentrations in impactites and in the crater in general, as well as in certain impactite bodies. It should be taken in mind that the natural process of transformation graphite to diamond significantly differs from the same accomplished during laboratory experiments. The laboratory synthesis occur in the homogenous metallic matrix, remaining in the solid state after the shock compression, which duration is much shorter than at the impact event. Moreover, the synthetic diamond does not suffer any displacement, any influence of hot silicate melt and some fluids.

8.2.1 Initial Processes

In the initial systems, the petrological processes are mainly reduced to shock transformations and heating of target rocks. During the compression stage, when the attenuating shock wave is passing through the target rocks, concentric hemispherical zones (if no account is taken of areas, adjoining the free surface) of altered crystalline rocks form, gradually passing into each other. The central evaporation zone, directly adjoining the impacting body, which is also subject to this process, turns

Table 8.1 Parameters of zones of target transformation

Zone of transformation	Pressure (GPa)	Outer radius of zone, km	Principal physical process and new-formed hyperbaric carbon phases
1	>100	9.5	Volatilization
2	100–60	11.3	Whole-rock melting, partly volatilization Graphite → diamond → graphite
3	60–50	12.0	Melting Graphite → diamond (diamond → graphite in parts)
4	50–35	13.6	Plastic deformations, selective melting Graphite → diamond
5	35–10	20.6	Plastic deformations
6	<10	Up to 70	Fracturing and shattering

to the melting zone and then to the slight crushing and fissuring zone around the periphery.

In case of the Popigai event, the evaluation of the peak pressure at the compression stage is $p = 620$ GPa (Masaitis 1984). Applying the law of shock wave attenuation (Zel'dovich and Raizer 1966; Bazilevsky et al. 1983; Melosh 1989), one can also evaluate the radii of concentric zones of full evaporation, full melting, plastic deformations and shock metamorphism of different intensity (Table 8.1). The above evaluations agree well with direct observations over the character of transformations of non-displaced (or subject to comparatively insignificant coherent displacements) crystalline rocks of the crater base, which are explored on the surface and are penetrated by boreholes in zones 5 and 6 (Table 8.1), i.e. within the peak ring, at the base of the annular trough, and at its outer edge. Thus, within the peak ring (r = 22.5 km), shock pressure, according to petrographic observations, did not exceed 8–10 GPa; near the annular trough axis (r = 28 km), it ranged within 4–5 GPa, and on the outer edge of the annular trough (r = 37.5 km) did not reach 1 GPa. Distribution of shock pressure in target rocks is schematically shown in Fig. 8.2, which is simultaneously illustrating the general pattern of mass displacement at subsequent stages of cratering.

Table 8.1 shows the position of zones of the most efficient diamond generation within the shock pressure interval from 35 to 60 GPa. Below this pressure level diamonds practically do not form, which, as it was shown above, follows from the study of shock-metamorphosed graphite-bearing gneisses, subjected to different compression and representing "frozen" elements of the above-mentioned zones. At a very high residual temperature, significantly exceeding the liquidus of acid rocks (T > 1700–1800 °C), resulting from compression above 60 GPa, diamonds are almost fully graphitized or oxidized, if there is no quick temperature drop (for example, during ejection of melt drops), to say nothing of the inner zone with even higher residual temperatures, where the forming melt is intensely overheated (up to 2000 °C and above). Possibly, under these conditions, the silicate melt, rich in SiO_2,

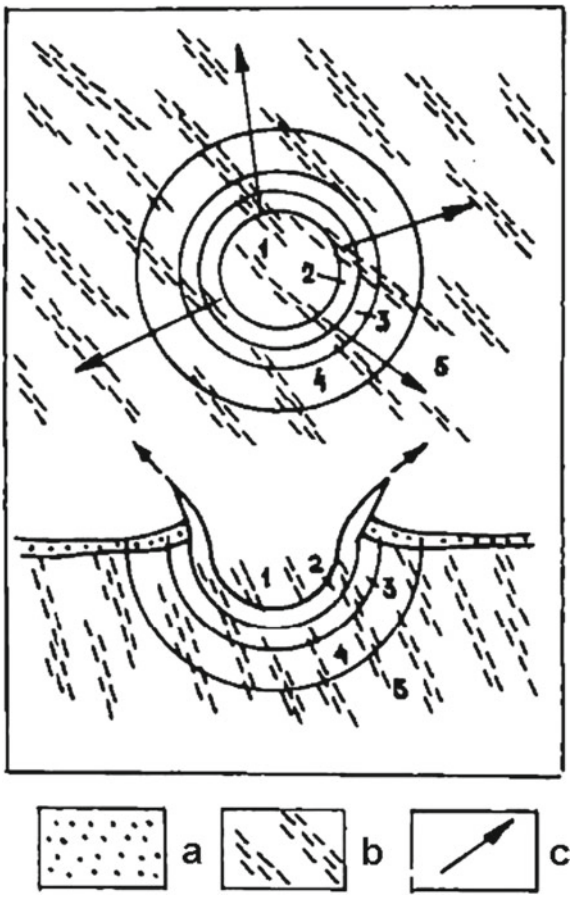

Fig. 8.3 Scheme of concentric zones of the shock transformation imposed on gneiss massif with an irregular distribution of graphite—plan (at top) and profile (at bottom). Zones of transformations: 1—evaporation, 2—melting, 3—plastic deformations, 4—fracturing and crushing; 5—undisturbed rocks. Target rocks: a—sedimentary (are not shown in the plan), b—crystalline, enriched by carbonaceous material in places; c—directions of radial ejection from zone 2 of melt portions enriched by carbonaceous substance transformed to hyperbaric phases (graphite + diamond)

could react both with relic graphite, and with diamond paramorphs, with generation of silicon carbide, similar to the industrial synthesis of this compound. Therefore, the zone of effective diamond generation is rather narrow in terms of width (about two and a half km). Further, the emphasis would be placed on certain processes, embracing the volume of substance in this zone, shown in Fig. 8.3.

External part of this zone (R = 13.6–12 km) after the passage of the shock wave remained in the solid-plastic state while the inner part (R = 12.0–11.3 km) turned into the melt. The rocks located closer to the center were also melted (R = 11.3–9.5 km). The estimation of the total volume of the rocks melted in the hemispherical layer according to the model in question (R = 12.0–9.5 km) approximately is about 1800 km^3, which almost exactly corresponds to the volume of the melt accumulated in the tagamites and suevites that preserved in the crater (excluding rock inclusions), and estimated by geological data at 1750 km^3.

An essential role in these processes is played by the differences in initial temperature of melts, generated at different distances from the center (R = 12.0–9.5 km). The presence of lechatelierite (melting temperature of quartz about 1700 °C), molten rutile grains, zircon, magnetite, and ilmenite (melting temperatures about 1300–1600 °C), occurrences of mullite (formation temperature 1100–1750 °C), moissanite (its synthesis proceeds at temperatures over 1800 °C) in tagamites points to a marked overheating of certain fractions above liquidus for the corresponding compositions. The series of mineralogical thermometers definitely points to the fact, that significant volumes of the melt had the temperature of 1100–1400 °C (Masaitis 1978). Thus, it might be presumed, that the initial temperatures ranged from 1100–1300 °C in the most remote zone to 1800 °C or more near the center.

The prevailing medium for the graphite substrate during diamond generation were biotite-garnet and some other gneisses, which most frequently occur as fragments in high-diamondiferous tagamites and suevites. Observations within the adjoining part of the Anabar Shield, where similar rocks are widespread, show, that graphite impregnation in crystalline rocks can reach 10 vol% in places. However, generally it is distributed irregularly as lenses, bands etc. Superposition of the shock-metamorphic concentric zonation on such a substratum with irregular distribution of graphite also resulted in an irregular distribution of diamond in the concentric zone of its most effective transition from graphite.

In some shock-metamorphosed gneisses from inclusions in impactites, up to 75% of the graphite turn into diamond. However, such rocks were compressed with the amplitude not more than 45 GPa, which might be confirmed by the presence of relics of garnet, which has not been fully transformed, whereas all the other silicate minerals are converted into diaplectic glass and impact glass. Apparently, the completeness of the solid-phase graphite transition is dependent not only on the compression degree, but also on the size of its grains and the aggregates formed by them, their degree of crystallinity, properties of silicate minerals, directly enclosing graphite aggregates etc. Observations on thin sections show, that in shock-metamorphosed graphite-bearing gneisses small idiomorphic graphite crystals are almost fully transformed to diamond, whereas relatively larger graphite scales and aggregates undergo only a partial transformation.

The analysis of shock alterations of tectosilicates leads to the conclusion, that in those cases, when their crystals are enclosed into larger grains of femic minerals, noted for a relatively higher acoustic impedance, higher levels of compression, than in those cases when tectosilicates form the rock groundmass, are required for plastic deformations and phase transitions. This enables to presume, that for the transition of graphite scales or particles into diamond in cases, when they are enclosed into large silicate crystals, a slightly higher pressure is necessary, than for similar scales, surrounded by feldspars and quartz.

Within the above-mentioned hemispherical layer with gradient pressure, the silicate matrix, enclosing graphite, in the rarefaction wave is partly transformed into the aggregate of impact melts of monomineral compositon. The density of inner energy at the expense of substance compression here is sufficient for the corresponding destruc-

tion of crystal lattice of the rock-forming minerals. This material is partly subject to plastic deformations with generation of diaplectic minerals and diaplectic glass.

Since the transformed massif represent the media with rather inhomogeneous physical properties, not only the differences in the degree of these changes on a micro- and macro-scale appear even on areas with similar pressure in the shock wave, but also significant shear stresses. At the same time, it should be born in mind, that certain parts of the imaginary gradient column of shock compression in the crystalline rock massif do not exist simultaneously, being transformed beyond the moving wave into a transit system immediately after its passage.

Transformation of rocks occur during the considered stage under conditions of a one-sided dynamic influence of the elastic precursor. It follows with an abrupt pressure increase, possibly, pulsating, intense compassion, characterized by a definite duration, and subsequent pressure decrease, accompanied by movement of substance, including that beyond the wave front. Some of the above-mentioned stressed-state phases can be reconstructed on the basis of analysis of the succession of destruction of rock-forming minerals and their aggregates (Masaitis 1982). The behaviour of graphite can also be considered with a certain share of probability within these processes (Val'ter et al. 1992)

A significant duration of the compression pulse during the considered crater-forming event (0.5–1.0 s) enables to conclude, that the shock wave arrival might be regarded as a two-stage compression. The entry of this wave may be considered as unilateral, whereas the subsequent long-term pulse results in its hydrostatic character. Such a succession of the processes is also confirmed by a number of mineralogical features of partly altered graphite scales and polycrystalline diamond paramorphs. The growth of the fine-grained nitrogen-bearing cubic diamond or its films on the paramorphs of lightly coloured polycrystalline diamonds directly within the altered gneisses is explained by diffusion (Val'ter et al. 1992). Such a process could, on the one hand, be supported by the above-mentioned duration of compression, and, on the other hand, by the influence of the high-density fluid, which also contained nitrogen. The participation of high-density fluid in this process, which also comprised water and carbon dioxide, is emphasized by the occurrence of these components in diamonds (Koeberl et al. 1997). The role of the volatile constituents and, primarily, their effect on phase transitions are not yet quite clear. Aqueous fluid is generated in compressed rocks both at the expense of pore moisture, and decomposition of water-bearing silicates. As it was shown by detailed studies of diaplectic glass and fusion glass (Feldman 1990), at the considered stage, such intensely compressed high-temperature fluid could cause a high-velocity transfer of certain constituents, primarily, alkalis and some others. At the same time, this process, most likely, occurs on a micro-scale (possibly, at distances not more than the first mm or a dozen of mm), without any changes in the bulk composition of rock within the samples of hand-specimen size. The role of this fluid in the formation of porous structure of melt glass under the starting relaxation, as well as during coesite crystallization at the expense of diaplectic glass, is doubtless (Masaitis et al. 1993). Dissociation of water and hydroxyl absorption by the melt (which is the more significant, the higher its temperature) resulted in the growth of the partial pressure of hydrogen in this coexisting fluid.

Such character of the fluid is also confirmed by the composition of chilled glass from suevites and microbreccias, characterized by a low degree of iron oxidation, which is lower, than that not only in gneisses, which served as an precursor for glass formation, but also in HT-tagamites. K_2O/Na_2O ratio is also rather high in glass. All this points to a significant overheating of the generated impact melt and agrees well with experimental data (Parfenova et al. 1976; Yakovlev et al. 1978).

8.2.2 Transitional Processes

Transitional petrological system is characterized by a wide range of the processes of displacement and accumulation of the altered substance of target rocks. They comprise the transformed material ejected as jets, currents, acoustic fluidized flows, fireball, gas clouds etc., consists of solid, liquid and gaseous phases.

As noted above, the transformation from the initial to the transitional system occurs beyond the shock wave front at each particular moment in each part of the semispherical layer, where graphite turns into diamond. Certain features of differential movements of the aggregate of monomineral melts and their mixing can be seen in specimens of chilled protoimpactities, ejected from this zone. These rocks, made up of monomineral pumiceous impact glass display traces of the starting flow of molten material and its homogenization as areas of fluidal textures and streaky bands of black polymineral glass. Such mixing, starting throughout the considered layer and in adjacent beds, further leads to a large-scale homogenization. Though such homogenization becomes essentially completed at the moment, when whole masses stops after the ejection along different trajectories, several observations indicate, that it mainly proceeds at the initial stages of substance movement. This is confirmed by the composition of thin tagamite veinlets and dykes, cutting blocks of shock-metamorphosed gneisses, enclosed into allogenic breccias. These injections formed prior to ejection of the crushed and molten material; however, their composition is practically indistinguishable from that of tagamites, which original melt seem to have undergone the complete mixing and ejection. There are other data, considered below, which also point to the high speed of this process.

The form and mechanism of transportation of the crushed and molten material directly in the transient crater, ejection plume, and gas and dust cloud (Fig. 8.2) can be, to a certain extent, reconstructed, processing from the aggregate state of substance of the observed rocks, their mode of occurrence, inner structure and relationships of the bodies composed by them. The character of displacement of the crushed and partly molten masses near the surface of the transient crater floor and under this surface and commonly regarded within the framework of the model of Z-flowage (Bazilevsky et al. 1983; Melosh 1989 etc.), passing into the ballistic jets. Two stages of ejection are commonly distinguished, i.e. initial and late (Gault et al. 1968; Melosh 1989, 2013; Kenkmann et al. 2014 etc.). The initial stage is associated with the action of the air shock wave, moving in front of the impactor, on the ground surface. This eventually leads to formation of tektites and tektite strewn field. The late stage is characterized

by the ejection of material upwards and to the sides along the ballistic trajectories with the velocities of several km per second. This ejection proceeds both in the form of dispersed fluidized systems, composed of gas, melt particles and rock fragments in different proportions. The dispersion rates of the ejected masses, which, along with a large size of the forming crater resulted in composite combination within the same bodies of the material of different initial rocks, transformed by shock compression to a variable degree, heated to different temperatures etc.

Taking into account a certain asymmetry in impactite and impactite breccia distribution in the Popigai crater relative to its center (Fig. 1.1), as well as the asymmetry of a number of elements of the inner structure, it might be concluded, that this was, most likely, caused by an oblique impact of the cosmic body, directed from the north-east to the south-west along the azimuth 220 ± 10° (Masaitis and Mashchak 1982). This agrees with experimental data, showing, that under the oblique impact the melt concentrates predominantly on front of the impact point (Gault and Wedekind 1978). It confirms a certain irregularity in the flow of the transformed target material and its ejection at the initial stage of movement. Judging by the similarity of composition of chilled bombs and impact glass fragments from suevites and microbreccias with that of tagamite composition, forming both large, and minor bodies, almost simultaneous homogenization occurs very fast during mixing of molten material and prior to its ejection along the ballistic trajectories and into the fireball.

The presence inside large sheeted bodies of two contrasting varieties of tagamites, differing in a number of textural-structural and, to a lesser extent, constitutional features, as well as abrupt contacts between them permits to distinguish their high-temperature (HT) and low-temperature (LT) facies. Such features of the former as a lower crystallinity degree, a smaller number of inclusions, their higher melting degree, a lower oxidation degree of iron, a smaller content of SiO_2, as well as normative orthoclase, albite, quartz, a smaller amount of initial dissolved water etc., allow presuming, that they formed from the melt fraction initially overheated above liquidus. Noteworthy is also a low content of impact diamonds in HT-tagamites, as well as the features of their more intense corrosion, due to influence high temperature. The above-mentioned shifts in composition of HT-tagamites, as compared to LT-tagamites are similar to those recorded in the course of experiments on selective evaporation of silicate melt (Yakovlev et al. 1978). Melt fractions, from which tagamites of both varieties formed, appeared at the expense of the same substrate; however, due to a slightly different position relative to the epicentral zone. Melt fractions could differ in temperatures approximately by 300–500 °C. These may resulted in different polymerization degree of the structures of corresponding liquids (Hess 1971). Immediately this feature interfered with the mutual immiscibility of fractions, when the corresponding jets stopped moving and composite bodies formed. Such an immiscibility, in places of a macroemulsion character, shows up at the boundaries of simple bodies of HT and LT tagamites as taxitic structures. These structures indicate that LT tagamites were in many instances less viscous, whereas HT tagamites already lost plasticity. Complete mixing in the junction zones of melt fractions with contracting temperature and viscosity occurred only in deeper and slowly cooled

parts of composite sheeted bodies of great thickness. There were also melt jets with intermediate tagamite varieties.

Impact diamonds, enclosed in tagamites and impact glass fragments, on the one hand, are the preserved relicts of completely or almost completely molten crystalline rocks. On other hand, they could result from the capture of shock-metamorphosed graphite-bearing material of such rocks as their fragments, subsequently subject to additional heating, melting, disintegration during further movement and mixing of the melt. A part of such fragments is, nevertheless fully preserved, enabling to judge confidently of the character of such processes.

There are, as yet, no data for the reliable evaluation of the relative quantities of diamonds, occurring in the tagamite matrix as independent grains or originally included in shock-metamorphosed gneisses comprised within small fragments. The negative correlation between the number of minor inclusions (above the level of approximately one-fourth of tagamite volume) and diamond content, as well as their marked corrosion, confirm the assumption, that most of them are localized in the glassy groundmass.

Capture and absorption of fragments of target rocks by the impact melt proceed along the entire route of its displacement and have a stagewise character. Apparently, the first portions of such more intensely heated fragments (particularly, their small fraction) have the time to fully dissolve in the overheated melt, whereas relatively cooler clasts, captured at the final section of this route, when the melt was markedly cooled due to contamination, degassing and, partly, adiabatic expansion, undergo only slight thermal changes. This can account for an almost constant presence of the preserved, slightly shock-metamorphosed clasts in the initially overheated melt fractions and demonstrates that the model of a single-stage capture and equalization of the temperature of the system (Floran et al. 1978; Grieve 1978; Onorato et al. 1978) requires a significant correction. The correlation exists between the extent of radial transport of the melt and the amount of clastic material, absorbed by it (Warren et al. 1996).

During transient crater growth, and downward and sideward displacements of its true bottom, the crushed and molten material was partially dragged along its surface, forming peculiar breccia masses at the base of thick tagamite bodies. In places, the melt together with crushed rocks penetrates the crater floor as injection veins and dykes.

As noted above, ray-like inhomogeneities in diamond distribution in impactities of the Popigai crater result from: (a) an irregular localization of graphite in target rocks, (b) superposition of concentric shock-metamorphic zonation, (c) subsequent centrifugal ejection of the molten and crushed material, containing certain amounts of diamonds (Fig. 8.3). A significant part of diamond-bearing material (about one-half) was dissipated into minor drops and particles during the ejection, which were later comprised into suevites. Small portion of pulverized melt was included into different displaced breccias, among them microbreccias. This was, to a major extent, associated with the impact of expanding gases, forming not only at the expense of evaporated matter of the impacting body and the target, but also, to a major

extent, generated under shock heating and alteration of water-saturated terrigenous and carbonate rocks of the sedimentary cover.

It is necessary to emphasize some specific features of such mixture masses, which under their further collapsing, result in formation of suevites. Their displacement occurred partly in a flow composed of gaseous, liquid, and solid material. Some flows and jets characterized by turbulent regime and combined with transport of isolated major outbursts of the melt and blocks of different rocks. Some of these flows may be similar to so-called pyroclastic ignimbrite-like currents. Subsequent accumulation of disordered chaotic masses forms thick suevite sequences. Irregular combination of suevites with fine grained clastic material (microbreccias), which have both gradual mutual transitions, and abrupt chilled contacts, point to significant differences in dynamic viscosity and temperature of certain jets of fluidized ejection. Reconstructions point to a definite lowering of the temperature of the material, at the expense of which suevites formed up the general section of the crater fill, approximately from 500–600 to 300–200 °C. Up the section occur a reduction of the relative amount of vitroclasts and intensely shock-metamorphosed crystalline rock fragments, reduction of sintering degree of vitroclasts etc. The relative admixture of small clasts of sedimentary rocks also increases; this particularly concerns the silty-psammitic fraction. All these also lower diamond content in suevites.

The suevites and microbreccias of the upper part of the general section was deposited from collapsing gaseous plume and dust clouds. Their accumulation was accompanied by a certain sorting of clastic material, condensation of water drops and formation of accretionary lapilli. The originated obscure-bedded suevites often contain gneiss coated bombs, which seem to be inserted into fine clastic material. Such rocks are, most likely, products of deposition from the radially flowage of base surges, which appeared by collapse of the vertical column of gas and dust.

8.2.3 Final Processes

Cooling and lithification are the main petrlogical processes, determining the evolution of the considered system and characterized by a significant duration.

Behaviour of the molten substance in thick sheeted bodies is primarily dependent on the initial temperature and its cooling rate under low pressures, Its evaluations for the crater of a large diameter, obtained by different researchers, lie within 10–100 thousand years; these evaluations are affected by a number of factors (composition and mass of the melt, temperature and thermal conductivity of the underlying and overlying rocks, the thickness of the latter, convective flows of fluids etc.). In small volume, the melt undergoes quick chilling with formation of glass and their subsequent devitrification or subsolidus crystallization.

Certain complication are introduced into simple schemes of cooling of large melt volumes by the presence of irregularly heated zones or areas, as well as large rock inclusions. A relatively slow cooling of the impact melt, resulting in its particular or full crystallization as applied to the impactites of some large craters is consid-

ered in a number of publications (Grieve 1975; Simonds et al. 1978 and references therein). The character of their crystallization is similar to that of magmatic masses of a similar composition, occurring on the surface or under the hypabyssal environment. Crystallization of the impact melt in places may have fractional character (Selivanovskaya 1987). Melting of inclusions, diffusion phenomena, caused by the presence of vapours and gases, may slightly disturb the regular general cooling. Release of the crystallization heat, which slightly slows down the cooling, can be of utmost significance.

Thermal evolution of large melt masses (and, correspondingly, its vitrification) is strongly affected by increase of its viscosity; thermal conductivity, in this case, is reduced, and cooling shows down. For this reason, no redistribution of crystalline and liquid phases occurs in the melt bodies of the Popigai crater, which is relatively rich in silica. The composition of cooling rocks is, to a certain extent, determined by their interaction with water vapours and solutions, atmospheric oxygen etc. This is accompanied by water absorption, particularly by glassy rocks, oxidation of iron, redistribution of certain constituents, which is particularly characteristic of small vitroclasts, making up significant part of the volume of suevites.

Thermal physical evaluation of the duration of cooling to the vitrification temperature, which is about 900 °C for the melt sheets containing 63% SiO_2, has been performed by Yu. P. Dobryansky (Val'ter and Dobryansky 2001). This stage comprises liquidus crystallisation of the melt and its interactions with minor clasts, and demonstrated that it can be evaluated for the Popigai crater at several hundred years. At the same time, evaluations of duration of complete melting of the inclusion relative to the acid crystalline rocks 10–30 m across indicate, that such a block can be fully molten in a year, to say nothing of minor clasts. It means, most probably, that the equilibrium temperature of large melt bodies at the moment when they stop, only insignificantly exceeds solidus. Significant viscosity of the melts at the moment of cessation also ensues from observations on relationships between high-temperature and low-temperature tagamites. In mixing zones of the corresponding melts, the directive structures are rare; contours of fragment-like small bodies of one variety, enclosed into the other one are often angular with abrupt boundaries between them.

Rate of the impact melt cooling was even higher in case of small bodies. This is confirmed by specific features of the microstructure of tagamites from them. Compositions of their liquidus phases, which are more high-temperature, than in large bodies, as well as by the appearance of less ordered clinopyroxenes in reaction rims around quartz clasts. Differences in the crystallinity degree of HT- and LT-tagamites are not likely, due to the fact, that a lesser number of crystallization centers appears in the melt, which was initially slightly overheated. It also undergoes the quenching stage earlier and without subsequent devitrification.

The residual glass of HT-tagamites contains an elevated amount of LOI, mainly dissociated water, removed at higher temperatures, than predominantly molecular water in low-temperature variety. Dissociated water is inherited from the high-temperature initial melt, capable of absorbing it in significant amounts. At low external pressure, under which tagamite cooling and crystallization occurs, elasticity of the fluid vapour is extremely low. Inversion of fluid regime from the reducing to

the oxidizing is most likely confined to the moment of quenching (900–1000 °C); however, the role of the fluid as an oxidizer is insignificant for the above reasons. This is also confirmed by the presence of the finest pyrrhotite particles in high-temperature tagamites, which results in supermagnetism of rocks. These practices, forming under the high-temperature reducing environment, seem to be frozen under the environment of quick cooling. More significant is role of the fluid as an oxidizer in low-temperature melts, where hypersthene, reacting with it, is partly replaced by biotite with an admixture of magnetite. Taking the above said into account, it might be presumed, that diamonds were subjected to corrosion, mainly due to the interaction the cooling melt, where alkalies were present as compounds with OH^- group are commensurable with the above values. Such a burn-out was most intense within a period prior to the melt quenching (temperature about 1025 °C or slightly lower), during which the convection stopped.

Experiments on impact diamonds oxidation under the air environment (Val'ter et al. 1992) demonstrate, that they burnt within the interval from 700 to 1100 °C; thermal resistance of dense light-colored grains, as well as larger grains, is higher. In the vacuum or in the reducing environment, graphitization of impact diamonds occurred at the temperature of 1000–1100 °C. Such process was more intensive in thick tagamite bodies, where light-colored grains preserved mostly. For suevites, in which fragments of diamond-bearing melt subjected to chilling, such a selection was not recorded, and dark-colored, graphite-bearing varieties account for an essential part of the diamonds.

Therefore, a period from the moment when the melt centrifugal displacement along the radii stops to its chilling was, generally, relatively short. It is within this time period, that the main stage of diamond oxidation occurred, recorded proceeding from the habit of irregular grains and paracrystals, as well as peculiar relief of their surface.

Futher cooling after chilling of crystallization residues, as well as subsequent, slightly shown hydrothermal processes (see Sect. 4.4), to a major extent, associated with leakage of atmospheric water into the heated sequences, practically do not affect most of the diamonds enclosed in rock. Essentially, this is the end of emplacement of diamondiferous impactite bodies as products of the above-characterized broad range of melt and rock generation within the evolving petrological systems (Fig. 8.4). This evolution is noted for a continuous alteration of thermodynamic (total entropy, enthalpy, total pressure and temperature), and some other characteristics (movement rate of melt masses and particles, effect of fluids etc.). At the final stages of the process, enthalpy, pressure, temperature, are coming back to the initial state, and only entropy (structural and constitutional) is conservatively recording the process of all the other stages. The evolution of the considered systems is accompanied by a number of transformations and mineralogical changes of carbonaceous substance, which is their constituent part.

Despite a significant success attained in the analysis of impact crater and its diamond-bearing rocks, many issues, concerning specific formation mechanisms of textural-structural and constitutional features of impactites and impact breccias, and the geological bodies made up of them, are not yet quite clear. In this connection,

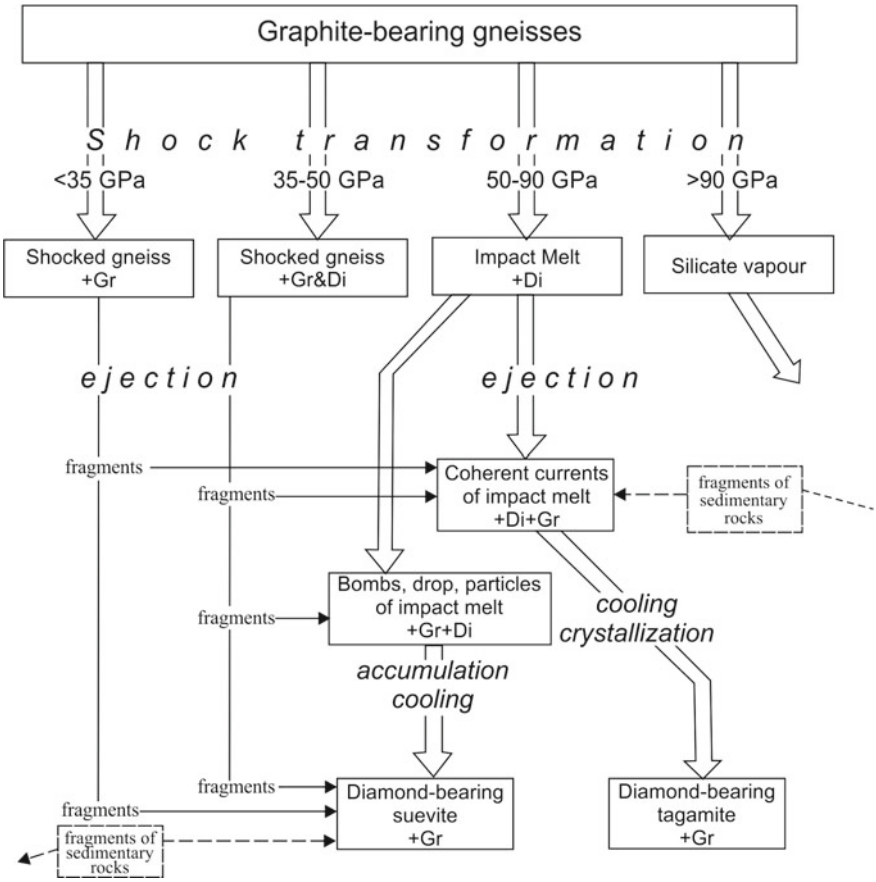

Fig. 8.4 Principal scheme of formation of diamond-bearing impactites. Gr—graphite, Di—diamond

the systems, considered above, and the processes in them are mainly qualitatively characterized. It is undoubtedly that all these questions may be dissolved during further detailed studies.

References

Bazilevsky AT, Ivanov BA, Florensky KP, Yakovlev OI, Feldman VL, Granovsky LB (1983) Impact craters on the Moon and planets (in Russian). Nauka Press, Moscow, 200 pp

Collins GS, Melosh HJ, Marcus RA (2005) Earth impact effects program: a Web-based computer program for calculating the regional environmental consequences of a meteoroid impact on Earth. Meteorit Planet Sci 40:817–840

Feldman VI (1990) Petrology of impactites (in Russian). Moscow University Press, Moscow, 299 p
Floran RJ, Grieve RAF, Phinney WC, Warner JL, Rhodes MJ, Jahn BM, Dence MR (1978) Manicouagan impact melt, Quebec, I: stratigraphy, petrology, and chemistry. J Geophys Res 83(B6):2737–2759
Gault DE, Wedekind JA (1978) Experimental studies of oblique impact. In: Proceedings of Lunar Planet Sci Conf IX, pp 3843–3876
Gault DE, Quaide WL, Oberbeck VR (1968) Impact cratering mechanics and structures. In: Short NM, French BM (eds) Shock metamorphism of natural materials. Mono Book, Baltimore, pp 87–99
Gohn GS, Koeberl K, Miller KG, Reimold WU (2009) Deep drilling in the Chesapeake Bay impact structure—an overview. Geol Soc Am Spec Pap 458:1–20
Grakhanov SA (2005) New data on distribution of lonsdaleite-bearing diamonds in the northeastern of Siberian platform. Trans (Dokl) Russ Acad Sci 405:779–782
Grakhanov SA, Shatalov VI, Shtyrov VA, Kychkin VR, Suleimanov AM (2007) Diamond placers of Russia (in Russian). Geo Press, Novosibirsk, 457 pp
Grieve RAF (1975) Petrology and chemistry of the impact melt of Mistastin Lake crater, Labrador. Geol Soc Am Bull 86:1617–1629
Grieve RAF (1978) Meteoritic component and impact melt composition of the Clearwater impact structures, Quebec. Geochim Cosmochim Acta 42:420–431
Hess PC (1971) Polymeric model of silicate melts. Geochim Cosmochim Acta 35:289–306
Ivanov BA (2005) Impacts of cosmic bodies as a geological factor (in Russian). In: Adushkin VV, Nemchinov IV (eds) Catastrophic influence of cosmic bodies. Academkniga Press, Moscow, pp 118–150
Kenkmann T, Poelschau MH, Wulf G (2014) Structural geology of impact craters. J Struct Geol 62:156–182
Koeberl C, Masaitis VL, Shafranovsky GI, Gilmour I, Langenhorst F, Schrauder M (1997) Diamonds from the Popigai impact structure, Russia. Geology 25:967–970
Krasheninnikov VA, Ahmetjev MA (eds) (1996) Geological and biological events in Late Eocene–Early Oligocene (in Russian). GEOS Publishing, Moscow, part 1, 313 pp, part 2, 249 pp
Masaitis VL (1978) High-temperature metamorphism and melting in impact craters. In: Problems of petrology of Earth crust and upper mantle (in Russian): Nauka Press, Novosibirsk, pp 188–194
Masaitis VL (1982) Problems of shock metamorphism (in Russian). VSEGEI Trans, New Ser 238:113–122
Masaitis VL (1984) Giant meteorite impact: some models and their consequences. In: Modern ideas of theoretical geology (in Russian). Nedra Press, Leningrad, pp 151–179
Masaitis VL (1993) Diamantiferous impactites, their distribution and petrogenesis (in Russian). Regionalnaya Geologija and Metallogenija 1:121–134
Masaitis VL (1998) Popigai crater: origin and distribution of diamond-bearing impactites. Meteorit Planet Sci 33:349–359
Masaitis VL (2010) Prospective zones of damage caused by the Popigai impact event. In: Finkelstein A, Huebner W, Shor V (eds) Protecting the Earth against collisions with asteroids and comet nuclei. SPb, Nauka. Proceedings of the International Conference “Asteroid-Comet Hazard-2009”, pp 211–215
Masaitis VL, Mashchak MS (1982) Bilateral symmetry of ring impact structures (in Russian). Meteoritika 41:150–156
Melosh HJ (1989) Impact cratering—a geological process. Oxford University Press, New York, 245 pp
Melosh HJ (2013) The contact and compression stage of impact cratering. In: Osinski GR, Pierazzo E (eds) Impact cratering: processes and products. Wiley, Chichester, pp 32–42
Morgan JV, Warner MR, Collins GS, Melosh HJ, Christeson GL (2000) Peak ring formation in large impact craters. Earth Planet Sci Lett 183:347–354

Morgan JV, Gulick SPS, Bralower T, Chenot E, Christeson G, Claeys P, Cockell C, Collins GS, Coolen MJL, Ferrière L, Gebhardt C, Goto K, Jones H, Kring DA, Le Ber E, Lofi J, Long X, Lowery C, Mellett C, Ocampo-Torres R, Osinski GR, Perez-Cruz L, Pickersgill A, Poelchau M, Rae A, Rasmussen C, Rebolledo-Vieyra M, Riller U, Sato H, Schmitt DR, Smit J, Tikoo S, Tomioka N, Urrutia-Fucugauchi J, Whalen M, Wittmann A, Yamaguchi KE, Zylberman W (2016) The formation of peak rings in large impact craters. Science 35(6314):878–882

Onorato PJK, Uhlmann DR, Simonds CH (1978) The thermal history of the Manicouagan impact melt sheet, Quebec. J Geophys Res 83(B6):2789–2798

Parfenova OV, Yakovlev OI, Kosolapov AI (1976) Some regularities of evaporization of target substance during meteorite impact (in Russian). Vestnik of Moscow State University, ser Geol 3:52–66

Pilkington M, Pesonen LJ, Grieve RAF, Masaitis VL (2002) Geophysics and petrophysics of the Popigai impact structure, Siberia. In: Plado J, Pesonen LJ (eds) Impacts in Precambrian shields. Springer, Berlin, pp 87–108

Poag CW (1996) Structural outer rim of Cheasapeake Bay impact crater: seismic and borehole evidence. Meteorit Planet Sci 31:218–226

Poag CW, Aubry MP (1995) Upper Eocene impactites of the US east coast: depositional origins biostratigraphic framework and correlation. Palaios 10:16–43

Poag CW, Koeberl C, Reimold WU (2004) The Chesapeake crater—geology and geophysics of a late Eocene submarine impact structure. Impact Studies Series. Springer, Heidelberg, 522 pp

Selivanovskaya TV (1987) Crystal fractionation of impact melts (in Russian). Meteoritika 46:128–135

Sherlock SC, Kelley SP, Parnell J, Green P, Lee P, Osinski GR, Cockell CS (2005) Re-evaluating the age of the Haughton impact event. Meteorit Planet Sci 40(12):1777–1788

Simonds CH, Floran RJ, McGee PE, Phinney WC, Warner JL (1978) Petrogenesis of melt rocks, Manicouagan impact structure, Quebec. J Geophys Res 83(B6):2773–2788

Val'ter AA, Dobryansky YP (2001) Cooling regimes in tagamite sheets and their influence on impact diamonds preservation (in Russian). Mineral J 23(4):56–66

Val'ter AA, Yeremenko AA, Kvasnitza VN, Polkanov YA (1992) Shock-generated carbon minerals (in Russian). Naukova Dumka Press, Kiev, 171 pp

Vermeesch PM, Morgan JV (2004) Chicxulub central crater structure: initial results from physical property measurements and combined velocity and gravity modeling. Meteorit Planet Sci 39:1019–1034

Vishnevsky SA, Afanasiev VP, Argunov KP, Pal'chik NA (1997) Impact diamonds: their features, origin & significance (in Russian). Siberian Branch of Russian Academy of Scence Press, Novosibirsk, 110 pp

Warren PH, Clayes P, Cedillo-Pardo E (1996) Megaimpact melt petrology (Chicxulub Sudbury and the Moon): effects of scale and other factors on potential for fractional crystallization and developments of cumulates. In: Ryder G, Fastovsky D, Gartner S (eds) The Cretaceous-Tertiary event and other catastrophes in Earth history. Geological Society of America Special Paper 307, pp 105–124

Yakovlev OI, Parfenova OB, Arkhangelskaya VN (1978) Modification of rock composition during impact melt formation (in Russian). Trans (Dokl) Acad Sci USSR 240:934–937

Zel'dovich YB, Raizer YI (1966) The physics of shock waves and of high-temperature hydrodynamic phenomena (in Russian). Nauka Press, Moscow, 686 pp

Conclusion

Impact interactions are one of the fundamental geological processes on the solid planetary bodies of the Solar system. The understanding of their role in the rock-forming and structure-forming processes, as well as their influence on global biotic phenomena, came into geology only in the last third of the twentieth century. At present, the results of comprehensive studies of impact structures on the Earth and the conditions of their formation are integrated into global natural science. These results occupy a certain place in the general system of studying outer space too.

The identification and geological study of ancient impact structures (or astroblemes) begun in Russia in the early 1970s, made it possible to obtain a large number of new data concerning their internal structure and composition of the rocks distributed in them, to develop methods for their subdivision and mapping, to reconstruct a number of mechanisms of rock formation. At the same time, the new type of diamondiferous bedrock, previously unknown in the world experience, was first established and evaluated. An important metallogenic significance of impact structures, many of which contain deposits of various mineral raw materials, was also shown.

The most significant results were obtained from the study of the Popigai structure. This ancient impact crater, with a diameter of 100 km, arose 35.7 million years ago in the northeastern edge of the Anabar Shield in the north of the Siberian Platform. It is distinguished by a complex multi-ring internal structure and is filled with rocks undergone intense shock transformations. The crater arose from the fall of a large cosmic body, which most likely had the composition of an ordinary chondrite. Dispersed substance of this body has been found in the rocks re-melted during the crater event. The gneisses and plagiogneisses including those containing graphite and subjected to impact melting, served as the initial substrate for the formation of diamond-bearing impactites. The accessory diamonds contained in the latter arose under shock compression of graphite and its transition in the solid state to the aggregate of hyperbaric phases of carbon. Impact diamonds are significantly different by many features from diamonds of endogenous origin that found in

V. L. Masaitis (ed.), *Popigai Impact Structure and its Diamond-Bearing Rocks*,
Impact Studies, https://doi.org/10.1007/978-3-319-77988-1

kimberlites and lamproites, but are characterized by a high hardness representing abrasive raw materials. In the impactites of the Popigai structure diamonds are found everywhere. At the same time, the primary uneven distribution of graphite in local rocks, on which the concentric zones of transformation superimposed, as well as the radial ejection of the melted and disintegrated material, caused radial-ray inhomogeneities in the distribution of diamonds and enrichment by them with certain separated areas. It was there that several unique (in terms of ore volumes and reserves) deposits of impact diamonds were identified. The destruction of diamond-bearing impactites on the surface and re-deposition of the products of their disintegration led to the formation of impact placers in the Popigai region. Impact diamonds belong to specific category of economic minerals occurred in impact structures.

In many respects, the Popigai impact structure is a unique geologic object, which presents a wide variety of impact breccias and impactites including diamondiferous ones, and where various morphostructural elements of a complex impact crater have been identified. This makes it possible to consider the Popigai as a special area not only deserving a further comprehensive study, but also a careful preservation. The Popigai crater is a source of information, which can answer many of the questions of the mechanism of impact cratering, the behavior of various rock materials (including carbonaceous materials) at super-high impulse pressures and temperatures, its movement and further evolution. It is important to establish the connection of the Popigai impact event with those or other biotic changes, as well as the correlation with other such events on Earth.

In this connection, previously accumulated geological and other materials including those obtained during drilling, geological mapping, study of rocks and minerals, are of considerable value. The presented work summarizing the data obtained, can contribute to the development of further studies of the Popigai structure and impact cratering in general.